Lehrstuhl für Elektrische Energiespeichertechnik
Fakultät für Elektrotechnik und Informationstechnik
Technische Universität München

Assessment and Optimization of Operating Stationary Battery Storage Systems

Cong Nam Truong

Vollständiger Abdruck der von der Fakultät für Elektrotechnik und Informationstechnik der Technischen Universität München zur Erlangung des akademischen Grades eines

Doktor-Ingenieur (Dr.-Ing.)

genehmigten Dissertation.

Vorsitzender:		Prof. Dr. Sebastian Steinhorst
Prüfer der Dissertation:	1.	Prof. Dr.-Ing. Andreas Jossen
	2.	Prof. Dr.-Ing. Thilo Bocklisch

Die Dissertation wurde am 19.11.2018 bei der Technischen Universität München eingereicht und durch die Fakultät für Elektrotechnik und Informationstechnik am 08.08.2019 angenommen.

Abstract

The reduction of carbon emissions is a global endeavor that requires increasing quantities of renewable energy sources. These introduce new challenges to the electrical power system. Energy storage systems are thought of as key component for the transition towards low carbon technology. This thesis is concerned with the assessment of battery energy storage and with improving the operation.

Storage systems are widely investigated with regard to their economics. The multitude of applications, evaluation metrics, and potential technologies complicate the generation of informative and comparable results. This thesis discusses the economic metrics, used for the assessment of battery storage systems. Each metric covered has its own benefits and disadvantages. The use of several metrics and in-depth assessments of the deployment of storage systems are advised. The question of the aggregate value added for the general public is addressed with a life-cycle analysis of battery storage systems on greenhouse gas emissions. This aspect shows their impact on the original motivation: the carbon reduction of the electric power system. In contrast to the economic benefits, the evaluation in respect of carbon emissions is derived with a global scope. Instead of analyzing the reduction of a system-bounded carbon footprint, the overall influence on the greenhouse gas emissions is taken into account. This ensures the assessment's meaning for the general public. Three applications are analyzed in case-studies to demonstrate the evaluation metrics. A misalignment of the economic incentives and the optimal operation, with regard to the carbon footprint, becomes apparent for the application of increasing self-consumption.

Another area in the field of energy storage is the optimal operation of storage systems. The state-of-the-art approaches are rule-based or optimization-based controllers. They both exhibit shortcomings that prevent optimal operation, either because they are suitable only for specific scenarios, are designed manually, or do not feature proper handling of prediction uncertainties, associated with renewable energy sources. A control algorithm is developed and presented in this work that alleviates the mentioned disadvantages. It is composed of the rule-based framework fuzzy logic control and of the meta-heuristic algorithm cuckoo search that solves the complex optimization problem of tuning the control parameters. The novel algorithm features versatility for the use with any system and application, real-time capability, optimized control, and systematic consideration of prediction uncertainties. Today, electrical battery storage systems are deemed to be too expensive for most use cases. The execution of multiple applications simultaneously, the multi-use, is suggested in academia and industry to increase their economic value. The multi-use operation of storage systems faces the issue of multiple stakeholders that take interest in the operation, in unbundled electricity markets, common in the European Union. A method to enable the multi-user operation of battery storage systems and an implementation concept, based on auction markets, are proposed in this thesis.

The thesis combines two related topics: The evaluation metrics set the optimal operating goals for battery storage systems. The control algorithms determine how the systems achieve these goals.

Kurzfassung

Die Vermeidung von CO_2 Emissionen ist eine globale Bestrebung, die eine Steigerung der erneuerbaren Energieerzeugung erfordert. Diese führen zu neuen Herausforderungen im Energieversorgungsnetz. Energiespeichersysteme werden als Schlüsselkomponente für den Wandel zu kohlenstoffarmen Technologien erachtet. Die vorliegende Dissertation befasst sich mit der Bewertung von Batteriespeichersystemen und der Verbesserungen des Betriebs.

Speichersysteme werden häufig unter wirtschaftlichen Aspekten analysiert. Die Vielzahl an Anwendungen, Bewertungsmethoden und potentieller Technologien erschweren das Generieren aufschlussreicher und vergleichbarer Ergebnisse. Diese Dissertation erörtert wirtschaftliche Metriken für die Bewertung von Batteriespeichersystemen. Jede behandelte Metrik hat ihre eigenen Vor- und Nachteile. Die Verwendung mehrerer Kennzahlen und eine ausführliche Analyse des Speichereinsatzes werden empfohlen. Der Gemeinnutzen von Batteriespeichersystemen wird durch die Life-Cycle Analyse für die Emissionen von Treibhausgasen untersucht. Dieser Aspekt zeigt die Bedeutung für die ursprüngliche Motivation, der Vermeidung von CO_2 Emissionen im Stromsektor. Im Gegensatz zu den wirtschaftlichen Analysen wird die Bewertung im Hinblick auf CO_2 Emissionen unter globalen Gesichtspunkten hergeleitet. Statt die CO_2 Emissionen für Systemgrenzen zu evaluieren, wird der Gesamteinfluss betrachtet. Dies gewährleistet die Bedeutsamkeit dieser Bewertung für die Allgemeinheit. Drei Speicheranwendungen werden in Fallstudien untersucht, um die Verwendung der Bewertungsmetriken zu demonstrieren. Hierbei stellt sich ein Widerspruch zwischen dem wirtschaftlichen Anreiz und des emissionsärmsten Betriebs von Batteriespeichern zur Eigenverbrauchserhöhung heraus.

Ein weiterer Bereich für Energiespeicher ist der optimale Betrieb von Speichersystemen. Heutige Methoden sind regelbasierte oder optimierungsbasierte Algorithmen. Beide weisen Unzulänglichkeiten auf, die einen optimalen Betrieb verhindern. Entweder sind sie auf spezielle Szenarien zugeschnitten, von Hand angepasst oder berücksichtigen Vorhersagefehler nicht systematisch. In dieser Dissertation wird ein Steueralgorithmus entwickelt der nicht die genannten Defizite aufweist. Dieser besteht aus einem formalisierten, regelbasierten Steuerungsansatz und einem meta-heuristischen Optimierer, der die Steuerparameter anpasst. Der vorgeschlagene Algorithmus ist für verschiedene Anwendungen und Technologien verwendbar, echtzeitfähig, optimiert und berücksichtigt Vorhersagefehler systematisch. Heute werden Batteriespeicher als zu teuer für die meisten Anwendungsfälle erachtet. Die zeitgleiche Erfüllung mehrerer Anwendungen, der Multi-Use, wird zur Verbesserung der Wirtschaftlichkeit empfohlen. Der Multi-Use Betrieb wird in liberalisierten Strommärkten, wie sie in der Europäischen Union üblich sind, mit dem Problem konfrontiert, dass mehrere Akteure am Betrieb interessiert sind. Ein Methode für den Multi-User Betrieb von Batteriespeichersystemen und ein Umsetzungskonzept, basierend auf Auktionsmärkten, werden in dieser Dissertation vorgeschlagen.

Die vorliegende Arbeit kombiniert zwei zusammenhängende Themen. Die Bewertungsmetriken bestimmen das optimale Betriebsziel für Batteriespeichersysteme. Die Steueralgorithmen bestimmen, wie diese Ziele erreicht werden.

Vorwort und Danksagung

Die vorliegende Arbeit wurde während meiner Zeit als wissenschaftlicher Mitarbeiter am Lehrstuhl für Elektrische Energiespeichertechnik der Technischen Universität München verfasst.

Zunächst möchte ich mich bei Herrn Prof. Dr.-Ing. Andreas Jossen bedanken, der mir diese Tätigkeit an seinem Lehrstuhl für gute 5 Jahre ermöglicht hat und mich fachlich betreut hat, um meine Forschungsarbeit in die richtigen Bahnen zu lenken. Prof. Dr.-Ing. Thilo Bocklisch möchte ich danken, für die Mitwirkung als 2. Mitberichter meiner Dissertation. Des weiteren danke ich Dr. rer. nat. Holger Hesse für die fachlichen Diskussionen und kritischen Fragen, die die Qualität der Arbeit gefördert haben.

Mein Dank gilt auch meinen ehemaligen und derzeitigen Kollegen, die für eine produktive, aber dennoch gute Atmosphäre gesorgt haben, bei der ich gerne am Lehrstuhl war. Besonders möchte ich mich bei Maik Naumann bedanken für die gemeinsame Entwicklung des Simulationsmodells *SimSES*. Die enge Zusammenarbeit war von grossen Vertrauen und zuverlässiger Unterstützung geprägt, die beruflich als auch persönlich gewinnbringend war.

Das Hauptprojekt während meiner Promotion war *EEBatt* und ich möchte mich bei allen Kollegen im Projekt für die Zusammenarbeit in dem spannenden Projekt bedanken. Dies gilt den Kollegen an der Technischen Universität München, aber auch den Kollegen von Varta Storage, ZAE Bayern und den Kraftwerken Haag. Im Rahmen des zweiten Forschungsprojektes *StorageLink* möchte ich mich bei meinen Kollegen von SmartPower bedanken.

Bei Prof. Dr. Petr Musilek möchte ich mich für die fachlichen Impulse und der Möglichkeit für einen mehrmonatigen Forschungsaufenthalt in Edmonton, Kanada bedanken. Die Dissertation ist auch mit Hilfe studentischer Arbeiten entstanden und ich möchte mich bei meinen Studierenden für ihr Engangement und das Vertrauen in mich als Betreuer bedanken.

Schliesslich möchte ich mich bei meinen Freunden und meiner Familie bedanken, die mich stets während der Promotionszeit unterstützt haben.

List of Publications

Journal Contributions (Lead Author)

C. N. Truong, M. Naumann, R. C. Karl, M. Müller, A. Jossen, and H. C. Hesse. "Economics of Residential Photovoltaic Battery Systems in Germany: The Case of Tesla's Powerwall". In: *Batteries* 2 (2) (2016), p. 14.

C. N. Truong, M. Schimpe, U. Bürger, H. C. Hesse, and A. Jossen. "Multi-Use of Stationary Battery Storage Systems with Blockchain Based Markets". In: *Energy Procedia 155* (2018), pp 3-16.

Conference Contributions (Lead Author)

C. N. Truong, L. Viernstein, M. Schimpe, R. Witzmann, A. Jossen, and H. C. Hesse. "Maximizing Solar Home Battery Systems' Contribution to the Energy Transition of the Power System". In: *Conference on Sustainable Energy Supply and Energy Storage Systems (NEIS)*, Hamburg, September 21-22, 2017.

C. N. Truong, D. C. May, R. Martins, P. Musilek, A. Jossen, and H. C. Hesse. "Cuckoo-search optimized fuzzy-logic control of stationary battery storage systems". In: *2017 IEEE Electrical Power and Energy Conference (EPEC)*. Saskatoon, SK, Canada, October 22-25, 2017.

C. N. Truong, M. Schimpe, M. Naumann, A. Jossen, and H. C. Hesse. "Impact of sub-components on the overall performance of stationary battery systems: Insights on the prototype Energy Neighbor". In: *International ETG Congress 2017*. Bonn, Germany, November 28-29, 2017.

Software Publications

M. Naumann, C. N. Truong. "SimSES: Software for techno-economic Simulation of Stationary Energy Storage Systems". 2017. DOI: 10.14459/2017MP1401541

Books (Co-Author)

J. Böttcher and P. Nagel. "Batteriespeicher - Rechtliche, Technische und Wirtschaftliche Rahmenbedingungen". De Gruyter, Oldenbourg (2018).

Journal Contributions (Co-Author)

M. Naumann, R. C. Karl, C. N. Truong, A. Jossen, and H. C. Hesse. "Lithium-ion Battery Cost Analysis in PV-household Application". In: *Energy Procedia 73* (2015), pp. 37-47.

M. Müller, L. Viernstein, C. N. Truong, A. Eiting, H. C. Hesse, and R. Witzmann. "Evaluation of grid-level adaptability for stationary battery energy storage system applications in Europe". In: *Journal of Energy Storage* (2017), pp. 1-11.

H. Hesse, R. Martins, P. Musilek, M. Naumann, C. N. Truong, and A. Jossen. "Economic Optimization of Component Sizing for Residential Battery Storage Systems". In: *Energies 10* (7) (2017), p. 835.

Y.-S. Cheng, Y. H. Liu, H. C. Hesse, M. Naumann, C. N. Truong, and A. Jossen. "A PSO-Optimized Fuzzy Logic Control-Based Charging Method for Individual Household Battery Storage Systems within a Community". In: *Energies 11* (2) (2018), p. 469.

M. Schimpe, M. Naumann, C. N. Truong, H. C. Hesse, S. Santhanagopalan, A. Saxon, and A. Jossen. "Energy efficiency evaluation of a stationary lithium-ion battery container storage system via electro-thermal modeling and detailed component analysis". In: *Applied Energy 210* (2018), pp. 211-229.

Oral Presentations

C. N. Truong. "Energiespeicher und deren netzintegrierter Betrieb III: Der Ortsnetzspeicher". *Otti-Seminar*, Regensburg, February 21st 2017.

C. N. Truong, M. Schimpe, I. Zilberman, M. Naumann, H. C. Hesse, and A. Jossen. "Impact of small-scale components on large-scale battery systems: Insights on the prototype Energy Neighbor". *Singapore Battery Meeting 2017*, Singapore, March 23rd 2017.

C. N. Truong. "Stationary Battery Storage Systems". *MIT Energy Club 2017*, Boston, May 2nd, 2017.

C. N. Truong, L. Viernstein, M. Schimpe, R. Witzmann, A. Jossen, and H. C. Hesse. "Maximizing Solar Home Battery Systems' Contribution to the Energy Transition of the Power System". *Conference on Sustainable Energy Supply and Energy Storage Systems (NEIS)*, Hamburg, September 22nd 2017.

C. N. Truong. "The Prototype *Energy Neighbor*". *Cluster-Forum Batterieinnovationen 2017*, Garching, October 5th 2017

C. N. Truong, M. Schimpe, M. Naumann, A. Jossen, and H. C. Hesse. "Impact of sub-components on the overall performance of stationary battery systems: Insights on the prototype Energy Neighbor". *International ETG Congress 2017*. Bonn, Germany, November 10th 2017.

C. N. Truong, M. Schimpe, U. Bürger, H. C. Hesse, and A. Jossen. "Multi-Use of Stationary Battery Storage Systems with Blockchain Based Markets". *12th International Renewable Energy Storage Conference (IRES 2018)*. Düsseldorf, March 13th 2018.

List of Contents

List of Abbreviations

BESS . . . . . battery energy storage system

BMS . . . . . battery management system

BOS . . . . . balance of system

C . . . . . graphite

CF . . . . . cash flow

DG . . . . . diesel generator

DOC . . . . . depth of cycle

EMS . . . . . energy management system

EOL . . . . . end-of-life

ESS . . . . . energy storage system

FEC . . . . . full equivalent cycle

GHG . . . . . greenhouse gas

GWP . . . . . global warming potential

IRR . . . . . internal rate of return

LCA . . . . . life-cycle assessment

LCOE . . . . . levelized cost of energy

LCOES . . . . . levelized cost of energy stored

LFP . . . . . lithium iron phosphate ($LiFePO_4$)

LHV . . . . . lower heating value

NCA . . . . . lithium nickel cobalt aluminium oxide

NMC . . . . . lithium nickel manganese cobalt oxide

NPV . . . . . net present value

OCV . . . . . open circuit voltage

PI . . . . . profitability index or NPV per EUR invested

PP . . . . . payback period

PV . . . . . photovoltaic

RES . . . . . renewable energy source

ROI . . . . . return on investment

SOC . . . . . state-of-charge

SOH . . . . . state-of-health

TCO . . . . . total cost of ownership

List of Formula Symbols

α_0	initial step size of Lévy flight	-
α_k	step size of Lévy flight at iteration k	-
C_{batt}	battery nominal capacity	As
ΔC_{batt}	battery capacity degradation	As
$\Delta C_{\text{batt}}^{\text{cal}}$	calendric battery capacity degradation	As
$\Delta C_{\text{batt}}^{\text{cyc}}$	cyclic battery capacity degradation	As
c_{el}	electricity price	EUR per kWh
c_{fuel}	fuel price	EUR per liter
$c_{\text{load}}^{\text{shed}}$	penalty for load shedding	EUR per kWh
c_{peak}	peak load charge	EUR per kW
c_{remun}	electricity feed-in remuneration	EUR per kWh
$\text{CF}_{\text{el}}^{\text{home}}$	cashflow of electricity costs of household without BESS or PV-unit	EUR
$\text{CF}_{\text{el}}^{\text{PVhome}}$	cashflow of electricity costs of photovoltaic (PV)-home without BESS	EUR
$\text{CF}_{\text{el}}^{\text{PVBESShome}}$	cashflow of electricity costs of PV-home with BESS	EUR
$\text{CF}_{\text{el}}^{\text{DG}}$	cashflow of electricity costs of diesel island grid	EUR
$\text{CF}_{\text{el}}^{\text{Hybrid}}$	cashflow of electricity costs of hybrid island grid with RES	EUR
$\text{CF}_{\text{el}}^{\text{HybridBESS}}$	cashflow of electricity costs of hybrid island grid with RES and BESS	EUR
$\text{CF}_{\text{el}}^{\text{PS,BESS}}$	cashflow of electricity costs with peak-shaving by BESS	EUR
$\text{CF}_{\text{el}}^{\text{PS,DG}}$	cashflow of electricity costs with peak-shaving by diesel generator	EUR
$\text{CF}_{\text{el}}^{\text{load}}$	cashflow of electricity costs without peak-shaving	EUR
$\Delta\text{CF}_{\text{el}}^{\text{BESS}}$	electricity cost reduction by BESS	EUR
$\Delta\text{CF}_{\text{el}}^{\text{DG}}$	electricity cost reduction by diesel generator	EUR
$\Delta\text{CF}_{\text{el}}^{\text{PV}}$	electricity cost reduction by PV-unit	EUR
$\Delta\text{CF}_{\text{el}}^{\text{RES}}$	electricity cost reduction by RES	EUR
$\text{CF}_{\text{return}}$	cashflow of returns	EUR
E_k^0	old virtual energy value of segment k before re-assignment	Ws
E^b	balanced energy or storable energy of BESS	Ws
E_k^b	virtual balanced energy segment or storable energy of application k	Ws
$E_{\text{batt}}^{\text{nom}}$	battery nominal energy capacity	Ws
$E_{\text{BESS}}^{\text{in}}$	energy charged by BESS	Ws
$E_{\text{BESS}}^{\text{loss}}$	BESS total energy losses	Ws
$E_{\text{BESS}}^{\text{nom}}$	BESS nominal energy capacity	Ws
$E_{\text{BESS}}^{\text{out}}$	energy discharged from BESS	Ws
$E_{\text{BESS}}^{\text{stby}}$	BESS energy loss by standby consumption	Ws
E_k^C	virtual energy capacity of BESS of application k	Ws
E_{DG}	diesel generated electricity	Ws
$E_{\text{grid}}^{\text{feedin}}$	energy feed-in to the electricity grid	Ws
$E_{\text{grid}}^{\text{purch}}$	energy purchased from electricity grid	Ws

$E^{\max}_{\text{housing}}$	energy capacity of batteries that fit into the housing	Ws
ΔE_k	virtual energy increase of segment k after ressource re-assignment	Ws
E^*_k	new virtual energy value of segment k after re-assignment	Ws
ΔE_{lk}	virtual energy assignment from application k to application l	Ws
E_{load}	load consumption	Ws
$E^{\text{shed}}_{\text{load}}$	shed load energy	Ws
E_{PS}	energy of load peaks shaved	Ws
E_{PV}	energy generated by PV-unit without curtailment	Ws
$E^{\text{curt}}_{\text{PV}}$	energy curtailed from PV-generation	Ws
$\Delta E^{\text{curt}}_{\text{PV}}$	reduced energy curtailment by BESS	Ws
$E^{\text{direct}}_{\text{PV}}$	PV-generated electricity directly consumed by household	Ws
$E^{\text{FC}}_{\text{PV}}$	PV-generated energy forecast	Ws
E_{RES}	energy generated by renewable energy sources without curtailment	Ws
$E^{\text{curt}}_{\text{RES}}$	energy curtailed from RES-generation	Ws
$E^{\text{direct}}_{\text{RES}}$	RES-generated electricity directly consumed	Ws
$E^{\text{FC}}_{\text{RES}}$	RES-generated energy forecast	Ws
E^r	residual energy of BESS	Ws
E^r_k	residual virtual energy segment of BESS of application k	Ws
$\epsilon^{\text{man}}_{\text{aux}}$	carbon emissions of producing auxiliary components of BESS	kg CO_2eq
$\epsilon^{\text{man}}_{\text{batt}}$	carbon emissions of producing batteries	kg CO_2eq
$\epsilon^{\text{man}}_{\text{BESS}}$	carbon emissions of producing a BESS	kg CO_2eq
$\epsilon^{\text{man}}_{\text{housing}}$	carbon emissions of producing BESS housing	kg CO_2eq
$\epsilon^{\text{man}}_{\text{inv}}$	carbon emissions of producing inverters	kg CO_2eq
ϵ_{BESS}	impact of operating BESS on overall carbon emissions	kg CO_2eq
$\Delta\epsilon_{\text{BESS}}$	reduction of carbon emissions with a BESS replacing a diesel generator	kg CO_2eq
ϵ_{DG}	carbon emissions caused by diesel generator's fuel consumption	kg CO_2eq
ϵ_{feedin}	carbon emissions of the electricity feed-in to the grid	kg CO_2eq
$\epsilon^{\text{purch}}_{\text{grid}}$	carbon emissions of the grid purchased electricity	kg CO_2eq
ϵ_{home}	carbon emissions of a PV-home without BESS	kg CO_2eq
$\epsilon_{\text{home,BESS}}$	carbon emissions of a PV-home with BESS	kg CO_2eq
ϵ_{Hybrid}	carbon emissions of hybrid island grid	kg CO_2eq
$\epsilon_{\text{HybridBESS}}$	carbon emissions of hybrid island grid with BESS	kg CO_2eq
ϵ_{load}	carbon emissions of the electricity consumption	kg CO_2eq
$\epsilon_{\text{PS,BESS}}$	carbon emissions of consumer with peak-shaving by a BESS	kg CO_2eq
$\epsilon_{\text{PS,DG}}$	carbon emissions of consumer with peak-shaving by a diesel generator	kg CO_2eq
$\epsilon^{\text{direct}}_{\text{PV}}$	carbon emissions of the directly consumed PV-generation	kg CO_2eq
η_{batt}	battery one-way conversion efficiency	pu
η_{BESS}	BESS round-trip efficiency including standby losses	pu
η_{DG}	diesel generator efficiency/fuel consumption rate	Ws per liter
$\bar{\eta}_{\text{DG}}$	average diesel generator efficiency/fuel consumption rate	Ws per liter
η_{inv}	inverter conversion efficiency	pu
$\gamma_{1,\text{FC}}$	skewness of forecast error	pu
$\gamma_{2,\text{FC}}$	kurtosis of forecast error	pu
I_{batt}	battery current	A
$I^{\text{max,chg}}_{\text{batt}}$	battery maximum absolute charge current	A

$I_{\text{batt}}^{\text{max,dchg}}$	battery maximum absolute discharge current	A
J	objective function	-
$J(x)$	fitness of solution x with regard to objective J	-
k	optimization iteration or application index	-
k_{max}	maximum number of optimization iterations	-
$m_{\text{container}}$	mass of a container for the housing of a BESS	kg
μ_{CS}	mean value for cuckoo-search	pu
μ_{FC}	mean value of forecast error normalized to nominal power of generator	pu
N	population size of cuckoo-search	-
n_{EOL}	cycle stability	-
p	normalized power	pu
P_{batt}	battery output power (positive charging, negative discharging)	W
$P_{\text{batt}}^{\text{nom}}$	battery nominal power	W
P_{BESS}	BESS output power (positive charging, negative discharging)	W
$P_{\text{BESS}}^{\text{adj}}$	output power adjusted by simulation model	W
$P_{\text{BESS}}^{\text{chg,max}}$	BESS absolute charging limit	W
$P_{\text{BESS}}^{\text{dchg,max}}$	BESS absolute discharging limit	W
$P_{\text{BESS}}^{\text{nom}}$	nominal/rated power of BESS	W
$P_{\text{BESS}}^{\text{ref}}$	reference power/power setpoint for BESS	W
P_{DG}	diesel generator output power	W
$P_{\text{DG}}^{\text{min}}$	diesel generator minimum output power	W
$P_{\text{DG}}^{\text{nom}}$	diesel generator rated power	W
$P_{\text{DG}}^{\text{ref}}$	diesel generator reference power/power setpoint	W
P_{grid}	electricity grid supply	W
$\hat{P}_{\text{grid}}$	peak grid power	W
$\Delta\hat{P}_{\text{grid}}$	peak grid load reduction	W
$P_{\text{inv}}^{\text{DC}}$	inverter power at DC side	W
$P_{\text{inv}}^{\text{nom}}$	nominal/rated power of inverter	W
$\tilde{P}_k$	power assigned to application k	W
P_k^{P}	priority power of application k	W
P_k^{ref}	reference power/power setpoint of application k	W
P_{load}	consumer load	W
$\hat{P}_{\text{load}}$	peak load	W
P_{net}	net/residual load	W
$\hat{P}_{\text{net}}$	net load generation peak	W
P_{PV}	PV-generation without curtailment at AC-side	W
$P_{\text{PV}}^{\text{curt}}$	PV-generation curtailed AC-power	W
$P_{\text{PV}}^{\text{lim,curt}}$	curtailment limit for PV-unit	W
$P_{\text{PV}}^{\text{nom}}$	PV-unit peak power/nominal power	W
$P_{\text{PV}}^{\text{out}}$	PV-generator AC output power after curtailment	W
$\Delta\hat{P}_{\text{red}}$	peak feed-in reduction	W
P^{rem}	remaining power capability during power assignment	W
$P^{\text{rem}*}$	new remaining power capability during power assignment step	W
P_{th}	threshold power	W
P_{wind}	wind generation without curtailment	W

$Q_{\text{batt}}^{\text{in}}$	battery stored charge	As
$Q_{\text{batt}}^{\text{out}}$	battery outstored charge	As
$r_{\|1\|}$	random number between 0 and 1 with uniform distribution	-
r_{annuity}	annuity factor	-
r_{aux}	auxiliary components' share of production emissions of a BESS	pu
r_{elitist}	probability of solution to mutate in an elitist way	pu
r_{fuel}	diesel generator gravimetric generation rate	Ws per gram
r_{i}	interest rate	pu per year
r_{mut}	mutation probability of solution	pu
r_{SC}	self-consumption rate	pu
r_{SD}	self-discharge rate	s^{-1}
r_{SS}	self-sufficiency rate	pu
$\rho_{\text{batt}}^{\text{man}}$	energy capacitiy specific emission factor for producing batteries	kg CO_2eq per kWh
$\rho_{\text{container}}^{\text{man}}$	gravimetric emission factor for producing standard containers	kg CO_2eq per kg
$\rho_{\text{inv}}^{\text{man}}$	rated power specific emission factor for producing inverters	kg CO_2eq per kW
ρ_{coal}	emission factor of coal-based electricity generation	kg CO_2eq per kWh
ρ_{DG}	emission factor of diesel	kg CO_2eq per liter
ρ_{grid}	emission factor of average electricity generation of power system	kg CO_2eq per kWh
ρ_{PV}	emission factor of PV-generation with production emissions converted to life-cycle electricity generation	kg CO_2eq per kWh
ρ_{RES}	emission factor of RES-generation with production emissions converted to life-cycle electricity generation	kg CO_2eq per kWh
R_i	battery inner resistance	Ω
R_k	rank of application k	-
σ_{CS}	standard deviation for cuckoo-search	pu
σ_{FC}	standard deviation of forecast error normalized to the nominal power of the generator	pu
SOC	state-of-charge	pu
SOC_{max}	upper SOC-limit	pu
SOC_{min}	lower SOC-limit	pu
t	time	s
T	defined time period	s
τ_{energy}	energy utilization rate	pu
τ_{time}	time utilization rate	pu
$t_{\text{BESS}}^{\text{idle}}$	BESS idle-time	s
$t_{\text{BESS}}^{\text{run}}$	BESS runtime	s
Δt	sample time	s
T_{dep}	depreciation period	years
$t_{\text{DG}}^{\text{idle}}$	diesel generator current idle-time	s
$t_{\text{DG}}^{\text{mustoff}}$	diesel generator minimum idle-time	s
$t_{\text{DG}}^{\text{run}}$	diesel generator current runtime	s
$t_{\text{DG}}^{\text{mustrun}}$	diesel generator minimum runtime	s
t_{total}	total time (i.e. current simulation time or current life time)	s
θ	random value generated with Gaussian distribution with standard deviation σ_{CS} and mean value μ_{CS}	-

U_{batt}	battery terminal voltage	V
$U_{\text{batt}}^{\text{max}}$	maximum battery charge voltage	V
$U_{\text{batt}}^{\text{min}}$	minimum battery discharge voltage	V
$U_{\text{batt}}^{\text{nom}}$	battery nominal voltage	V
U_{OCV}	battery open-circuit-voltage	V
V_{DG}	diesel volume consumed by diesel generator	liter
w	energy density	J per m^3
x	optimization solution	-
x^*	Pareto optimal solution of population	-
x_{gen}^k	generated solution of iteration k	-
x_{pop}^k	solution of population of iteration k	-
$x_{\text{r1}} \dots x_{\text{rn}}$	randomly chosen solution of population	-

Part I

Introduction and Fundamentals

1 Introduction

1.1 Energy Storage for Low-Carbon Power Systems

Global warming is observed in the last 50 years with the fastest increase rates of the average global temperature in the recorded history [1]. Greenhouse gases (GHG) have been identified as main cause of the anthropogenic climate change [2]. Figure 1.1 illustrates the correlation of atmospheric carbon dioxide concentration and the global annual average temperature [3]. Climate change is projected to have a rogue impact on ecological systems, biodiversity, and mankind [4–6]. This leads to global effort and inter-governmental collaboration to slow down global warming. Agreements, such as the *Kyoto Protocol* [7] and the *Paris Agreement* [8] are compound to combat climate change, by mitigating the carbon emissions, among other measures.

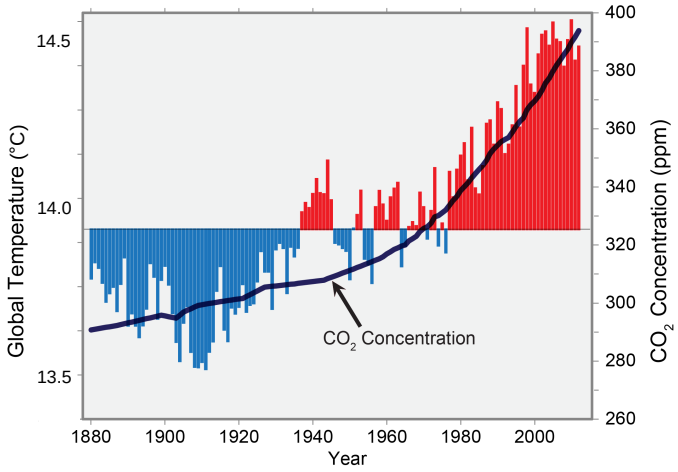

Figure 1.1: Global annual average temperature has increased by more than 0.8°C since 1880. Red bars show temperatures above the long-term average, and blue bars indicate temperatures below the long-term average. The black line shows atmospheric carbon dioxide (CO2) concentration in parts per million (ppm). Despite year-to-year fluctuations in temperature due to natural processes, such as the effects of El Niños, La Niñas, and volcanic eruptions, the long-term global warming trend is clearly visible. [3]

25% of human-induced emissions are attributed to the electricity sector [9] and power systems worldwide are shifting from fossil-fuel generation towards low-carbon technologies [10]. Germany is taking the lead with its *Energiewende*, the popular term for the shifting of the power system towards renewable energy source (RES). The German federal government is committed to achieve a share of 80% RES in the total electricity production by the year 2050 [11]. The share of RES in the electricity production increased from 7% to 30.1% in the years 2000 to 2016 [12]. At the same time, the German government pledged to issue the nuclear power phase-out, induced by the *Fukushima Daiichi* nuclear disaster in 2011 in Japan [13; 14]. This narrows the options of low-carbon electricity generation down to RES.

Growing shares of RES increase the intermittency and uncertainty. This introduces a number of challenges for the electrical power system, having increased the demand for flexibility in power grids in recent years [15]. With 27% of all RES capacity installed in low voltage grids in 2015 [16], the integration of high shares of RES introduces problems for the low voltage-distribution grid. 98% of all PV-units in Germany are connected to the low voltage-distribution networks [17]. Voltage deviations caused by RES are one of the main issues for distribution system operators [18].

Energy storage systems (ESS) are acknowledged as a key component to facilitating the transition of power systems towards low-carbon technology [19]. Pumped hydro storage systems have been part of the power system since the early 20^{th} century and represent the dominant share of all grid-connected ESS [20; 21]. With arising challenges caused by RES and the higher flexibility of battery energy storage system (BESS), new applications for ESS of different qualities and sizes emerge [22–24]. The amount of projects for grid-scale BESS installations is growing steadily [25]. BESS' capability to relieve the grid of RES-induced problems have already been investigated [26; 27]. BESS are often discussed to mitigate challenges like over-voltage or overloading of grid equipment, that are associated with high shares of RES (Fig. 2.1).

High battery prices, however, prevent a widespread adoption of BESS [22; 28; 29]. The technical feasibility of BESS to alleviate RES-induced grid problems has been shown, however, there are currently no financial incentives for BESS in Germany for grid-supporting operation [30]. Further issues for beneficial operations of BESS are the market mechanisms that are not necessarily aligned with the technically optimal operation of the BESS [31].

1.2 Scope of the Thesis

Objectives

BESS are widely claimed as a key component for the decarbonization of the power system. The benefits of some applications for the general public is, however, questionable [32]. This raises the question of other non-obvious disadvantages of operating BESS. Besides cost savings, the deployment of BESS with regard to GHG-emissions as not sufficiently clarified.

The benefit of BESS for its application and consequently the impact on the power system is determined by its operation strategy [33; 34]. Even though the battery prices are rapidly falling [35], the BESS' financial return requires further improvement. Operating BESS for single, dedicated applications leads to low utilization [36], resulting in insufficient revenue that prevents widespread adoption and integration into the electricity grid. Multi-use is suggested in the literature to improve the economics of BESS [37] but there is a lack of appropriate operation methods [38]. Based on the status quo, following research objectives for this Ph.D. thesis are therefore defined:

1. Development of a modeling framework for accurate simulations of BESS and the respective application.
2. Derivation of assessment methods for a true valuation of BESS.
3. An examination of the alignment of climate benefits and economic incentives for the BESS operation.
4. Development of control methods to improve the BESS performance.

Outline of the Thesis

The thesis is composed of four parts: Part I: Introduction and Fundamentals, Part II: Evaluating Stationary Battery Storage Systems, Part III: Improving Battery Storage Operation, and Part IV: Conclusion and Outlook.

Figure 1.2 illustrates the structure of the thesis. Part I provides the fundamentals for the thesis. Part II derives evaluation methods for the operation of BESS. These evaluation methods can be understood as objectives and set the goals for favorable operation. Part III is concerned with the approach of how to reach any desired objective (preferably the goals suggested in Part II). A method to incorporate multiple stakeholders is presented, in consideration of unbundled electricity markets, common in the European Union. Part IV concludes the thesis and gives an outlook, suggesting options for future research.

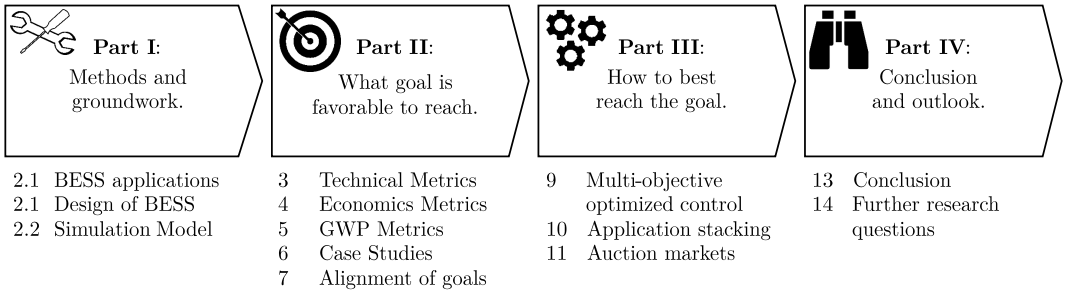

Figure 1.2: Graphical outline of thesis.

The remainder of Part I provides the fundamentals for the thesis. An overview of stationary BESS is given in Chapter 2. Three applications are described further analyzed in Section 2.1: PV-home storage, peak-shaving, and hybrid renewable-diesel island grids. The prototype *Energy Neighbor* is presented as the basis for stationary BESS. The simulation framework *SimSES* used throughout the thesis is presented in Section 2.2.

Part II covers the evaluation of operating BESS. Chapter 3 describes technical evaluation metrics and presents literature reviews on the economics and the carbon emissions of BESS. The business model of BESS for the three applications and a discussion of economic metrics are presented in Chapter 4. Chapter 5 gives an approximation of the GHG emitted by the production of stationary BESS and derives the influence of operating BESS in the three applications on the carbon emissions. Case studies on the three applications apply the derived evaluation approaches in Chapter 6. The Part concludes with a discussion on the evaluation of BESS in Chapter 7.

Part III is concerned with improving the operation of BESS. It starts with Chapter 8 that outlines the motivation, classifies approaches for the operation strategies, and conducts a literature review. Chapter 9 presents an algorithm, developed to operate optimally towards any desired (multi-) objective, features real-time capabilities, and exhibits robustness against prediction uncertainties. Another method to operate BESS for multiple stakeholders is presented in Chapter 10. Chapter 11 presents a concept for transferring both operation methods to business logic and allow financial accounting of the BESS operation to several stakeholders. The findings of this Part are concluded in Chapter 12.

Part IV closes the thesis. Chapter 13 concludes the thesis and an outlook is given in Chapter 14.

2 Fundamentals

2.1 Stationary Battery Storage Systems

2.1.1 Storage Applications

This section gives a short overview of the energy storage applications covered in this thesis. The PV-home storage, peak-shaving, and hybrid renewable-diesel island grid are explained. The PV-home storage is an example for small-scale applications. Peak-shaving represents an application for BESS of commercial scale. The hybrid renewable-diesel island grid is an application for BESS of utility scale.

2.1.1.1 PV-Home Storage

PV-home storage is one of two major applications for BESS deployment in Germany [39] with continuously increasing installation [40]. They are installed at households with a rooftop PV-unit and aim at increasing the household's self-consumption, by storing surplus PV-power, instead of feeding it into the grid and later consuming it at low generation periods.

The purpose of increasing a household's self-consumption is to reduce the owner's electricity bill [41; 42]. The case covered in this thesis is based on the German case, where PV-units below 10 kW are legally remunerated with a fixed feed-in rate for 20 years [43; 44]. The financial benefits for the BESS owner stem from the price spread between the electricity price and the feed-in tariff for PV-generated electricity. Besides increasing the self-consumption, surveys show that other common motivations for purchasing a home BESS are to hedge against rising electricity prices, a desire for increased autonomy against utility companies, and to support the integration of RES [40].

A number of publications have assessed the economic impact of purchasing solar home BESS [28; 29; 45–48]. They generally conclude that PV-home storage systems are economically favorable only in few cases. Considering battery prices of 2015, the savings of such systems under German market conditions commonly undercut the battery investment cost within the projected system lifetime [28; 47].

Undesired voltage deviations that compromise grid operation are caused by feed-in peaks of the PV-unit, especially in low voltage distribution grids [18]. The issue is illustrated in Figure 2.1. The blue curve depicts the voltage level of the line, normalized to the nominal voltage. A sufficiently high and simultaneous generation of PV-power raises the voltage U at the opposite end from the transformer above legal and safety limits. Another possible issue is the violation of the grid equipment's power capacity. The orange curve in the Figure shows the apparent power S that exceeds the line's power capacity at its transformer end.

Voltage control is either conducted by limiting the feed-in peak of RES [26; 27; 34; 49–54], reactive power provision [55; 56], or by combining both methods [18; 57–62]. Reducing the peak power of the feed-in power into the grid is favorable for the distribution grid operator [51], but BESS owners are

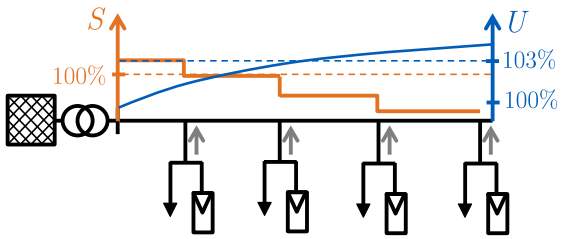

Figure 2.1: Illustration of normalized apparent power flow S and voltage U along low-voltage grid line with several rooftop solar panels. The orange curve shows the apparent power. The blue curve depicts the voltage along the lines. (Graphic by Lorenz Viernstein; published in [31].)

not directly rewarded financially. Segundo Sevilla *et al.* suggest that curtailment is an economically attractive option for the power system to enable high PV-penetration in distribution grids [63]. Reinforcement of the grid infrastructure is an alternative option, however, associated with high costs that could be avoided by integrating BESS [64]. Future incentives for minimizing the peak feed-in are, therefore, plausible and the peak feed-in reduction is assessed in this thesis.

2.1.1.2 Peak-Shaving

Peak-shaving is an application that is relevant for commercial electricity consumers with an electricity contract that includes peak power charges. These charges are determined by the load peak over a defined period of time, usually a year. Consumers with a load of more than 100 MWh per year are subject to peak power charges in Germany. The peak is determined as mean value over a time period of 15 minutes. The highest peak of the present year defines the peak power charge that is recalculated if the actual peak load does not match the anticipated value. [65–69]

BESS deployed for peak-shaving supply the load that exceeds the desired maximum peak load. This way the peak grid power is limited to that maximum value and the BESS avoids higher peak power charges. Alternative options for peak-shaving are diesel generators, that provide the load power exceeding the peak load threshold, or demand-side management. Demand side management is the scheduling of controllable loads to avoid large load peaks. It requires coordination of numerous loads [70].

The economic benefits of peak-shaving strongly depend on the load profile of the consumer and the contract with the grid operator. Thus each individual case needs to be studied. The case regarded in this thesis is based on the German scenario and is valid for annual load energy to peak load ratios higher than 2500 h. Besides reducing the electricity bill of the consumer, the peak power charges reflect the financial and operational burden for the grid operator. The required grid capacity is determined by the occurring power peaks and if the power peaks exceed the grid capacity, expensive grid-reinforcement is required. Peak-shaving reduces the power peak in the grid and improves the utilization of the electricity grid [71].

2.1.1.3 Hybrid Renewable-Diesel Island Grid

An island grid is an isolated electricity grid without connection to another (larger) electricity grid [72]. Island grids exist on, but are not limited to geographical islands [73]. Electricity grids in remote areas, for example, are isolated island grids, if the connection to the larger grid is technically, or economically not feasible [74].

The integration of RES, such as PV and wind turbines, in an island grid, requires controllable dispatch units that are capable of providing energy for the load in time periods without RES generation. BESS are capable of fulfilling this task [75], yet conventional generators are usually part of hybrid renewable-diesel islands because a 100% share of RES would require very large amounts of BESS [76].

The case regarded in this thesis is a hybrid renewable-diesel island grid that is composed of consumers, PV-units, wind turbines, a diesel generator, and a BESS. The RES provide the load if they can. Any surplus energy is stored in the BESS for later use, in times of insufficient RES generation. The diesel generator supplies the load if neither RES nor BESS can provide the load.

The analysis of the island grid in this thesis is limited to power- and energy flows. Stability issues, such as frequency, and spinning reserve, and line losses, are neglected. Another simplification is to treat the grid participants as single entities, instead of distributed units.

2.1.2 Model Battery Storage System: The Energy Neighbor

The *Energy Neighbor* is a stationary BESS that has been developed in the research project *EEBatt*. It is the basis for the simulation model and used for the estimation of the global warming potential (GWP) of producing BESS in this thesis. The *Energy Neighbor* has been developed by the Technical University of Munich (TUM), in cooperation with the project partners VARTA Storage GmbH and ZAE Bayern. The BESS is tested in cooperation with the local grid operator and utility company of the Kraftwerke Haag Gruppe. The field test has been executed in the Bavarian village Moosham in Oberbayern, Germany. The prototype BESS *Energy Neighbor* (Figure 2.2) is installed in a rural low voltage distribution grid that experiences challenges to date caused by a large share of RES. A large portion of the system description in this Section has been published before [77].

Figure 2.2: Photography of the prototype battery storage system *Energy Neighbor*.

2.1.2.1 Similar Demonstration Systems

The amount of projects for grid-scale BESS installations is continuously emerging [25], however, only little information about best practices and experiences in the setup of BESS has been published.

Thien *et al.* describe their lessons learned in planning and operating a 5 MW BESS within the research project M5Bat [78]. Koller *et al.* assess the topology and experience with a 1 MW and 250 kWh demonstration BESS installed 2012 in Zurich, Switzerland [79]. The *M5Bat* BESS serves frequency response services and participates in energy wholesale markets for arbitrage. The Zurich BESS is

installed within the urban grid and provides frequency reserve, applies peak-shaving, and is capable of work in an island operation mode.

2.1.2.2 Goal and Demonstration-Grid

The field test grid in Moosham consists of about 50 households and a total installed PV-capacity of about 300 kWp. The goal of the system is to enhance the local grid's self-consumption of its PV-generated electricity, relieve the grid, and provide secondary control reserve. The self-consumption is increased by storing the generated surplus energy and supplying the load at low generation periods.

The grid experiences over-voltage issues during peak PV-feed-in periods. The occurring voltage-rise may exceed legal limits (see Figure 2.1). Figure 2.3 shows the simulation results of the grid in Moosham. The top figure is the worst-case of the grid without the *Energy Neighbor*, the bottom figure shows the alleviating effect of connecting 2 stub lines to a ring line and the BESS. A rising number of rural, low voltage distribution grids face this problem [80]. The operation of the *Energy Neighbor* aims at relieving this issue, by charging during the peak production periods, hence reducing the current that causes the undesired voltage rise.

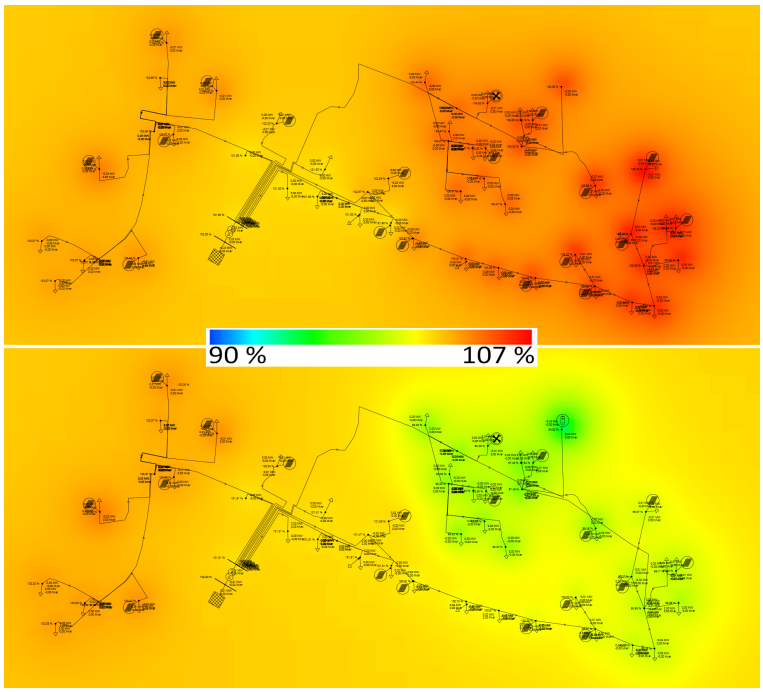

Figure 2.3: Visualization of the simulated grid in Moosham. The colors illustrate the normalized voltage level. The top figure is the worst-case of the grid without the *Energy Neighbor*, the bottom figure shows the alleviating effect of connecting 2 stub lines to a ring line and the BESS. [64]

The *Energy Neighbor* is intended to simultaneously serve another application to demonstrate its ability to use multiple sources of revenue. Such multi-use scenarios have been proposed for the increased profitability of BESS [37]. Dedicated shares of the BESS-capacity provide secondary control reserve because the idle and active time periods complement the primary application well [81]. The academic prototype system is, however, not viable because of effective regulations: Increasing the self-consumption of the chosen village-grid results in twofold taxation of the electricity produced by the RES. This prevents possible business cases under current legislation in Germany.

Challenges of Developing Stationary Battery Storage Systems

BESS are subject to a variety of interdependent effects that need to be taken into account. Best practices for the design of BESS are yet to be determined.

(Electro-) Chemical side-reactions within the battery-cells cause aging, i.e. battery capacity degradation and increasing inner resistance. Both impair the overall system's performance with regard to energy capacity and efficiency. The aging of battery-cells is very sensitive towards non-optimal handling, e.g. certain temperatures, charging- or discharging-currents, and average state-of-charge (SOC). The battery-cells compose about 50% of the overall BESS cost, requiring careful system design even more.

2.1.2.3 System Overview

The *Energy Neighbor* is situated in a single 20-foot ISO standard container for both power electronics and batteries, to allow straightforward transport and installation. The current experimental configuration of 8 independent battery-racks weighs about 7000 kg. The nominal energy capacity of the *Energy Neighbor* is 192 kWh and the rated power is 248 kW.

Each battery rack is connected to the electricity grid via one-stage inverter with rated powers of 16 kW and 36 kW. A battery-rack consists of 13 battery-modules, that are connected in series. The battery-modules each comprise of 192 battery cells with 16 cells connected in series and 12 in parallel. Table 2.1 gives an overview on the key-properties of the system.

Table 2.1: Datasheet of the *Energy Neighbor*.

Parameter	Value
Energy capacity	192 kWh (8x24 kWh batt.-racks)
Power capability	248 kW (2x16 kW, 6x36 kW)
Housing	20' ISO standard container
Total weight	$\sim$ 7000 kg
Batt.-type	LFP:C, cylindrical 26650
Batt.-module	16s12p battery cells
Batt.-rack	13s1p battery modules
Converter type	One-stage inverter per rack
Grid level	400 V low voltage
Applications	Increase of self-consumption
	Grid-relief
	Secondary control reserve

The partition of the BESS into several independent battery-racks allows modular scaling of the total number of battery-racks and consequently the energy capacity and power capability. The BESS can therefore easily be adapted to the application and scenario it is intended for. The module voltage is below 60 V, thus no additional training is legally required, for assembly and handling of the modules [82].

The *Energy Neighbor* is connected to the low voltage distribution grid and thereby allows deployment for a large number of applications. BESS in low voltage grids can serve more applications than BESS placed in higher voltage grids [36] and still address issues in higher voltage grids [64].

2.1.2.4 Battery Technology

The choice of the battery technology influences a variety of factors that determine the system performance and may change the constraints and issues for design considerations for the auxiliary components fundamentally. Lithium-ion technology is currently the most widespread battery type in the major fields: automotive, stationary application, and consumer electronics. The main reason to use lithium-ion batteries is the combination of long lifespan, high power and energy density, and technical maturity. Even within lithium-ion technology, the choice of the different cell-chemistries for the anode and cathode of the battery cells, significantly changes the system properties with regards to safety, lifetime, energy density, ease of state-estimation, and more.

The *Energy Neighbor* consists of lithium iron phosphate ($LiFePO_4$) (LFP) batteries with a graphite (C) anode. The battery-cells are of cylindrical 26650 format and they are connected with a 16s12p configuration to form modules. Even though LFP:C exhibits lower energy density than other lithium-ion chemistries, other beneficial properties outweigh the disadvantage. The energy density is not as important for stationary applications [21], in contrast to mobile applications, where size and weight are crucial. LFP used as cathode material, tends to exhibit much larger cycle-stability than lithium nickel cobalt aluminium oxide (NCA) and lithium nickel manganese cobalt oxide (NMC) [83], that dominate the automotive sector.

Estimating the states of the battery, i.e. its state-of-charge and momentary power capability is crucial to exploit the full potential of the system. The chosen LFP:C-chemistry exhibits a very flat open circuit voltage (OCV), over a wide range of the SOC (Figure 2.4). The battery voltage is more sensitive towards other factors like cell-temperature, current, and relaxation state. Consequently, the information about the SOC that can be concluded from the battery voltage is imperfect.

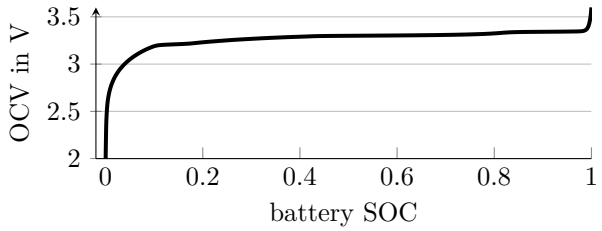

Figure 2.4: Open-circuit voltage of chosen lithium-iron-phosphate battery at 25 °C. Mean value of voltage during charging and discharging is shown.

2.1.2.5 System Management

The BESS needs to be managed at different component levels (Figure 2.5). The battery management system (BMS) supervises the battery states, to keep the operation of the BESS within constraints. This avoids system failure and accelerated aging. The BMS is designed in a master-slave concept. The BMS-slaves monitor the battery modules and send information to the BMS-master, that supervises the battery rack. It communicates with the energy management system (EMS) and approves the charging and discharging operations.

Decisions about the charging and discharging of BESS are made in the EMS. The distinction of BMS and EMS allows independent development of both components, reducing the complexity of coordinating the separate development teams.

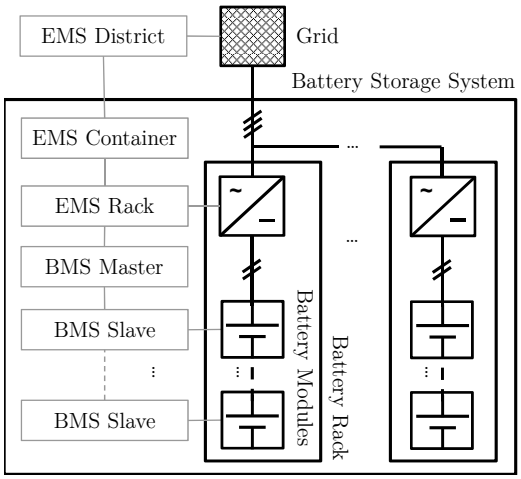

Figure 2.5: Illustration of battery to grid connection with dedicated inverters and hierarchy of management system.

Battery Management System

The battery management system (BMS) estimates the battery SOC, executes the balancing of the serially connected battery-cell compounds, and communicates the relevant information to higher system management entities. State-estimation of batteries is a complicated task and subject to inaccuracies because of the high nonlinearity of battery cells. The relatively low sensitivity of the OCV towards the battery SOC compared with its higher sensitivity towards other factors considerably enhances the complexity of estimating the battery's SOC.

Batteries in mobile applications are usually fully charged regularly, reaching an accurately defined full-state that can be used as a reference to readjust the estimated state. Applications for stationary BESS experience the problem of drifting SOC-estimation because the batteries are not necessarily reaching certain states routinely. This is especially an issue for applications with a medium average SOC and relatively small SOC-swings, such as primary control reserve for frequency control. The estimation error is accumulating over time, resulting in necessary re-calibration cycles to re-adjust the SOC estimation. To ensure comparable condition, these re-calibration cycles may require a long time and inhibit standard operation. In addition, energy drain, caused by the batteries' self-discharge, the idle consumption of power electronic devices, and (dissipative) balancing, interferes with the state-estimation.

Varying temperatures and manufacturing differences of the battery-cells result in an increasing spread of their SOC. Balancing of the battery-rack is necessary, to keep the SOC gaps of the serially connected batteries to a minimum and enable exhaustive utilization of their capacities. The *Energy Neighbor* is equipped with dissipative balancing because of the method's simplicity and small investment cost. The balancing resistance is $33\,\Omega$, resulting in a discharge current of $97\,\mathrm{mA}$ for a nominal voltage of $3.2\,\mathrm{V}$ for each parallel battery-cell compound. This is equivalent to a C-rate of 0.27% per hour. The chosen balancing method is the commercial standard, however, causes inefficiencies because energy is dissipated into heat and cannot be utilized. The activation of the balancing in the *Energy Neighbor* is based on the battery-cell voltage. Temperature deviations cause the terminal voltage of the battery cells to diverge. The OCV is more sensitive to the temperature than to the SOC. The balancing does not actually result in converging SOC of the parallel battery compounds if the temperature deviation

within the battery rack is too severe.

Energy Management System

The energy management system (EMS) is divided into internal and external systems. The external EMS district is responsible for the BESS operation strategy and aims at maximizing the benefit of BESS operation. The internal EMS container attempts to maximize the system efficiency by distributing the power output among the battery racks, considering the efficiency of each component. The EMS rack is the communication interface for the higher EMS levels and the power electronics. It also controls the stand-by consumption of the BESS components.

2.1.2.6 Power Electronics

The battery-racks are individually interfaced to the low voltage distribution grid with direct one-stage inverters. One-stage inverters are more cost effective than their two-stage counterparts that contain an additional DC/DC converter. Omitting the additional conversion step also leads to higher efficiency, but requires higher DC-voltage as input. A battery-rack voltage of at least $\sqrt{2} \cdot 400\,\mathrm{V} = 565\,\mathrm{V}$ is required, to allow direct connection of the AC-side of the inverter to the 400 V low voltage grid.

The trade-offs for the efficiency increase and component-cost savings are stricter safety requirements for the operation and development of the BESS. The omitted galvanic insulation of the topology requires the installation of additional residual-current measurement units, to detect electric faults. The high voltage-levels raise the legal requirements for the maintenance and development personnel. Additional training and qualification, as well as expensive testing and maintenance equipment and facilities, are compulsory [82]. These cost drivers need to be carefully assessed, to justify the improved BESS efficiency.

Dedicated inverters are used for each individual battery-rack. This allows higher efficiency at partial loadings of the BESS. Figure 2.6 illustrates the efficiency curve of a single, central inverter in comparison with an aggregated efficiency curve of two dedicated, individual inverters over the normalized output power of the power electronics setup. Subsequent activation of the inverters avoids operating any of them in partial load, where the efficiency drops significantly. The resulting efficiency curve is calculated by compressing the original efficiency curve to half of the nominal power. The remaining curve above 0.5 of the normalized output power is calculated as the total efficiency of an inverter at nominal output power and a second identical inverter with the respective power output. The efficiency at 0.8 is for example calculated with the in- and output power of the inverter at 1.0 of the nominal output power and at 0.6. The resulting efficiency is calculated based on the input and output power of both inverters.

Using independent inverters for shares of the BESS also enhances the system reliability against failures of the inverter. The malfunction of one battery-rack can be compensated by the remaining functional racks.

An important issue is the idle-consumption of the inverters [84]. Minimizing the idle-consumption leads to an increase of the system efficiency. More importantly, the output on the AC-side is measured to deliver specific power values for the application. The idle-consumption of the inverter is supplied by the batteries, which may lead to an unintentional deep-discharge and consequently to damage of the battery-rack, which must be avoided.

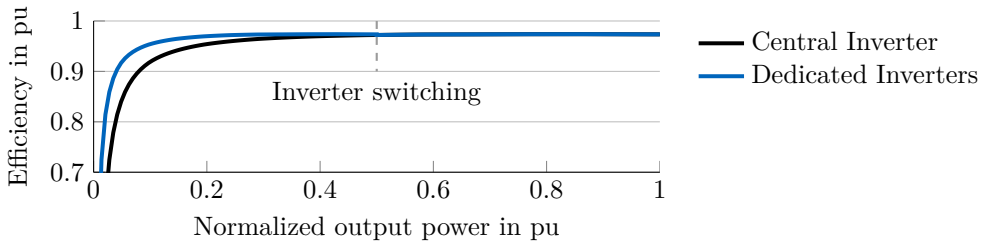

Figure 2.6: Inverter efficiency of a single central inverter compared with the achievable efficiency with two dedicated, individual inverters for each battery-rack. The *Energy Neighbor* contains eight individual inverters.

2.1.2.7 Thermal Management

Battery aging is highly sensitive to the temperature and has a significant influence on the economic viability of BESS [28]. Precise temperature control, however, requires careful engineering and may result in additional electricity consumption for air conditioning. The conflicting goals of reduced aging and achieving high efficiency need to be balanced.

The thermal management concept of the *Energy Neighbor* comprises of a multi-zone approach (Figure 2.7). While heat dissipating and temperature resistant inverters are placed in the *Hot-Zone*, the components that benefit from moderate temperatures are located in the *Cool-Zone*.

The *Hot-Zone* has a wide temperature range, requiring little cooling and consequently little to no energy expense. This is where heat-dissipating components, such as inverters, and components with broad temperature tolerance are located. The *Cool-Zone* contains temperature sensitive components (i.e. batteries) and is kept at a more restricted temperature range. The thermal absorption in this zone is very small because of the spatial segregation of both thermal zones. Unnecessary cooling of heat-dissipating components and undesired heating of sensitive components are minimized this way.

In addition to the container internal multi-zone concept, extra vents allow for switching between fresh-air and circulating air supply. Their proper control allows to further increase the efficiency.

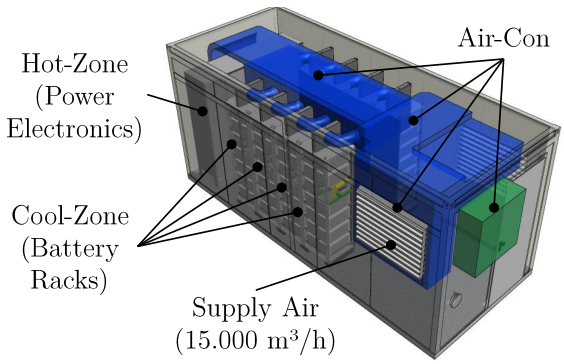

Figure 2.7: Thermal management with multi-zone concept. Main heat producers and low sensitivity components are placed in the *Hot-Zone*. The *Cool-Zone*, where the batteries are located, is kept at favorable temperatures.

The thermal management within the racks is also designed to avoid varying aging progress of the batteries within a battery-rack. An air-channel is located at the center of a battery-rack from the top to the bottom. At each row of battery modules vents on the side of the air-channel allow air to flow

through the modules for temperature regulation. The vents' width increases from top to bottom to avoid the air-flow to drop along the vertical axis, This way, similar cooling of the battery-modules is achieved.

The battery-cells in the modules are geometrically arranged to cause obstructed perfusion of the air-flow. Instead of a chessboard pattern arrangement, the battery-cells are positioned in a shifted manner, to maximize the convective heat transfer through air-turbulences.

2.1.2.8 Summary

The battery storage container prototype system presented is meant to alleviate the stress on the grid imposed by a relatively large amount of RES. Features and drawbacks of the system-design choices are analyzed and discussed in detail.

Auxiliary components are necessary to enable the operation of the batteries, but the choice of the battery technology substantially impacts all other components of a BESS. The decision to use lithium iron phosphate batteries is based on the technology's favorable safety and aging properties, as well as the dispensable role of energy density for stationary application. The associated issue of flat OCV significantly influences the accuracy and complexity of state-estimation and consequently, the effectiveness of the balancing method applied. The auxiliary components depend on the characteristics of the chosen battery technology and require adaption for each technology. Furthermore, a sophisticated thermal management concept has been implemented in the *Energy Neighbor*.

The grid connection topology determines the achievable conversion efficiency and at the same time the control complexity. Dedicated inverters for each battery-rack have been installed in the system, as these allow higher efficiency at partial output power. The chosen one-stage inverter reduce investment cost and enhance overall efficiency, however, require high battery voltages that are monitored by additional safety components.

The presented *Energy Neighbor*'s structure is not intended to be a best practice approach, but rather to illustrate and share the insights gained during the project *EEBatt*. The system is a prototype, offering the potential for further improvement.

2.2 Simulation Model: SimSES

2.2.1 Background

The simulation model *Simulation of Stationary Energy Storage (SimSES)* has been originally developed by Maik Naumann and the author of this thesis. The source-code is published as an open-source tool under the BSD 3-clause license [85]. The model's purpose is to simulate stationary ESS in their respective application. At the same time, the technical effects within the system, such as conversion losses or battery aging are considered.

The modeling framework is programmed in the commercial *MathWorks MATLAB®* software. The main benefit is the modular structure of the framework. It allows coupling of models from different developers and hereby promotes collaboration. The goal for the development of the tool is to enable rapid analysis of any issue that concerns the operation of stationary BESS. The states and variables

during the simulation are stored and saved. This allows detailed analyses after the simulation run. A re-programming of essential components is avoided by re-use of existing components allowing new researchers to focus on the area of interest. Another benefit of re-use is that the perpetual review and revision of the code improves it and reduces the probability of bugs.

SimSES utilizes the object-oriented programming paradigm that simplifies consistent data handling. It also enables the inheritance of classes. This way further developments of the basic model is immediately transferred to specialized models and all applications, without the need for manual incorporation of the new features into numerous model variants.

Both developers contributed equally to the tool. Maik Naumann focused on the aging model, the input-data handling, and the acquisition of input parameters. The author of this thesis was mainly responsible for the operation strategies, power electronics, and the battery model. The integration of all components and sub-models into a framework, plotting functions, and evaluation functions were equally developed. Both did support and assist each other in all areas of the development.

SimSES is further maintained and developed at the Institute for Electrical Energy Storage Technologies by younger Ph.D. students. Numerous publications, student, and Ph.D. theses have been generated based on the simulation framework. Together with internships and working students, they have contributed to the development of the simulation framework, in return.

2.2.2 Model Framework

The model simulates the BESS's charging and discharging behavior and its performance on the respective given applications. The simulation model includes load, generation units, and the BESS [86]. Conversion losses are considered for the battery inverter (2.1) and the battery (2.13). The BESS is connected to the low-voltage grid via inverter without an additional transformer. Stand-by consumption of inverter, thermal management, and auxiliary components are neglected in this thesis.

Measured profiles of solar generation P_{PV}, wind generation P_{wind}, and consumer load P_{load} at the AC-side are used. The power flows of the relevant components are computed (Figure 2.8): diesel generator (DG) output P_{DG}, the electricity grid supply P_{grid}, and BESS power P_{BESS} (positive sign for charging, negative sign for discharging), considering (power-dependent) one-way efficiencies of inverter η_{inv} and battery η_{batt}.

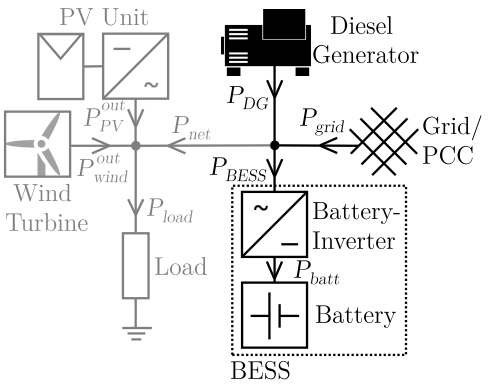

Figure 2.8: Overview of the simulated power flows in the model. Components implemented as fixed profiles at the AC-side are depicted in grey. The more elaborate models are shown in black.

The BESS provides the output power according to the reference power $P_{\text{BESS}}^{\text{ref}}$ (also power setpoint) while maintaining the allowed operating range, with regard to SOC (2.6), power (2.2), current (2.10), and battery voltage limits (2.11). The operating limits of the BESS are considered, regardless of the power requested by the controller. The output power is limited to the momentary power capability of the battery system. Hence, BESS specific constraints do not need to be further considered as constraints in the formulation of optimization problems.

The load and renewable generation (wind and solar) are implemented as fixed profiles originating from measurements. The power outputs of controllable units (i.e. BESS and DG) are determined during simulation time by the effective operation strategy.

The toolbox structure of the model allows switching of sub-models, such as power flow model and equivalent circuit model for the battery. Both are used for the simulation and described in Section 2.2.3.2. The model includes output power dependent conversion losses of inverters and battery cell efficiency.

2.2.3 System Model

2.2.3.1 Inverter Model

The inverter is implemented as an efficiency model with a power dependent efficiency curve η_{inv} (2.1). The function and the parameters are taken from Notton *et al.* [87] The inverter power may not exceed its nominal power (2.2).

$$\eta_{\text{inv}} = f\left(p = \frac{P_{\text{BESS}}}{P_{\text{inv}}^{\text{nom}}}\right) = \frac{p}{a \cdot p^2 + p + p_0} \tag{2.1}$$

$$|P_{\text{BESS}}| \leq P_{\text{inv}}^{\text{nom}} \tag{2.2}$$

The DC-power $P_{\text{inv}}^{\text{DC}}$ of the inverter is calculated based on the AC-power P_{BESS} and the respective efficiency η_{inv} (2.3). The power at the DC-side of the inverter is passed to the battery model as reference battery power to calculate the SOC change and to verify that the battery can provide the calculated power.

$$P_{\text{inv}}^{\text{DC}} = \begin{cases} \eta_{\text{inv}} \cdot P_{\text{BESS}} & \text{for } P_{\text{BESS}} > 0 \\ \frac{1}{\eta_{\text{inv}}} \cdot P_{\text{BESS}} & \text{for } P_{\text{BESS}} < 0 \end{cases} \tag{2.3}$$

The battery output power P_{batt} returned by the battery model is the effective power. If it is different from the calculated inverter DC-power, the inverter AC-power is adjusted accordingly. Two possible cases are considered: If the SOC-limit de-rates the battery power, the output is adjusted to the same ratio of the adjusted power and the initial DC-power of the inverter (2.4). In this case, the BESS operates at the working point, originally computed, until the limit is reached. At this point in time, the output is reduced to 0. The working point is therefore not adjusted with another efficiency value, but the adjusted output $P_{\text{BESS}}^{\text{adj}}$ is equivalent to the average of the power over time.

$$P_{\text{BESS}}^{\text{adj}} = P_{\text{BESS}} \cdot \frac{P_{\text{batt}}}{P_{\text{inv}}^{\text{DC}}} \tag{2.4}$$

If power or current limits de-rate the original DC-power, the valid AC-power $P_{\text{BESS}}^{\text{adj}}$ of the inverter is

adjusted with the respective efficiency for the DC-power determined by the battery. In this case, the calculated output power occurs over the entire sample time period.

$$P_{\text{BESS}}^{\text{adj}} = \begin{cases} \frac{1}{\eta_{\text{inv}}} \cdot P_{\text{batt}} & \text{for } P_{\text{BESS}} > 0 \\ \eta_{\text{inv}} \cdot P_{\text{batt}} & \text{for } P_{\text{BESS}} < 0 \end{cases} \tag{2.5}$$

Inverter Model Parameters

Two parameter sets are used for the inverter's power flow model. The first set is a power dependent efficiency curve that corresponds to the *Type 2* high-efficiency inverter described by Notton *et al.* [87]. The second set corresponds to the *Type 1* inverter described in the same publication. The parameters for the efficiency curve (2.1) are given in Table 2.2.

Table 2.2: Parameters of two inverter types for efficiency formula [87].

	a	p_0
Type 1	0.0437	0.0145
Type 2	0.0345	0.0072

Figure 2.9 depicts the efficiency curve of the two inverter types used. Efficiencies above 90% are achieved for normalized power outputs larger than 10%, while partial loads below 10% of the nominal inverter power result in significantly lower efficiencies.

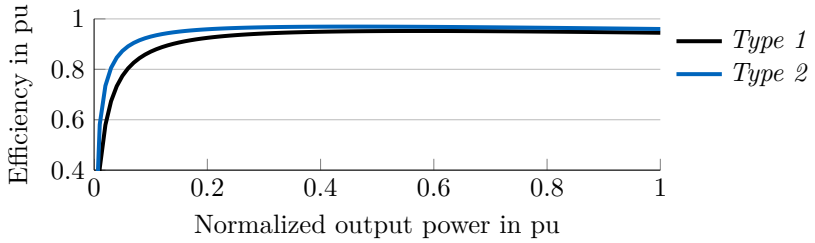

Figure 2.9: Efficiency curves of inverter model [87].

2.2.3.2 Battery Model

Electric Model

Two simulation models for the battery are used. The first model is an equivalent circuit model with a measured OCV and an inner resistance. The second model is a power flow model.

The battery models maintain the allowed operating range with regard to SOC (2.6), current (2.10), battery voltage limits (2.11), and power (2.12). The operating limits of the BESS are considered, regardless of the power requested by the controller. The output power is limited to the momentary power capability of the battery system. Hence, BESS specific constraints do not need to be further considered as constraints in the formulation of optimization problems.

$$\text{SOC}_{\text{min}} \leq \text{SOC} \leq \text{SOC}_{\text{max}} \tag{2.6}$$

The equivalent circuit model of the battery is directly coupled to the inverter model by its power value (2.7). The model uses the DC-power of the inverter as input and calculates whether this power can be met by the battery. If this is not the case, the maximum battery power is computed and utilized as DC-power. The output power is based on the current, the terminal voltage, and the SOC that are calculated in the model. It includes a SOC-dependent open-circuit voltage U_{OCV} and an inner resistance R_i that is influenced by the direction and amplitude of the battery current I_{batt}, the SOC, and the battery cell temperature. The explicit parameter values are obtained by lookup-table based linear interpolation. The terminal voltage U_{batt} depends on the inner resistance R_i, the battery current I_{batt} and the open-circuit voltage U_{OCV} (2.8). The SOC-change is determined by the battery current I_{batt}, the battery capacity C_{batt}, and the self-discharge rate r_{SD} (2.9).

The battery model is subject to the current limits (2.10) and voltage limits (2.11). The limits are given as absolute, positive values. The signs, therefore, need to be considered in the equations. The voltage limit leads to a de-rating of the current if the battery voltage is near its limit. The over-voltage caused by the current at the inner resistance may not lead to the terminal voltage to exceed its limit. All values are kept constant within a sample time period.

$$P_{\mathrm{batt}} = U_{\mathrm{batt}} \cdot I_{\mathrm{batt}} \tag{2.7}$$

$$U_{\mathrm{batt}} = U_{\mathrm{OCV}} + R_i \cdot I_{\mathrm{batt}} \tag{2.8}$$

$$\frac{d}{dt}\mathrm{SOC} = \frac{I_{\mathrm{batt}}}{C_{\mathrm{batt}}} - r_{\mathrm{SD}} \tag{2.9}$$

$$-I_{\mathrm{batt}}^{\mathrm{max,dchg}} \leq I_{\mathrm{batt}} \leq I_{\mathrm{batt}}^{\mathrm{max,chg}} \tag{2.10}$$

$$U_{\mathrm{batt}}^{\mathrm{min}} \leq U_{\mathrm{batt}} \leq U_{\mathrm{batt}}^{\mathrm{max}} \tag{2.11}$$

The battery power flow model takes the DC-power of the inverter as input and verifies, whether this power is provided by the battery. The effective power is subject to the battery's power limit constraint (2.12). The SOC in this model refers to the energy level stored in the BESS normalized to the nominal energy capacity (2.13). It deviates from the common definition of coulombic charge (2.9).

The output power constraint for the battery power flow model is the battery's power limit (2.12). The battery's output power is adequate to the inverter power on its DC-side. A battery SOC of 100%, for example, allows full discharge power, but no charging power (2.6).

$$|P_{\mathrm{batt}}| \leq P_{\mathrm{batt}}^{\mathrm{nom}} \tag{2.12}$$

$$\frac{d}{dt}\mathrm{SOC} = \begin{cases} \eta_{\mathrm{batt}} \cdot \frac{P_{\mathrm{batt}}}{E_{\mathrm{BESS}}^{\mathrm{nom}}} - r_{\mathrm{SD}} & \text{for } P_{\mathrm{batt}} > 0 \\ \frac{1}{\eta_{\mathrm{batt}}} \cdot \frac{P_{\mathrm{batt}}}{E_{\mathrm{BESS}}^{\mathrm{nom}}} - r_{\mathrm{SD}} & \text{for } P_{\mathrm{batt}} < 0 \end{cases} \tag{2.13}$$

Battery Model Parameters

Both models are parameterized with in-house measurements of a commercial LFP battery cell with a C anode (Table 2.3). The allowed operating voltage range is 2.0-3.6 V and the inner resistance is about 28.5 mΩ, depending on the battery's SOC and temperature. The equivalent circuit model is scaled to the assumed battery pack configuration with a nominal voltage of 650 V. Influences of additional connectors or variation of the battery cell parameters are very small [88] and therefore neglected. The self-discharge r_{SD} rate is 0.1% per month.

Table 2.3: Battery cell parameters for the simulation model. [89; 90]

Parameter	Value	Unit
Battery type	LFP:C	
Nominal capacity	3.0	Ah
Nominal voltage	3.2	V
Voltage range	2.0-3.6	V
Max. charge current	2.85	A
Max. disch. current	20	A
Resistance $R_{\mathrm{DC,10s}}$	28.5	mΩ
Self-discharge rate	0.1	%/month

Aging Model

Batteries degrade over their lifetime because of electro-chemical side-reactions. The results are decrease of usable capacity and increasing inner resistance. This has significant impact on the operation of BESS and needs to be considered for the sizing of BESS. It influences the BESS performance in long-term operation.

The model is built as two-step computation. First the parameters that influence aging are reduced by battery stress characterization stress methods. The regarded influence parameters are the SOC, cell temperature, depth of cycle, relative current or power (C-rate), and charge-throughput. Several stress characterization methods with varying properties are implemented.

The reduced stress data are then used as input for the battery lifetime models that consist of calendar aging model and cycle aging model. These are added to obtain the overall capacity fade and performance decrease. Several models with varying degree of complexity are implemented in the simulation framework. Different battery technologies based on datasheets, or warranty information are implemented as simple models. Literature-based aging models with formulas and parameters are integrated as well. The most sophisticated model is the lifetime model derived from experiments conducted by Maik Naumann [89].

The aging models are executed periodically with the simulation. They update the parameters of the battery model accordingly, to ensure further simulation with the correct battery capabilities. This way the deteriorating battery performance is reflected in its operation with as little offset as possible.

One method is pointed out specifically because it has been used for the PV-home storage case study. The method to estimate cycle aging of batteries is based on literature methods [48; 91–95]. Cyclical degradation depends only on the inflicted stress on the battery; the aging progress itself does not influence the aging speed, hence time-dependency is neglected in the system simulation.

The depth of cycle (DOC) describes the amplitude between the peak and the minimum state of-charge within a cycle and determines the cycle-aging. The cycle-counting algorithm detects half-cycles. These are distinguished between charging, discharging, and resting periods of the batteries. The cycle-counter determines the cycles by detecting zero-crossing of the battery terminal power-flow. Every time the power flow changes to zero, the end of a half-cycle is declared and the difference of the SOC at the beginning and at the end of the detected cycle is calculated to obtain the DOC.

The calendric capacity degradation $\Delta C_{\mathrm{batt}}^{\mathrm{cal}}$ (2.14) and the cycle degradation $\Delta C_{\mathrm{batt}}^{\mathrm{cyc}}$ (2.15) depend on the calendar lifetime t_{cal} and the cycle stability n_{EOL}. The calendar lifetime is the time period

t_{EOL} until 20% of the capacity is diminished by calendric aging. The cycle stability n_{EOL} describes the number of full equivalent cycles FEC until the battery degrades by 20% of its capacity just by cycle aging. Each cycle k with its respective DOC contributes to the cycle aging (2.15). Assuming independence of calendric and cycle aging, a superposition approach to account for both simultaneous aging effects is used to calculate the current capacity degradation ΔC_{batt} based on the current lifetime t and the occurred cycles k (2.16).

$$\Delta C_{\mathrm{batt}}^{\mathrm{cal}} = \frac{0.2 \cdot C_{\mathrm{batt}}}{t_{\mathrm{EOL}}} \cdot t \tag{2.14}$$

$$\Delta C_{\mathrm{batt}}^{\mathrm{cyc}} = \sum_{k} \frac{0.2 \cdot C_{\mathrm{batt}}}{n_{\mathrm{EOL}}(\mathrm{DOC}_k) \cdot \mathrm{DOC}_k} \tag{2.15}$$

$$\Delta C_{\mathrm{batt}} = \Delta C_{\mathrm{batt}}^{\mathrm{cal}} + \Delta C_{\mathrm{batt}}^{\mathrm{cyc}} \tag{2.16}$$

2.2.3.3 Diesel Generator Model

The diesel generator is implemented with certain operational constraints that are satisfied during the simulation: The diesel generator keeps its output power P_{DG} between the minimum and nominal output power (2.17). It only ramps down, if the current runtime $t_{\mathrm{DG}}^{\mathrm{run}}$ exceeds the diesel generators minimum runtime $t_{\mathrm{DG}}^{\mathrm{mustrun}}$ (2.18). The diesel generator only ramps up, if the current idle time $t_{\mathrm{DG}}^{\mathrm{idle}}$ exceeds the minimum idle time $t_{\mathrm{DG}}^{\mathrm{mustoff}}$ (2.19). The process of ramping up and down is neglected. Fuel is assumed to be always available and the fuel consumption V_{fuel} is computed with the diesel generator's efficiency η_{DG}, its output power P_{DG}, and the lower heating value (LHV) of diesel (2.20).

$$P_{\mathrm{DG}}^{\mathrm{min}} \leq P_{\mathrm{DG}} \leq P_{\mathrm{DG}}^{\mathrm{nom}} \tag{2.17}$$

$$t_{\mathrm{DG}}^{\mathrm{run}} \geq t_{\mathrm{DG}}^{\mathrm{mustrun}} \tag{2.18}$$

$$t_{\mathrm{DG}}^{\mathrm{idle}} \geq t_{\mathrm{DG}}^{\mathrm{mustoff}} \tag{2.19}$$

$$V_{\mathrm{fuel}} = \int_t \frac{P_{\mathrm{DG}}}{\eta_{\mathrm{DG}} \cdot \mathrm{LHV}}\, dt \tag{2.20}$$

Diesel Model Parameters

The power dependent generation rates per liter of diesel are taken from literature and named after the respective first authors of the publication Guinot, Ashari, and Bortoloni [96–98].

The generation efficiency of the diesel generator given by Ashari and Guinot is described by (2.22). The curves describe the energy output as Joule per LHV of fuel and transformed to $\mathrm{kWh_{el}}$ per liter for the simulation. Bortoloni *et al.* describe the fuel consumption in kg per $\mathrm{kWh_{el}}$ with (2.23). A density of 0.835 kg/l is used to convert the diesel fuel's mass into the volume. The given equation is re-formulated into $\mathrm{kWh_{el}}$ per liter for the simulation. The LHV of diesel is 34.7 MJ/l.

$$p = \frac{P_{\mathrm{DG}}}{P_{\mathrm{DG}}^{\mathrm{nom}}} \tag{2.21}$$

$$\eta_{\mathrm{DG}} = a + b \cdot p + c \cdot p^2 + d \cdot p^3 + e \cdot p^4 + f \cdot p^5 + g \cdot p^6 \tag{2.22}$$

$$r_{\mathrm{fuel}} = \begin{cases} a + b \cdot p + c \cdot p^2 + d \cdot p^3 & \text{for } 0.25 \leq p \leq 1 \\ r_0 & \text{for } 0 < p < 0.25 \end{cases} \tag{2.23}$$

The parameters for the efficiency curves are given in Table 2.4.

Table 2.4: Parameters of power dependent diesel generator consumption [96–98].

	Eq.	a	b	c	d	e	f	g	r_0
Ashari	(2.22)	0.24	0.084	0	0	0	0	0	-
Guinot	(2.22)	0.011	2.8753	-15.116	42.045	-62.194	46.2	-13.54	-
Bortoloni	(2.23)	0.369	-0.605	0.808	-0.330	-	-	-	0.263

Figure 2.10 shows the electricity generated per liter of fuel over the normalized output of the diesel generators.

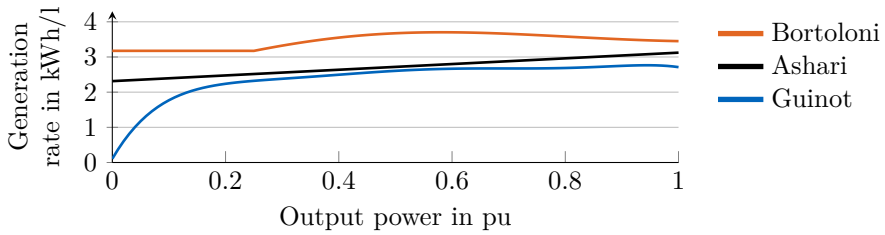

Figure 2.10: Electricity generation rates of the diesel generator types per liter of diesel. [96–98]

A direct emission factor of 2.625 kg CO_2eq/l and an indirect factor of 0.526 kg CO_2eq/l for the diesel consumption is assumed [99].

2.2.4 Application Models

2.2.4.1 PV-Home Storage Model

Figure 2.11 displays the relevant components of the PV-home storage model: PV-unit, household load, electricity grid, and BESS.

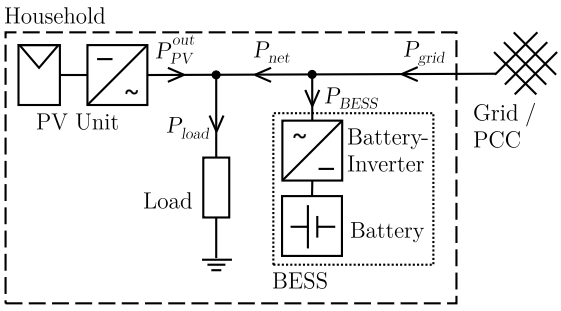

Figure 2.11: Topology of the modeled PV-household with relevant components.

The simulation model computes the power flow between solar generation P_{PV}, household load P_{load}, BESS P_{BESS}, and the electricity grid P_{grid}, considering inverter efficiency η_{inv}, and battery one-way efficiency η_{batt}. The net load P_{net} is determined by the solar generation P_{PV} and the household load P_{load} (2.24). The BESS output power P_{BESS} then determines the remaining power supplied by the grid P_{grid} (2.26). The grid power is subject to the constraint that limits the feed-in to a curtailment limit $P_{\mathrm{PV}}^{\mathrm{lim,curt}}$ (2.27). Any feed-in power above that limit is curtailed $P_{\mathrm{PV}}^{\mathrm{curt}}$ and the power output $P_{\mathrm{PV}}^{\mathrm{out}}$

differs from the theoretic generation P_{PV} (2.25).

$$P_{\mathrm{net}} = P_{\mathrm{load}} - P_{\mathrm{PV}} \tag{2.24}$$

$$P_{\mathrm{PV}} = P_{\mathrm{PV}}^{\mathrm{curt}} + P_{\mathrm{PV}}^{\mathrm{out}} \tag{2.25}$$

$$P_{\mathrm{grid}} = P_{\mathrm{net}} + P_{\mathrm{BESS}} + P_{\mathrm{PV}}^{\mathrm{curt}} \tag{2.26}$$

$$-P_{\mathrm{grid}} \leq P_{\mathrm{PV}}^{\mathrm{curt,lim}} \tag{2.27}$$

German regulations impose a limit of 70% of the PV-unit's capacity [44]. The specific subsidy for PV-home storage by the *KfW*-bank further tighten the curtailment limit to 50% of the PV-unit's peak power [100].

PV-Home Storage Operation Strategies

German regulations impose additional constraints that need to be considered for the operation strategies. The BESS may not charge from the grid, but only store the household's PV-generated energy. It is also not allowed to discharge power into the grid, but only provide the load. The BESS charging limit $P_{\mathrm{BESS}}^{\mathrm{chg,max}}$ (2.28) and discharging limit $P_{\mathrm{BESS}}^{\mathrm{dchg,max}}$ (2.29) depend on the algebraic sign of the net load P_{net}.

$$P_{\mathrm{BESS}}^{\mathrm{chg,max}} = \begin{cases} 0 & \text{if } P_{\mathrm{net}} > 0 \\ P_{\mathrm{net}} & \text{else} \end{cases} \tag{2.28}$$

$$P_{\mathrm{BESS}}^{\mathrm{dchg,max}} = \begin{cases} P_{\mathrm{net}} & \text{if } P_{\mathrm{net}} > 0 \\ 0 & \text{else} \end{cases} \tag{2.29}$$

Two rule-based operation strategies are used in this thesis. Both calculate reference powers $P_{\mathrm{BESS}}^{\mathrm{ref}}$ for the BESS, depending on the momentary production net load P_{net}. Figure 2.12 illustrates the power flows of a PV-home with storage and the different operation strategies.

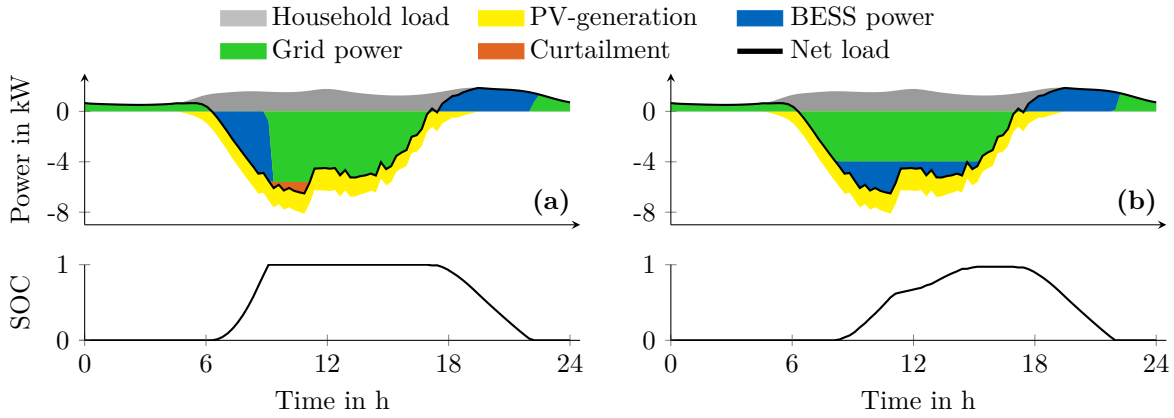

Figure 2.12: Illustration of the evaluated control algorithms. On the left (a) is the *Direct Charge* operation strategy. The right plot (b) shows the *Dynamic Feed-in Limit* operation strategy.

The first operation strategy is the *Direct Charge* operation strategy (Figure 2.12 (a)). It is the simplest and most intuitive algorithm and achieves the maximum self-consumption rate. The BESS stores all

occurring power surplus and discharges to meet the net load (2.30).

$$P_{\mathrm{BESS}}^{\mathrm{ref}} = -P_{\mathrm{net}} \tag{2.30}$$

The second control algorithm is the *Dynamic Feed-in Limit* operation strategy (Figure 2.12 (b)) [101]. It relies on a forecast of load and PV-production to calculate the lowest possible threshold P_{th} for the excess power that can be stored in the BESS, each day (2.31). This method aims at limiting the feed-in peak of the day to the power threshold P_{th}. The algorithm represents the theoretical optimum for peak feed-in reduction while maximizing the self-consumption, given the future load and generation are perfectly known. The discharging policy of the BESS discharges to fully meet the load, avoiding power purchased from the grid. The *Dynamic Feed-in Limit* is simplified for this thesis, neglecting sophisticated enhancements, originally proposed [50].

$$P_{\mathrm{BESS}}^{\mathrm{ref}} = \begin{cases} -P_{\mathrm{net}} - P_{\mathrm{th}} & \text{for } -P_{\mathrm{net}} > P_{\mathrm{th}} \\ 0 & \text{for } 0 < -P_{\mathrm{net}} \leq P_{\mathrm{th}} \\ -P_{\mathrm{net}} & \text{for } -P_{\mathrm{net}} \leq 0 \end{cases} \tag{2.31}$$

The discharging behavior of the *Dynamic Feed-in Limit* operation strategy is identical with the *Direct Charge* operation strategy (2.30) because high load power peaks are assumed not to occur simultaneously at night and lead to voltage violations in the grid. Therefore, no shifting is required.

2.2.4.2 Peak-Shaving Model

The components of a consumer with a BESS or a diesel generator for peak-shaving are shown in Figure 2.13. The left Figure (a) shows the model with the BESS, the right Figure (b) shows the configuration with a diesel generator.

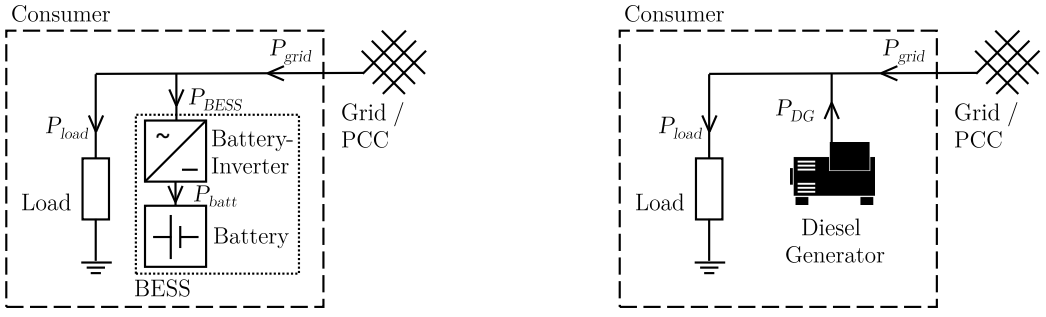

Figure 2.13: Topology of modeled consumer for peak-shaving with a BESS (a) and with a diesel generator (b).

The BESS charges from the grid during base load periods. During peak load periods, the BESS discharges to partially supply the load and reduce the grid power (2.32). In the second case, the diesel generator ramps up to reduce the grid peaks (2.33).

$$P_{\mathrm{grid}} = P_{\mathrm{load}} + P_{\mathrm{BESS}} \tag{2.32}$$

$$P_{\mathrm{grid}} = P_{\mathrm{load}} - P_{\mathrm{DG}} \tag{2.33}$$

Peak-Shaving Operation Strategy

The operation strategy for peak-shaving prevents the grid power P_{grid} from exceeding the pre-determined peak-shaving threshold P_{th}. If the load exceeds the limit, the BESS provides sufficient power to keep the grid power at that limit. As soon as the load falls below the limit, the BESS charges to prepare for future load peaks (2.34).

$$P_{\text{BESS}}^{\text{ref}} = P_{\text{th}} - P_{\text{load}} \tag{2.34}$$

The BESS is not capable of providing the necessary power, if the lower SOC-limit is reached and the BESS cannot discharge further or if the BESS's power capability is insufficient to buffer the peak. The analysis in this thesis is performed with a perfect forecast of the load. The threshold for maximum peak-reduction is pre-determined and the BESS is parameterized to be able to provide the necessary power at all times. Figure 2.14 shows the power flows with the consumer load, grid power, and the BESS charging and discharging.

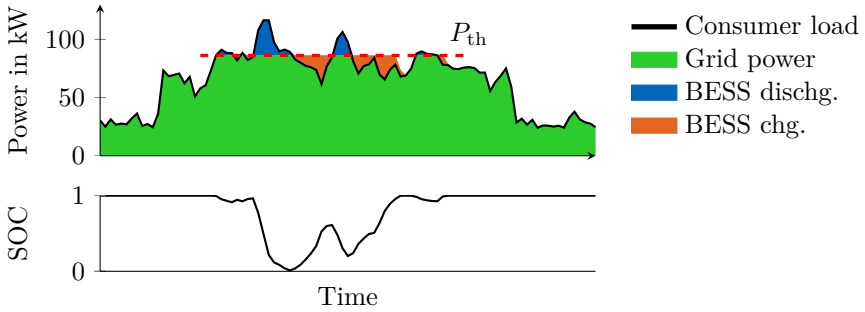

Figure 2.14: Illustration of peak-shaving operation. The BESS discharges to keep provide the consumer load and keep the grid power below the peak-shaving limit P_{th}. It immediately charges energy to prepare for the next peak.

2.2.4.3 Hybrid Renewable-Diesel Island Grid Model

All relevant components of a hybrid renewable-diesel island grid are shown in Figure 2.15. The model includes RES, load, diesel generator, and BESS.

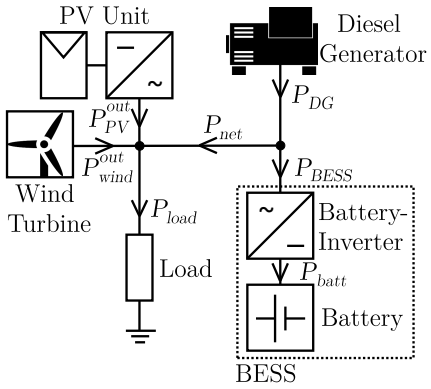

Figure 2.15: Topology of modeled island grid with components.

The deciding variable for the operation of the island grid is the net load (2.35). Negative values describe

surplus RES energy generation that is either stored in the BESS or curtailed to keep the grid power balance. Positive net loads mean that the RES cannot provide the load by themselves and need to be assisted by the BESS or the diesel generator.

$$P_{\text{net}} = P_{\text{load}} - P_{\text{PV}} - P_{\text{wind}} \tag{2.35}$$

The BESS can only store available power that is excess RES-generation and diesel generator power if the diesel generator is active (2.36). The BESS may not contribute to curtailment: If the generated power exceeds the required load and must be curtailed or consumed by switchable loads, the BESS cannot further discharge. Equation (2.37) describes the absolute value of the discharging limit. The limits have a degree of freedom and allow the BESS to support the diesel generator or induce the diesel generator to generate more power to charge the BESS. It may also not sufficiently supply the load and cause the diesel generator to remain in run-mode.

$$P_{\text{BESS}}^{\text{chg,max}} = \begin{cases} -P_{\text{net}} & \text{if DG is off} \\ -P_{\text{net}} + P_{\text{DG}}^{\text{nom}} & \text{else} \end{cases} \tag{2.36}$$

$$P_{\text{BESS}}^{\text{dchg,max}} = \begin{cases} P_{\text{net}} - P_{\text{DG}}^{\text{min}} & \text{if DG is active} \\ P_{\text{net}} & \text{else} \end{cases} \tag{2.37}$$

Loads that are not supplied do not impair the grid operation in the simulation. The shortage of supply is introduced as load shedding. Stability of the grid is not regarded.

Hybrid Renewable-Diesel Island Grid Operation Strategies

The two operation strategies described in this Section are shown in Figure 2.16. The operation strategies are used for the case study (Section 6.3) or as a reference for the presented operation strategy (Chapter 9).

The first operation strategy (*On-Off*) operates the diesel generator in two modes: off and running with full power output. The BESS stores any power generation surplus provided by wind and PV. Otherwise, the net load is provided by the BESS (2.38). The diesel generator ramps up to full power output if the BESS cannot sufficiently provide the load (2.39). The excess generated power is stored by the BESS (2.40).

$$P_{\text{BESS}}^{\text{ref}} = -P_{\text{net}} \tag{2.38}$$

$$P_{\text{DG}}^{\text{ref}} = \begin{cases} 0 & \text{for } P_{\text{BESS}} = -P_{\text{net}} \\ P_{\text{DG}}^{\text{nom}} & \text{for } P_{\text{BESS}} > -P_{\text{net}} \end{cases} \tag{2.39}$$

$$P_{\text{BESS}}^{\text{ref}} = P_{\text{DG}} - P_{\text{net}} \qquad \text{if DG is running} \tag{2.40}$$

The second operation strategy (*load follow*) operates the diesel generator in load following mode. The load is matched by the BESS first and the diesel generator produces electricity only if the BESS cannot provide the load or the generator is currently running because of its minimum runtime constraint. If the diesel generator must run because of the runtime constraint (2.18), it matches the load (2.41) and

the BESS stores the excess power (2.42), if available.

$$P_{\mathrm{DG}}^{\mathrm{ref}} = P_{\mathrm{net}} \tag{2.41}$$

$$P_{\mathrm{BESS}}^{\mathrm{ref}} = -P_{\mathrm{net}} + P_{\mathrm{DG}} \tag{2.42}$$

If the load exceeds the nominal power $P_{\mathrm{DG}}^{\mathrm{nom}}$, the BESS attempts to provide the remaining load. In case the load is below the diesel generator's minimum output power $P_{\mathrm{DG}}^{\mathrm{min}}$, the generator will run at its minimum output power (2.17) and the excess generated energy is stored in the BESS (2.42).

If the diesel generator may turn off or remain off, the BESS attempts to provide the net load (2.43). In case the BESS is not capable of providing the load, the diesel generator supports the BESS (2.44). Excess power generation that cannot be stored in the BESS is curtailed.

$$P_{\mathrm{BESS}}^{\mathrm{ref}} = -P_{\mathrm{net}} \tag{2.43}$$

$$P_{\mathrm{DG}}^{\mathrm{ref}} = P_{\mathrm{net}} + P_{\mathrm{BESS}} \tag{2.44}$$

The BESS output power reference is adapted, if the diesel generator reference $P_{\mathrm{DG}}^{\mathrm{ref}}$ cannot be met because of its power constraint (2.17), to avoid unnecessary curtailment of the generated power. If the diesel generator needs to run, it will try to match the load. P_{DG} is subject to the diesel generator's constraints (2.17)-(2.19) at all times.

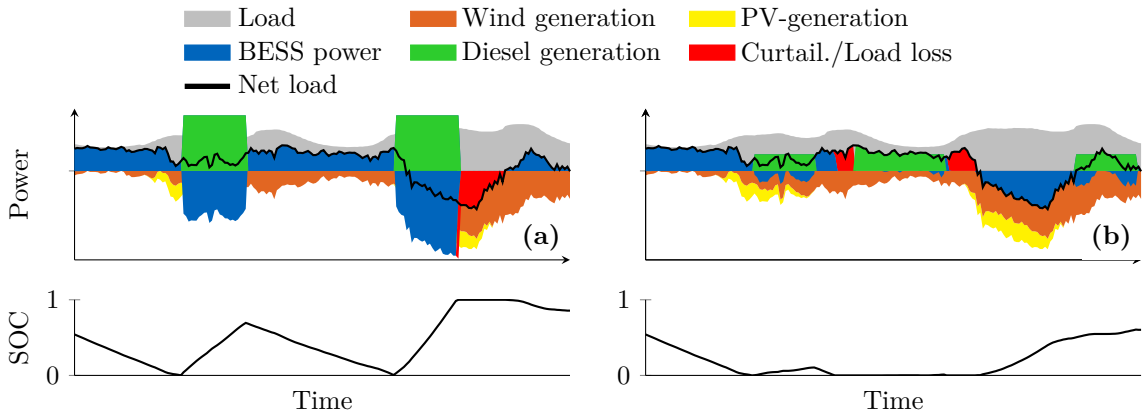

Figure 2.16: Illustration of the reference operation strategies. The left figure (a) shows the *On-Off* operation strategy. The right figure (b) depicts the *load follow* operation strategy.

Part II

Evaluating Stationary Battery Storage Systems

3 State of the Art

3.1 Technical Metrics

3.1.1 Efficiency

The efficiency η describes the share of power that is usable after a conversion step [84]. This value is found in data sheets of BESS and usually describes the efficiency of the inverter. The second parameter associated with efficiency is the standby consumption of the BESS $E^{\mathrm{stby}}_{\mathrm{BESS}}$. The standby consumption is sometimes given for single components, such as auxiliary electronics or the inverter. The values describe the technical performance of the BESS, but the real performance during operation may deviate from those numbers.

The round-trip efficiency η_{BESS} is related to energy storage and describes the share of energy that can be used after the storing process (3.1). The equation is valid for identical SOC at the beginning and the end of the measurement. The standby consumption $E^{\mathrm{stby}}_{\mathrm{BESS}}$ of all BESS components need to be considered in the calculation together with the conversion losses η_{conv}. [84]

$$\begin{aligned}\eta_{\mathrm{BESS}} &= \frac{E^{\mathrm{out}}_{\mathrm{BESS}}}{E^{\mathrm{in}}_{\mathrm{BESS}}}\bigg|_{\mathrm{SOC_0=SOC_{end}}} = 1 - \frac{E^{\mathrm{loss}}_{\mathrm{BESS}}}{E^{\mathrm{in}}_{\mathrm{BESS}}}\bigg|_{\mathrm{SOC_0=SOC_{end}}} = \\ &= \frac{\eta_{\mathrm{conv}} \cdot E^{\mathrm{in}}_{\mathrm{BESS}} - E^{\mathrm{stby}}_{\mathrm{BESS}}}{E^{\mathrm{in}}_{\mathrm{BESS}}}\bigg|_{\mathrm{SOC_0=SOC_{end}}}\end{aligned} \tag{3.1}$$

The round-trip efficiency calculated is only valid for the specific system configuration and cycle-procedure because of the power-dependent efficiencies of inverter and batteries. Using the round-trip efficiency for evaluation and comparison purposes is fairly complicated and requires numerous consideration. The German Energy Storage Association (BVES) for example developed a guideline to correctly evaluate the efficiency of PV-home storage systems [102]. A total of 26 partners that consist of universities, research institutes, and companies have contributed to the guideline.

3.1.2 Charge and Energy Throughput

The coulombic full equivalent cycles $\mathrm{FEC_Q}$ describe the charge throughput for the battery (3.2). The energy full equivalent cycles $\mathrm{FEC_E}$ is similar but refers to the energy throughput (3.3). [103]

$$\mathrm{FEC_Q} = \frac{Q^{\mathrm{in}}_{\mathrm{batt}} + Q^{\mathrm{out}}_{\mathrm{batt}}}{2 \cdot C^{\mathrm{nom}}_{\mathrm{batt}}} \tag{3.2}$$

$$\mathrm{FEC_E} = \frac{E^{\mathrm{in}}_{\mathrm{batt}} + E^{\mathrm{out}}_{\mathrm{batt}}}{2 \cdot E^{\mathrm{nom}}_{\mathrm{batt}}} \tag{3.3}$$

3.1.3 System Utilization

The time utilization rate τ_{time} that is the ratio between of the BESS's working time $t_{\text{BESS}}^{\text{run}}$ and the total time t_{total} [84]. The runtime is defined as the overall time period when the BESS supplies or charges power to serve its application (3.4). The idle time $t_{\text{BESS}}^{\text{idle}}$ is the remaining time when the BESS waits for its operation.

$$\tau_{\text{time}} = \frac{t_{\text{BESS}}^{\text{run}}}{t_{\text{total}}} = 1 - \frac{t_{\text{BESS}}^{\text{idle}}}{t_{\text{total}}} \tag{3.4}$$

A similar approach to assess the system utilization is the energy utilization rate τ_{energy}. The energy utilization rate is the ratio of the energy throughput and the theoretic maximum energy throughput, that is the system charges and discharges at nominal power level without interruption [84]. It is related to the full equivalent cycles but includes time-dependency. Low values indicate that the BESS is either operating for short times and/or mostly in partial power.

$$\tau_{\text{energy}} = \frac{E_{\text{BESS}}^{\text{in}} + E_{\text{BESS}}^{\text{out}}}{P_{\text{BESS}}^{\text{nom}} \cdot t_{\text{total}}} = \frac{(1 + \eta_{\text{BESS}}) \cdot E_{\text{BESS}}^{\text{in}}}{P_{\text{BESS}}^{\text{nom}} \cdot t_{\text{total}}} \tag{3.5}$$

3.1.4 Self-Consumption and Self-Sufficiency

The self-consumption rate r_{sc} is usually associated with the PV-home storage application. It is used as a performance indicator of PV-home storage and often for marketing purposes. The self-consumption rate describes the share of RES-generated energy that is consumed $E_{\text{RES}}^{\text{direct}}$ in relation to the total RES-generated energy E_{RES} (3.6) [50]. In the PV-home context, the consumed energy refers to the direct use of the RES-generated energy $E_{\text{RES}}^{\text{direct}}$ and the stored energy $E_{\text{BESS}}^{\text{in}}$.

$$r_{\text{sc}} = \frac{E_{\text{RES}}^{\text{direct}} + E_{\text{BESS}}^{\text{in}}}{E_{\text{RES}}} \tag{3.6}$$

The benefit of a high self-consumption rate is a lower electricity bill under German legislation. Consequently, high self-consumption rates mean that less self-generated PV-energy is sold to the grid.

The self-sufficiency rate r_{ss} is similar to the self-consumption rate, but its reference is the load, instead of the generated energy [50]. It illustrates the share of the load supplied by RES-generated energy (3.7).

$$r_{\text{ss}} = \frac{E_{\text{RES}}^{\text{direct}} + E_{\text{BESS}}^{\text{out}}}{E_{\text{load}}} = \frac{E_{\text{RES}}^{\text{direct}} + \eta_{\text{BESS}} \cdot E_{\text{BESS}}^{\text{in}}}{E_{\text{load}}} \tag{3.7}$$

The self-sufficiency rate is more objective than the self-consumption rate because BESS losses decrease the self-sufficiency rate, while the BESS losses are not considered in the self-consumption rate. Both metrics self-consumption rate and self-sufficiency rate are virtual metrics, for simpler representation of the BESS performance.

3.2 Literature Review of Evaluation of Economics and Carbon Emissions

The literature reviews below reveal that no unified method to assess ESS exists in the literature. The majority of publications focus on the economics of ESS, as they are less abstract than environmental impacts and are the main barrier for widespread adoption of ESS in the grid. A variety of metrics exist, that need to be analyzed. Economic considerations of ESS are non-conform and the results from several papers are usually not easily comparable. Especially the evaluation of the carbon footprint of ESS is not established and incomplete reflection of the influence of ESS are common.

3.2.1 Economics

The main barrier for the deployment of energy storage systems in the grid are the costs [22; 29]. A fraction of the body of publications that is concerned with the economics is discussed below.

Some contributions assess the overall result of a system coupled with ESS. A common research question tackled in publications is the optimal sizing of RES and BESS for island grids. Publications often use the levelized cost of energy (LCOE) for the assessment and various island and ESS-technologies have been investigated [104–107].

Denholm *et al.* evaluate the economics of ESS for increasing the penetration of PV power plants. They utilize the LCOE of the PV-plant as economic minimization objective [108]. Wissem *et al.* conduct an optimization of an autonomous PV system. The objective is to minimize the overall LCOE [109].

Weniger *et al.* analyze the performance of PV-home storage systems and base their conclusions on the annual cost and savings achieved by the BESS [50; 110]. Their conclusive evaluation criterion is the average electricity price over the operation lifetime. Merei *et al.* conduct a techno-economic analysis of PV-battery-systems for commercial applications [111]. They discuss both annuity costs and average electricity costs.

The publications above analyze the economics of a power system or a building. The authors evaluate the performance with the overall cost of the regarded system and do not explicitly isolate the benefit of the BESS. The most common goal is the reduction of electricity cost, hence most authors utilize the LCOE that can be directly compared to the electricity cost of alternatives.

The levelized cost of energy stored (LCOES) (4.22) is considered for technology comparisons, among other metrics. Battke *et al.* compared the life-cycle costs for various storage technologies [46]. They use a literature review, expert interviews, and Monte Carlo simulations for their assessment. Pawel *et al.* compare different storage technologies based on the LCOES [112]. The author uses different assumptions that specifically favor one technology. Quoilin *et al.* utilize the LCOES to assess the economics of increasing the self-consumption with PV-home storage systems [113]. The LCOES is comparable to the LCOE and based on the delivered energy. It does, however, not take into account possible savings or revenues of ESS, deployed to serve applications.

Other contributions apply different metrics, but also exclude possible revenues and restrict their results to the costs. Hittinger *et al.* evaluate the cost-effectiveness of several BESS technologies for four different applications: Frequency regulation, baseload wind integration, load-following wind integration, and peak-shaving [114]. They calculate the annualized cost of providing the particular service,

the cost-of-service. Jallouli *et al.* analyze the economics of a stand-alone PV power unit [115]. They couple the PV-unit with a BESS and a hydrogen system. Their results are the net present value (NPV) (4.19) of the costs.

Metrics that exclusively consider the expenses of ESS are suitable for the comparison of different storage technologies. The LCOES, in particular, is suitable to compare ESS with generation units. More comprehensive evaluations of ESS need to include the revenue and savings expected from the respective application.

Celik *et al.* assess the optimal sizing of PV-home storage and conduct a life-cycle cost analysis [116]. Heymans *et al.* analyze the economics of second use electric vehicle batteries for two applications [117]. They obtain the offset of overall cost achieved by BESS for their economic analysis. Göbel *et al.* investigate the profitability of residential BESS [118]. The authors above use the NPV to quantify their results.

Hesse *et al.* optimize the size of PV-home storage systems [119]. They rely on the return on investment (ROI) (4.17) for the objective function of their optimization. The authors give an overview of the cost factors of BESS that determine the ROI in another publication [22]. They also identify the major contributing mechanisms for the cost factors.

The internal rate of return (IRR) (4.23) is another metric used for economic assessments. Braun *et al.* investigate the economics of PV-home lithium-ion BESS for increasing the household's self-consumption, based in the IRR [120].

Some authors conduct evaluations with several metrics. DiOrio *et al.* conduct several case studies for peak-shaving and load-shifting on the economics of BESS [121]. Their financial metrics are the NPV and the payback period (4.18). Colmenar-Santos *et al.* analyze the economics of PV-home storage [122]. They use the NPV, the IRR, and the payback period as key metrics. The fact that they use several metrics, is an indicator that each is more suitable for another purpose.

Similar to the LCOE or LCOES, a more intuitive way of assessing the economics of ESS is to use annual financial metrics. Battke *et al.* investigate the economics with regard to demand-pull policies [123]. They assess the ESS in annual profit (or loss) per installed electric capacity in EUR/kW per year. Rathgeber *et al.* break the economics of ESS down to two equations [48]. They use the annuity method to take into account different user classes, that vary in their interest rate assigned to the capital costs and the intended payback period. The method is the NPV referenced to one year. Their evaluation method is limited to an energy-based point of view. Applications, where power values are the key metrics, such as frequency control or peak-shaving are not considered in their framework.

Both annual profit (or loss) per installed capacity and annuities directly quantify the economic performance over the period of a year. They depict an illustrative metric that is easy to use.

Another metric introduced especially for the assessment of ESS is the profitability index or NPV per EUR invested (PI) (4.24). Hoppmann *et al.* use the PI to evaluate the economic viability of battery systems for PV-homes [41]. Naumann *et al.* analyzed the cost of PV-home storage systems with lithium-ion batteries [28]. They utilize the ROI as a figure of merit, based on the NPV values of cost and revenue without mentioning the term PI. Stephan *et al.* discuss the benefit of stacking applications [37]. They undermine their conclusions with the PI.

Profitability is the key parameter for the deployment of BESS and therefore most common performance metric in the literature. The number of different metrics utilized indicates that there is no common

understanding on what metric to use and that the metrics are each suitable for different purposes. The main differences are the scopes of the analyses. Either the whole power system or building is regarded, rendering distinct metrics for ESS unnecessary. A comparison of storage technologies does not require considering the revenue of the application, given that the technologies only differ in the costs they induce. The LCOES is based on the established LCOE for energy generation. The metric is therefore illustrative but requires that the focus on energy is sufficient. Any application that requires considering the powers (e.g. frequency control or peak-shaving) cannot be evaluated with the LCOES. A more detailed discussion of the different economic evaluation metrics follows in Section 4.2.

Table 3.1: Overview of literature reviewed on the economic metrics used.

Economic metric	Sources
LCOE of generation system	[50; 104–111]
annuity costs of generation system	[111]
levelized cost of energy stored (LCOES)	[46; 112; 113]
Annualized BESS costs	[114]
net present value (NPV) of BESS costs	[115]
net present value (NPV) of BESS costs and savings	[116–118; 121; 122]
return on investment (ROI) of BESS	[22; 119]
internal rate of return (IRR) of BESS	[120; 122]
payback period of BESS	[121; 122]
annual profit	[48; 123]
profitability Index (PI)	[28; 37; 41]

3.2.2 Carbon Emissions

ESS are regarded as a key component to reduce the carbon emissions of the electric power system. The major share of scientific publications that assess BESS focus on the economics. Less attention has been paid to the specific impact of BESS on the GWP.

Pettinger *et al.* estimated the ecological amortization time for different BESS [124]. The energy output of the BESS is assumed to directly compensate for the energy required for producing the BESS. This approach lacks the consideration that energy input is needed before and falsely treats the BESS energy output identical to emission-free energy generation.

Denholm *et al.* [125] compare different ESS technologies based on a life-cycle assessment. They do not consider possible positive effects of ESS but focus on the energy output. The approach is similar to the analysis of electricity generation units and suitable for technology comparison.

Immendoerfer *et al.* compare the life-cycle assessment of a pumped hydro storage with a lithium-ion BESS over a timespan of 80 years [126]. Both ESS are scaled to similar nominal energy capacity and annual energy output. The parameters of the ESS are, however, not identical. While the pumped hydro storage has a nominal power of 1 GW, the BESS is parameterized with a much larger nominal power of 9.6 GW. Forcing identical parameter assumptions would lead to unreasonable parameters for one of the technologies. In addition, the BESS is oversized by 10% to account for the aging of the batteries. Their results show that the GWP of the BESS operation contributes to more than 90% of the total GWP. Immendoerfer's approach illustrates the issue of technology comparisons and supports the claim that different ESS are suitable for different applications.

Hiremath *et al.* present a comparison of life-cycle assessment for four stationary BESS technologies

in six different applications [127]. They acknowledge that a normalization of the impact to the total electricity delivered over the lifetime of the ESS allows a more realistic comparison, rather than normalizing them against the mass, volume, or the storage capacities. The cradle-to-gate impact is smaller than the emissions caused by BESS losses in all cases and all technologies regarded. The operational impact on the GWP is not correctly depicted. The emissions of the charging energy are considered, but an alternative use of the charging energy is disregarded in the analysis. The increase of self-consumption, for example, has a very low emission factor because the BESS is solely charged by the PV-unit, but grid feed-in instead of storing the energy is not considered. Their results are therefore meaningful for the comparison of technologies, but not convincing for the assessment of the applications' benefit.

Vandepaer *et al.* compare the environmental impacts of lithium metal polymer batteries with lithium-ion batteries [128]. The functional unit they utilize is one MWh delivered by the BESS. Their results show that the battery manufacturing stage drives the majority of environmental impacts in the scenarios. The investigated application for the BESS is to store electricity of intermittent electricity production source and use it to deliver it at a later time. The reason for the negligible impact of the operation is that the BESS store wind-generated energy with very small emission values. Similar to Hiremath, the alternative use of the generated energy is not considered.

Stenzel *et al.* conduct a life-cycle assessment for a real BESS with 5 MW nominal power and 5 MWh nominal energy capacity [129]. The BESS provides primary control reserve in Germany. Their assessment of the BESS is compared to the operation of coal power plants, however, lacks the holistic view and does not represent a fair comparison. The provision of primary control reserve with coal power plants also leads to a base electricity supply that serves loads. This reference is compared to BESS that provide the same amount of primary control, but do not supply the same amount of energy. As such the comparison is between a system (coal power plant), that provides primary control reserve and at the same time generates a certain amount of energy, and another system (BESS) that provides primary control reserve without generating the same amount of energy. This difference needs to be considered for a meaningful comparison.

The literature discussed above is partially suitable for comparing different technologies, but the approaches are not conclusive with regard to the carbon reduction achieved by the applications. The contributions also show that the technology comparison is complicated because identical system parameters may not be realistic or applicable for all technologies. The reference for comparisons, such as a different system or an alternative use to storing the energy, are either neglected or not correctly considered in all papers above.

Arbabzadeh *et al.* investigate an island grid with gas-turbine, wind turbine, and vanadium redox flow batteries [130]. They conclude that wind turbines reduce the carbon emissions and BESS further reduce the emission rate, only if sufficient wind turbines are installed.

Stenzel *et al.* conduct a life-cycle assessment for the annual electricity production of an island grid [131]. Their results show that RES with BESS annually reduce the environmental impacts by approx. 43%. The main contributor to the environmental impact is the diesel generator even if coupled with RES and BESS.

The two examples above illustrate that the assessment of BESS in isolated island grids is more straightforward than the assessment for grid-connected applications.

McKenna *et al.* investigated the environmental impact of lead-acid batteries that perform load shifting

in the United Kingdom [132]. Their analysis includes the production and the usage of the BESS. They conclude that the losses of the BESS increase the net fossil fuel generation leading to a negative environmental impact. The carbon emissions for operation are about five times higher than the production induced emissions in their investigation.

Jones *et al.* investigate the financial and environmental benefit of PV-home storage [133]. Their results show that the carbon reduction originates from the PV-unit and is not improved by the BESS. They draw the same conclusion as the author of this thesis in a previous publication [31].

De Sisternes *et al.* analyzed the value of energy storage in a de-carbonized electricity system [134]. They conclude that BESS are capable of reducing the carbon emissions of a power system if strong reliance on RES is imposed. A more mixed generation composition with nuclear power plants renders ESS less useful in their results.

Lin *et al.* investigate the impact of ESS for power system reserve [135]. Their results show that adding energy storage does not necessarily reduce the emission, but the properties of the power system determine the impact on the GWP. Systems with high renewable penetration levels and significant renewable curtailment enable ESS to reduce emissions. In other systems the results are mixed. They also found that enhancing dispatch algorithms improve the net carbon emissions by ESS operation.

The four authors above all conducted a meaningful life-cycle assessment of ESS, where the beneficial effects of operating the systems are correctly considered. Their results show that the power system parameters and the intention of operating ESS determine, whether the deployment of ESS is beneficial or not. The authors did not narrow down the critical factors for the net outcome of the carbon emissions.

Zheng investigates the impact of different ESS technologies for load shifting and peak-shaving strategies, economically optimized in a demand response scheme [136]. The analysis includes the generator dispatch curve based on the New York electric system. Both operation strategies shift the electricity generation from high-emission generators to generators with lower emission rates. The emissions decrease only in one of the 14 cases investigated. The generation shift to low-emission generators does not generally compensate for the losses induced by ESS operation.

Abdon *et al.* compare different storage technologies regarding their economic value and environmental impact [137]. They acknowledge that ESS need to charge renewable energy that would otherwise have been curtailed, in order to provide electricity with lower emissions than the grid average. Their benefit depends on the emission mitigation achieved by substituting conventional supply.

Arbabzadeh *et al.* conduct a sensitivity analysis on the influence of the environmental impact of BESS [138]. Both BESS parameters and power system parameters are analyzed. The results show that the parameter influence depends on the application. Applications with high energy throughput, such as time-shifting or frequency regulation benefit from high round-trip efficiencies of the BESS and heat rates of the displaced generators. Other applications with low utilization, such as power reliability, are more dependent on the BESS's service life and the system production burden.

The author of this thesis previously published an analysis of the GWP of BESS for PV-homes in a rural distribution grid [31]. The conclusion is that the key action for reducing carbon emissions is avoiding the curtailment of RES-generated energy. The increase of self-consumption, in contrast, does not reduce the carbon emissions, but the losses caused by the BESS increase the net load and consequently the carbon emissions instead.

The last four publications presented here, conclude that grid-connected applications need to shift the energy generation from high-emission systems to low-emission generators. The losses induced by BESS operation need to cause less energy consumption than the savings of the respective application.

4 Economics

4.1 Financial Benefit of Storage Operation

This section describes the mechanisms for the revenue and savings of BESS for the applications PV-home storage, peak-shaving, and hybrid renewable-diesel island grid. The equations capture the main factors that determine the economic benefit.

4.1.1 PV-Home Storage

The German case is regarded for the PV-home costs. A fixed rate c_{remun} is applied for the remuneration of the feed-in of self-generated electricity (i.e. by the PV-unit). The BESS only charges surplus PV-generated power and only discharges to provide the household consumption.

PV-generated electricity can be fed into the grid for a fixed remuneration rate c_{remun} or stored for later use and avoid purchase from the grid for the electricity price c_{el}. The electricity costs $\text{CF}_{\text{el}}^{\text{home}}$ of the household without PV-unit or BESS are defined by the load E_{load} (4.1). The total electricity costs $\text{CF}_{\text{el}}^{\text{PVhome}}$ for a household with a rooftop PV-unit are reduced by the self-consumed electricity $E_{\text{PV}}^{\text{direct}}$ and the grid feed-in $E_{\text{grid}}^{\text{feedin}}$ (4.2). A BESS coupled with a PV-unit further reduces the electricity costs $\text{CF}_{\text{el}}^{\text{PVBESShome}}$ by reducing the grid purchase by the BESS supplied energy $E_{\text{BESS}}^{\text{out}}$ and possibly by reduction of the energy curtailment $E_{\text{PV}}^{\text{curt}}$. The grid feed-in is reduced by the energy stored in the BESS $E_{\text{BESS}}^{\text{in}}$ (4.3).

$$\text{CF}_{\text{el}}^{\text{home}} = E_{\text{load}} \cdot c_{\text{el}} \tag{4.1}$$

$$\begin{aligned}\text{CF}_{\text{el}}^{\text{PVhome}} &= E_{\text{grid}}^{\text{purch}} \cdot c_{\text{el}} - E_{\text{grid}}^{\text{feedin}} \cdot c_{\text{remun}} = \\ &= \left(E_{\text{load}} - E_{\text{PV}}^{\text{direct}}\right) \cdot c_{\text{el}} - \left(E_{\text{PV}} - E_{\text{PV}}^{\text{direct}} - E_{\text{PV}}^{\text{curtail}}\right) \cdot c_{\text{remun}}\end{aligned} \tag{4.2}$$

$$\begin{aligned}\text{CF}_{\text{el}}^{\text{PVBESShome}} &= E_{\text{grid}}^{\text{purch}} \cdot c_{\text{el}} - E_{\text{grid}}^{\text{feedin}} \cdot c_{\text{remun}} = \\ &= \left(E_{\text{load}} - E_{\text{PV}}^{\text{direct}} - E_{\text{BESS}}^{\text{out}}\right) \cdot c_{\text{el}} - \left(E_{\text{PV}} - E_{\text{PV}}^{\text{direct}} - E_{\text{PV}}^{\text{curtail}} - E_{\text{BESS}}^{\text{in}}\right) \cdot c_{\text{remun}}\end{aligned} \tag{4.3}$$

The electricity bill reduction achieved by installing a PV-unit $\Delta\text{CF}_{\text{el}}^{\text{PV}}$ is given by equation (4.4). PV-generated energy reduces the electricity purchased and are fed into the grid for a remuneration. The BESS reduces the grid purchase, but at the same time reduces the feed-in energy, thus the remuneration (4.5).

$$\Delta\text{CF}_{\text{el}}^{\text{PV}} = E_{\text{PV}}^{\text{direct}} \cdot (c_{\text{el}} - c_{\text{remun}}) + \left(E_{\text{PV}} - E_{\text{PV}}^{\text{curt}}\right) \tag{4.4}$$

$$\begin{aligned}\Delta\text{CF}_{\text{el}}^{\text{BESS}} &= E_{\text{BESS}}^{\text{out}} \cdot c_{\text{el}} - \left(E_{\text{BESS}}^{\text{in}} - \Delta E_{\text{PV}}^{\text{curt}}\right) \cdot c_{\text{remun}} = \\ &= E_{\text{BESS}}^{\text{in}} \cdot (c_{\text{el}} \cdot \eta_{\text{BESS}} - c_{\text{remun}}) + \Delta E_{\text{PV}}^{\text{curt}} \cdot c_{\text{remun}}\end{aligned} \tag{4.5}$$

The external factors that determine the revenue are the electricity price, remuneration price, and

the curtailment limit imposed. The BESS parameters that determine the achievable revenue are the efficiency, the stored energy, and the avoided curtailment.

4.1.2 Peak-Shaving

Consumers exceeding a certain amount of load energy (usually commercial customers) are subject to paying power prices c_{peak} for the largest occurring load peak $\hat{P}_{\text{grid}}$ within a defined time period. Peak-shaving (PS) serves the purpose to reduce the load peaks and achieve a lower peak power price. The electricity costs of a consumer under the mentioned tariff scheme, without peak-shaving by either diesel generator or BESS consist of both, purchased energy E_{load} and peak load charge (4.6).

The electricity bill for peak-shaving by a diesel generator, including fuel cost, is given by (4.7). The LHV and the average system efficiency of the diesel generator are included in the equation. Consumers that perform peak-shaving by a BESS have different electricity costs (4.8).

$$\text{CF}_{\text{el}}^{\text{load}} = \hat{P}_{\text{load}} \cdot c_{\text{peak}} + E_{\text{load}} \cdot c_{\text{el}} \tag{4.6}$$

$$\text{CF}_{\text{el}}^{\text{PS,DG}} = \hat{P}_{\text{grid}} \cdot c_{\text{peak}} + (E_{\text{load}} - E_{\text{PS}}) \cdot c_{\text{el}} + E_{\text{PS}} \cdot \frac{c_{\text{fuel}}}{\bar{\eta}_{\text{DG}} \cdot \text{LHV}} \tag{4.7}$$

$$\text{CF}_{\text{el}}^{\text{PS,BESS}} = \hat{P}_{\text{grid}} \cdot c_{\text{peak}} + \left(E_{\text{load}} + E_{\text{BESS}}^{\text{loss}}\right) \cdot c_{\text{el}} \tag{4.8}$$

The diesel generator reduces the peak load charge and supplies the associated peak-shaving energy E_{PS}. This energy replaces the grid-purchased energy of the same amount and causes fuel consumption and costs c_{fuel} instead (4.9). The diesel generator's efficiency $\bar{\eta}_{\text{DG}}$ describes its average efficiency. This depends on the explicit operation of the diesel generator. The BESS is assumed to achieve an identical peak-reduction as the diesel generator. The grid-purchase, in this case, is not replaced by (fossil-fuel based) self-generated energy but is increased to compensate for the BESS-losses $E_{\text{BESS}}^{\text{loss}}$ (4.10).

$$\Delta\text{CF}_{\text{el}}^{\text{DG}} = \Delta\hat{P}_{\text{grid}}^{\text{PS}} \cdot c_{\text{peak}} - E_{\text{PS}} \cdot \left(\frac{c_{\text{fuel}}}{\bar{\eta}_{\text{DG}} \cdot \text{LHV}} - c_{\text{el}}\right) \tag{4.9}$$

$$\Delta\text{CF}_{\text{el}}^{\text{BESS}} = \Delta\hat{P}_{\text{grid}}^{\text{PS}} \cdot c_{\text{peak}} - E_{\text{PS}} \cdot \left(\frac{1}{\eta_{\text{BESS}}} - 1\right) \cdot c_{\text{el}} \tag{4.10}$$

The external factors for the revenue of peak-shaving are the peak power price and the characteristics of the load, i.e. how much energy is required to peak-shave a certain amount of power. The main factors concerning the BESS are its nominal energy and the inverter's nominal power.

4.1.3 Hybrid Renewable-Diesel Island Grid

The economic aim for the island grid is to reduce the fuel costs of the diesel generator and to establish a stable, non-interrupted power supply. Added RES to the power system provide the load for certain times, depending on the wind and solar irradiation. The BESS compensates for the time-mismatch of electricity supply by RES and electricity demand.

The equation of the operational costs of island grids with only a diesel generator is determined by the load E_{load}, the fuel cost c_{fuel}, the LHV of diesel, and the diesel generator's average efficiency $\bar{\eta}_{\text{DG}}$ (4.11). RES supply part of the load $E_{\text{RES}}^{\text{direct}}$ and reduce the diesel generator output by that amount (4.12). Equipping the RES with a BESS further reduce the diesel generator energy by the energy supplied by

the BESS (4.13). In all cases, they comprise the energy provided by the diesel generator E_{DG} and the associated fuel price c_{fuel}.

$$\mathrm{CF}_{\mathrm{el}}^{\mathrm{DG}} = E_{\mathrm{load}} \cdot \frac{c_{\mathrm{fuel}}}{\bar{\eta}_{\mathrm{DG}} \cdot \mathrm{LHV}} \tag{4.11}$$

$$\mathrm{CF}_{\mathrm{el}}^{\mathrm{Hybrid}} = \left(E_{\mathrm{load}} - E_{\mathrm{RES}}^{\mathrm{direct}}\right) \cdot \frac{c_{\mathrm{fuel}}}{\bar{\eta}_{\mathrm{DG}} \cdot \mathrm{LHV}} \tag{4.12}$$

$$\mathrm{CF}_{\mathrm{el}}^{\mathrm{HybridES}} = \left(E_{\mathrm{load}} - E_{\mathrm{RES}}^{\mathrm{direct}} - E_{\mathrm{BESS}}^{\mathrm{out}}\right) \cdot \frac{c_{\mathrm{fuel}}}{\bar{\eta}_{\mathrm{DG}} \cdot \mathrm{LHV}} \tag{4.13}$$

The saving contributions achieved by RES (4.14) and BESS (4.15) are isolated below.

$$\Delta\mathrm{CF}_{\mathrm{el}}^{\mathrm{RES}} = E_{\mathrm{RES}}^{\mathrm{direct}} \cdot c_{\mathrm{fuel}} \tag{4.14}$$

$$\Delta\mathrm{CF}_{\mathrm{el}}^{\mathrm{BESS}} = E_{\mathrm{BESS}}^{\mathrm{out}} \cdot c_{\mathrm{fuel}} \tag{4.15}$$

The external factors for the revenue are the fuel price and the correlation of RES-generation periods and load. The technical factors are the amount of energy, the RES can directly provide for the load, the energy the BESS supplies, i.e. the nominal energy and the average system efficiency $\bar{\eta}_{\mathrm{DG}}$. For evaluating the overall economic outcome for the island grid, the investments for RES and BESS are considered in the analysis.

4.2 Discussion of Economic Metrics

The high initial investments for installing BESS are the main barrier for the wide-spread deployment of BESS [40]. As batteries constitute a large portion of the overall system costs and they are subject to aging, possible replacement of the battery component needs to be considered [28].

The replacement costs are not the only component that increases the complexity of economic analyses for BESS, but the operating costs need more precise assumptions as well. Due to the sensitivity of battery aging to the battery temperature, the costs of the thermal management need to be considered, together with other factors. Some applications, for example, require the participation of the BESS at spot markets, to ensure a certain SOC-range for BESS to be able to meet the requirements of its application. Smaller factors such as the standby consumption of auxiliary components are often overlooked, but accumulate to a significant sum that may change the outcome of economic analyses.

For BESS to be economically reasonable, their revenue or achieved cost savings need to exceed the cost they cause. The remaining manuscript will treat cost savings and revenue achieved by BESS equally. BESS are limited in their ability to store energy that needs to be considered for the performance of BESS for each application. As aging has a major influence on the nominal energy of a BESS, this factor needs to be considered over the lifetime of such systems.

The complexity of assessing the economics of BESS is discussed in this Section. Several assessment metrics, commonly found in the scientific literature are presented and each evaluated based on criteria for economic metrics.

4.2.1 Evaluation Criteria of Economic Metrics

Economic metrics for the assessment of BESS should meet certain criteria to be acknowledged as favorable metrics. Five criteria are proposed that serve as qualitative indicators and framework to evaluate and compare existing economic metrics. The criteria proposed are meaningfulness, the extent of applicability, clarity, ease of use, and objectiveness.

Meaningfulness describes the property, whether an economic metric gives a meaningful assessment of the economic viability. The user of the metric should be able to rely on the computed number and the metric should give a good estimate of the overall value of the BESS.

The extent of applicability describes that the metric is *open*: applicable to any storage technology and any application. Instead of specialized metrics, that are useful only for a small number of applications or technologies, general assessment methods are favored.

Clarity means that the metric is understandable for the user. The easier the metric is to understand, the more suitable it is to inform and explain to others.

Ease of use is the factor of how straightforward a metric is to use. This is related to the number of assumptions and parameters and the accuracy of the BESS operation required. A large number of parameters and the need for very accurate technical models result in an unfavorable ease of use.

Objectiveness is the compound of clarity and ease of use. This criterion determines, how robust an assessment metric is against manipulations by favorable assumptions by the user. Even though objectiveness is not an independent factor, it is explicitly considered because of its importance.

4.2.2 Return on Investment

A common metric to evaluate the benefit of an investment is the return on investment (ROI) [22; 119]. The ROI is the ratio of the cash flows of the generated return $\mathrm{CF}_{\mathrm{return}}$ (4.16) over the entire depreciation period T_{Dep} against the investment (4.17). A value of 1 means that the return and investment are equal. Values below 1 denote a deficient investment and values above 1 mean that the investment achieves positive returns.

$$\mathrm{return} = \sum_{T_{\mathrm{Dep}}} \mathrm{CF}_{\mathrm{return}} \tag{4.16}$$

$$\mathrm{ROI} = \frac{\mathrm{return}}{\mathrm{investment}} \tag{4.17}$$

The ROI is a meaningful measure because the savings/revenues are included. However, the time delay of the return is not discounted. The ROI is easily applicable to a range of applications and storage technologies. Savings can be treated as revenue and allows the analysis of investment deferral. It exhibits high clarity because the ROI is a common metric that is understandable. Its ease of use is of medium quality because quite some assumptions are required to predict the future revenue of the BESS. This includes future electricity prices and future storage prices in case of replacement costs.

The objectiveness of the ROI can be quite low. This is especially relevant if the assumptions are not clearly stated. In such a case, the figure can be misleading. Another issue is the disregard of the time factor for the economic value of cash flows.

4.2.3 Payback Period

The payback period (PP) gives the number of years, when the cumulated cash flow of the earnings of the years n beginning with the first year surpasses the investment (4.18) [121; 122]. The shorter the payback period is, the more attractive the investment is.

$$\text{investment} = \sum_{n}^{\text{PP}} \text{CF}_{\text{return}} \tag{4.18}$$

The payback period has a low to medium meaningfulness. It presumes positive returns and only considers the time period until cumulated return and investment are equal. Any economic implication after that period is neglected, therefore neither aging is not correctly considered, nor are future cash flows discounted. The metric is easy to understand and illustrates the quality of the investment. It is also easy to use without the need to assume a depreciation period or interest rate. Required assumptions are limited to future cost and revenue. In case of assessing the economic value of BESS for deferral of grid reinforcement, the payback period is not applicable because grid deferral does not generate regular revenue. The applicability of the payback period is therefore low.

The objectiveness of the payback period is at a medium level because any revenue potential that arises after the payback period is dismissed. The comparably low number of required assumptions reduce the options for manipulating the result.

4.2.4 Net Present Value

The net present value (NPV) describes the sum of all projected cash flows of the regarded period T_{Dep}, discounted to today's value (4.19) [118]. The interest rate r_i is required for the NPV and all metrics based on the NPV.

$$\text{NPV} = \sum_{n}^{T_{\text{Dep}}} \text{CF}_{\text{return}} \cdot (1 + r_i)^{-n} - \text{investment} \tag{4.19}$$

The NPV exhibits medium meaningfulness. It is good in terms of absolute valuation, but the value is not related to the required investment to achieve the NPV. In terms of clarity, the NPV is also average. No relation to the required investment and the introduction of the interest rate as an additional parameter degrade the clarity. The NPV is rather complex to use. The number of required assumptions, such as depreciation period, interest rate, and future prices require upfront thoughts and consideration. In terms of applicability, the NPV is similar to the ROI. It is well suitable to include parameters and constraints and not limited to certain applications or scenarios.

The NPV shows medium objectiveness, because of the detachment from the investment. Together with the number of parameters and assumptions, the NPV can be manipulated.

The annuity of an investment is another metric, similar to the NPV. It calculates the NPV to even, annual cash flows (4.21), based on the interest rate and the time period (4.20) [48]. The reference to a single year allows easier comparison of different investments with diverse depreciation periods. It is

treated and evaluated equally to the NPV in this thesis.

$$r_{\text{annuity}} = \frac{(1+r_i)^T_{\text{Dep}} \cdot r_i}{(1+r_i)^T_{\text{Dep}} - 1} \tag{4.20}$$

$$\text{annuity} = r_{\text{annuity}} \cdot \text{NPV} \tag{4.21}$$

4.2.5 Levelized Cost of Energy Stored

A widespread metric that describes the cost-effectiveness of BESS is the levelized cost of energy stored (LCOES) [46; 112; 113]. It denotes the total cost of ownership (TCO) for the BESS divided by the total delivered energy $E^{\text{out}}_{\text{BESS}}$ (4.22). The total cost of ownership is the sum of all cash flows, including investment cost, operating cost, and revenues/savings.

$$\text{LCOES} = \frac{\text{TCO}}{\text{E}^{\text{out}}_{\text{BESS}}} \tag{4.22}$$

The LCOES is based on the LCOE that describes the cost of generating energy. Naumann introduced sub-types of the LCOES that refer to the earnings and profit [28]. Further modifications with regard to the reference energy have also been proposed. The profit per energy installed correlates the profit to the nominal energy of the BESS, instead of the delivered energy.

The LCOES is a general financial figure, as only little assumptions for the application is required. The revenue achieved by the BESS is disregarded and the metric is good to technically compare different ESS.

Because of the disregard of the revenue, the metric is not very meaningful. It does not reflect the context of the BESS operation. The reference towards energy describes power-based applications, such as primary control reserve, incorrectly. Because the LCOE is a known metric for the cost of generated energy, the derived LCOES has a high clarity. It is an understandable metric in the energy sector and is established in the industry already. The figure is easy to use because only few assumptions are required, compared to other metrics. Only parameters relevant for the costs are required, namely the future cost and the depreciation period T_{Dep}. The LCOES is not generally applicable because it only considers the costs and ignores the revenues, achieved by the BESS.

The high clarity and favorable ease of use give the impression that the metric exhibits a rather high objectiveness. However, the seemingly fixed assumptions can be modified. The impact of the depreciation period and the provided energy can be easily concealed, as demonstrated by Pawel [112]. The author compares three different storage technologies and concludes that redox-flow batteries exhibit the lowest LCOES. Careful analysis of the paper reveals that 365 cycles per year and a power of 1 MW are assumed for all technologies, but the redox-flow system provides four times more energy than the reference systems, hence the denominator for the LCOES is four times higher.

4.2.6 Internal Rate of Return

The internal rate of return (IRR) is a hypothetical rate so that the return of the BESS over the depreciation period T_{Dep} discounted with the IRR amounts to the initial investment (4.23) [120].

$$\text{investment} = \sum_{n}^{T_{\mathrm{Dep}}} \frac{\mathrm{CF}}{(1+\mathrm{IRR})^n} \tag{4.23}$$

The IRR yields a good trade-off with regard to accuracy against the number of required assumptions. Financial constraints or cost caused by the replacement of the battery may render the IRR useless because the IRR yields multiple solutions.

The metric has a high meaningfulness, but the replacement of the battery may prevent the applicability of the IRR. The IRR exhibits a medium clarity, as it is a common financial metric, but more complicated to explain than the ROI, NPV, or the LCOES. It is medium with regard to the ease of use, as no interest rate assumption is required. The IRR is also well applicable to different analyses and assumptions.

The objectiveness is on a medium level because the number of parameters allows a rather easy manipulation of the results. However, omitting the interest rate eliminates one factor that allows subtle manipulation of results.

4.2.7 Profitability Index

The ROI and NPV, introduced above, each have weaknesses. While the ROI does not take into account the time fade of financial value, the NPV does not put investment and revenue into context. The profitability index or NPV per EUR invested (PI) combines both metrics and compensates for both disadvantages [37]. Similar to the ROI, the PI is the ratio of the sum of all cash flows within the depreciation period and the investment. The PI additionally discounts all cash flows to the NPV (4.24).

$$\mathrm{PI} = \frac{\mathrm{NPV}}{\text{investment}} \tag{4.24}$$

The PI has a high meaningfulness, as it combines both ROI and NPV. Both, accuracy by discounting the cash flows and context to the required investment are given. The clarity of the metric is high. It is similar to the ROI and therefore comparably easy to understand, but the combination with NPV may be confusing. Because of the high amount of required assumptions, the PI features a low ease of use. Similarly to both ROI and NPV, the PI is well applicable and well suitable to include varying conditions and circumstances.

The large number of assumptions degrade the objectiveness of the metric to a medium level. Unlike the NPV, it properly accounts for the amount of required investment and in addition, considers the time factor.

4.3 Concluding Economic Metrics

None of the metrics can be the sole value for the decision on whether to purchase a BESS or not, but several metrics and numbers need to be considered, instead. There is no clarity on which metric to

use. Table 4.1 gives an overview of the qualitative comparison of the economic metrics presented.

Table 4.1: Qualitative assessment of economic metrics for evaluation of energy storage systems.

	Meaningfulness	Clarity	Ease of use	Applicability	Objectiveness
ROI	**	***	**	***	*
PP	*	**	***	*	**
NPV	**	**	*	***	**
LCOES	*	***	***	*	**
IRR	***	**	**	***	**
PI	***	***	*	***	**

The requirement for comparisons based on any metric is that the assumptions are identical for each case. Future cost and revenue projections are required for all metrics, to correctly asses the cash flows and replacement costs. This requires an elaborate, technical simulation of the BESS to accurately consider declining BESS performance, caused by aging. Aging, future revenue, and cost are important for the reliability of the results but are uncertain.

5 Carbon Emissions

This chapter covers the carbon emissions associated with producing and operating BESS. First, the life-cycle assessment method is presented in Section 5.1. An approximation for the production-induced emissions of a BESS is derived in Section 5.2. The impact of operating BESS on the GHG emissions are derived for the applications PV-home storage, peak-shaving and hybrid renewable-diesel island grid in Section 5.3.

5.1 Life-Cycle Assessment

The life-cycle assessment (LCA) is a systematic method to determine the environmental impact of a product. It is a well-established and internationally acknowledged method, defined in the ISO standards 14040 and 14044 [139]. The life-cycle assessment calculates environmental and human health impacts, as well as resource depletions which result from the necessary processes over the whole life-cycle of a product or process, including its inputs (materials, energy) and outputs (emissions, waste). Manufacturing with its upstream processes and all energy requirements throughout the life-cycle are included. The upstream processes are processes that happen before those that are directly linked to the item or system to be assessed, such as raw material extraction, the energy required for extraction, production steps, and disposal at the end of life.

The method requires an accurate accounting of all energy and emissions related to the construction, operation, and decommissioning of the system, as well as environmental impacts resulting from these. This requires a complete bill of material and energy balances for each component of the system, including its manufacturing and installation.

The end of life of Li-ion BESSs is not considered in this thesis because of non-established recycling infrastructures. However, studies on recycling of batteries for electric vehicles show that especially for resource depletion and acidification a high reduction can be expected [140–145], while the energy savings and GWP are determined by the chosen recycling process [129]. The life-cycle inventory (LCI) data sources vary. Studies, reports, and the *ecoinvent* database [146] are utilized for the life-cycle inventory.

The GWP in CO_2eq is chosen for the life-cycle impact analysis (LCIA). Both, IPCC2007 standard [147] and IPCC2013 standard [148] are applied for the GWP-assessment. The mean value of both standards is used in this thesis. The system boundary includes cradle-to-gate stage processes, i.e. raw materials extraction, materials processing, product manufacture, transportation, and installation [125; 126; 128; 129; 132; 134; 137; 149]. The life-cycle assessment is used in this thesis to quantify the impact of BESS in the production and use-phase.

5.2 Production Induced Carbon Emissions

The *Energy Neighbor* is used as example system with an existing bill of materials. The system weighs about 7 t and has eight independent inverters. Six 36 kW and two 16 kW inverters are used in the system. The energy capacity of the LFP:C batteries amounts to 192 kWh. Monitoring and control electronics are included in the analysis. A bottom-up approach for estimating the carbon emissions of the production has been conducted. The components have been itemized and each component's CO_2eq emission has been estimated based on existing literature values or by their material composition.

Robert Hierle collected most of the data and conducted the first analyses in his master thesis [150]. The author of this thesis continued the work and generalized the findings.

5.2.1 Breakdown of Components

The components of the *Energy Neighbor* are itemized in this Section and each component's production-induced emissions are calculated. The results are used for a bottom-up approximation of the carbon emissions of the overall BESS.

5.2.1.1 Mass of Battery Storage System

The mass composition of *Energy Neighbor* is given in Figure 5.1. Total weight of the BESS is 7 t. Batteries amount to 4 t of the mass, that is a share of 57.2%. The inverters contribute to the mass with 227 kg, including relevant components for operation. This corresponds to only 3.2% of the total BESS mass. Electronic components for safety, monitoring, control, and all other functions add about 367.6 kg to the BESS mass. That is a contribution of 5.3%. The last large component is the ISO-container that contributes 34.3% of the overall mass with a weight of 2.4 t.

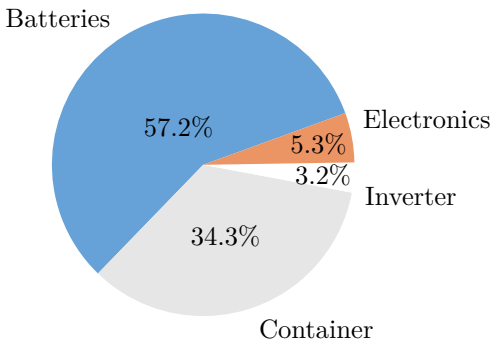

Figure 5.1: Mass composition of the *Energy Neighbor*. Its total weight is 7 t.

5.2.1.2 Emissions of Producing Battery Cells

Emissions of different battery-technologies are given in Table 5.1. These energy specific values are taken from a review of Peters *et al.* [151]. The LFP:C-batteries with 192 kWh of nominal energy capacity have a mass of about 4 t. This includes the connectors, mechanical attachment, and housing components of the battery module and rack.

Table 5.1: Energy-specific emission factors per kWh of energy capacities for battery technologies [151].

	Spec. emissions ($kg\,CO_2eq/kWh$)		
Technology	Min.	Avg.	Max.
LFP	30	161	275
NMC	40	160	245
NCA	50	116	170

The emissions caused by producing the batteries are obtained by multiplication of the energy-specific emission factor $\rho_{\text{batt}}^{\text{man}}$ and the nominal energy capacity $E_{\text{batt}}^{\text{nom}}$ (5.1). The resulting total emissions based on the energy capacity and energy specific values in Table 5.1 caused by producing the batteries in the *Energy Neighbor* amount to 5.8 to 52.8 $t\,CO_2eq$. The emissions with the average value is 30.9 $t\,CO_2eq$.

$$\epsilon_{\text{batt}} = \rho_{\text{batt}}^{\text{man}} \cdot E_{\text{batt}}^{\text{nom}} \tag{5.1}$$

The values strongly vary because of a comparably weak basis of original life-cycle inventory data. Not only is original inventory data scarce, but the studies investigated by Peters *et al.* made different assumptions regarding the manufacturing energy demand. The choice of the battery chemistry has a smaller influence on the environmental performance than the assumptions for the energy demand of the manufacturing processes. [151]

5.2.1.3 Emissions of Producing Inverters

The CO_2eq emissions emitted by the production of inverters are estimated based on values of specific inverter sizes, given in the *ecoinvent* database and publications (Table 5.2) [146; 149; 152]. The inverter values from the *ecoinvent* database are condensed to the mean value of IPCC2007 and IPCC2013 with a global market share of 32% in Europe and 68% for the rest of the world. This impacts the assumed energy mix for the production processes.

Table 5.2: Production emissions of reference inverters [146; 149; 152].

Nominal power	kW	0.5 [146]	2.5 [146]	7.5 [149]	100 [152]	500 [146]
IPCC 2007	$kg\,CO_2eq$	48.01	237.70	-	-	14,180
IPCC 2013	$kg\,CO_2eq$	48.96	242.80	-	-	14,510
Mean emissions	$kg\,CO_2eq$	48.49	240.25	612	3978	14,345
Spec. emissions	$kg\,CO_2eq/kW$	96.97	96.10	81.60	39.78	28.69

The power-dependent emissions are approximated with a logarithmic function (5.2). The original curve describes the embodied energy for the production of inverters [153]. It is adapted to represent the carbon emissions of inverter manufacturing.

$$\rho_{\text{inv}}^{\text{man}} = -b \cdot \ln\left(\frac{P_{\text{inv}}^{\text{nom}}}{\text{kW}}\right) + c \tag{5.2}$$

The parameters b and c are fit to minimize the mean squared error (MSE) of the curve and the data values to $\text{MSE} = 45.88\,(kg\,CO_2eq/kW)^2$ (Figure 5.2). The best fit is achieved for $b = 11.23\,kg\,CO_2eq/kW$ and $c = 97.96\,kg\,CO_2eq/kW$.

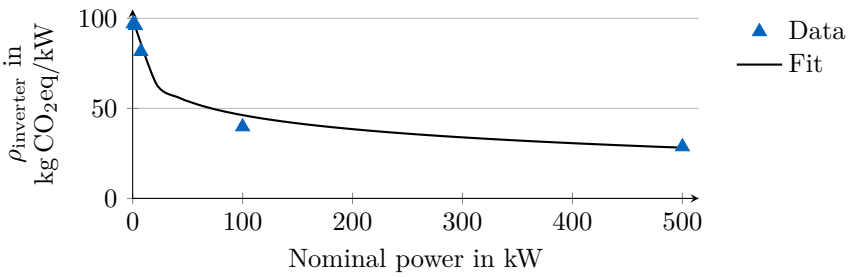

Figure 5.2: Power-specific emissions of inverters. The blue line depicts the function fit, the blue triangles are the reference values [146; 149; 152].

The total CO_2eq emissions for each of the inverter are calculated with (5.3). The total CO_2eq emissions of the inverters installed in the *Energy Neighbor* amount to 14.6 t CO_2eq.

$$\epsilon_{\text{inv}} = \rho_{\text{inv}}^{\text{man}} \cdot P_{\text{inv}}^{\text{nom}} \tag{5.3}$$

5.2.1.4 Emissions of Producing Auxiliary Electronics

The estimation of the electronic components has been conducted with several approaches. Devices such as circuit breaker, relays, or contactors have been disassembled and the materials have been weighed. The emissions for the materials are then summed according to their mass portion for the estimated total carbon emissions of the respective device. Other devices, such as processors have been estimated with similar components found in the *ecoinvent* database [150].

The chosen approaches are associated with uncertainties regarding the results. As the mass of the electronic components amounts to only 5.3% of the overall mass, the inaccuracy's impact is neglected. The estimated carbon emission caused by auxiliary electronic components add up to 2.50 t CO_2eq in the minimum case and to 3.79 t CO_2eq in the maximum case, respectively.

5.2.1.5 Emissions of the System Housing

The last component of the *Energy Neighbor* is the container that accounts for 34.3% of the BESS mass with its 2.4 t. It is made of steel and the weight-specific emission factor is estimated at 5.9 kg CO_2eq/kg to 7.2 kg CO_2eq/kg. The total carbon emissions caused by producing a container of this mass amounts to 14.16 t CO_2eq up to 17.28 t CO_2eq.

5.2.2 Emissions of a Battery Storage System

The obtained results of analyzing the *Energy Neighbor* with a bottom-up approach are summarized in this Section and compared to available numbers found in literature to ensure plausibility.

5.2.2.1 Emissions of Producing the Energy Neighbor

The carbon emissions induced by producing a BESS similar to the *Energy Neighbor* add up to 37.1 t CO_2eq in the minimum case, 88.5 t CO_2eq in the maximum case, and amount to 64.35 t CO_2eqwith average values. The fraction of the components batteries, inverter, electronics, and the container are

shown in Figure 5.1. Assuming the lower emissions case, the inverters and housing cause the major share of the carbon emissions (77%), while the battery emissions only amount to 16%. In the upper emissions case the batteries contribute to 60% of the emissions and 48% in the average case.

The resulting emissions amount to 193.2 t CO_2eq to 460.9 t CO_2eq per MWh nominal energy capacity of the *Energy Neighbor*, with an average of 335.2 t CO_2eq per MWh. It would need to replace 193 to 576 times its energy capacity of coal-generated electricity ($\rho_{coal} = 0.8 - 1.0\,t/MWh_{el}$) to make up for the production emissions.

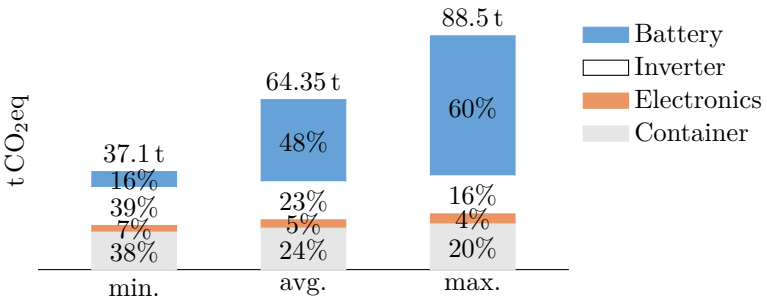

Figure 5.3: Production emissions of the *Energy Neighbor* with LFP:C batteries.

5.2.2.2 Comparison with other Systems

A life-cycle assessment for a 5 MW BESS with a nominal energy capacity of 5 MWh has been conducted by Koj *et al.*, but no absolute numbers are given [154]. In their case, battery cells and inverter contribute to 50% of the carbon emissions. Their BESS is situated in a concrete building instead of a stainless steel container and the respective emissions are calculated. This leads to lower carbon emission contributed by the housing. The remaining components' contributions to the carbon emissions are of the same magnitude.

Immendoerfer *et al.* [126] conducted the life-cycle assessment for a pumped hydro storage and a BESS in comparison. They do not give explicit absolute numbers for the final result, but they assume an annual energy output of 1855 GWh/a and total losses of 0.379 MWh per MWh of energy generated for the BESS. The total losses include internal energy consumption, e.g. ventilation and lighting of the system. With the given relative shares of more than 90% of the carbon emissions caused by the system losses, the resulting overall GWP of the BESS is 38,870 Mt CO_2eq, including its use-phase. The contribution of the production amounts to 4-5%. Scaling the resulting emissions of the BESS down to a BESS with a nominal capacity of 1 MWh and nominal power of 1 MW by simple division results in about 155 t CO_2eq to 195 t CO_2eq per MWh.

The numbers are 20% to 58% lower than the values obtained from the *Energy Neighbor*. Beside uncertainties, different system design could be the reason for the deviation. The prototype system *Energy Neighbor* has an unusually high nominal power and uses several small inverters that have higher power-specific emissions (see Figure 5.2). Smaller total inverter size and fewer, larger inverters would equalize the carbon emissions of the systems. Other issues are the uncertain data sets. The specific emissions for the LFP:C batteries, for example, deviate by a factor of almost 10.

5.2.3 Generalized Approximation of Production Emissions of Battery Storage Systems

Based on the findings of the *Energy Neighbor*, an approximation of the production induced emissions of BESS, in general, is derived. The emissions of producing BESS with different sizes and battery technologies can be approximated.

The battery is linearly scaled with its nominal energy capacity (5.1). The mean values for the energy-specific emission factors from Table 5.1 apply and are listed in Table 5.3.

The inverters are scaled according to (5.3) depending on the structure of the system. Several inverters in a system are each calculated with their individual emissions according to their nominal power and summed.

The BESS is assumed to be situated in 20' ISO-containers. The container is estimated to have sufficient space for a certain energy capacity of batteries $E^{\text{max}}_{\text{housing}}$. The maximum capacity of the container to accommodate LFP:C batteries is roughly estimated to 300 kWh. Other battery technologies are estimated by scaling according to their energy densities w. The estimated maximum energy capacity in a container for different battery technologies is given in Table 5.3.

Table 5.3: Battery parameters for emission approximation.

		LFP	NMC	NCA
Energy density [22]	kWh/m^3	278	355	676
Container capacity	kWh	300	383	728

The total number of containers for hosting a larger energy capacity is taken into account together with the gravimetric emission factor $\rho^{\text{man}}_{\text{container}}$ and the mass of one container $m_{\text{container}}$ (5.4). Using fixed, concrete buildings for containing the batteries would reduce the carbon emissions, but is not further regarded in this thesis.

$$\epsilon_{\text{housing}} = \rho^{\text{man}}_{\text{container}} \cdot m_{\text{container}} \cdot \left\lceil \frac{E^{\text{nom}}_{\text{BESS}}}{E^{\text{max}}_{\text{housing}}} \right\rceil \tag{5.4}$$

The auxiliary components have a comparably small contribution to the overall system's emission and are accounted with a share of $r_{\text{aux}} = 7\%$ of the total BESS emissions (5.5).

$$\epsilon_{\text{aux}} = \frac{r_{\text{aux}}}{1 - r_{\text{aux}}} \cdot (\epsilon_{\text{batt}} + \epsilon_{\text{inv}} + \epsilon_{\text{housing}}) \tag{5.5}$$

The total emissions for the production of BESS are the sum of the components' emissions (5.6). It depends on the battery technology, the system's nominal energy capacity, and the number of inverters and their nominal power. Emissions of housing and auxiliary components are included in the equation.

$$\epsilon^{\text{man}}_{\text{BESS}} = \epsilon_{\text{batt}} + \epsilon_{\text{inv}} + \epsilon_{\text{housing}} + \epsilon_{\text{aux}} \tag{5.6}$$

5.3 Calculating Emissions of Operating Battery Storage Systems

The emissions of RES include the production and installation of the respective generator. The necessary balance of system (BOS) components, i.e. support structures, electronics, cables, and inverters are considered. This approach has been performed by Peng *et al.* for PV systems [155]. While the emissions of producing and installing the generator can be apportioned to the generated electricity, this approach is not straightforward for BESS. The energy discharged from BESS is determined by their application and their operation strategy. The emissions of producing and installing BESS is explicitly excluded in this Section, but the impact of operating BESS on the use of the generated energy is the key subject. Similarly, the emissions of diesel generators are limited to the emissions of fuel consumption, as the operation depends on the operation strategy in the regarded applications.

5.3.1 PV-Home Storage

The aim of a PV-home storage is to reduce the energy purchase from the electricity grid and thus achieve a higher self-sufficiency rate for the household. The energy flow of a PV-home with storage is illustrated in Figure 5.4. The fundamental principle of the PV-home storage emissions has been published before [31]. The topic is further discussed in this Section.

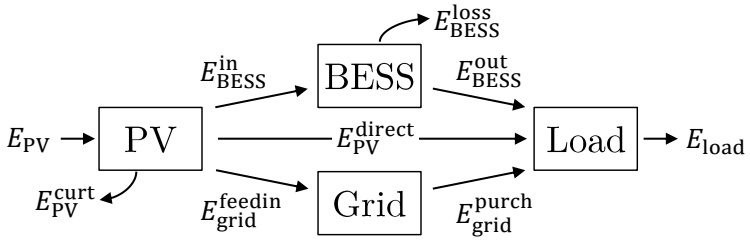

Figure 5.4: Illustration of energy flows in PV-Home with BESS.

The PV-generated energy E_{PV} provides the load directly $E^{\text{direct}}_{\text{PV}}$, feeds the grid $E^{\text{feedin}}_{\text{grid}}$, is curtailed $E^{\text{curt}}_{\text{PV}}$, or charges the BESS $E^{\text{in}}_{\text{BESS}}$ (5.7). The load E_{load} is supplied directly by the PV-unit $E^{\text{direct}}_{\text{PV}}$, by the grid $E^{\text{purch}}_{\text{grid}}$, or by the BESS $E^{\text{out}}_{\text{BESS}}$ (5.8). The regulations for PV-home storage in Germany stipulate that the BESS may only charge surplus PV-generated energy and discharge $E^{\text{out}}_{\text{BESS}}$ only to provide the household load.

$$E_{\text{PV}} = E^{\text{direct}}_{\text{PV}} + E^{\text{feedin}}_{\text{grid}} + E^{\text{curt}}_{\text{PV}} + E^{\text{in}}_{\text{BESS}} \tag{5.7}$$

$$E_{\text{load}} = E^{\text{direct}}_{\text{PV}} + E^{\text{purch}}_{\text{grid}} + E^{\text{out}}_{\text{BESS}} \tag{5.8}$$

The load E_{load} and the directly consumed PV-generated energy $E^{\text{direct}}_{\text{PV}}$ are independent of the BESS operation, hence identical for PV-homes with and without BESS. The motivation for increasing the self-consumption in Germany, besides financial benefits, is the reduction of the carbon footprint of the household ϵ_{load} [40]. The emissions caused by the load ϵ_{load} consist of the emissions of the purchased grid energy $\epsilon^{\text{purch}}_{\text{grid}}$, the PV-generated energy $\epsilon^{\text{direct}}_{\text{PV}}$, and the BESS stored energy ϵ_{BESS} (5.9). The purchased energy is generated and causes emissions with the average grid emission factor ρ_{grid}.

Operating a BESS to increase the self-consumption leads to increased battery energy output $E^{\text{out}}_{\text{BESS}}$

and therefore reduces the emissions caused by the household's load ϵ_{load} because a larger share of the load is supplied by the PV-generated energy, instead of grid-purchased electricity (5.10). The claim that the BESS lowers its owner's carbon footprint, is therefore correct on a local scope and the conclusion is similar to the analysis of the island grid (Section 5.3.3).

$$\begin{aligned}
\epsilon_{\text{load}} &= \epsilon_{\text{grid}}^{\text{purch}} + \epsilon_{\text{PV}}^{\text{direct}} + \epsilon_{\text{BESS}} = \\
&= E_{\text{grid}}^{\text{purch}} \cdot \rho_{\text{grid}} + E_{\text{PV}}^{\text{direct}} \cdot \rho_{\text{PV}} + E_{\text{BESS}}^{\text{in}} \cdot \rho_{\text{PV}} = \\
&= \left(E_{\text{load}} - E_{\text{PV}}^{\text{direct}} - E_{\text{BESS}}^{\text{out}}\right) \cdot \rho_{\text{grid}} + E_{\text{PV}}^{\text{direct}} \cdot \rho_{\text{PV}} + \frac{1}{\eta_{\text{BESS}}} \cdot E_{\text{BESS}}^{\text{out}} \cdot \rho_{\text{PV}} = \\
&= E_{\text{load}} \cdot \rho_{\text{grid}} - E_{\text{PV}}^{\text{direct}} \cdot (\rho_{\text{grid}} - \rho_{\text{PV}}) - \left(\rho_{\text{grid}} - \frac{\rho_{\text{PV}}}{\eta_{\text{BESS}}}\right) \cdot E_{\text{BESS}}^{\text{out}} \qquad (5.9)
\end{aligned}$$

$$\epsilon_{\text{BESS}} = -\left(\rho_{\text{grid}} - \frac{\rho_{\text{PV}}}{\eta_{\text{BESS}}}\right) \cdot E_{\text{BESS}}^{\text{out}} \qquad (5.10)$$

As the reduction of greenhouse gas emissions is not a local issue, a broader scope needs to be considered. The discourse above does not take into account the interaction of the PV-home's grid feed-in energy. This effect is therefore considered in the following derivation. This step is crucial for the final conclusion and represents the key difference to the island case, where increasing the self-sufficiency rate is essential for the BESS to reduce the carbon emissions of operating the hybrid renewable-diesel island grid.

The feed-in energy is assumed to displace fossil-fuel generated electricity. The feed-in energy is generated with an emission factor of the PV-unit ρ_{PV} and replaces the same amount of energy that would have been generated with the average emission factor of the grid ρ_{grid}. The emissions of producing and installing PV-units are converted to the total energy generation over the PV-units' cycle lives to obtain the emission factor ρ_{PV}. Energy curtailment is included in this conversion and treated as generated energy for the emission calculation.

Considering the energy balance of the PV-generated energy (5.7), we obtain the emission reduction by grid feed-in electricity (5.11). The generated energy E_{PV} could replace the grid energy. The actual displaced grid energy requires discounting curtailment $E_{\text{PV}}^{\text{curt}}$, direct PV-supply $E_{\text{PV}}^{\text{direct}}$, and BESS-stored energy $E_{\text{BESS}}^{\text{in}}$.

$$\begin{aligned}
\epsilon_{\text{feedin}} &= E_{\text{grid}}^{\text{feedin}} \cdot (\rho_{\text{PV}} - \rho_{\text{grid}}) = && \text{with (5.7)} \\
&= \left(E_{\text{PV}} - E_{\text{PV}}^{\text{direct}} - E_{\text{PV}}^{\text{curt}} - E_{\text{BESS}}^{\text{in}}\right) \cdot (\rho_{\text{PV}} - \rho_{\text{grid}}) && (5.11)
\end{aligned}$$

Equation (5.11) applies if the amount of imported and exported energy does not significantly influence ρ_{grid}. This is fulfilled for this case because the amount of energy produced by the household's PV-unit (several MWh) is smaller by a factor of 10^8 compared to the traded energy in Germany (several 100 TWh) [156].

The resulting net-emissions of a PV-home without BESS ϵ_{home} are determined by the load E_{load}, the PV-generated energy E_{PV}, and the curtailed energy $E_{\text{PV}}^{\text{curt}}$ (5.12).

$$\begin{aligned}
\epsilon_{\text{home}} &= \epsilon_{\text{load}} + \epsilon_{\text{feedin}} && \text{with (5.9) and (5.11)} \\
&= E_{\text{load}} \cdot \rho_{\text{grid}} + \left(E_{\text{PV}} - E_{\text{PV}}^{\text{curt}}\right) \cdot (\rho_{\text{PV}} - \rho_{\text{grid}}) && (5.12)
\end{aligned}$$

Operating PV-home storage causes a reduction of the purchased grid energy $E_{\text{grid}}^{\text{purch}}$, as well as a

decrease of the feed-in grid energy $E_{\text{grid}}^{\text{feedin}}$. Reducing the purchased grid energy leads to reduced generation of fossil-fuel-based electricity, while a reduction of the feed-in grid energy decreases the amount of fossil-fuel-based electricity that is displaced by PV-energy. Concluding the equations (5.9) and (5.11) reveal that the BESS influences the net emissions of a PV-home $\epsilon_{\text{home,BESS}}$ both positively and negatively (5.13).

$$
\begin{aligned}
\epsilon_{\text{home,BESS}} &= \epsilon_{\text{load}} + \epsilon_{\text{feedin}} = \\
&= E_{\text{load}} \cdot \rho_{\text{grid}} - E_{\text{PV}}^{\text{direct}} \cdot (\rho_{\text{grid}} - \rho_{\text{PV}}) - E_{\text{BESS}}^{\text{out}} \cdot \left(\rho_{\text{grid}} - \frac{\rho_{\text{PV}}}{\eta_{\text{BESS}}} \right) + \\
&\quad + \left(E_{\text{PV}} - E_{\text{PV}}^{\text{direct}} - E_{\text{PV}}^{\text{curt}} - E_{\text{BESS}}^{\text{in}} \right) \cdot (\rho_{\text{PV}} - \rho_{\text{grid}}) = \\
&= E_{\text{load}} \cdot \rho_{\text{grid}} - E_{\text{PV}} \cdot (\rho_{\text{grid}} - \rho_{\text{PV}}) - E_{\text{BESS}}^{\text{out}} \cdot \left(\rho_{\text{grid}} - \frac{\rho_{\text{PV}}}{\eta_{\text{BESS}}} \right) + \\
&\quad + \frac{E_{\text{BESS}}^{\text{out}}}{\eta_{\text{BESS}}} \cdot (\rho_{\text{grid}} - \rho_{\text{PV}}) + E_{\text{PV}}^{\text{curt}} \cdot (\rho_{\text{grid}} - \rho_{\text{PV}}) = \\
&= E_{\text{load}} \cdot \rho_{\text{grid}} - E_{\text{PV}} \cdot (\rho_{\text{grid}} - \rho_{\text{PV}}) + E_{\text{BESS}}^{\text{out}} \cdot \left(\frac{1}{\eta_{\text{BESS}}} - 1 \right) \cdot \rho_{\text{grid}} + \\
&\quad + E_{\text{PV}}^{\text{curt}} \cdot (\rho_{\text{grid}} - \rho_{\text{PV}})
\end{aligned}
\tag{5.13}
$$

The BESS emissions are the difference between the home case without BESS (5.12) and with BESS (5.13) are determined by the energy provided $E_{\text{BESS}}^{\text{out}}$. The non-perfect efficiency η_{BESS} increases the emissions, while a reduction of energy curtailment $\Delta E_{\text{PV}}^{\text{curt}}$ decreases the carbon emissions (5.14). The reduction of the energy curtailment is determined by the system's operation strategy.

$$
\epsilon_{\text{BESS}} = E_{\text{BESS}}^{\text{out}} \cdot \left(\frac{1}{\eta_{\text{BESS}}} - 1 \right) \cdot \rho_{\text{grid}} - \Delta E_{\text{PV}}^{\text{curt}} \cdot (\rho_{\text{grid}} - \rho_{\text{PV}}) \tag{5.14}
$$

The Sankey diagrams of the energy flows for a PV-home without and with storage are illustrated in Figure 5.5. Green color denotes the energy from PV-generation. Red energy flows depict the energy losses. Energy flows in grey illustrate the energy purchase from the grid. Blue bars illustrate the usage of the energy.

A large share of PV-generated energy is fed into the grid without PV-home storage (Figure 5.5 (a)). The timing mismatch of PV-generation and load is compensated by grid purchase to supply the load and with grid feed-in to use the PV-generated energy. Curtailment of the PV-generated power because of regulatory curtailment limits and grid losses contribute to the overall energy losses.

The energy flow looks different for a PV-home with storage (Figure 5.5 (b)). The BESS stores part of the PV-generated energy that does not coincide with the household's load. The energy is later used to provide the household consumption and consequently reduce the grid-purchased energy. While the reduction of the grid-purchased energy reduces the electricity costs, the energy feed-in into the grid is likewise reduced, diminishing the revenue obtained by feed-in remuneration. The reduction of energy curtailment has a positive effect on the energy efficiency of the PV-home, but may be dominated by the BESS-losses.

The optimal operation with regard to carbon emissions would be to minimize the BESS losses and at the same time minimize the PV energy curtailment. The consequent operation mode would be to

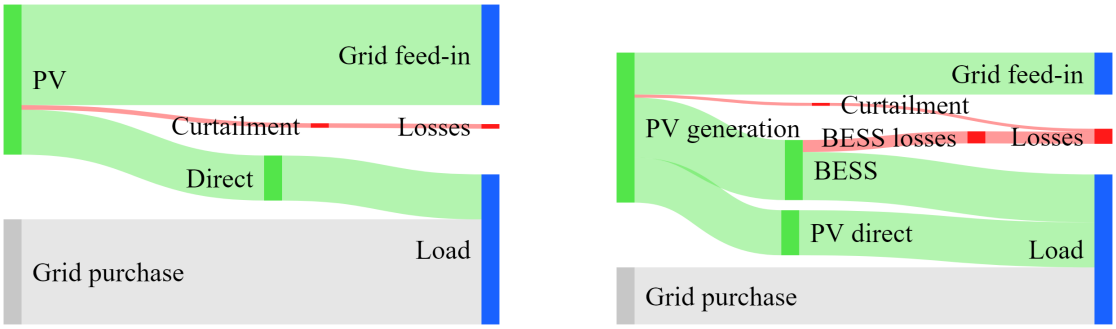

(a) (b)

Figure 5.5: Sankey diagram for PV-home without storage (a) and PV-home with storage to increase self-consumption (b).

only store otherwise curtailed PV energy. This is, however, not aligned with the financial incentives for PV-home storage.

Charging the BESS is not equal to avoiding wasting energy from RES. In the PV-home storage case, the PV-generated electricity is stored in the BESS for later use, instead of using the energy to provide another load in the grid. The BESS, in addition, causes energy losses. For this application to have a positive effect on the carbon emissions, the reduction of grid losses, and curtailment need to outweigh the BESS losses. Grid losses have not been considered, but only amount to 3.884% in Germany (2014), 6.3% in OECD countries (2015), and 9.6% in non-OECD countries (2015) [157; 158]. The case study (Section 6.1.2) shows that their contribution to the overall losses are much lower than curtailment and conversion losses.

5.3.2 Peak-Shaving

Peak-shaving is not usually associated with RES or carbon emissions. The goal is to reduce the peak power charge of the electricity bill. The implication for the carbon emissions is evaluated by comparing the deployment of BESS to two alternative options: First, the absolute impact of operating the BESS in this application is derived. The second assessment compares the carbon emissions of peak-shaving with a diesel generator.

The energy flow for peak-shaving is shown in Figure 5.6. The load is normally supplied by the grid. In the event of peaks that need to be avoided, the peak-shaving device, either diesel generator or BESS, provides power to reduce the grid load peak.

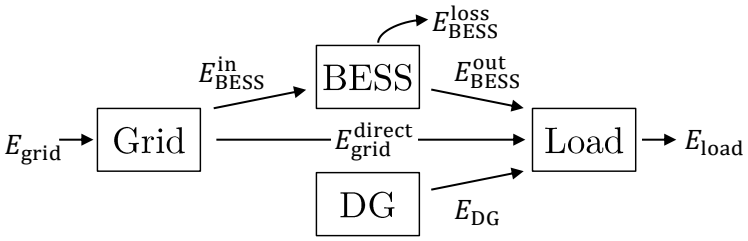

Figure 5.6: Illustration of energy flows for consumer with BESS for peak-shaving.

Providing the load peaks with the diesel generator reduces the amount of grid-purchased energy by

the amount of the diesel generator's energy output (5.15). The emissions of this case $\epsilon_{\mathrm{PS,DG}}$ consist of the purchased grid energy $E_{\mathrm{grid}}^{\mathrm{direct}}$ and the diesel generator's fuel consumption with the respective emission factors (5.16). The added emissions of peak-shaving with a diesel generator ϵ_{DG} amount to the diesel generator's operational emissions minus the displaced grid purchase (5.17).

$$E_{\mathrm{load}} = E_{\mathrm{grid}}^{\mathrm{direct}} + E_{\mathrm{DG}} \tag{5.15}$$

$$\begin{aligned}\epsilon_{\mathrm{PS,DG}} &= E_{\mathrm{grid}}^{\mathrm{direct}} \cdot \rho_{\mathrm{grid}} + E_{\mathrm{DG}} \cdot \frac{\rho_{\mathrm{DG}}}{\bar{\eta}_{\mathrm{DG}} \cdot \mathrm{LHV}} = \\ &= E_{\mathrm{load}} \cdot \rho_{\mathrm{grid}} + E_{\mathrm{DG}} \cdot \left(\frac{\rho_{\mathrm{DG}}}{\bar{\eta}_{\mathrm{DG}} \cdot \mathrm{LHV}} - \rho_{\mathrm{grid}} \right)\end{aligned} \tag{5.16}$$

$$\epsilon_{\mathrm{DG}} = E_{\mathrm{DG}} \cdot \left(\frac{\rho_{\mathrm{DG}}}{\bar{\eta}_{\mathrm{DG}} \cdot \mathrm{LHV}} - \rho_{\mathrm{grid}} \right) \tag{5.17}$$

For peak-shaving with a BESS the charging process needs to be considered. The overall load is supplied by the energy drawn from the grid $E_{\mathrm{grid}}^{\mathrm{direct}}$ and the BESS power output $E_{\mathrm{BESS}}^{\mathrm{out}}$ (5.18). The electricity purchase comprises the load energy E_{load} and the BESS system losses $E_{\mathrm{BESS}}^{\mathrm{loss}}$ (5.19). The overall emissions of this case $\epsilon_{\mathrm{PS,BESS}}$ are determined by the amount of electricity purchased from the grid (5.20). Thus the BESS increases the emissions ϵ_{BESS} because of its system losses (5.21).

$$E_{\mathrm{load}} = E_{\mathrm{grid}}^{\mathrm{direct}} + E_{\mathrm{BESS}}^{\mathrm{out}} \tag{5.18}$$

$$\begin{aligned}E_{\mathrm{grid}}^{\mathrm{purch}} &= E_{\mathrm{grid}}^{\mathrm{direct}} + E_{\mathrm{BESS}}^{\mathrm{in}} = \\ &= E_{\mathrm{load}} + E_{\mathrm{BESS}}^{\mathrm{loss}}\end{aligned} \tag{5.19}$$

$$\begin{aligned}\epsilon_{\mathrm{PS,BESS}} &= E_{\mathrm{grid}}^{\mathrm{purch}} \cdot \rho_{\mathrm{grid}} = \\ &= \left(E_{\mathrm{load}} + E_{\mathrm{BESS}}^{\mathrm{loss}} \right) \cdot \rho_{\mathrm{grid}}\end{aligned} \tag{5.20}$$

$$\begin{aligned}\epsilon_{\mathrm{BESS}} &= E_{\mathrm{BESS}}^{\mathrm{loss}} \cdot \rho_{\mathrm{grid}} = \\ &= \left(\frac{1}{\eta_{\mathrm{BESS}}} - 1 \right) \cdot E_{\mathrm{BESS}}^{\mathrm{out}} \cdot \rho_{\mathrm{grid}}\end{aligned} \tag{5.21}$$

Both peak-shaving cases are compared in the following. The premise is that both diesel generator and BESS need to provide the same energy for peak-shaving (5.22). Using a BESS compared to a diesel generator avoids diesel generator-generated energy, but grid electricity is used instead. The amount of grid electricity purchase is increased by the BESS system losses (5.23).

$$E_{\mathrm{PS}} = E_{\mathrm{DG}} = E_{\mathrm{BESS}}^{\mathrm{out}} \tag{5.22}$$

$$\begin{aligned}\Delta\epsilon_{\mathrm{BESS}} &= \epsilon_{\mathrm{DG}} - \epsilon_{\mathrm{BESS}} = \\ &= E_{\mathrm{PS}} \cdot \left(\frac{\rho_{\mathrm{DG}}}{\bar{\eta}_{\mathrm{DG}} \cdot \mathrm{LHV}} - \rho_{\mathrm{grid}} \right) - \left(\frac{1}{\eta_{\mathrm{BESS}}} - 1 \right) \cdot E_{\mathrm{PS}} \cdot \rho_{\mathrm{grid}} = \\ &= E_{\mathrm{PS}} \cdot \left(\frac{\rho_{\mathrm{DG}}}{\bar{\eta}_{\mathrm{DG}} \cdot \mathrm{LHV}} - \frac{\rho_{\mathrm{grid}}}{\eta_{\mathrm{BESS}}} \right)\end{aligned} \tag{5.23}$$

Sankey diagrams for peak-shaving with a diesel generator (Figure 5.7 (a)) and with a BESS (Figure 5.7 (b)) are given. Grey flows represent the energy drawn from the grid. The brown flow illustrates the diesel generator-generated energy. Red energy flows depict the occurring losses. The blue bar illustrates the use of electricity. The diesel generator consumes fuel to provide the electricity required

to execute peak-shaving. The generated energy replaces the same amount that would otherwise be drawn from the grid. The BESS for peak-shaving increases the overall electricity purchased by the grid because of the system losses.

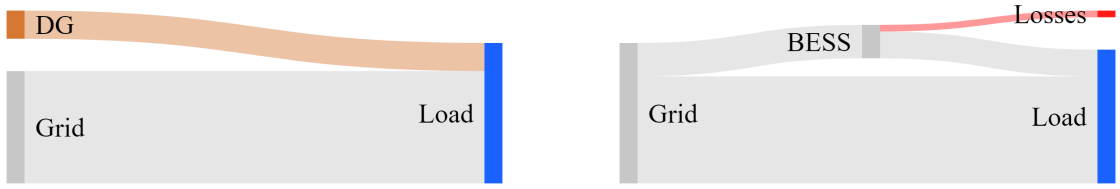

(a) (b)

Figure 5.7: Sankey diagram for peak-shaving with a diesel generator (a) and a BESS (b).

From a carbon emission focused point of view, peak-shaving only introduces energy losses that deteriorate with the system efficiency and increase the generated electricity. The composition fo the emissions are different for peak-shaving by a diesel generator and BESS. While diesel generator-generated electricity is expected to have a higher emission factor than the average electricity generation within the grid, the BESS losses need to be compensated by added energy generation of the power system.

5.3.3 Hybrid Renewable-Diesel Island Grids

BESS for hybrid renewable-diesel island grids increase the utilization of RES and reduce fossil-fuel based generation. Conventional generators provide the load, in times of insufficient RES-generation. The BESS's task is to store the excess RES-generated energy, that would otherwise be curtailed, and supply the load instead of the diesel generator. Figure 5.8 illustrates the simplified energy flows in an island grid. The following discussion of the principal mechanisms for the GWP neglects operational inefficiencies that require more diesel generator generation.

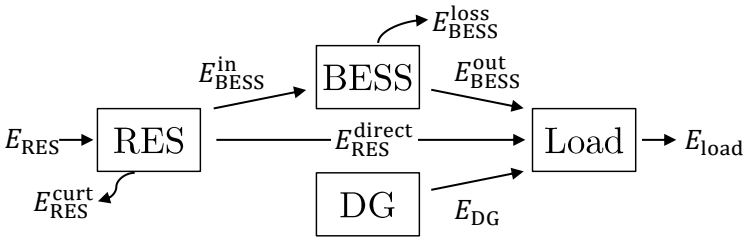

Figure 5.8: Illustration of energy flows in island grids with BESS.

RES-generated energy E_{RES} either directly provides the load $E^{\text{direct}}_{\text{RES}}$, is stored in the BESS $E^{\text{in}}_{\text{BESS}}$, or is curtailed $E^{\text{curt}}_{\text{RES}}$ (5.24). The load is supplied directly from RES $E^{\text{direct}}_{\text{RES}}$, by the BESS $E^{\text{out}}_{\text{BESS}}$, or by the diesel generator E_{DG} (5.25). BESS operation is associated with energy losses $E^{\text{loss}}_{\text{BESS}}$ (5.26).

$$E_{\text{RES}} = E^{\text{direct}}_{\text{RES}} + E^{\text{in}}_{\text{BESS}} + E^{\text{curt}}_{\text{RES}} \tag{5.24}$$

$$E_{\text{load}} = E^{\text{direct}}_{\text{RES}} + E^{\text{out}}_{\text{BESS}} + E_{\text{DG}} \tag{5.25}$$

$$E^{\text{loss}}_{\text{BESS}} = E^{\text{in}}_{\text{BESS}} - E^{\text{out}}_{\text{BESS}} = \left(\frac{1}{\eta_{\text{BESS}}} - 1\right) \cdot E^{\text{out}}_{\text{BESS}} \tag{5.26}$$

RES are the primary source to feed the load. Surplus power is stored in the BESS for later use. We assume that the BESS is charged only with RES surplus and the remaining excess RES-generated power is curtailed (5.24). The BESS provides the load if RES-generated power is insufficient. Only if RES and BESS cannot sufficiently supply the load, the diesel generator provides the necessary power.

The power system's carbon emissions ϵ_{Hybrid} without BESS are caused by RES and diesel generator fuel consumption (5.27). RES emission factors apportion the emissions of producing and installing the RES among the energy produced over the system lifetime. This allows a straightforward comparison with fossil-fuel based generation.

$$\begin{aligned}\epsilon_{\text{Hybrid}} &= E_{\text{DG}} \cdot \frac{\rho_{\text{DG}}}{\bar{\eta}_{\text{DG}} \cdot \text{LHV}} + E_{\text{RES}} \cdot \rho_{\text{RES}} = \\ &= \left(E_{\text{load}} - E_{\text{RES}}^{\text{direct}}\right) \cdot \frac{\rho_{\text{DG}}}{\bar{\eta}_{\text{DG}} \cdot \text{LHV}} + E_{\text{RES}} \cdot \rho_{\text{RES}}\end{aligned} \tag{5.27}$$

Operating BESS influences the carbon emissions $\epsilon_{\text{HybridES}}$ of the island grid. It reduces curtailed RES energy by storing that energy, to provide the load at later times, and consequently reduce the energy production of the diesel generator (5.28). The more energy the BESS stores, the higher the carbon reduction is (5.29). Higher BESS efficiencies further improve the carbon reduction. The negative sign of the BESS emissions indicates that the BESS operation reduces carbon emissions.

$$\begin{aligned}\epsilon_{\text{HybridBESS}} &= E_{\text{DG}} \cdot \frac{\rho_{\text{DG}}}{\bar{\eta}_{\text{DG}} \cdot \text{LHV}} + E_{\text{RES}} \cdot \rho_{\text{RES}} = \\ &= \left(E_{\text{load}} - E_{\text{RES}}^{\text{direct}} - E_{\text{BESS}}^{\text{out}}\right) \cdot \frac{\rho_{\text{DG}}}{\bar{\eta}_{\text{DG}} \cdot \text{LHV}} + E_{\text{RES}} \cdot \rho_{\text{RES}}\end{aligned} \tag{5.28}$$

$$\begin{aligned}\epsilon_{\text{BESS}} &= \epsilon_{\text{HybridBESS}} - \epsilon_{\text{Hybrid}} = \\ &= -E_{\text{BESS}}^{\text{out}} \cdot \frac{\rho_{\text{DG}}}{\bar{\eta}_{\text{DG}} \cdot \text{LHV}} = \\ &= -\eta_{\text{BESS}} \cdot E_{\text{BESS}}^{\text{in}} \cdot \frac{\rho_{\text{DG}}}{\bar{\eta}_{\text{DG}} \cdot \text{LHV}}\end{aligned} \tag{5.29}$$

The Sankey diagrams of hybrid renewable-diesel island grids without and with BESS are shown below in Figure 5.9. The red colored energy flows show the losses in the power system. The green colored energy flows represent the energy generated from RES. The brown color is associated with energy generated from fossil fuel. The blue bar illustrates the energy, that is utilized.

An island grid without BESS (Figure 5.9 (a)) only utilizes the RES-generated energy that coincides with the load. The remaining RES generation is lost by curtailment. The consumers' load that does not coincide with RES generation needs to be supplied by the diesel generator.

The diagram for the island grid with a BESS (Figure 5.9 (b)) shows that the BESS stores a share of the otherwise curtailed RESs' excess energy and supplies the load at other times. The BESS causes losses, but the avoided diesel generator-generated energy is equal to the energy provided by the BESS.

5.4 Concluding Carbon Emissions

An approximation of the production induced emissions has been derived. It is based on a bottom-up analysis of the prototype system *Energy Neighbor* and is compared to other values in the literature. This allows taking the production into account that needs to be compensated by the operation of BESS

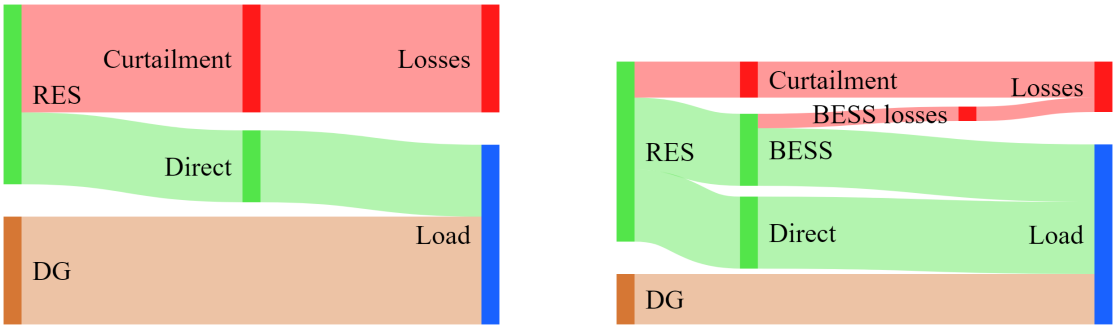

(a) (b)

Figure 5.9: Sankey diagram for island grid without storage (a) and with storage to increase RES-utilization (b).

for a positive net reduction of the carbon footprint.

The net impact of operating BESS for three different applications on the carbon emissions has been developed. The mechanisms are considered in a global manner to obtain the true net effect, instead of displacing the cause of emissions to a process outside of the analysis. This way a credible method of evaluating BESS' direct impact on the GWP is available.

The literature review unveils that analyses of the GWP with narrow system limits are at risk to yield distorted results and possibly wrong conclusions. Evaluation methods need to incorporate thorough comparisons with reference scenarios to achieve eligible results and enable qualified conclusions.

The mechanisms reveal that the key-process to reduce the carbon emissions is to increase the utilization of RES-generated energy and thereby avoid the use of fossil-fuel generated electricity. The results are determined by the properties of the respective power system, with regard to its carbon emissions of the generated energy. The BESS efficiency is another key factor. Low efficiencies cause more losses that need to be compensated by increased fossil-fuel-based generation. Shifting of the energy generation towards lower carbon technology needs to compensate for the introduced system losses.

Other targets for the operation of BESS, such as the increase of a household's self-consumption have no immediate positive effect on the overall carbon footprint. The positive coincidental effect of avoiding curtailment does reduce the carbon footprint. The self-consumption is an ineffective incentive for the reduction of the carbon footprint and even counteracts that goal. Instead, BESS operation needs to aim at increasing the power system's energy efficiency, reduce curtailment losses, solve stability issues, or drive down public economic cost. Applications and corresponding elicited BESS operation need to be reassessed and aligned to one of the mentioned goals, if necessary.

While PV-home storage for increase self-sufficiency adds carbon emissions, as well as raise general public cost [32], peak-shaving may potentially reduce the general public cost of the power system transformation, by deferring the necessity of grid reinforcement. Reducing the peak load avoids the occupancy of the grid's power capacity. The application has therefore potential to reduce the costs of the overall power system.

Other indirect consequences of the deployment of BESS, such as appealing the installation of RES are not regarded in this thesis.

6 Case Studies

6.1 PV-Home Storage in Germany

Two case studies are performed for the PV-home storage application in Germany. First, an economic case study is presented that has been published previously [29]. The second study investigates the impact of BESS on the carbon emissions and has been presented before [31].

The economic case study is based on the first version of the *Powerwall*, a BESS announced by *Tesla Motors, Inc.* (Palo Alto, California, USA). The product was of particular interest, as the announcement promised a price that was 75% lower than the market price at that time, attracting considerable attention in the industry and media.

The carbon emissions study was performed and presented independently, with different technical parameters for the BESS. It also considers the emissions of an entire community grid, instead of a single household.

6.1.1 Economic Case Study

In spring 2015, *Tesla Motors, Inc.* (Palo Alto, California, USA) announced the *Powerwall*, a BESS developed for residential PV-systems, surprising the renewable energy industry and gaining attention in the media. The technical specifications are similar to previous lithium-ion battery systems, but the announced system cost is significantly below the market prices of the time. The average retail price in the German market in the first half of 2015 was about 2000 EUR/kWh [40]. The price of the *Powerwall* in Germany was announced to be about 500 EUR/kWh [159], reducing the specific price by a factor of four compared to previous average prices for lithium-ion based systems. It, however, remained vague as to what exactly was included in the announced price.

In this case study, the economic benefit of a system with technical data based on *Tesla*'s announcements regarding the *Powerwall* is assessed for the German market. The aim is to give a reliable evaluation of *Tesla's Powerwall* and to estimate the conditions under which the storage systems become financially favorable.

6.1.1.1 Parameters

Technical Parameters

The simulation is conducted with parameter sets matching typical single-family houses in Germany with a rooftop PV-system installation. Simulated PV-system sizes ranges from 1 kWp to 10 kWp. PV-systems with sizes above 10 kWp operate under different economic framework conditions in Germany [44] and are not considered in this study.

The average annual consumption of four- and six-person households is 4300 kWh and 4750 kWh, respectively [160]. Households with more than average power load are found to be more likely to invest in PV-systems and BESS to reduce their dependency on the grid-electricity price [40]. Simulations are run with a scaled annual consumption from 1000 kWh to 10,000 kWh to cover all relevant consumption scenarios. Two reference households are discussed in detail: The *average household* with an annual load of 4500 kWh and a PV-unit with 5 kWp peak power and a *large household* with an annual load of 7000 kWh and a PV-unit with 8 kWp peak power.

The annual load of the *average household* represents the average four- to six-person household with the most common PV-system size of 5 kWp in Germany [161]. The *large household* has a larger annual load than the German average of four- to six-person households. A large share of households that consider the purchase of a BESS share this trait [40]. This household is assumed to have a PV-system of 8 kWp installed on the roof, the second most common PV-system size, within the investigated range [161].

The load profile utilized for the simulation consists of 15-minute mean values of the average of about 100 measured households in Germany over a year [12] (Figure B.1). Consequently, fast load variations and prolonged periods without major electricity use (for example, during holidays of individual households), are not captured. The generation profile has been measured with a sample time of one minute at a PV-system in Munich, Germany, in 2009 (Figure B.2). Both profiles are scaled to match the PV-system's peak power and annual consumption of the household respectively.

Tesla claims that no maintenance is required after the system's commissioning, thus no operational costs are considered in the cost calculations throughout the storage lifetime. The battery capacity is guaranteed to retain at least 60% after 10 years [159]. The simulation includes the battery's capacity fade; the replacement of the battery after the warranty period is not considered to keep the number of scenarios overseeable. It is important to note that a system lifetime below the assumed depreciation period of 20 years corrupts the achievable savings.

The PV-home storage is analyzed for both, DC and AC-coupling. Coupling at the DC-side of the PV-unit is cheaper because no additional inverter is needed. AC-coupling is more expensive but required for retrofitting existing PV-unit installations. The conversion losses are simulated accordingly to the topology, shown in Figure 6.1.

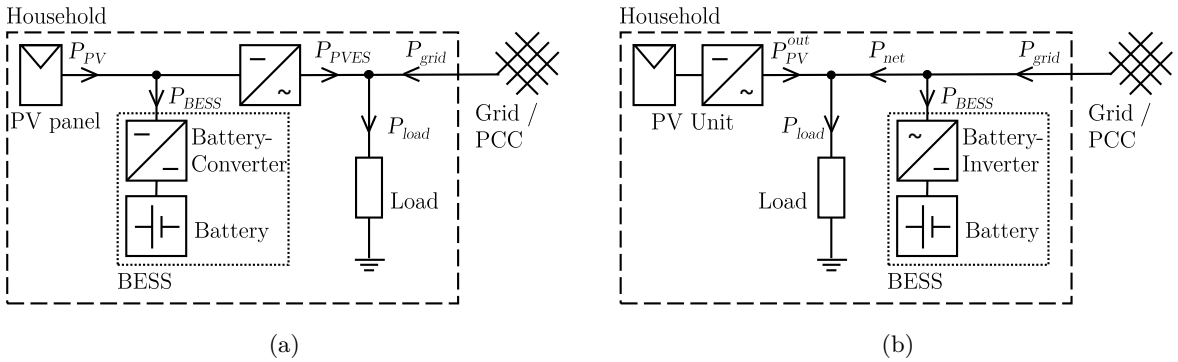

Figure 6.1: Connection topologies for BESS in a PV-home. DC-coupled BESS is shown on the left (a). AC-coupling of BESS on the right Figure (b).

Two aging characteristics are simulated. The first parameter set is a cycle stability of 5000 full cycles until the capacity degrades to 80% of its nominal value. The second parameter set is a cycle stability of 3000 full cycles. Both characteristics are based on the degradation curve described by

Rosenkranz *et al.* [162]. According to their model, smaller DOCs lead to reduced aging when compared to large DOCs. The model curve is scaled to attain 5000 full cycles for the battery with a capacity degradation to 80% of its initial value, as announced for the *Powerwall* product [163]. The cycle aging parameters are given in Table 6.1. The respective amount of equivalent full cycles for each occurring DOC is obtained with piecewise cubic interpolation of the given parameter set.

Table 6.1: Number of full equivalent cycles with different DOCs until end-of-life (EOL) of SOH= 80% is reached.

DOC in %	2.5	5	10	25	50	80	100
Reference aging	30,800	19,800	14,500	9,500	6,900	5,500	5,000
Strong aging	18,500	11,900	8,700	5,700	4,100	3,300	3,000

The calendrical aging is assumed with 15 years to 80% remaining capacity [28]. The same battery chemistry is used in the *Powerwall* (Table 6.2). Cycle aging and calendrical aging are added to obtain the overall battery aging.

Table 6.2: Powerwall device datasheet according to Tesla (denoted with superscript d) and assumptions (denoted with superscript a) used in case study.

Parameter	Value	Unit
Usable energy capacity^d	6.4	kWh
Nominal power^d	3.3	kW
Battery cycle efficiency^d	92.5	%
Calendrical lifetime^a	15	years
Cyclical lifetime^a	5,000	Full cycles
Price^a	3,615	EUR

Economic Parameters

The BESS's performance is assessed based on the PI. A depreciation period of 20 years is chosen for BESS, equivalent to the endorsed depreciation period for PV-systems [164]. An interest rate of 4% p.a. and an inflation rate of 2% p.a. result in a real interest rate of about 2% being in the same range as other publications [165–169]. The most significant parameters (electricity price, household size, remuneration rate, subsidies, coupling-topology, and aging characteristics) are varied to cover the possible range of the BESS's value.

The average electricity price for German private households in 2015 amounted to 28.72 ct/kWh [169]. Two scenarios for the electricity price development are analyzed. First a constant electricity price of 28.72 ct/kWh and secondly a rising electricity price with an annual price increase of 4.55% p.a. starting with 28.72 ct/kWh. The constant electricity price refers to a constant nominal electricity price and results in overall decreasing real electricity costs considering the effects of inflation. The rising electricity price is an extrapolation of the average annual price increase of the historic electricity price development from 2000 to 2014 [170].

The following cost assumptions are based on an AC-coupled system in 2016. Several publications suggest a specific inverter price of 350 EUR/kW for micro-inverters [170–172]. The inverter, therefore costs a total of 1250 EUR, hence the whole price for AC-coupling amounts to 6250 EUR. The DC-coupled BESS does not require an additional inverter and the total costs amount to 5000 EUR.

The regulations in Germany, including a subsidy for BESS that requires a stricter limit of the in-feed power of the installed PV-system capacity, such as the subsidy by the KfW-Bank [173] are considered. The assumptions for the subsidy are that it funds 30% of the BESS investment and imposes a feed-in limit of 50% of the PV-unit's peak power. The BESS is assessed with and without subsidy. This concerns the subsidy imposed curtailment limit of 50% and the legal curtailment limit of 70% of the installed PV-power.

The savings generated by a PV-home storage stem from the spread between electricity purchase price and feed-in remuneration. The remuneration is granted for 20 years according to the German renewable energy act (EEG) [43; 44] and equals to 12.31 ct/kWh in 2016. The first rooftop PV-units were installed in the year 2000 and their remuneration after the guaranteed time period (after 2019) is uncertain. A remuneration of 3.21 ct/kWh based on the average price at the EPEX-SPOT day-ahead market in the time period of January and September 2015 is assumed [174]. The electricity price is calculated for the time period from 2020 to 2040, accordingly.

Table 6.3 outlines the electricity price scenarios for each investigated parameter set, and the two example households that are investigated in detail.

Table 6.3: Reference households and electricity price assumptions analyzed.

	Variant 1	Variant 2
Electricity price scenario	constant price 28.72 ct/kWh	increasing price 28.72 ct/kWh in 2016 with 3.55% increase p.a.
Reference households	average household	large household
Load	4500 kWh/a	7000 kWh/a
PV-unit	5 kWp	8 kWp

The reference scenario for the parameter sensitivity is given in Table 6.4 along with the alternative parameter variants.

Table 6.4: Overview of the reference scenario and the investigated parameter variations.

	Reference scenario	Alternative parameter variant
System coupling	DC-coupling 5,000 EUR	AC-coupling incl. inverter 6,250 EUR
Cycle aging	5000 full cycles	3000 full cycles
Subsidy	30% of the full price 50% feed-in limit	no subsidy 70% feed-in limit
Remuneration	12.31 ct/kWh	3.21 ct/kWh

6.1.1.2 Results and Discussion

Figure 6.2 depicts the results of the different parameter variants. The left bars without border show the results for the *average household*. The right bars with a black border represent the results of the *large household*. The variations from the reference scenario are given on the x-axis. The bars show the PIs for the electricity price scenarios. Blue bars represent the rising electricity price scenario. The results for the constant electricity price are depicted by the grey bars. The grey line between the blue

and grey bars represents a PI of 0%.

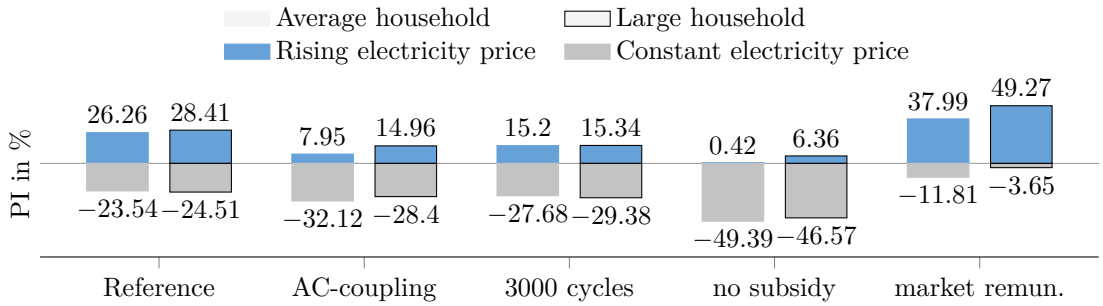

Figure 6.2: Comparison of the PI for different scenarios. The bars show the PIs for the electricity price scenarios. Blue bars represent the rising electricity price scenario. Grey bars with a black edge show the results of the constant electricity price scenario. The left bars without border represent the *average household* (5 kWp/4500 kWh). The right bars with a black border show the results of the *large household* (8 kWp/7000 kWh). Bar groups shows the different scenarios. The deviations from the reference scenario are given in the description on the x-axis.

The BESS achieve PIs in the reference scenarios that range from -24% to 26% for the *average household* and -25% to +28% for the *large household*. Each sensitivity scenario in Figure 6.2 shows a significant change of the PI compared to the reference scenario on the left. Hence every single investigated variation parameter strongly influences the probability of the BESS being able to generate a positive return within a time period of 20 years.

Choosing to purchase an additional inverter to enable AC-coupling of the BESS reduces the PI to ranges from -32% to +8% and from -28% to +15% for each of the two respective households.

Batteries that exhibit strong aging and have a cycle stability of only 3000 full cycles instead of 5000, reduce the PI to a spectrum of -28% to +15% and -30% to +15%, respectively. The impairment is more severe for the large household. This indicates that the BESS size is too large for small households. The extra energy capacity serves as a buffer, compensating for the aging. The capacity decrease is more perceivable at the larger household, where the BESS is utilized more intensely.

The scenario where the subsidy is omitted yields a strong decline of the PI to spans from -49% to 0% and from -47% to +6%, respectively. A very low remuneration of electricity feed-in increases the household's incentive to store the self-generated energy for later use. The soared PI without subsidy ranges from -12% to +38% and from -4% to +49% respectively.

Reimbursement by subsidy directly translates to an improved PI. A more severe PV-feed-in limit, however, has a noticeable negative influence on the PI. Lower feed-in limits cause larger waste of the PV-generated electricity. Figure 6.3 shows the decrease of the PI for stricter curtailment limits. The added losses yield noticeable impacts for lower feed-in limits.

The PI over all simulated PV-system sizes and annual loads are shown in Figure 6.4 for the reference scenario (Table 6.4). The numbers in Figure 6.4 (a) are calculated assuming a constant electricity price of 28.72 ct/kWh over 20 years. Figure 6.4 (b) shows the PI for the rising electricity price scenario.

The PI increases with both the PV-system size and the annual load, until saturation is reached. This results in an U-shaped contour: Neither the annual load nor the PV-size directly correlate with the economics of the BESS. Instead, both variables yield matching values for the BESS to achieve the optimal PI.

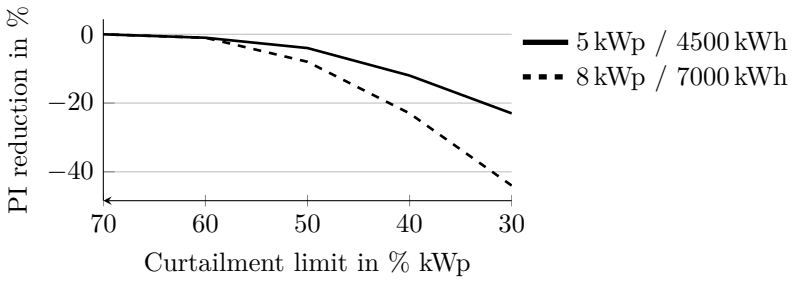

Figure 6.3: Change of the PI caused by curtailment limits lower than 70% for the BESS with a remuneration rate of 12.31 ct/kWh. The solid curve shows the PI change for the *average household* (5 kWp/4500 kWh). The dashed curve depicts the *large household* (8 kWp/7000 kWh). The losses are more severe for larger PV-systems and increase with decreasing curtailment limits.

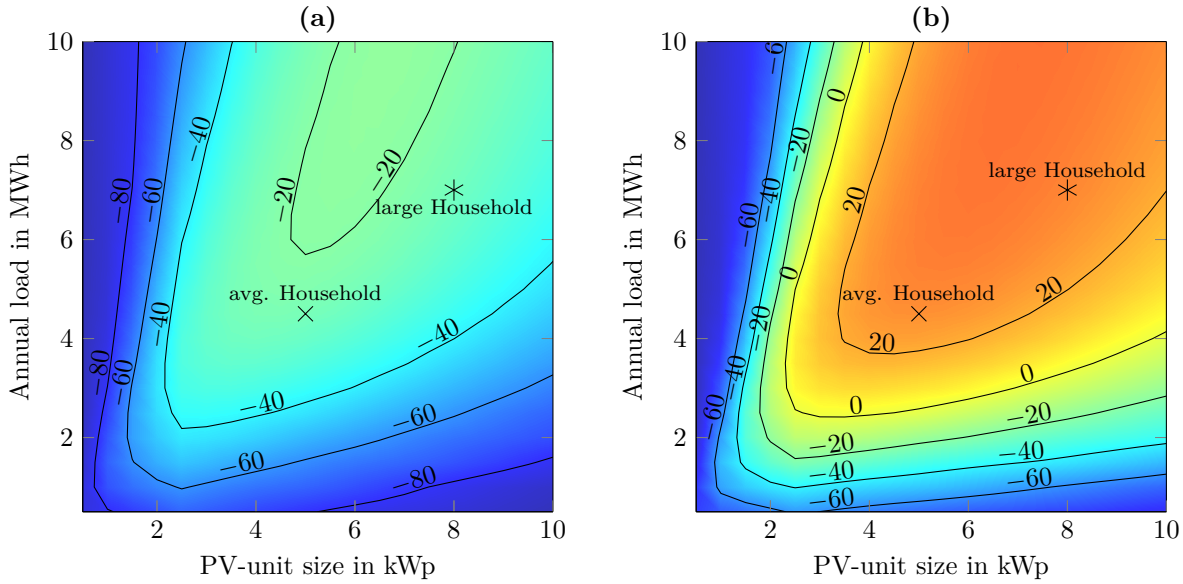

Figure 6.4: Overview of the PI in % for reference case. The left Figure (a) illustrates the PI for a constant electricity price. The right Figure (b) shows the PI assuming a rising electricity price.

The Figure shows that the PI decreases for larger loads and PV-sizes below 6 kW because they lead to more direct supply by the PV-produced energy. The excess PV-produced energy is not sufficient to fully charge the BESS, if the self-consumption is high, hence the BESS is not completely utilized and appears oversized for the desired application. Smaller loads, however, generate situations where the energy demand does not consume the entire energy stored in the BESS. In this case the BESS is not fully discharged until the next charging period.

Larger PV-systems experience more curtailment losses. The storage-subsidy lowers the feed-in limit, hence the increased losses account to the cost of the BESS, reducing its PI. Consequently, the additional curtailment losses reduce the PI of households with larger PV-units,

In case of a constant electricity price (Figure 6.4 (a)), the cost savings generated by the BESS cannot compensate for the system's investment cost. Hence, deploying the BESS results in financial losses, assuming the reference scenario.

In the increasing electricity price scenario (Figure 6.4 (b)), the BESS is economically beneficial for households with an annual load larger than 4000 kWh and a PV-system size of at least 4 kWp. The majority of PV-systems below 10 kWp yield a capacity of 5 kWp and the average 4-person household consumes more than 4000 kWh p.a., hence the average single-family house in Germany with a rooftop solar facility achieves positive returns in this scenario.

The development of the electricity price has a major impact on the economics of BESS. The span between the chosen scenarios of constant nominal electricity prices and of energy prices that increase by 4.55% p.a. exceeds 50 percentage points difference in the resulting PI in some cases.

6.1.1.3 Summary of PV-Home Storage Economic Case Study

The results show no distinct trend on the possible economic benefit regarding PV-home BESS in the price range of *Tesla*'s *Powerwall*. The product can be an economically viable purchase now with a PI over 25% in some of the discussed cases with a rising electricity price. These numbers further improve in future scenarios with lower remuneration rates and increasing electricity prices. Some investigated scenarios yield a negative PI for the BESS, including the majority of scenarios with a constant electricity price. This emphasizes the need to accurately analyze the situation for each installation to obtain a realistic economic estimation. The high impact and distinct uncertainty of future electricity prices need to be taken into account for such economic estimations.

Each of the investigated parameters exhibits a high impact on the total economics of BESS. Varying both the electricity price and the remuneration rate underline the immense relevance of the price gap between them for the economics of increasing the self-consumption.

The analysis regarding system coupling and the impact of subsidies emphasizes the significance of total system costs. The anticipated subsidy scheme of the *KfW*-bank significantly improves the financial benefit of installing a BESS.

The announced subsidy scheme is expected to require grid-relieving feed-in limits: electrical energy storage systems are endowed with funding, provided the grid feed-in power is limited to a certain fraction of the PV-systems peak power. Stricter limits will lead to larger energy waste in cases where *direct charging* control algorithms are used. Residential BESS are technically capable of reducing the power peak injected into the grid and diminish curtailment losses, hence providing more grid-relief, without significantly compromising the benefits to the BESS-owner [175].

The economic value of BESS heavily depends on the load and generation profile: a large increase of self-consumption, by usage of storage, results in higher savings. Households with large PV-systems and high annual load and households with little simultaneity of load and generation are especially favorable. The results illustrate that BESS with a usable capacity of 6.4 kWh, seem to be oversized for the average German BESS-buyer.

6.1.2 Carbon Emissions Case Study

The case study in the following has been presented and published at the *Conference on Sustainable Energy Supply and Energy Storage Systems* 2017 [31]. The net emissions caused by operating PV-home BESS on the low voltage-distribution grid with 57 households have been investigated. The operation strategy has a significant impact on the outcome. Combination of BESS with PV feed-in curtailment

and the impact on the grid's hosting capacity is also subject of the case study. Only active power control by BESS is considered and preceding carbon emissions caused by the production of BESS is not included in the analysis. The emissions of producing the PV system is implicitly included in the emission factor ρ_{PV}.

6.1.2.1 Technical Parameters

To assess the BESS' impact on the low voltage grid, a typical village grid is used for the simulation [176]. The grid consists of 57 households and a transformer with a rated power of 400 kVA. Since spatial distribution of RES has a big impact on voltage distribution, every household is assigned a PV unit to minimize the regarded variants and to isolate the effect of the applied BESS operation strategy. All houses have uniform PV unit sizes and BESS system properties for a small number of analyzed cases.

Individual load profiles are used for each household, to achieve a realistic load profile calculation [177]. The annual consumed energy of the households ranges from 1527 kWh to 4673 kWh, with a mean value of 2823 kWh. Because of the spatial proximity of the houses, a single measured PV generation profile is applied to all PV units. The profile is measured at the AC-side of a solar panel in Munich, Germany in 2009 (Figre B.2). The solar panel is assumed to have operated at the maximum power point in the entire time. The influence of varying roof and PV setup directions, which in practice influence the PV production in terms of amplitude and of the temporal profile, is neglected in this work.

PV feed-in limits of 50%, 70%, and 100% (i.e. no limit) of the installed PV capacity are simulated. The simulations are run for the low voltage distribution grid with and without BESS.

The solar home BESS are uniformly chosen with 4.0 kWh usable energy and 4.0 kW rated power for all simulations. This size is considered to be favorable for the most common household size in Germany [28]. The inverter is modeled with the *Type 1* efficiency curve (Figure 2.9). The study is conducted with the power flow battery model described in Section 2.2.3.2. The parameters are taken from Table 2.3).

Three different operation strategies are used to run the BESS. First the *Direct Charge* and the *Dynamic Feed-in Limit* are used. The third operation strategy is the avoid curtailment operation strategy (*avoid curtailment*). It only stores energy that would otherwise be wasted by curtailment. The mechanics is like the *Dynamic Feed-in Limit*'s, but the threshold P_{th} is fixed at the curtailment limit of the PV feed-in.

Perfect forecasting data is assumed to be available to avoid the influence of prediction errors on the performance of the *Dynamic Feed-in Limit*. The remaining energy that can be stored by the BESS is estimated without considerations of the system's output dependent efficiency. This results in a slight impairment on the self-sufficiency rate, apparent in Figure 6.5.

Emission factors for the PV produced electricity unit and the average produced energy in the power system are required to assess the grid's impact on the total balance of greenhouse gas emissions. The emission factor for the PV produced electricity ranges between 10.5 g CO_2eq/kWh and 50 g CO_2eq/kWh for several technologies [155]. The worst case value of 50 g CO_2eq/kWh is used in this work. The average emission factor of the electricity production in Germany was 534 gCO_2eq/kWh in 2015 [178] and is used for the grid electricity.

6.1.2.2 Simulation

The simulation uses two models, the BESS model is simulated for each household individually. The resulting profiles are then handed to the grid simulation model to obtain the effects on the electricity grid. The electricity grid is modeled as a standard load-flow model [179]. The simulation has been conducted with a commercial grid software. Apparent, real and reactive power, as well as voltage, are computed at all nodes and the transformer to obtain the grid's hosting capacity. This also includes the evaluation of grid losses. Steady-state operation of the grid phases is assumed, neglecting transient effects. The simulation is run for one year and the results represent one year.

The *hosting capacity* of the grid is defined as the maximum installable RES power that does not lead to limit violations. For lines and the transformer, the rated current is set as the maximum admissible limit. Node voltages are limited to rise 3% above the state without connected generation units, as defined by AR 4105 [180]. The hosting capacity of the low voltage grid is determined for the different BESS operation strategies and curtailment limits, by increasing the nominal power of every PV unit in 0.5 kW steps for the simulation. The different profiles of each household are generated by the BESS simulation and passed to the grid simulation. A complete data set for the consideration of losses and self-sufficiency rate is obtained by performing a load flow calculation for a whole year and verifying the adherence to the limits.

6.1.2.3 Results and Discussion

For the assessment of the BESS' impact on the distribution grid, the self-sufficiency rate, the energy balance, and the greenhouse gas emissions are calculated. The values refer to the entire low voltage distribution grid, instead of single households.

The impact of installing solar home BESS on the hosting capacity of the distribution grid are shown in Table 6.5. Results on BESS' increase in the self-sufficiency rate (Figure 6.5) are comparable to literature values [47]. The losses for different BESS cases and the resulting CO_2eq balance for the different scenarios are discussed.

Hosting Capacity and Self-Sufficiency

The hosting capacity of the example distribution grid without relieving means, obtained from the simulations, is a total of 256.5 kWp. This corresponds to equipping each of the 57 households with a 4.5 kWp PV unit.

Imposing a curtailment limit of 70% on the feed-in of PV power raises the installable PV power by 44.4% to 6.5 kWp per house. The potential PV unit size on each household rises to 9.0 kWp if a more severe curtailment limit of 50% is in effect.

Deployment of BESS with *Direct Charge* does not increase the hosting capacity of the investigated low voltage distribution grid (Table 6.5). Voltage violations appear as early as in the case without BESS. BESS with the chosen size and the *Dynamic Feed-in Limit*, in contrast, are capable of increasing the hosting capacity by 44.4%. The effect is similar to a curtailment limit of 70%. BESS with *Dynamic Feed-in Limit* are therefore capable of increasing the PV hosting capacity of distribution grids. Other BESS sizes would lead to a different increase of the hosting capacity. The *avoid curtailment* operation strategy does not noticeably contribute to the self-sufficiency rate and is therefore not shown.

The resulting self-sufficiency rate r_{ss} is saturating after reaching a certain amount of PV-power in the distribution grid is shown in Figure 6.5. BESS significantly elevate the self-sufficiency rate for the distribution grid, almost doubling the number. The *Direct Charge* achieves a slightly higher self-sufficiency rate than the *Dynamic Feed-in Limit*. Inaccuracies of estimating the remaining storing capacity of the BESS lead to slightly inferior results compared to the *Direct Charge*. The *Dynamic Feed-in Limit* enables larger PV unit sizes, establishing the potential for higher self-sufficiency rate.

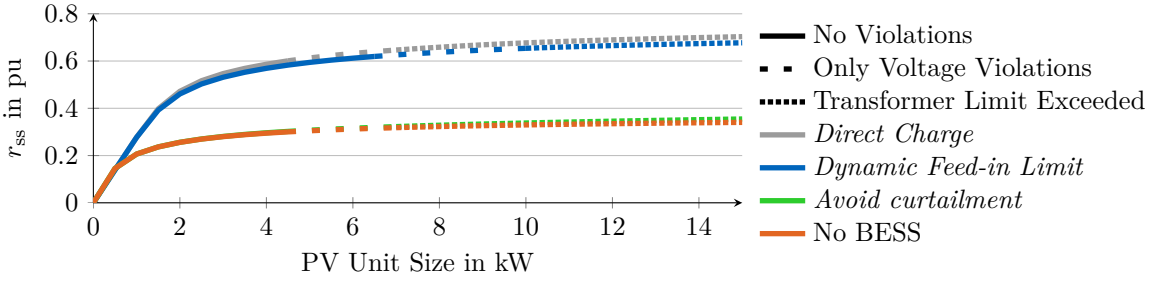

Figure 6.5: Self-sufficiency rate over PV-size. Solid lines show the self-sufficiency rate r_{ss} for feasible operation where no voltage violations occur. PV unit sizes at the dashed lines cause voltage limit violations according to simulations. Dotted lines illustrate PV unit sizes where the transformer limit is exceeded.

Energy Analysis

The resulting amounts of exported PV-energy, produced PV-energy, household consumption, imported grid energy, and losses are shown in Figure 6.6 on the left bar of each group. The resulting net export energy is depicted by the white bar with a black border on the right of each group. The x-axis indicates the scenario, describing the curtailment limit, the BESS case (either the operation strategy or nor BESS at all), and the respective PV size per house.

Increasing the installed PV power does not increase the time correlation between load and generation. Consequently, the imported energy is not reduced significantly, but the amount of exported energy rises (Figure 6.6).

Running all BESS with *Dynamic Feed-in Limit* results in similar PV hosting capacity as a 70% curtailment limit for the specific BESS size; the BESS introduce significant losses, though (Figure 6.7). The BESS reduce the imported energy, as well as the exported energy. Consequently, the resulting net export energy decreases. BESS reduce the amount of energy flowing through the lines and as a consequence the grid losses. The losses caused by BESS are, however, significantly higher and outweigh

Table 6.5: Hosting capacity of the low voltage distribution grid for different curtailment limits and battery deployment scenarios. The capacity of the PV unit of each house P_{PV}^{unit}, the total installed capacity in the grid P_{PV}^{grid}, and the increase of the hosting capacity $\Delta P/P_0$ for each scenario compared to the scenario without BESS and curtailment are given.

	no curtail. lim. (100%)			70% curtail. lim.	50% curtail. lim.
	no BESS	direct	feed-in limit		
P_{PV}^{unit}	4.5 kWp	4.5 kWp	6.5 kWp	6.5 kWp	9.0 kWp
P_{PV}^{grid}	256.5 kWp	256.5 kWp	370.5 kWp	370.5 kWp	513.0 kWp
$\Delta P/P_0$	-	0%	44.4%	44.4%	100.0%

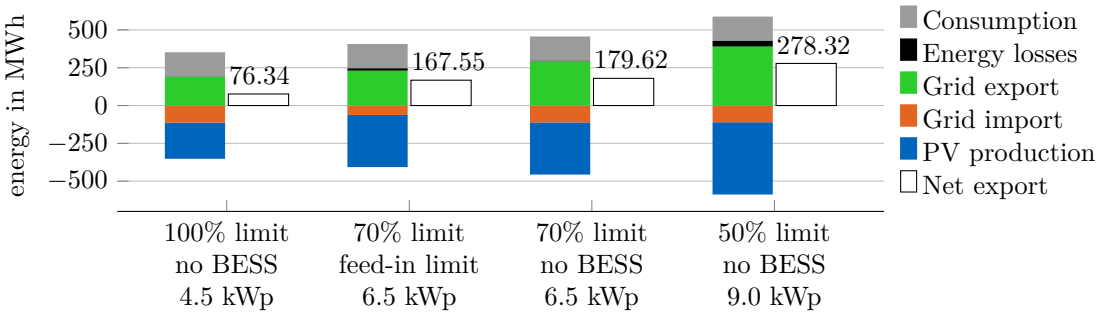

Figure 6.6: Energy balance of the scenarios for the largest PV unit sizes without voltage limit violations.

the line loss reduction.

A curtailment limit at 70% of the PV peak power causes curtailment losses smaller than the grid losses for the chosen load and PV profiles. Imposing a limit of 50%, in comparison, leads to a significant rise of the curtailed energy.

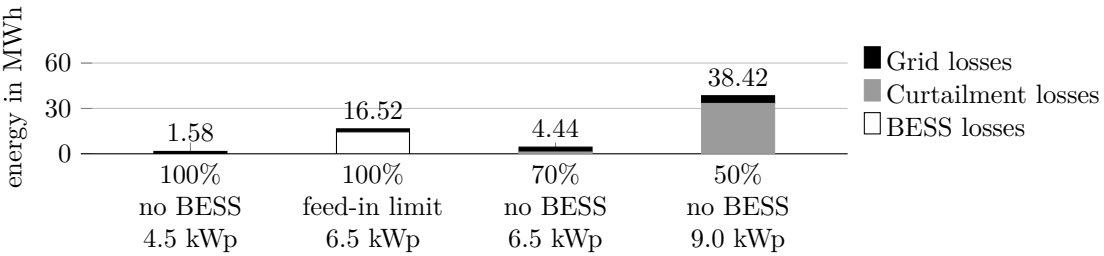

Figure 6.7: Detailed losses of the scenarios for the largest PV unit sizes without voltage limit violations. The labels on the x-axis denote the curtailment limits, BESS scenarios, and the PV unit sizes per household.

Figure 6.8 displays the losses in the distribution grid for the case of a 50% curtailment limit and a 9.0 kWp PV unit size. The *Direct Charge* has no noticeable effect on the curtailment losses but adds BESS losses. The *Dynamic Feed-in Limit*, in contrast, achieves a substantial reduction of the curtailment losses that is larger than the internal BESS losses, leading to an overall loss reduction. The total losses are smaller than the losses in the case of PV systems without BESS.

The results are improved further by the *avoid curtailment* operation strategy. As increasing the self-consumption is not an objective, but only storing the energy that would be curtailed, the achieved self-sufficiency rate is barely higher than in the case without BESS. The smaller energy throughput decreases the total BESS losses.

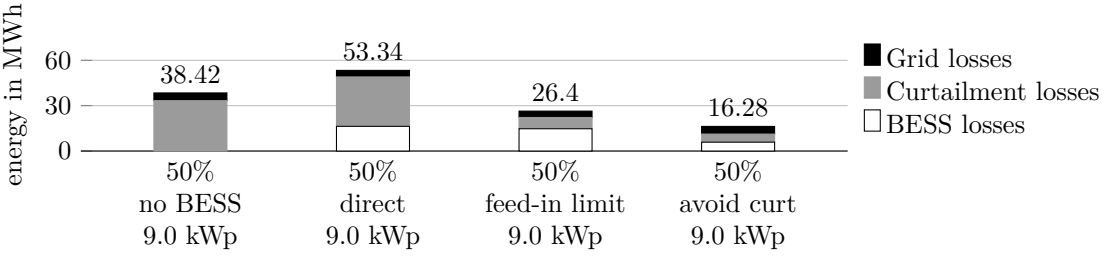

Figure 6.8: Detailed losses for a 50% curtailment limit for different BESS scenarios.

Emissions of the Distribution Grid

The total emissions of the distribution grid without PV units amount to 86 t CO_2eq if supplied exclusively by the power system. The emission reduction of the 57 households for different PV unit sizes, BESS operation, and curtailment limits are shown in Table 6.6. Non-feasible cases are shown for reference but put in brackets to mark that voltage violations occur.

Table 6.6: Carbon emission reduction by the PV units of the distribution grid for different PV unit sizes in the grid, curtailment limits, and BESS deployment scenarios. The reference scenario without PV units leads to the distribution grid emitting 86 t CO_2eq. Configurations, where voltage violations occur, are shown in brackets.

	no curt. lim. (100%)		70% curt. lim.		50% curt. lim.		
P_{PV}	4.5 kWp	6.5 kWp	4.5 kWp	6.5 kWp	4.5 kWp	6.5 kWp	9.0 kWp
no BESS	115 t	(165 t)	114 t	165 t	107 t	153 t	211 t
direct	107 t	(157 t)	106 t	156 t	100 t	146 t	203 t
feed-in limit	108 t	158 t	108 t	158 t	107 t	157 t	217 t
avoid curt.	-	-	115 t	165 t	113 t	162 t	222 t

PV-units cause a reduction of the distribution grid's emissions. Equipping every house with a 4.5 kWp PV unit leads to sufficient replacement of fossil-fuel based energy so that the grid at last saves more CO_2eq emissions than it requires to serve its load.

Avoiding curtailment with BESS yields a positive effect on the emission balance. Operating BESS with *Dynamic Feed-in Limit* generally results in fewer losses, hence higher carbon reduction, compared to the *Direct Charge* operation strategy. In the case of 50% curtailment limit, BESS with *Dynamic Feed-in Limit* avoid more losses than they cause, resulting in an improved CO_2eq balance. The *avoid curtailment* operation strategy outperforms the *Dynamic Feed-in Limit* in all cases and avoids more curtailed energy than the losses it inflicts in general.

The comparison of similar PV unit sizes with different curtailment limits shows that imposing such limits impairs the carbon balance because of the curtailment losses. Increasing the installed PV unit size has a tremendous impact on the reduction of the carbon emissions. Besides further reducing the imported energy, the replacement of fossil-fuel based electricity with the exported energy contributes more to the positive record.

The results on the carbon emissions of the entire distribution grid are based on several simplifying assumptions. The precision of the computed CO_2eq emissions is determined by the accuracy of the computed energy amounts and the correctness of the underlying emission factors.

The exported energy is assumed to fully replace electricity in the power system, that would otherwise be generated by fossil-fuel power plants. Further grid losses in higher voltage levels have not been considered. The amount of replaced energy and avoided CO_2eq emissions are therefore slightly overestimated.

The emission factor of the actually replaced energy is likely to be higher than the grid's average emission factor. Especially controllable generation units' output, such as gas turbines or coal-fired thermal plants, is probably reduced to balance the additional renewable energy. Coal-fired power plants produce energy with almost double the emissions per kWh than the average generation [181; 182]. Assuming the grid average emission factor for the replaced electricity is an approximation. The influence on the dispatch of conventional power generation needs to be analyzed further for more

accurate results.

The production of the BESS needs to be taken into account to assess the overall effect of the systems. Assuming that all households have identical BESS with LFP:C batteries, the resulting carbon emissions of producing and installing the systems, amount to 1.37 t CO_2eq per household. The total emissions of the BESS in the distribution grid equal to about 77.8 t CO_2eq. The numbers for the inverter and batteries are calculated with average assumptions for the parameters, according to (5.6). The housing and auxiliary components are assumed to contribute to 29% of the total emissions, like in the average case shown in Figure 5.3. That means that the BESS with the *avoid curtailment* operation strategy reduce sufficient carbon emissions of a curtailment limit of 50%, to justify their emissions after 13, 9, and 7 years in case of PV-units with peak powers of 4.5 kWp, 6.5 kWp, and 9.0 kWp.

6.1.2.4 Conclusion

Operating BESS introduces losses that outweigh the curtailment losses of PV up to a curtailment of 70% of the installed capacity. This deteriorates the carbon balance in a setting that corresponds to the German legislation today. Even though BESS are acknowledged to be a key component to support low-carbon energy sources, they may be ineffective, even in established applications, such as increase of self-consumption. The charging and discharging behavior of BESS determine their benefit.

Increasing the self-consumption is not positively correlated with the reduction of carbon emission and the goal by itself does not promote the integration of RES. The increase of self-sufficiency rate is useful for reducing the carbon emissions in cases, where the feed-in peak is reduced. It is remarkable that carbon reduction does not occur in scenarios, that correspond to the current situation in Germany (for the utilized profiles).

Significant energy waste appears for a curtailment limit of 50%. BESS improve the carbon balance if they avoid energy waste by storing and later use. The energy waste would otherwise be replaced by fossil-fuel based electricity. Solely avoiding curtailment losses, without aiming at increasing the self-sufficiency rate, results in fewer BESS losses and further carbon reduction. BESS are therefore a beneficial solution to avoid carbon emission if a 50% curtailment limit is put into effect.

Increasing the self-consumption leads to a poorer CO_2eq balance in all cases, compared to the case that does not aim at increasing the self-consumption. Not using BESS is superior to BESS with *Direct Charge*, and BESS that only avoid curtailment reduce more carbon emission than BESS with the *Dynamic Feed-in Limit*. Consequently, increasing households' self-consumption does not increase the utilization of RES, hence reduce the usage of fossil fuel or necessarily result in grid relief. It solely improves an individual household's electricity bill.

The simulated cases without curtailment of the PV feed-in show that BESS with the *Dynamic Feed-in Limit* increase the potential of installable PV units in the low voltage distribution grid. Exploiting the additional potential and increasing the installed PV capacity, improves the carbon emission balance.

BESS are thus capable of deferring grid upgrades, enabling high shares of RES. Grid-relieving operation may, therefore, avoid additional cost for the general public. Pursuing such a task is, however, not incentivized, even though suggested for BESS in the literature.

Instead of rewarding self-consumption, the reduction of energy losses or grid-relief to increase the *general* use of renewable generated electricity should be incentivized. Increasing the hosting capacity of a distribution grid is, however, only useful if the grid's current hosting capacity is fully utilized.

Policy and regulations are determining the explicit usage of BESS and decide whether residential BESS are useful for reducing CO_2eq emission or just exploit the market financially without generating real value. The incentives should align with the overall target of reducing greenhouse gas emissions.

6.2 Peak-Shaving for a Sawmill and a Grocery Store

Peak-shaving is studied for two scenarios. The first scenario is a sawmill in Bavaria, the *Weiss Holz- und Palettenwerk GmbH* in Julbach. The data were kindly provided by its shareholder-managing director Dipl. Inform. (FH) Jürgen Martlmüller. The plant produced 1.5 million pallets in the year 2015 and consumed about 1.8 GWh of electrical energy. A large share of the load is covered by on-site combined heat and power plants (CHP). The electricity purchased from the grid amounts to 459.06 MWh per year. The influence of the combined heat and power plant is not further considered and peak-shaving is analyzed for the factory with the existing generation schedule of the combined heat and power plants.

The second scenario studied is a grocery store in Germany. The commercial load amounts to 438.93 MWh per year. Both consumers are subject to peak load charges because their consumptions exceed 100 MWh [66].

6.2.1 Parameters

6.2.1.1 Technical Parameters

The load profiles are actual measurements with a sample time of 15 minutes over the period of a year. The annual load of the sawmill accounts to 459.06 MWh and has a power peak of 184.39 kW (Figure B.3). Two combined heat and power plants with a nominal electrical power output of 140 kW. The heat generation is used in the sawmill for drying processes, further improving its efficiency but is not regarded in this thesis. The schedule for the combined heat and power plants is one base-load generator that runs continuously without interruption and another peak-load generator that is switched on from Monday to Thursday at 6:45 in the morning to 15:45 in the afternoon and on Friday 6:45 in the morning to 13:30 in the afternoon. The grocery store consumes 438.93 MWh electricity per year and the load profile peak is 142.45 kW (Figure B.4). Table 6.7 gives a brief overview of both consumers' parameters.

Table 6.7: Parameters of consumers for peak-shaving study.

	Sawmill	Grocery store	Unit
Annual load	459.06	438.93	MWh
Peak load	184.39	142.45	kW

The BESS has been varied from 0 to 500 kWh nominal energy capacity. The achievable threshold for peak-shaving has been iteratively determined for each BESS size. The inverter size is chosen accordingly with the nominal power rounded up to full kilowatts.

The diesel generator's nominal power is identical. All mentioned efficiency curves of the diesel generator are simulated and the results compared (Figure 2.10). The curve given by Guinot *et al.* is chosen as the standard case [96].

Table 6.8: BESS parameters for peak-shaving study.

Parameter	Value	
Nominal energy capacity	10 - 500	kWh
Nominal inverter power	10 - 80	kW
Battery model	equivalent circuit model	Table 2.3
Inverter type	Type 2	Figure 2.9 [87]

6.2.1.2 Economic Parameters

Since peak-shaving is exercised in a commercial context, shorter depreciation periods than for the residential PV-home case apply. A depreciation period of 5 years is the commercial standard [48], 10 years is chosen as a trade-off for longer-term investments, and 20 years is the longest depreciation period analyzed, for comparison with other applications. The reference depreciation period is 10 years. The interest rate is assumed to be 2% [29].

An overview of the grid charges with respect to the load peak prices has been surveyed (Table A.1). The peak prices range from 42 to 180 EUR/kW per year for the annual peak load. A price of 139 EUR/kW per year is chosen as reference price because the sawmill is located in the area of the grid operator *Bayernwerk* in the medium voltage grid, where this price applies. The respective electricity price is 0.005 EUR/kWh according to the price for consumers at the medium voltage grid with an annual utilization time (Jahresbenutzungsdauer) of over 2500 h given in Figure A.3.

A parameter variation of the battery prices is based on literature values and an example quotation from a manufacturer (see Figure A.1). The prices are assumed with 550 EUR/kWh of battery capacity from the quotation. A buffer for peripheral components has been added to obtain this number that serves as the standard reference. Hesse *et al.* surveyed a price of 752 EUR/kWh nominal battery energy capacity [119].

The inverter price is assumed with 120 EUR/kW being the current lower end of inverter market prices confirmed by several manufacturers (Q2 2018). This price is compared with literature values of 155 EUR/kW in the analysis [119].

Diesel generator costs are taken from a quotation (Figure A.2) and amount to 162 EUR/kW. Maintenance cost for running the diesel generator is assumed with 0.08 EUR/kW for 24 h [96] and the startup cost of 0.19 EUR/kW is used [183]. The diesel fuel price is varied between 0.7 EUR/l [98], 2 EUR/l, and 3 EUR/l [96]. 2 EUR/l is the chosen reference price. The overview of the economic parameters is given in Table 6.9.

6.2.2 Results

The simulation results for both cases, sawmill and grocery store are presented and discussed in this section. The economic results are given as annuities to allow an easier comparison of outcomes with different depreciation periods.

Figure 6.9 (a) shows the maximum peak reduction by the BESS. The solid line represents the sawmill case and the dashed line the grocery store. The inverter is set with the respective nominal power rounded to the next higher full kW value.

Table 6.9: Economic parameters of the peak-shaving case.

Parameter	Value	Unit	Sources
Depreciation period	5 / 10 / 20	years	[48]
Peak power charge	42 / 139 / 180	EUR/kW/a	Table A.1, Figure A.3
Electricity price	0.005	EUR/kWh	Figure A.3
Diesel generator price	162	EUR/kW	Figure A.2
Battery price	550 / 752	EUR/kWh	[119], Figure A.1
Inverter price	120 / 155	EUR/kW	[119]
Fuel price	0.7 / 2 / 3	EUR/l	[96; 98]
Diesel generator maint.	0.08	EUR/kW/d	[96]
Diesel generator start	0.19	EUR/kW	[183]

The achieved peak reduction is greater for the grocery store profile than the sawmill load profile, up to a BESS size of 440 kWh. The peak reduction achieved at the sawmill increases with the BESS size in a steady manner. The peak reduction at the grocery store exhibits a steep slope in the beginning that slowly abates with larger BESS sizes.

The BESS' utilization rates are shown in Figure 6.9 (b). They increase with the BESS size. This is because BESS are simulated to reduce the peak as much as possible. Larger BESS, therefore reduce more peaks and need to operate more frequently. The time utilization rates, shown as blue lines, are higher for the grocery store case (dashed line). This indicates that the grocery store's load profile comprises more and spikier peaks than the sawmill's load profile.

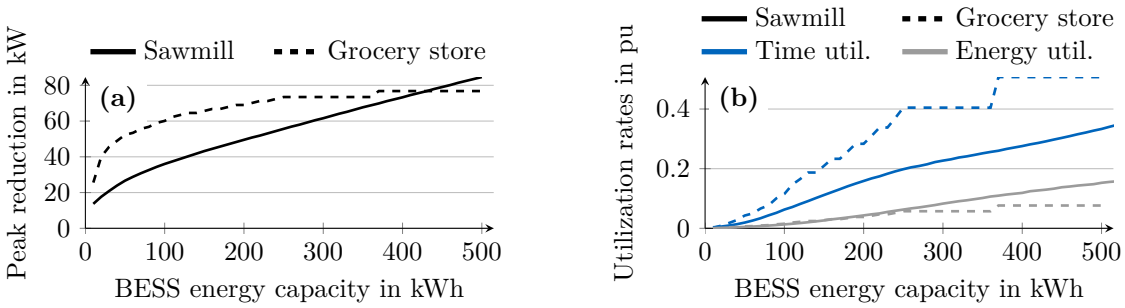

Figure 6.9: Peak reduction of BESS for peak-shaving at both cases over the BESS nominal capacity on the left (a). Time and energy utilization rates of BESS for peak-shaving at both scenarios on the right (b).

A parameter variation of the depreciation period for the BESS has been conducted and the effect on the net saving annuities is depicted in Figure 6.10. The sawmill case is represented by solid lines. The dashed lines represent the grocery store case. The depreciation periods 5 years, 10 years, and 20 years are indicated by the colors grey, blue, and orange, respectively. The BESS achieves higher net savings for the grocery store than for the sawmill. Smaller system yield net-savings, while the savings of larger peak reduction do not justify the added investment costs for larger BESS in the sawmill case. A depreciation period of 5 years, the business standard, results in BESS deployment being hardly economical.

Small BESS achieve positive net savings for all parameter variations in the grocery store case. Longer periods for the depreciation are obviously favorable for BESS investments because the costs for BESS virtually all incur at the beginning as investment costs. Longer depreciation periods stretch these costs

to more time periods and add the achieved revenues/savings fairly linearly.

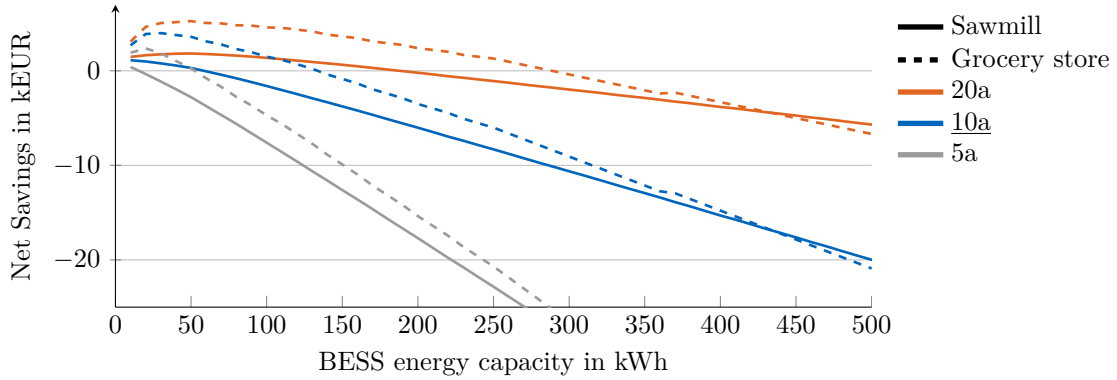

Figure 6.10: Sensitivity of depreciation period on the net savings.

Figure 6.11 (a) depicts the net savings for both consumer cases with varying BESS prices. Solid and dashed lines represent the sawmill and the grocery store. The quotation based price is denoted by blue, literature values are displayed with grey lines. Cheaper BESS significantly improve the profitability of the application. The impact of the BESS price is of similar magnitude for both peak-shaving cases and increase with larger BESS.

A sensitivity of the peak prices on the BESS net savings is illustrated in Figure 6.11 (b). The peak prices cause the incentive for peak-shaving and specify the achieved savings. The prevailing price range in Germany renders BESS to being economically both viable or non-viable, depending on the contract with the grid operator. The consumer cases are again distinguished by solid and dashed lines. The annual peak load charges are indicated by the different colors orange, blue, and grey for 42 EUR/kW, 139 EUR/kW, and 180 EUR/kW.

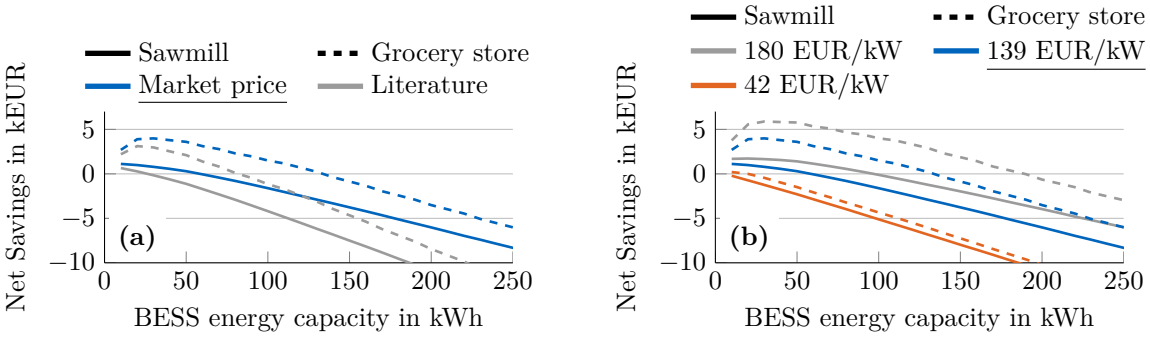

Figure 6.11: Sensitivity of battery prices (a) and peak prices (b) on the net savings.

The BESS reference case is compared to peak-shaving with a diesel generator in Figure 6.12. The standard diesel generator with a consumption curve taken from Guinot *et al.* is computed with varying fuel prices. The black, dashed lines represent the BESS. The solid lines denote the savings by the diesel generator with fuel prices of 0.7 EUR/l, 2.0 EUR/l, and 3.0 EUR/l in grey, blue, and orange.

The diesel generator is more economical in the sawmill case (Figure 6.12 (a)) for most peak-shaving limits, regardless of the fuel prices. The diesel generator is favorable in the grocery store case (Figure 6.12 (b)) for the low fuel price of 0.7 EUR/l. BESS and diesel generator yield comparable net savings for a fuel price of 2.0 EUR/l and the savings shift in favor of the BESS for larger peak load reduction. BESS become economical even earlier if the fuel price is 3.0 EUR/l.

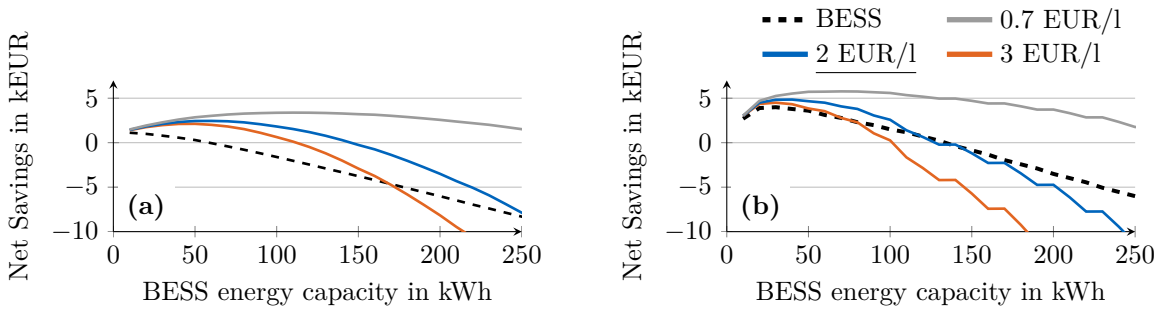

Figure 6.12: Sensitivity of fuel prices on the net savings. Left figure (a) represents sawmill case. Right figure (b) shows the savings for the grocery store.

Figure 6.13 shows the economics of diesel generator for peak-shaving with different efficiency curves. The diesel generator type does not impact the net savings significantly. The efficiency curves from Guinot, Ashari, and Bortoloni are represented by the blue, orange, and grey solid lines. All diesel generator types improve the net savings compared to a BESS in the sawmill case (Figure 6.13 (a)). In the grocery store case (Figure 6.13 (b)), BESS are generally more expensive, except against the Guinot type diesel generator for larger peak load reduction. The high-efficiency diesel generator with parameters from Bortoloni *et al.* is more economical for greater peak reductions.

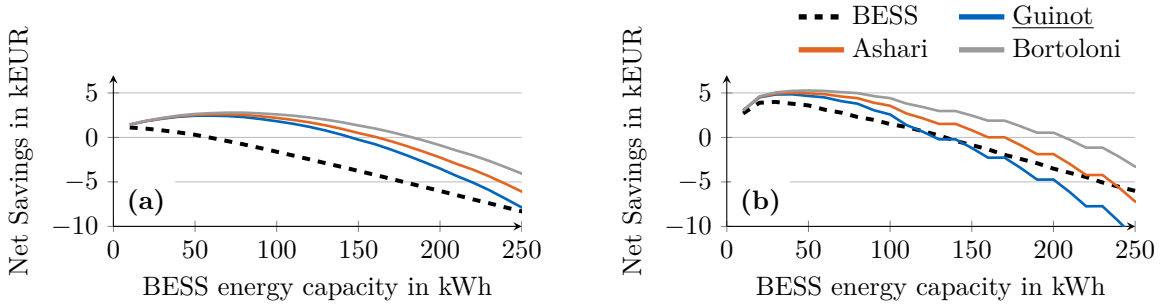

Figure 6.13: Sensitivity of the diesel generator type on the net savings for the sawmill case (a) and the grocery store case (b).

Figure 6.14 plots the carbon reduction achieved by the BESS compared to the diesel generator types. The production of all components is included in this analysis. The diesel generators are represented by the same colors as before (Figure 6.13). Larger BESS with greater peak reduction of the load profile save carbon emission compared to diesel generators in both consumer cases.

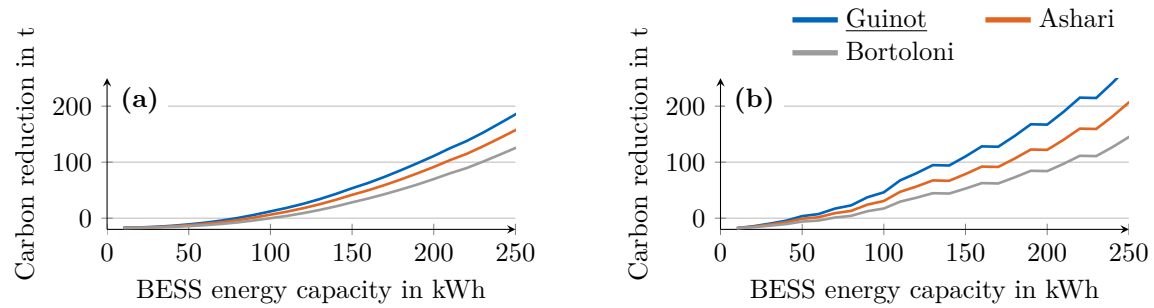

Figure 6.14: Sensitivity of diesel generator type on carbon reduction by BESS instead of diesel generator. Sawmill case on the left (a). Grocery store case shown on the right (b).

6.2.3 Summary

Two cases for peak-shaving are studied in this chapter. The first case is an sawmill, the second case is a grocery store.

The sawmill case achieves marginal or negative returns in most parameter cases. This becomes apparent in Figure 6.9 (a) that depicts the achievable peak reduction over the BESS energy capacity. The achievable peak reduction per storage capacity is too low and the peak charges cannot compensate for the required investment costs. The properties of the peaks are not favorable for BESS, as they contain more energy that need to be provided for the peak reduction.

The grocery store case yields a different result. BESS for peak-shaving achieve positive returns for a wide range of parameter assumptions. The achievable peak reduction is significantly higher in this case (Figure 6.9 (a)) and is reflected in the net savings. The choice of the depreciation period has a large impact on the financial results. Longer depreciation periods shift the results in favor of the BESS. The BESS price and the peak charge naturally influence the profits.

A comparison with diesel generators shows that the diesel generator case is more economic in the reference scenario. The carbon emissions, in contrast, are reduced by using BESS, instead of diesel generators for larger peak reductions. The results also show that the fuel price is more important than the specific diesel generator type, but it may still change the outcome of the results.

6.3 Hybrid Renewable-Diesel Island Grid in Graciosa

The hybrid renewable-diesel island grid case is based on Graciosa Island, one of the Azores islands that belong to Portugal. The grid parameters are chosen according to Stenzel *et al.*, who analyzed the effect of BESS on the power system of Graciosa [131]. The modeled grid consists of the consumers' load, a diesel generator, a BESS, a PV unit, and a wind turbine (Figure 2.15). The BESS aims at minimizing the fuel consumption of the diesel generator, by shifting the load to times with excess renewable energy generation.

6.3.1 Parameters

6.3.1.1 Technical Parameters

The load and RES-generation profiles of the island grid simulation are not taken from Graciosa, but from Tenerife, another island that is approximately 1500 km away from Graciosa island. Tenerife is part of the Canary Islands of Spain. The profiles are publicly provided by the local utility company with a sample time of 10 minutes and the profiles of the year 2016 are used [184]. This affects the electric load, solar generation, and wind generation. The latitude of the solar generation profile is $28°16'07''$N and a total of 114.9 MWp is installed in Tenerife. 36.7 MW of wind generation capacity is installed in the island grid and the electrical load amounts to 3.45 TWh/a [185]. The annual PV-generation of the profile amounts to 1835 kWh per kWp installed. The wind turbines generated 2174 kWh electricity per kW installed in 2016.

The measured load profile of January 1st to December 31st 2016 is scaled to match the annual load of Graciosa Island with 14 GWh/a (Figure B.5) The renewable generation profiles are scaled to match

the installed capacity of Graciosa Island that has a wind generation capacity of 4.5 MW (Figure B.7) and PV-generation capacity of 1.0 MWp [131] (Figure B.6). The parameters of both islands are shown in Table 6.10.

Table 6.10: Parameters of islands Graciosa and Tenerife [131; 185].

Parameter	Graciosa	Tenerife	Unit
Load	14	3450	GWh/a
PV capacity	1.0	114.9	MWp
Wind capacity	4.5	36.7	MW
Latitude	29°15'06"	28°16'07"	

The simulation is run with varying RES-generation capacity and BESS nominal energy capacity. The RES range from 1 MW to 20 MW total installed RES capacity, with a fixed ratio of 1:4.5 for PV units and wind turbines, like in the Graciosa island grid. The BESS nominal energy is varied between 2 MWh and 40 MWh with a fixed nominal power of 6 MW.

Two reference scenarios are chosen for further sensitivity analyses. The scenarios consist of a total RES capacity of 5.5 MW with a BESS with 5.3 MWh energy capacity and 16 MW and 16 MWh, respectively.

Table 6.11: RES and BESS parameters for the study on hybrid renewable-diesel island grid.

Parameter	Value	
RES installed capacity	1 - 20	MW
Wind:PV ratio	2:9	
Nominal energy capacity	2 - 40	MWh
Nominal inverter power	6	MW
Battery model	equivalent circuit model	Table 2.3
Inverter type	Type 1	Figure 2.9

The island's diesel generator is used to provide the electrical load, whenever the renewable energy sources and the BESS cannot provide the required electrical power. The maximum load of the profile is about 2.3 MW and the model diesel generator has a nominal power of 2.5 MW_{el}.

Once it is turned on, it is required to run a minimum uptime of six hours before being able to shut down again. Similarly, if the diesel generator is shut down, it needs to stay off for at least six hours. The minimum off-time is taken from Carrion *et al.* [186]. They used this assumption for a unit commitment problem for thermal unit commitment problems. Diesel generators today should be more versatile with fewer constraints. Another constraint of the diesel generator is the minimum output power of 30% of the nominal power [187]. The diesel generator model is described in Section 2.2.3.3 and the parameters utilized are given in Table 6.12.

6.3.1.2 Economic Parameters

The depreciation period for the power system is 20 years. The diesel fuel price variation is identical to the peak-shaving study between 0.7 EUR/l [98], 2 EUR/l, and 3 EUR/l [96]. The interest rates are 0%, 2% [29], and 4%. The parameter variation of the battery prices done like in the peak-shaving case study. The prices are 550 EUR/kWh (see Figure A.1) and 752 EUR/kWh [119]. The inverter price is assumed identical to the peak-shaving study with 120 EUR/kW and 155 EUR/kW [119]. The diesel

Table 6.12: Diesel generator parameters.

Parameter		Value	Source
Model type		power-flow model	
Efficiency	η_{DG}	power dependent	[96–98]
Nominal power	$P_{\mathrm{DG}}^{\mathrm{nom}}$	2.5 MW_{el}	
Min. output power	$P_{\mathrm{DG}}^{\mathrm{min}}$	30% $P_{\mathrm{DG}}^{\mathrm{nom}}$	[187]
Min. runtime	$\tau_{\mathrm{DG}}^{\mathrm{mustrun}}$	6 h	[186]
Min. downtime	$\tau_{\mathrm{DG}}^{\mathrm{mustoff}}$	6 h	[186]

generator costs are also equivalent to the peak-shaving study with 162 EUR/kW.

Costs for PV units are 1250 EUR/kWp and maintenance cost of 12.50 EUR/kWp/a [17]. Specific costs for wind turbines are 1120 EUR/kW and annual maintenance of 56 EUR/kW [188]. The overview of the parameters is given in Table 6.13.

Table 6.13: Economic parameters of the island grid case.

Parameter	Value	Unit	Sources
Interest rate	0 / 2 / 4	%	[28]
Diesel generator price	162	EUR/kW	Figure A.2
PV price	1250	EUR/kWp	[17]
Wind turbine price	1120	EUR/kW	[188]
Battery price	550 / 752	EUR/kWh	[119], Figure A.1
Inverter price	120 / 155	EUR/kW	[119]
Fuel price	0.7 / 2 / 3	EUR/l	[96; 98]
Diesel generator maint.	0.08	EUR/kW/d	[96]
Diesel generator start	0.19	EUR/kW	[183]
PV maint.	12.50	EUR/kWp/a	[17]
Wind turbine maint.	56	EUR/kW/a	[188]

6.3.2 Results

Figure 6.15 shows the time utilization rate of the BESS deployed on the hybrid renewable-diesel island. The utilization rates are depicted in a contour plot over the BESS size from 0 to 40 MWh (x-axis) and the total RES power from 0 to 20 MW. The utilization rate increases with the BESS size. Smaller BESS exhibit longer idle-times because they are fully charged or empty for long time periods, being incapable of further storing surplus energy or supplying the load, respectively.

Figure 6.16 gives an overview of the NPV of the net savings. The left Figure 6.16 (a) shows the net savings achieved by RES without BESS. Larger RES increase the savings that saturate with increasing power capacity. This is the case when the benefits rise slower than the investment costs of the RES.

The added savings by the BESS are shown in the middle Figure 6.16 (b) and the total net savings of both components are shown on the right Figure 6.16 (c), compared to the diesel only case. The BESS net savings depend on both, the BESS size and the installed RES capacity. Larger BESS decrease the net savings at a certain size because the added savings do not compensate for the larger BESS costs. The benefits of BESS also decrease for larger RES.

The RES contribute more to the overall savings than the BESS. The BESS still increases the savings in

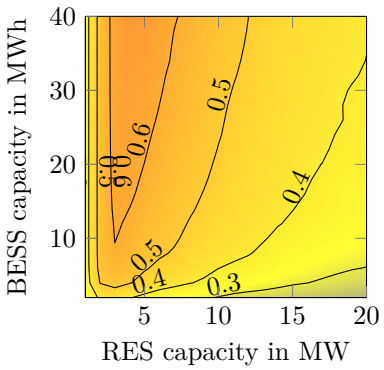

Figure 6.15: Time utilization rate of BESS in pu.

all cases. The largest total net savings are achieved with 13 MW installed RES capacity and 16 MWh energy capacity of the BESS, marked in the Figure as a triangle.

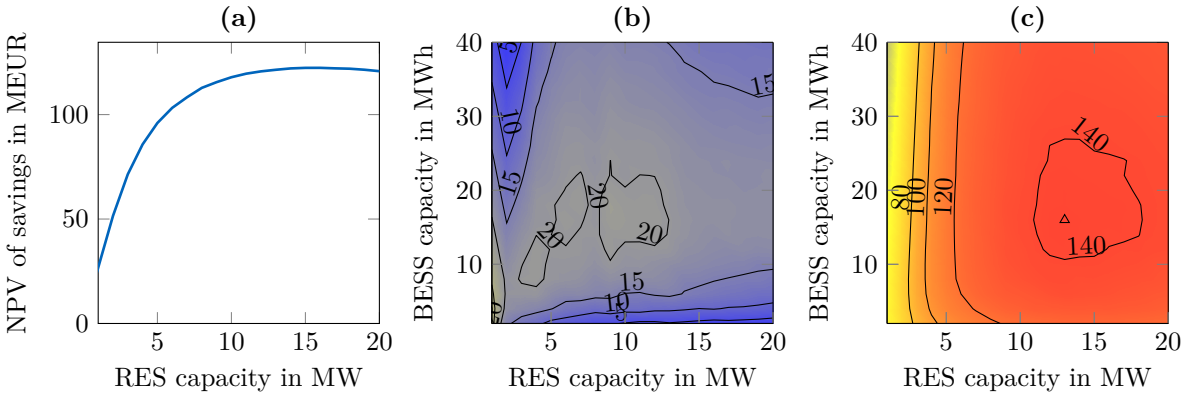

Figure 6.16: NPV of net savings of RES without a BESS (a), the NPV of the added savings of a BESS (b), and the NPV of the total savings of both components (c) in million EUR.

The PI of the configurations are shown in Figure 6.17. Smaller investments are more favorable for the PI because the revenue rises slower with larger components than the necessary investment costs.

With regard to the carbon reduction, the RES contribute considerably more than the BESS, as shown in Figure 6.18. Larger RES and larger BESS improve the carbon footprint of the island grid. The largest parameters of the sensitivity range achieve the best results. The carbon reduction by fuel savings outweigh the emissions caused by producing RES and the BESS.

Table 6.14 gives a cost overview of three cases: a hybrid renewable-diesel island grid with 5.3 MWh BESS and 5.5 MW of RES, a hybrid renewable-diesel island grid with 16 MWh BESS and 16 MW RES, and a diesel island grid without BESS or RES. Deploying RES and BESS shifts the costs away from the fuel cost towards their investment costs. The fuel costs constitute a large share of all costs in all cases and is tremendously reduced by RES and BESS.

Figure 6.19 shows the influence of the fuel price. The white bars with a black edge on the left of each bar group represent a fuel price of 0.7 EUR/l. The blue bars in the middle of the group depict the reference case with 2.0 EUR/l and the grey bars on the right of each bar group show the NPV of the net savings, assuming a total fuel price of 3 EUR/l. The left bar group shows the net savings of the small case, the right group illustrates the net savings for the 16 MWh BESS and 16 MW of RES. The

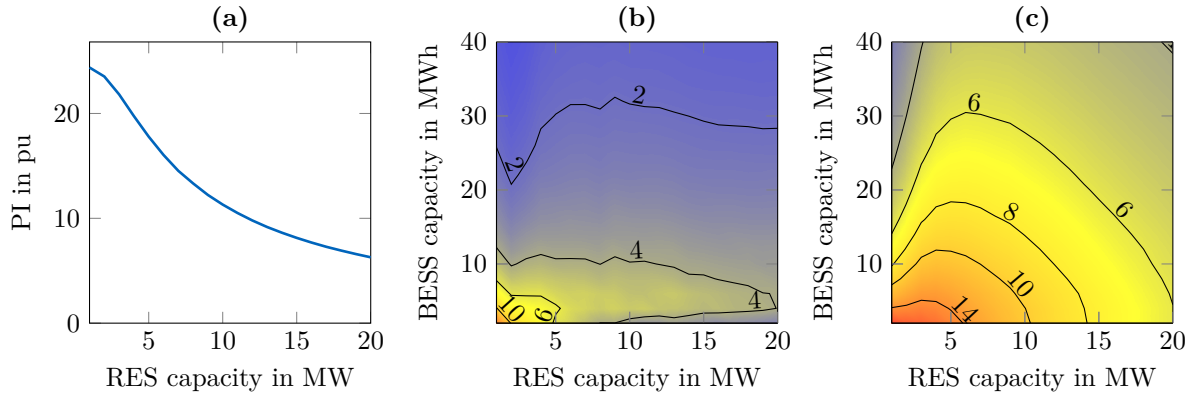

Figure 6.17: Profitability index of RES without BESS (a), PI of the BESS and its added value (b), and the PI of both components (c) in pu.

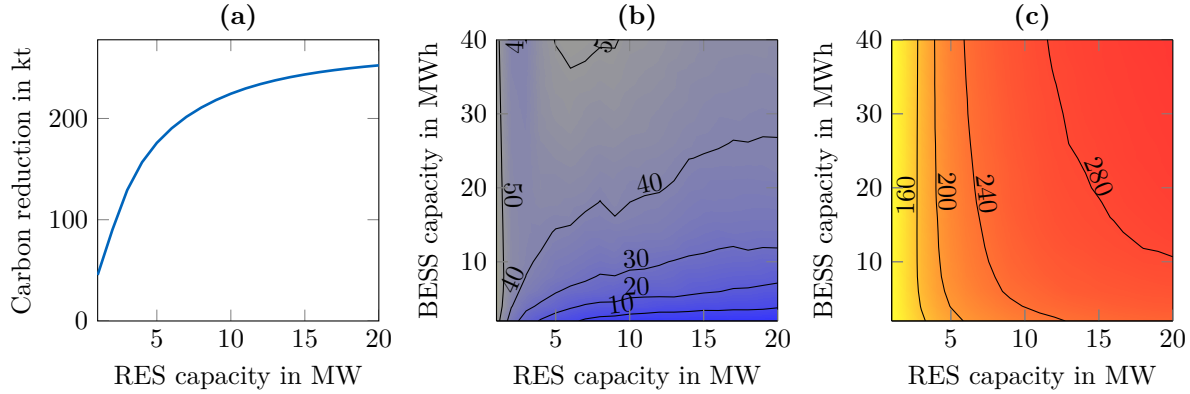

Figure 6.18: Carbon reduction by RES without BESS (a), further reduction by the BESS (b), and carbon reduction by both components (c) in kilotons.

fuel price has a tremendous impact on the economics that is higher than the chosen size for RES and BESS. Assuming the cheaper diesel price reduces the net savings by 80% in the larger case. More expensive diesel for 3 EUR/l increases the achieved savings by more than 60% for the larger island case. This is congruent to the fact that the fuel costs are the largest contributor to all costs.

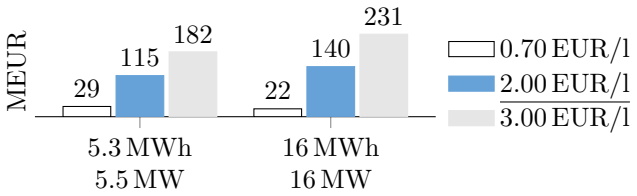

Figure 6.19: Sensitivity of the NPV of the net savings to the fuel prices.

The impact of the interest rate is shown in Figure 6.20 (a). The influence is not negligible for the depreciation period of 20 years. Discounting the net savings with an interest rate of 2% reduces the NPV by about 20% of the cash flows. An interest rate of 4% discounts the NPV by more than 35% of the nominal net savings.

The BESS price surprisingly has a minor influence on the overall net savings, as shown in Fig-

Table 6.14: Costs (MEUR) of island grid with 5.3 MWh BESS and 5.5 MW RES, 16 MWh BESS and 16 MW RES, and island grid with only diesel generator.

Island case	Small Island 5.5 MW RES 5.3 MWh BESS	Large Island 16 MW RES 16 MWh BESS	Diesel	shares/%		
Diesel gen. invest	0.41	0.41	0.41	0%	1%	0%
PV invest	1.25	3.64	-	1%	5%	-
Wind invest	5.04	14.66	-	5%	22%	-
BESS invest	3.63	9.52	-	4%	14%	-
Wind maint.	4.12	11.99	-	4%	18%	-
Diesel gen. start	3.69	1.27	0	4%	2%	0%
Fuel cost	73.55	24.66	206.73	80%	37%	100%
Total	91.92	66.74	207.20			

ure 6.20 (b). This is because of the tremendous savings by reducing the fuel consumption in the first place. BESS costs are more ponderous at marginal cases that achieve lower revenues/savings.

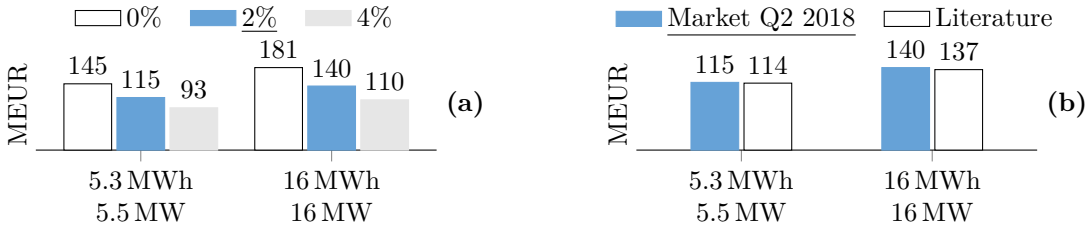

Figure 6.20: Sensitivity of the NPV of the net savings to the interest rates (a) and to BESS prices (b).

The sensitivity of different diesel generator types (Figure 6.21) with respective efficiency and fuel consumption is shown in Figure 6.21. The small reference island with a 5.3 MWh BESS and 5.5 MW total RES is shown on the left (a) and the larger reference is represented on the right (b). The grey bar represents the operational costs of the hybrid renewable-diesel island grid with respective configuration. The blue bar stacked on top represents the savings achieved by both RES and BESS. The total heights of the stacked bars with the respective value on top depict the reference costs of the same island grid without RES and BESS. Higher fuel consumption because of worse efficiencies increases the operational costs and therefore also the achievable savings by RES and BESS.

The results illustrate that the diesel generator itself or the composition of conventional generators are substantial for the costs and savings. Model-based assessment requires adequate accuracy of these generators to achieve reliable results.

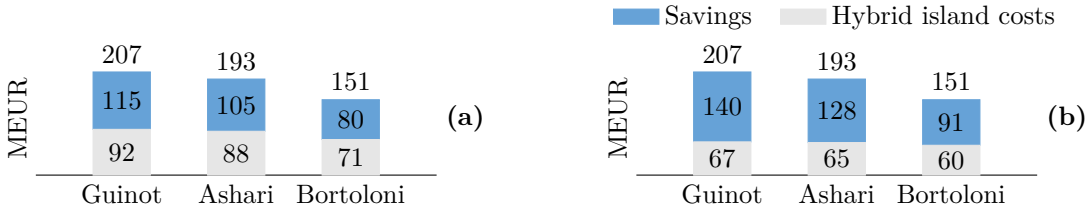

Figure 6.21: Sensitivity of the NPV of the net savings to the diesel generator type for the small reference island (5.3 MWh and 5.5 MW) (a) and for the large reference island (16 MWh and 16 MW) (b).

The carbon emissions are significantly influenced by the diesel generator types, as well (Figure 6.22). The stacked bar plots are similarly structured as in the previous Figure 6.21. The grey bars represent the hybrid renewable-diesel island grid's total emissions. The blue bars stacked on top represent the carbon reduction achieved by equipping the island grid with RES and BESS and the sum on top are the emissions if the island grid would operate only with the diesel generator. Savings are larger for less efficient diesel generators, but so are absolute emissions.

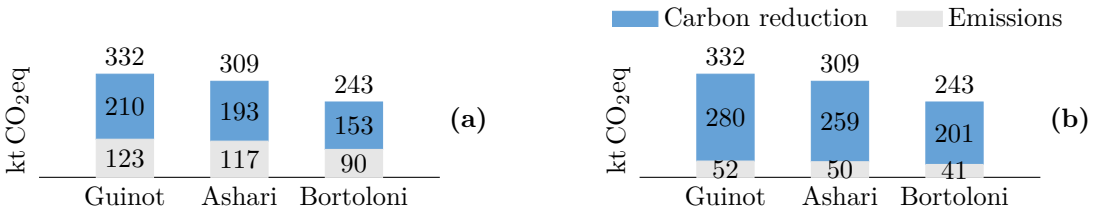

Figure 6.22: Sensitivity of CO_2eq emission reduction to the diesel generator type. Sensitivity for the small reference island on the left (a), results for the large reference island on the right (b).

6.3.3 Summary

A case study for Graciosa island is conducted. The BESS is deployed to increase the use of RES-generated energy and avoid fuel consumption by the diesel generator.

The installation of RES and BESS in the island grid yields tremendous savings and carbon reduction. The major contributor to the benefits are the RES, but the BESS benefit is perceivable.

The economic metrics PI and NPV indicate distinct optima for the sizing of RES and BESS. PI favors small components, while the NPV designates 13 MW of RES and a 14 MWh BESS to achieve the highest net savings. Carbon reduction is higher for systems that even exceed the analyzed range of 20 MW RES and 40 MWh BESS.

Fuel costs constitute a large share, even for large RES and BESS. Consequently, the fuel price has a heavy impact on the economics. Yet, BESS achieve positive net savings even for very low fuel prices.

The interest rate has a moderate impact on the economic outcome. The BESS price has a surprisingly small influence on the savings. This is because the savings are immense in the first place, rendering the importance relevantly low.

The large role of the fuel is reflected in the sensitivity of several diesel generator types. The varying diesel consumption influences both, financial savings and carbon reduction, significantly.

7 Concluding Storage Evaluation

Part II deals with the evaluation of stationary BESS. Technical evaluation metrics for stationary BESS are described and the literature review on economics, and carbon emissions of BESS is reviewed. The economic goals of the applications increasing the self-consumption, peak-shaving, and integrating RES in an island grid, are described. Different economic metrics are analyzed and discussed.

The analysis of economic metrics and the case studies show that any assessment of BESS requires consideration of multiple factors and metrics. Each metric that is regarded in isolation may (mis-)lead to false conclusions. The hybrid renewable-diesel island grid case, for example, shows that PI and NPV indicate different optimum solutions for the system sizing.

Technical metrics do not give exhaustive insights about system performance but are more suitable for identifying possible improvements. The efficiency of BESS is an exception. It is a key parameter that determines other technical metrics, economics and the GWP of BESS for different applications. The BESS performance improves in all areas with higher efficiencies. This metric must not be underestimated because low values are easily reached, impairing the performance of the whole system.

A method for approximating the carbon emissions of producing BESS is derived in this Part. The method is generic and enables transferring the results to other BESS with varying sizes and technologies. The method is based on a bottom-up, component-wise analysis of the *Energy Neighbor*. Both, literature values and the life-cycle inventory database *ecoinvent* are used for data.

The overall impact on the carbon emissions by operating BESS for the three specific applications is derived. A holistic approach is chosen to capture the overall carbon value of BESS, instead of shifting the emissions' cause out of the assessment scope. This avoids overly optimistic valuations of BESS in their respective application.

Case studies demonstrate, how to evaluate BESS. They illustrate that evaluation metrics should not be utilized in isolation. Different metrics lead to different conclusions and may not be informative. A thorough study of such results and cases is necessary.

The case studies show the potential of BESS for the applications. The PV-home storage systems in Germany are not favorable with regard to economics and GWP. PV-home storage systems that only avoid curtailment losses instead of increasing the self-consumption combined with a curtailment limit of 50% achieve the largest carbon reduction of all cases analyzed. Peak-shaving depends on the load profile that defines the achievable peak reduction per storage energy capacity. The first case at the sawmill shows negative returns for the deployment of BESS for peak-shaving, while the second case at the grocery store leads to positive net savings. The carbon footprint, in contrast, is not reduced in this application. BESS yield remarkable benefits for RES-integration in island grids. The case study on Graciosa island shows tremendous savings and a significant reduction of the carbon emissions compared to island grids with only diesel generators. The results are sensitive to the parameter assumptions. Especially the battery prices are expected to further decline. This may render currently non-profitable deployment to profitable cases and needs to be re-assessed in the future.

GWP analyses reveal that economic incentives for deploying BESS in different applications do not necessarily align with carbon reduction objectives. This is especially apparent for increasing the self-consumption in the residential context. While the personal carbon footprint is improved, the application worsens the carbon footprint for the general public. The case study shows that increasing the self-consumption even increases the fossil fuel electricity generation and the carbon emissions. A fixed feed-in limit of 50% for the PV-units combined with BESS to only avoid curtailment losses achieved the most favorable carbon reduction of the investigated cases.

The displacement of grid energy is assumed to avoid emissions with an emission factor of the average grid. The emission factor of displaced energy is most likely higher because especially fossil-fuel-based generators, such as gas-turbines or coal-fired power plants keep the power system balance. Coal-fired power plants, for example, generate energy with almost double the emissions compared to the grid average [181; 182]. This constitutes an underestimation of the carbon reduction by displacing fossil-fuel generated energy [31]. Larger carbon reduction of PV feed-in further worsens the effect of increasing the self-consumption on the carbon emissions.

Jägemann *et al.* discuss the inefficiency of PV-home storage systems for the general public [32]. They conclude that increasing the self-consumption raises the public cost. Even though the self-sufficiency (also energy autonomy) is the main motivation for many decentralized communities [189]. The metric should, nevertheless, be avoided as objective because it contradicts its own underlying motivation to decarbonize the power system.

The SolarPower Europe association recently published a whitepaper that proposes specific changes of regulations to enable and facilitate grid-supporting operation of solar with storage [30].

Von Appen *et al.* agree that the current regulatory framework for PV-home storage systems in Germany (i.e. its incentives) do not foster grid-relieving operation of BESS [190]. They suggest a change of the regulatory framework to incentivize grid-relieving BESS operation. They do not question the use of increasing the self-consumption but acknowledge that other objectives, such as avoiding curtailment or limiting the feed-in are beneficial goals. The author of this thesis doubts the benefit of increasing the self-consumption fundamentally and suggests that the grid-relief should not only be included in the incentives but replace any incentive for increasing the self-consumption.

Part III

Improving Battery Storage Operation

8 Motivation and Fundamentals

8.1 Motivation

BESS face profitability issues because of their high costs [22; 28; 29]. Even though the battery prices are rapidly falling [35], the BESS' economic return during operation requires further improvement. The benefit of BESS for its application and consequently the impact on the power system is determined by its operation strategy [33; 34]. Operating BESS for single, dedicated applications leads to low utilization [36], resulting in insufficient revenue that prevents widespread adoption and integration into the electricity grid.

In order to increase the stream of revenue and thus improve the economic value of BESS, serving multiple applications (multi-use) has been proposed and shown to have promising potential [36]. However, only a few algorithms have been published and they exhibit some considerable weaknesses. The value of multi-use can only be reliably determined if interdepending and possibly conflicting effects of applications are taken into account [36; 37].

Multi-use results in a dynamic dispatch of BESS and is not compatible with rather static electricity markets and regulations. Multiple applications within one system require a conciliating mechanism that maps the BESS efforts and resulting benefits to market-based obligations. This is especially relevant in unbundled energy markets, common in the European Union, where the ownership and operation of BESS need to be decoupled. This allows value generation of shared BESS across different market players.

8.2 Classification of Multi-Use Operation

Synonyms for the multi-use of BESS in the literature include multi-objective, multi-purpose, and stacked services. Multi-use generally describes the concurring execution of multiple applications. The author of this thesis classifies the existing approaches for multi-use into two categories: *multi-objective optimized control* and *stacking of applications*.

The literature review reveals two distinct types of multi-use of BESS. First the *multi-objective optimized control*, where timing and value of the output power determine the performance towards the set of applications. Secondly the *stacking of applications*, that leads to a distinct partitioning of the BESS resources (power, energy capacity, and energy stored). The latter allows a straightforward mapping of the BESS usage to market logic.

Multi-Objective Optimized Control

The first type of multi-use is the *multi-objective optimized control*. In this operating mode, the BESS meets several objectives by adapting the output power with regard to absolute value and timing. The

BESS serves multiple objectives but the battery power or energy capacity (the battery resources) cannot be assigned clearly to an objective. It may also be impossible to determine separate power profiles for each goal.

Examples of this multi-use type have been proposed by Weniger *et al.* [47] and Zeh *et al.* [51]. Both authors proposed the operation of PV-home battery systems that increase a household's self-consumption and at the same time reduce the peak feed-in of the PV unit during mid-day, to relieve rural distribution grids with high shares of RES.

Figure 2.12 illustrates how both goals are achieved, compared to the conventional direct charging behavior. The black line describes the net load of the household. The blue area shows the BESS charging (negative values) and discharging (positive values) behavior. The green area displays power exchanged with the grid. Negative values illustrate energy that is fed into the grid.

The *Direct Charge* operation strategy shown in Figure 2.12 (a) stores an excess generated energy in the BESS immediately to maximize the self-consumption. The grid relieving operation in Figure 2.12 (b) exhibits a smaller peak of the feed-in. Instead of immediately storing any surplus power, the charging time is shifted towards midday and the energy of the high generation period is stored instead of fed into the grid. The *Dynamic Feed-in Limit* operation strategy, shown in Figure 2.12 (b), pursues both goals of maximizing the self-consumption and at the same time decreasing the feed-in peak of the household, while the direct strategy does not aim at reducing the peak. Both operation strategies shown require the entire energy storage capacity and the BESS resources cannot be distinctly allocated to the objectives.

Application Stacking

The second type of multi-use is the *stacking of applications* by partitioning the storage. This multi-use type divides the physical energy capacity, nominal power, and state of charge (SOC) of the BESS into virtual segments and associates each segment to one specific application. Each application requires a certain power profile that can be independently assigned to a segment and the resulting physical output is the sum of the applications' output power.

Fig. 8.1 illustrates this operation mode and displays the allocation of BESS resources to the applications A and B over time. The applications may only use these resources and cannot exceed the assigned resources. A redistribution of the resources is depicted twice in Figure 8.1 at t_1 and t_2.

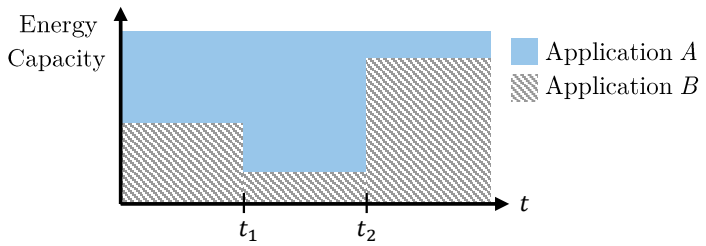

Figure 8.1: Illustration of time-varying energy capacity distribution for two applications (AP).

A fixed partitioning of the battery segments would be the static case for this multi-use type, while a sequential alternation of applications represents the most dynamic case of *application stacking*.

The disadvantage of this operation mode is that the capability of the system may not be fully utilized,

as the limits may lead to either under-utilization of the BESS or to the insufficient fulfillment of the application's objective. Any reduction of the assigned BESS resource for the application increases the utilization of that BESS resource but diminishes the capability for the respective application. The available BESS resources for the remaining applications, however, increase.

8.3 Literature Review

The following literature review analyzes algorithms for the EMS of BESS. The scenarios of the reviewed contributions are not comparable but are tested in different scenarios and applications. The review is based on the underlying structures of the algorithms that have been analyzed and abstracted. The given results have not been considered because they would require a pre-analysis and consequently a normalization of the scenarios and assumptions. The abstraction of the reviewed algorithms and the resulting classification is comparable to the review conducted by Weitzel *et al.* [38].

8.3.1 Multi-Objective Optimized Control

Different algorithms for the optimal energy management of stationary energy storage systems have been proposed in the recent past. Yet unresolved issues remain throughout the literature, such as incorporating demand response in a commercial context, integrating different planning horizons for different markets, applying adequate solution techniques for usage-related model formulations, and systematic uncertainty handling [38].

The control methods can be roughly classified into two categories: rule-based algorithms and optimized scheduling algorithms. Rule-based controllers comprise of parametric and fuzzy logic controllers. Optimized scheduling algorithms are deterministic, stochastic and robust optimization algorithms, and model predictive control (MPC). Some approaches, such as adaptive MPC and optimized rule-based control, utilize principles of both classes and are regarded as a hybrid. A similar classification of control approaches for hybrid energy storage systems has been presented before [191]. A more detailed discussion in the following section outlines the subtle differences between the categories. Table 8.1 provides an overview of the classification.

Table 8.1: Classification of control algorithms.

	Rule-based	Optim.-based
Parametric controller	x	
Fuzzy logic controller	x	
Determ. optim.		x
Stoch. / Robust optim.		x
MPC		x
Adaptive MPC	(x)	x
Optim. rule-based control	x	(x)

8.3.1.1 Rule-Based Algorithms

Rule-based controllers use input variables to calculate the BESS output according to predetermined rules. They are designed for specific applications and goals and determine their output at the instant

of operation. We classify rule-based algorithms for the control of BESS into two different classes: parametric and fuzzy logic.

For the application of increasing the self-consumption of households coupled with PV-generation, parametric control algorithms have been proposed to additionally minimize the feed-in limit of the PV-system [101]. Zeh *et al.* improved the robustness by considering the BESS state and the predicted sunshine duration [51]. This serves the purpose to relieve the local distribution grid and avoid voltage issues at peak PV-production periods [18]. A similar controller is proposed to reduce the load peak and defer the reinforcement of distribution infrastructure [192]. In this case, perfect foresight of local demand and generation is assumed. Another proposed controller smoothes the fluctuation in a residential microgrid based on forecast generation and load [193]. Moshövel *et al.* develop a parametric controller that adapts its parameters, based on the deviations of the real system state from the predicted system state [42]. Kennedy *et al.* propose a voltage-based controller to reduce the network stress [194]. Their controller is not limited to determining the active power of the BESS but also includes the reactive power. Fleer *et al.* investigate the impact of different parametric controllers for primary control reserve [195].

Parametric controllers generally exhibit a few disadvantages: They need to be designed by experts and often require time-consuming parameterization for every system. They also require manual tuning and non-optimal performance is a common outcome. Different applications and objectives require complete re-development of the control algorithm. Methods to cope with prediction-errors have been presented, but do not seem to follow a systematic approach.

Fuzzy logic control is a general approach to develop rule-based controllers from a linguistic representation of the desired system behavior. Fuzzy logic-based algorithms for the control of stationary BESS have been proposed in several works.

The controller proposed by Lühn *et al.* is used only for certain time periods and parametric algorithms are active in the remaining time [196]. This requires decision criteria for switching between the control modes. Arcos-Aviles *et al.* propose a fuzzy logic controller for the energy management of a microgrid to smooth the power profiles [197]. The controller's parameters, its membership functions, and ruleset are parameterized manually. The forecast profiles are included as input to determine the setpoint and the prediction error is used as input for the reference setpoint correction.

The results shown with fuzzy logic control-based algorithms are usually promising, but they are very specific to the demonstration scenarios. Their performance under different circumstances usually remains unclear and the parameter tuning is often incomprehensible. Rule-based control algorithms are easier to develop with the fuzzy logic control-framework, however, the parameter tuning is not straightforward and requires extensive knowledge about the application and the fuzzy logic approach. Also compensating for prediction errors has been approached differently for each individual case.

8.3.1.2 Optimized Scheduling

Optimized scheduling algorithms determine the power setpoints of the BESS for each sample time period of the optimization horizon, by means of optimization algorithms. Optimized scheduling algorithms do not react on events below the sample time of the power setpoints unless enhanced by additional rule-based methods. The sample time cannot be infinitely small because the computation time of the optimization depends on the number of power setpoints that are treated as optimization

parameters. Among these algorithms, we distinguish three different subtypes that can be partially combined: Deterministic optimization, stochastic and robust optimization, and model predictive approaches.

Deterministic optimization does not consider prediction uncertainties. The results are therefore only feasible for perfect prediction or may be regarded as a retrospective optimization to obtain the theoretic best performance. Consequently, the control algorithms require high-quality forecast and are sensitive to forecast errors [198; 199]. They suffer from low time-resolution in prediction data. The method can be applied with different optimization algorithms, such as linear programming [119], dynamic programming [200], or differential evolutionary algorithm [201]. The fundamental principle of prediction based scheduling is, however, independent of the explicit method and not limited to these algorithms.

Stochastic and robust optimization approaches capture the ambiguity of predictions, by considering a multitude of scenarios with varying prediction data. Stochastic optimization relies on a large number of scenarios, while robust optimization reduces the number of scenarios to the most significant ones, for example, a best- and a worst-case scenario.

Nejad *et al.* propose stochastic optimization for the energy management of microgrids, including energy storage and controllable loads. They run Monte-Carlo simulations to increase the microgrid's expected operational profit [202]. Choi *et al.* describe a control method for a microgrid energy storage system based on robust optimization. Their algorithm requires a detailed system model and includes a variety of constraints [203].

Model predictive control or receding horizon control is the repeated optimization after a determined time to consider updated and more certain information on the prediction and the system. This approach aims to decrease the accumulation of the errors caused by prediction uncertainty. Each time, the optimization is executed, the current system state and an updated forecast are utilized with the assumption that the near-term forecast is more accurate.

The model predictive control has been suggested for the control of BESS in a microgrid [204; 205] and also as controller of multiple microgrid units [206]. Zheng *et al.* propose a short-term scheduling by means of convex optimization to minimize the cost for distribution system operators caused by forecast uncertainties [207]. Model predictive control is also suitable to consider battery degradation, but the combination with prediction uncertainties has not been investigated [208]. Arnold *et al.* use a 2-step optimization, where the energy storage system is scheduled the day before and a nested model predictive control is used to minimize the impact of the prediction error [209]. Oliviera *et al.* compared optimization-based control with parametric controllers [210]. They have shown that receding horizon optimization with simplified models is sufficiently accurate if the optimization problem is solved with a certain frequency.

While the impact of prediction errors is reduced by employing model predictive control, compared to the deterministic optimization, the extent of the performance deterioration is still strongly determined by the forecast quality and time-resolution, as well as the frequency of the optimization. Model predictive control captures power changes that have longer time-periods than the sample time of its resulting output. Any power deviation below that sample time is not captured by the scheduling method but requires a real-time controller.

Following papers combine model predictive control with stochastic optimization approaches to capture the prediction uncertainties and use the receding horizon method to utilize the updated system state

and a more accurate forecast of the near-term.

Kumar *et al.* suggest that deterministic model predictive control may cause significant inefficiencies and propose a stochastic model predictive control instead, which is basically a two-stage stochastic programming problem [211]. This approach can be further improved by reducing the number of forecast scenarios with a backward reduction method [212]. Niknam *et al.* propose a gravitational search algorithm to determine the output power of all units in a microgrid and use a 2m point estimate method to consider the prediction uncertainties [213]. Lara *et al.* develop a robust energy management for isolated microgrids. Their approach comprises a nested robust optimization, where the day-ahead unit commitment determines the target state-of-charge (SOC) of the BESS, and a more frequent optimal power flow optimization compensates for the forecast errors. They use polyhedral uncertainty sets to obtain probabilistic characteristics of the forecast system [214].

Optimization-based control algorithms that determine the explicit power output are highly sensitive to prediction errors. They are also incapable of real-time control of energy storage systems and are therefore at risk of undesired system behavior.

8.3.1.3 Hybrid Approaches

Both rule-based control and optimization algorithms are combined in several publications. One option is an adaptive, model predictive control that pre-determines an optimization-based scheduling and uses a rule-based controller during operation to compensate for prediction errors. Another hybrid approach is to utilize a rule-based controller and predictively optimize its parameters. Weitzel *et al.* describe this approach as policy function approximation, where the policy (i.e. control parameters) of the BESS-controller is determined, instead of the explicit power output [38].

Following publications are adaptive, model predictive control approaches: Wang *et al.* introduce a nested 2-stage hierarchical control algorithm. The global tier is a feed-forward controller based on convex optimization. The local tier is a rule-based feedback controller, where the energy storage system is used to compensate for the prediction uncertainties and keep the grid power at the predicted level [215]. Qin *et al.* propose a 2-step model predictive control. The first step determines the power output schedule and the parameters of the correction term for the second step. The second step optimizes the output power using the correction parameters to shift the operation towards the globally desired solution. The correction factor considers the SOC, as well as the best and worst case prediction, to hedge against prediction errors [216]. Sachs *et al.* use a two-layer model-predictive control for the energy management system of a diesel-PV-battery island grid, where the first layer is an optimal control problem. The second layer is a boundary value problem that improves the system robustness against prediction errors, by shifting the diesel generator's operation. They achieve improved robustness with an additional controller to keep the reference point determined in the first layer, by means of operating reserve [217].

Policy function optimization methods have also been suggested: Barelli *et al.* propose a rule-based controller for the load management of a residential microgrid [218]. The control-parameters are tuned by an artificial neuronal network that uses historic and predicted weather data for the tuning process. Mueller *et al.* utilize a simple, parametric controller and optimize its parameters in a model-predictive manner [219]. Abdoos *et al.* also suggest parameter tuning of a rule-based controller. They utilize a particle swarm algorithm for the optimization [220]. Henri *et al.* use a similar approach, where different operation strategies that best satisfy the objectives in the prediction based simulation of the system are

chosen. Instead of a general controller with parameters, a control algorithm is chosen from a fixed set of possible control algorithms [221]. Mamun *et al.* optimize a parametric controller with a differential evolutionary algorithm to satisfy multiple objectives [222]. Their controller aims at maximizing the economic revenue achieved by the BESS and at the same time minimizing battery degradation. The parametric controllers used by the authors above are suitable only for the specific application.

Fuzzy logic controllers can, for example, be tuned by differential evolution to best follow the optimal power flow previously determined by linear programming [223]. Fossati *et al.* use a genetic algorithm to determine the optimal parameters of a fuzzy logic controller for the control of a microgrid. The fuzzy logic controller controls the BESS power and is optimized by the genetic algorithm based on the forecast power generation and load. No prediction errors have been considered [224].

The challenge of prediction errors needs to be combined with optimization and has not been researched exhaustively [38]. The method proposed in this paper falls into the category of policy function optimization but extends the mentioned literature. By combining the rule-based fuzzy logic controller with an optimization algorithm, we achieve the control algorithm's general applicability for different applications, real-time capability, optimal performance, and at the same time a robustness against prediction uncertainties.

8.3.2 Application Stacking

The concept of multi-use has been proposed in numerous publications, to improve the economic value of BESS. The majority of the reviewed manuscripts analyze specific sets of applications and propose particular solutions. The multi-use category, *multi-objective optimized control* is more prevalent in the literature, as this problem can be solved by established multi-objective optimization, that has been proven to be effective on other topics. There are fewer publications that propose a *stacking of applications* and even less that explicitly describe the methodology.

Fitzgerald *et al.* [36] state that multi-use customer-sited BESS deliver maximum service and value to the customers and the grid. They claim that the value of applications cannot be generalized and that regulations are the main barrier for the market participation of BESS since behind-the-meter assets are hindered by regulations to receive payment for deferral services, grid services, or wholesale markets. Their meta-study does not describe the necessary BESS operation to capture the value of multiple applications.

Another shortcoming of numerous papers is the assumption of perfectly known future profiles, such as load and renewable power generation. Their methods are not tested against forecast errors and likely to be sensitive to uncertainties. Some papers simulate multi-use of BESS but do not discuss conflicting applications [225; 226].

Tsakgou *et al.*[225] describe a stacking of services without reservation of BESS resources for the specific applications. They show an example, where the power requests do not occur at the same time.

Di Wu *et al.*[226] optimize the hourly output and the amount of balancing service of an energy storage system. They introduce optimality constraints to achieve a sequential order of the applications.

Other publications determine the optimal power output of BESS for several applications by means of numerical optimization algorithms but do not consider the presence of multiple stakeholders. While their approaches achieve good results, they are limited to cases with a single stakeholder, who attempts

to serve several applications. If several stakeholders seek to serve different, potentially conflicting applications, by operating the BESS, the remuneration remains unclear with these methods. There is no apparent procedure to determine the financial obligations and to achieve mutual agreements on the operation of the BESS.

Megel *et al.* [227] suggest a time-varying stacking of two applications and the corresponding allocation of the energy capacity of the BESS. They have not looked into the issue of sharing the system among several stakeholders.

Stephan *et al.* [37] assessed the economic value of BESS with a variety of applications. They conclude that combining applications can improve the investment attractiveness substantially. Their analysis is limited to two applications at a time, where the primary application is given priority, while the secondary application is served only if sufficient idle capacity is available based on pre-known profiles.

Metz *et al.* [228] optimize multiple applications, considering perfect forecast of the BESS profiles. The benefits are summed up, but a single stakeholder is assumed and the resource splitting of the BESS among several stakeholders has not been considered.

Zeh *et al.* [81] propose a multitasking of BESS to provide both secondary control reserve and grid-friendly storing of PV-generated energy. They consider the strict separation of energy capacities as necessary, to avoid a clash of different storage tasks. They also mention that legal proof of delivery for certain applications requires the installation of measuring devices. Concepts for metering devices designed specifically for the multi-use of BESS have been proposed [229].

Hollinger *et al.* [230] describe a multi-use method for home BESSs that provide primary control reserve and increase the self-consumption of the household. The state-of-charge determines the power output for increasing the household's self-consumption. The introduced rules of operation modify the output for the second application and aim to keep the BESS capable of providing primary control reserve.

9 Multi-Objective Optimized Control

This chapter presents a general-purpose method for the control of BESS with the *multi-objective optimized control* approach. The algorithm combines the real-time capability and wide applicability of a general fuzzy logic controller and the short-term optimal parameter tuning of the control parameters by a cuckoo-search algorithm with model prediction in a receding horizon manner. Having the cuckoo-search algorithm tune the control parameters of the fuzzy logic controller, instead of the reference power/ power setpoint of the BESS, raises the algorithm's robustness against prediction errors. The methodology is outlined in Section 9.1. The algorithm's performance is demonstrated for two case studies in Section 9.2. The chapter concludes with a summary in Section 9.3. Most of a published manuscript is used in this chapter [231].

9.1 Proposed Control Algorithm

In this section, the proposed control algorithm is outlined (Figure 9.1). First, the general structure and the interdependency of fuzzy logic control and cuckoo-search are explained before the implementation of each method and the constraint handling is described.

9.1.1 Overview of the Algorithm Structure

The core of the algorithm is the fuzzy logic controller that determines the BESS's output power based on the input values. The fuzzy logic controller's parameters are tuned by predictive model-based optimization. Recurring tuning of the fuzzy logic controller's parameters is executed with the cuckoo-search. An overview of how the fuzzy logic controller and cuckoo-search are coupled in the proposed algorithm is shown in Figure 9.1. The cuckoo-search optimizes the controller parameters with regard to the objective function J. After determining the optimal parameters x^* based on the simulation with the forecast profiles, the fuzzy logic controller is run with the actual profiles.

9.1.2 Description of Methods

9.1.2.1 Cuckoo-Search

The cuckoo-search is a bio-inspired meta-heuristic algorithm that mimics the behavior of cuckoos that lay eggs in nests and look for most promising habitats. Meta-heuristic algorithms generally show good performance at solving global optimization problems [232]. They usually require only little knowledge about the problem and exhibit the capability of avoiding local minima due to their stochastic nature. It cannot be mathematically proven that they are able to always find the global optimum. However, their results are usually satisfactory for various real-world problems. [233]

The modified cuckoo-search by Li *et al.* [234] is adopted in this paper. Different solution candidates

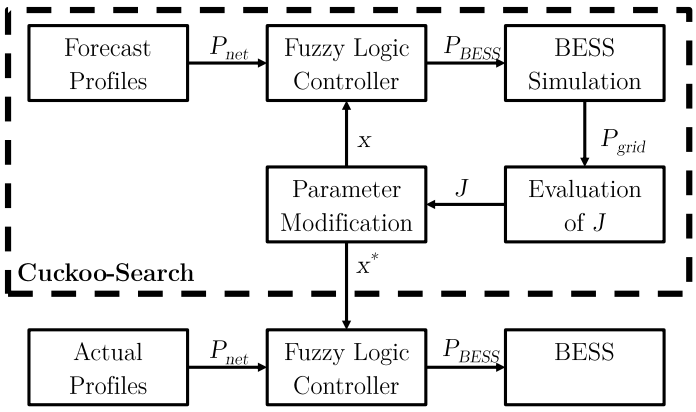

Figure 9.1: Structure of the simulation-based rolling-horizon fuzzy logic control optimization. The cuckoo-search is executed $k_{\max}$ times. The best parameter-set x^* is then used for the actual (simulated) control of the BESS until the reeding horizon is reached and the cuckoo-search is run from this new starting point.

are created with random generation of the parameters x until the number of solutions reaches the population size N. The cuckoo-search consists of three steps that are repeated every optimization iteration k: *Lévy flight*, *selection*, and *discovery*. *Lévy flight* produces N new solutions x^k_{gen}, each based on one existing solution x^{k-1}_{pop} (9.1). The *Lévy flight* is a random walk with step-lengths that have a Lévy distribution [235].

$$x^k_{\text{gen}} = x^k_{\text{pop}} + \alpha_k \cdot \mathit{Lévy} \tag{9.1}$$

These generated solutions are evaluated by computing the objective function value (fitness) $J(x)$ of each solution x. Depending on the respective fitness, a fraction of the solutions is kept for further optimization in the *selection* step. The nests x^{k-1}_{pop} and cuckoos x^k_{gen} are randomly assigned pairwise and the fitness values $J(x^k_{\text{gen}})$ and $J(x^{k-1}_{\text{pop}})$ of each pair are compared. Of each pair, the solution with superior fitness is kept for further optimization, while the remaining solution is discarded (9.2).

$$x^{k+1}_{\text{pop}} = \begin{cases} x^k_{\text{pop}} & \text{for } J(x^k_{\text{pop}}) < J(x^k_{\text{gen}}) \\ x^k_{\text{gen}} & \text{otherwise} \end{cases} \tag{9.2}$$

The subsequent *discovery* step randomly choses a share of the population and between (9.3) and (9.4), introducing additional stochasticity to the production of new solution candidates. The variable $r_{|1|}$ denotes a random number between 0 and 1 with uniform distribution: $r_{|1|} \sim \mathcal{U}([0,1])$ that is generated each time. x_r denotes the parameters of a randomly chosen solution. x^* are the parameters of a randomly chosen Pareto candidate. φ is a random value generated from a Gaussian distribution with the standard deviation σ_{CS} and mean value μ: $\varphi \sim \mathcal{N}\left(\mu_{\text{CS}}, \sigma^2_{\text{CS}}\right)$.

$$x = x_{r1} + \varphi \cdot (x_{r2} - x_{r3}) \tag{9.3}$$

$$x = x^* + \varphi \cdot (x_{r1} - x_{r2} + x_{r3} - x_{r4}) \tag{9.4}$$

The explicit choice of meta-heuristic algorithms is not essential for the proposed control-structure. Meta-heuristic, swarm optimization algorithms exhibit similar characteristics. They are population-

based, hence a number of solution candidates exist and they basically consist of three mechanisms: a random walk, a mutation technique, and an elite mechanism.

The *Lévy flight* is the mechanism corresponding to the random walk that provides the search algorithm with explorative properties. The search space is expanded by the random walk and not limited by the existing population.

The mutation mechanism of the cuckoo-search is the *discovery* step. New parameters are generated, based on the existing population and the purpose is to search the solution space within the area covered by the population and improve the existing solution. Depending on the explicit search algorithm, this could be implemented as an exchange of parameter values (e.g. genetic algorithm [232]) or some kind of calculation based on the existing parameter values, such as deviating the search direction towards existing solutions (e.g. particle swarm [232]).

The elite mechanism emphasizes the current (Pareto-) optimal solutions and aims at increasing the convergence rate towards the global optimum. The presented cuckoo-search integrates this mechanism in its *selection* step, where inferior solutions are discarded. The elite is further included in the discovery strategy, where the best solution x^* is the origin of the discovery step (9.4).

Cuckoo-search is employed to recurrently optimize the fuzzy logic parameters for the desired behavior, determined by the objective function J. The forecast profiles are used within the cuckoo-search to determine the solutions' fitness and choose the optimal parameter set. The fuzzy logic controller is simulated for each solution candidate x over the predetermined look-ahead time horizon, to obtain the corresponding BESS behavior and consequently the solutions' fitness. The optimization parameters x describe the fuzzy logic controller's parameters, that is the coordinates of the membership functions.

The simulation within the cuckoo-search utilizes the simplified models, that is a power dependent one-way conversion efficiency of the inverter with a resolution of 10 values. The values correspond to the efficiency curve of the *Type 1* inverter (Figure 2.9). A power flow model for the battery with a constant conversion efficiency of 95% is used. The model outside of the cuckoo-search utilizes the more sophisticated model, where the inverter has the output power dependent efficiency of the *Type 2* inverter described (Figure 2.9). The EC-model is used for the battery outside of the cuckoo-search. The purpose of utilizing simplified and less accurate models is to accelerate the optimization speed and, more importantly, to emulate a model error between optimization and simulation model. The proposed control algorithm is ultimately tested for controlling a real BESS with an inevitably erroneous system model for the parameter optimization.

The Lévy flight mechanism (9.1) continuously decreases its step size α_k to 30% of its initial length α_0 towards the last optimization iteration $k_{\max}$ (9.5). This results in a smaller search area for the existing solution candidates x and aims at more refined solutions and improved search convergence at later optimization stages. Lévy flight is followed by the selection step, to discard inferior solutions and keep the superior solutions (9.2).

$$\alpha_k = \alpha_0 \cdot \left(1 - \frac{k}{k_{\max}} \cdot 0.7\right) \tag{9.5}$$

The mutation mechanism randomly chooses a share of the population to modify their parameters. During the first iteration $k = 1$ of the optimization, half of the solutions has a low chance to mutate (probability of 12%). The remaining solutions mutate each with a high probability of 85%. The number of solutions with a high mutation probability r_{mut} steadily decreases to 0 at the end of the

optimization run, where every solution has a low probability of 12% to mutate (9.6). The mutation probability is randomly assigned to each solution with uniform distribution.

$$r_{\text{mut}} = 0.5 \cdot \left(1 - \frac{k}{k_{\max}}\right) \tag{9.6}$$

Of the randomly chosen individual solutions for the mutation, their chance r_{elitist} to mutate in an elitist way (9.4) and the probability of more random mutation (9.3) is 0% against 100% at the first optimization iteration $k = 1$. This probability continuously shifts with the optimization progress to 100% and 0% distribution at the last optimization iteration $k = k_{\max}$ (9.7). The search area shifts towards the best solution candidate x^*.

$$r_{\text{elitist}} = \frac{k}{k_{\max}} \tag{9.7}$$

At the end of the optimization a Pareto candidate is chosen as the result of the multi-objective optimization. The method implemented for the solution choice takes the two outer Pareto candidates to span a subspace. The distances are normalized to the value range defined by all Pareto candidates. The solution with the largest distance to the spanned subspace is chosen as final result.

9.1.2.2 Fuzzy Logic Control

The fuzzy logic approach changes the exact matching of input and output of conventional functions to an approximate matching, by applying a continuous, real-valued logic instead of the discreet Boolean logic. This blurring is usually associated with a qualitative description of ranges (e.g. high and low) and therefore allows for the development of controllers based on linguistically expressed behavior.

Fuzzy logic controllers are usually expert-designed and tuned, to obtain the desired behavior. The fuzzy logic approach has proven to be capable of controlling complex or unfamiliar systems with noisy inputs [236]. It is therefore powerful in dealing with vague inputs and nonlinear systems and promising for the control of BESS in uncertain environments.

Fuzzy logic controllers express the input by assigning the values to membership functions that describe the input value's degree of membership to the specific membership function. A Takagi-Sugeno fuzzy logic controller is implemented, hence the output membership functions have singular values. The Takagi-Sugeno type fuzzy logic controller has a computational advantage over the Mamdani type fuzzy logic controller, as the defuzzification step is omitted [237].

The unity of all membership functions and their weights corresponding to the input value are then subject to the ruleset. Any combination of the input membership functions is assigned to separate output membership functions. The ruleset for the mapping of the membership functions consists of *AND* operations. Uniform heights and weights are chosen for the membership functions of the fuzzy logic controller. The ruleset determines the weight of the output membership function of the fuzzy logic controller, based on the fuzzified input. The rules are mapped to exact output values and the resulting output of the fuzzy logic controller is determined by the weighted average of the outputs, instead of conventional defuzzification. The output value of the fuzzy logic controller represents the BESS's reference power $P_{\text{BESS}}^{\text{ref}}$. An illustration of the Takagi-Sugeno fuzzy logic controller with two inputs that each have three membership functions is shown in Figure 9.2.

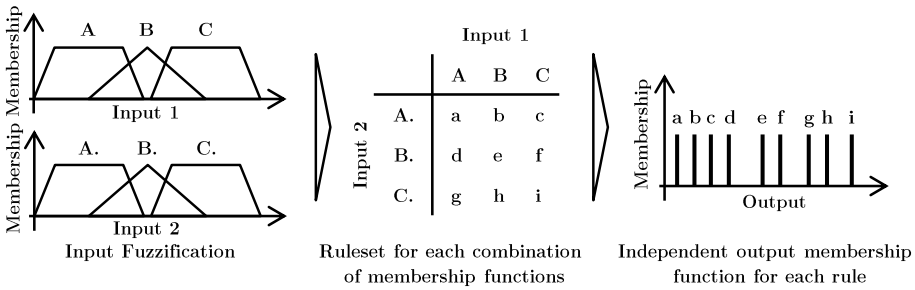

Figure 9.2: Illustration of the Takagi-Sugeno fuzzy logic controller. All combinations of the input membership functions are combined the ruleset. Each rule is assigned to an independent output membership function. The the input values' degree of membership to each membership function are the weight of the output membership function. The resulting output is the respective weighted average of the output membership functions.

The fuzzy logic controller determines the reference output power of the BESS based on the input variables that can be chosen arbitrarily. Each input has been varied with two and three membership functions in all combinations and the number with the best results were chosen for further analysis. For each input variable, both outer membership functions are trapezoidal. The remaining membership functions in between are triangular. All possible combinations of input membership function are assigned to separate output singletons in a mutually exclusive way.

The parameter set for the optimization fully describes all membership functions of the fuzzy logic controller. The parameters x for the optimization represent the position of the membership functions' defining points. Each outer trapezoidal membership function of the input variables is described by four values, each triangular membership function by three values, and each output singleton by one value. The outer two values of the trapezoidal values are treated as non-tunable parameters and kept at their original position.

9.1.2.3 Constraint Handling

Operational constraints of the BESS are handled by the simulation model and cannot be violated by the control algorithm. Constraints with regards to the membership functions are considered by the cuckoo-search's repair functions. The effective constraints are illustrated in Figure 9.3. The membership functions are required to overlap or at least connect, and the outer edge of any membership function cannot exceed the center of a neighboring membership function. The left edge B_L of the right membership function is, for example, subject to $\mathrm{A}_C \leq \mathrm{B}_L < \mathrm{A}_R$.

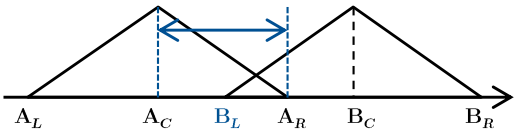

Figure 9.3: Illustration of membership function constraints.

If a newly generated solution either by *Lévy flight* or *discovery* violates any of the given constraints, the positions are reassigned to different membership functions to satisfy the constraints. If, for example, $\mathrm{B}_L > \mathrm{A}_R$, their positions are switched: B_L will be placed at the position of A_R and vice versa.

9.2 Case Studies

The proposed algorithm's capability is demonstrated for two scenarios, a PV-home storage and a BESS for a hybrid renewable-diesel island grid. Its results are compared to reference algorithms under different assumptions. Both, ideal assumptions, as well as more realistic ones that include prediction errors of the generation and load profiles, are used for the assessment.

Measurements of renewable energy production and measured as well as synthetic load profiles are used for the simulation of the scenarios. Objective functions illustrate the metrics for the evaluation of the operation strategies performance for each scenario.

The aim is to maximize the benefit of operating BESS with regard to the chosen goals. Guidance on whether to invest in BESS or not and the optimal sizing need to be assessed for each case individually and are not subject of this work.

The simulations were conducted on a *Dell Precision T7610 with Intel Xeon E5-2650 v2* workstation with 2.60 GHz with *MATLAB R2017b 64 bit*. The computation time depends on the number of the fuzzy logic controllers inputs. With the given optimization parameters of 80 iterations and a population of 45 solutions, the optimization of two inputs requires on average 71 seconds, three inputs 85 seconds and four input values require 110 seconds. The simulation of the PV-home case conducts three optimization runs per day to capture the forecast-based net load profile, obtain an updated forecast at the beginning of the peak-generation period, and to allow for a correction after the peak-generation period. It takes about 85 minutes for the two input fuzzy logic controller and 100 minutes for the three input fuzzy logic controller for the simulation and optimization time of 28 days. The simulation of the island grid with an optimization frequency of four per day requires about 205 minutes for a simulation period of 28 days. The island grid performs more optimization because the generation period is not limited to daylight periods because of the wind generation.

9.2.1 Scenarios and Assumptions

9.2.1.1 Battery Energy Storage System

Two parameter sets are used for the inverter's power flow model, described in Section 2.2. The first set is a power dependent efficiency curve that corresponds to the *Type 2* high-efficiency inverter. The second set is a less accurate efficiency curve consisting of 10 values, based on the *Type 1* inverter (Figure 2.9). The sample time of the simulation is set to $\Delta t = 15\,\text{min}$.

9.2.1.2 PV-Home Storage

The first scenario is a household with a rooftop solar unit and a PV-home BESS. The simulation and analysis span over a time period of 28 days. A week of each season has been chosen to generate a set of days to avoid seasonal influence in the operation strategy's performance. Each continuous week contains only days with solar generation to enable (reasonable) BESS operation.

The operation is compared with the *Dynamic Feed-in Limit*(Figure 2.12 (b)). The reference operation strategy does not emulate the actual *Dynamic Feed-in Limit* but simplified to copy the behavior of algorithms that optimize the immediate power output of the BESS instead of (dis-)charging policies that consider the momentary situation. No correction method to compensate for prediction errors

is implemented, thus the *Dynamic Feed-in Limit*'s effectively reduced feed-in peak may be less than anticipated. The algorithm is executed with a perfect forecast and normally distributed forecast error to schedule the future BESS output power. This way the theoretic optimum and a non-perfect BESS behavior that shows the algorithm's sensitivity to prediction uncertainties are obtained.

9.2.1.3 Objective of PV-Home Storage

The evaluation metric is the reduction of the feed-in peak $\hat{P}_{\text{grid}}$ of the grid power P_{grid} of each day, compared to the daily generation peak $\hat{P}_{\text{net}}$ of the net load P_{net} (9.8). The fuzzy logic controller's parameters x are optimized with regard to simultaneously minimizing both objective functions J_1 (9.9) and J_2 (9.10) by the cuckoo-search.

$$\hat{P}_{\text{red}} = \hat{P}_{\text{net}} - \hat{P}_{\text{grid}} \tag{9.8}$$

$$\min_x J_1 = \min_x \left(-r_{\text{ss}}\right) \tag{9.9}$$

$$\min_x J_2 = \min_x \left(-\hat{P}_{\text{red}}\right) \tag{9.10}$$

9.2.1.4 Load and Generation of PV-Home

The investigated household is a large household in Germany with an annual electricity consumption of 7000 kWh and a rooftop PV unit with a capacity of 8.0 kWp [29]. The load is modeled as a synthetic load profile of an individual household, obtained from a profile generator [177].

The generation profile of the PV unit is measured from a solar panel with a tilt angle of 0° at a latitude of 48°08′59″ N. The energy produced per kWp installed is 899.34 kWh per year. The measurements were taken at the AC-side of the inverter in 2009 (Figure B.2). Both load and generation profiles are scaled to the values of the chosen household parameters.

The BESS has a usable energy capacity of 4.0 kWh and a rated power of 4.0 kW, suggested as the optimal size for the most common household size in Germany [28]. Table 9.1 gives an overview of the household parameters.

Table 9.1: Household model parameters.

Parameter	Value	Unit
Household load	7,000	kWh/a
Rooftop PV unit size	8.0	kWp
PV energy production	899.34	kWh/kWp/a
BESS useable energy	4.0	kWh
BESS nominal power	4.0	kW

9.2.1.5 Forecast of PV-Home Profiles

Realistic prediction errors for generation are implemented to analyze their impact on the operation strategy. The modeled prediction error for the PV production is based on statistical errors of actual predictions. A normal error distribution is assumed and a standard deviation σ_{FC} of 0.1924 normalized to the PV-peak power is used in this work to model the prediction error. The average 24h ahead baseline prediction of the solar utilities Tucson Electric Power (Arizona), Green Mountain Power (Vermont),

and Smyrna (Tennessee) of the year 2013, given by Zhang *et al.*, are used to calculate the standard deviation [238].

The erroneous forecast is generated based on the actual profile that has been measured. The hourly average value of the profile is used as the base and offset with a random, normal distributed error generated with the respective standard deviation σ_{FC}. This produces hourly prediction values with the respective standard deviation (Figure 9.4). The synthesized forecast is similar to actual forecasts with respect to uncertainty, as we use the same statistical parameters to generate them.

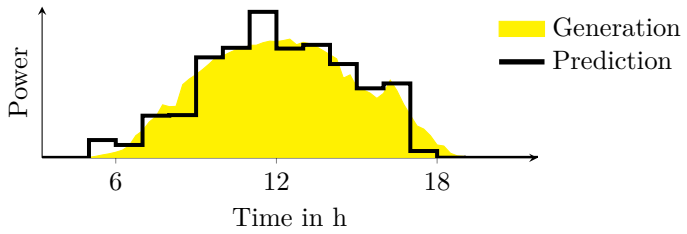

Figure 9.4: Illustration of the synthetic prediction error.

The optimization of the fuzzy logic controller parameters uses an updated short-term forecast of the PV-generated energy in addition to the modeled prediction error, described above. Adapted predictions are based on a clear-sky prediction and the PV generated energy of the day. The short-term prediction method is illustrated in Figure 9.5. The clear-sky prediction depends on the latitude, tilt angle, the azimuth angle of the PV-panel, and the time and date of the year. The intensity of direct sun radiation is calculated and assumed to correspond to the output power of the PV-unit. At the time of the optimization, the PV-generated energy of the previous three hours is compared to the theoretic maximum generated energy according to the clear-sky prediction. The fraction of the actually generated energy (yellow area) is then multiplied with the clear-sky prediction (grey, dashed line), to obtain the adapted PV-prediction (blue line). The next three hours of PV-generation forecast are assumed to equate that adapted prediction, while more distant future predictions remain according to the forecast described above. This update is considered for the calculation of the PV-generated energy forecast only.

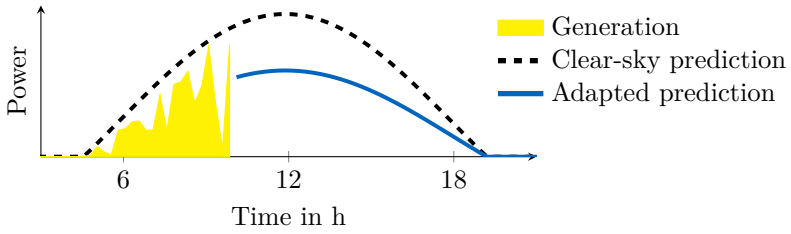

Figure 9.5: Illustration of the short-term adapted clear-sky prediction.

The load is less generalizable and its predictability correlates with the number of households considered. Single households are hardly predictable without additional information. The load of the previous day is used as persistent forecast.

9.2.1.6 Optimization Parameters and Fuzzy Logic Structure

The cuckoo-search algorithm is executed with 45 nests and a total of 80 iterations. The cuckoo-search's parameter standard deviation σ_{CS} is 0.4 and its mean value μ_{CS} is 0.5. The simulation is run eight

times to account for the stochastic mechanisms of cuckoo-search and to ensure that the result is not a single outlier.

Two well-performing fuzzy logic controllers have been identified from the simulation results. The first controller uses the net load P_{net} and the BESS's SOC as input, each with three membership functions. Fuzzy logic controllers with lower numbers of membership functions achieved inferior results. The second analyzed fuzzy logic controller uses the generated energy forecast of the look-ahead period as an additional input value for the computation of the output value. The numbers of the input membership functions with the best results are two membership functions for the net load and three membership functions each for the inputs SOC and energy generation forecast. The number of output singletons comprises of the amount of all possible combinations of the input membership function, thus 9 values for the output of the first fuzzy logic controller and 18 values for the second controller. Table 9.2 gives an overview of the input parameters and the membership functions.

Table 9.2: Configuration of fuzzy logic controller for PV-home case.

fuzzy logic controller Parameter	2 inputs membership	3 inputs functions
net load	3	2
SOC	3	3
energy gen. forecast	0	3
output	9	18

The outputs of the fuzzy logic controllers are subject to the constraints that the BESS may only discharge to provide the household's load (9.11) and only charge excess PV-generated energy (9.12).

$$0 \geq P_{\text{BESS}}^{\text{ref}} \geq -P_{\text{net}} \qquad \text{for } P_{\text{net}} \geq 0 \tag{9.11}$$

$$0 < P_{\text{BESS}}^{\text{ref}} \leq -P_{\text{net}} \qquad \text{for } P_{\text{net}} < 0 \tag{9.12}$$

The look-ahead period for the cuckoo-search that performed best for the chosen objective is 24 hours and the cuckoo-search's recurrence is three times each day at 3 AM, 10 AM, and 1 PM.

9.2.1.7 Hybrid Renewable-Diesel Island Grid

The second scenario is the hybrid renewable-diesel island grid of Graciosa Island, already analyzed in Section 6.3. A total of 28 days have been chosen for the simulation (days 40-46, 137-143, 235-241, and 324-330 of the year 2016). One week for each of the four seasons has been chosen to obtain a representative set of days and avoid seasonal influence on the overall performance of the operation strategies.

The BESS is parameterized with a nominal power of 6 MW and usable energy of 5.3 MWh, identical to Stenzel *et al.* [131].

9.2.1.8 Objective for Island Grid Storage

The objective J for the optimization consists of the fuel cost of the diesel generator and the cost of load shedding (9.13). The load shedding is introduced to force the BESS to supply the required net load. The economic assumptions for the diesel operation are fuel costs c_{Fuel} of 2 EUR/l [96] and a penalty

$c_{\text{load}}^{\text{shed}}$ of 800 EUR/MWh$_{el}$ for load energy $E_{\text{load}}^{\text{shed}}$ that is shed/not supplied. The penalty is chosen to be higher than the electricity produced by the diesel generator, to prioritize the supply of the load [239].

$$J = c_{\text{Fuel}} \cdot V_{\text{Fuel}} + E_{\text{load}}^{\text{shed}} \cdot c_{\text{load}}^{\text{shed}} \tag{9.13}$$

9.2.1.9 Forecast of Island Grid Profiles

The modeling of the prediction errors for PV and the load is identical to the PV-home case. The PV error is a normal distribution with a standard deviation σ_{FC} of 0.1924 normalized to the nominal PV-peak power. The load forecast is the persistence of the previous look-ahead period of 24 hours.

The forecast of the wind generation is modeled as hourly predicted values, according to probability density functions analyzed by Hodge *et al.* [240]. They describe the prediction errors with a hyperbolic distribution, that are modeled in the same way as the PV-prediction error. The hourly average of the actual profile is offset with a random value, generated with the respective error distribution.

The forecast is modeled using the error parameters of the *Spanish case* (Table 9.3) presented by Hodge *et al.*, with a mean value μ_{FC} of 0.0162, a standard deviation σ_{FC} of 0.0514, a skewness $\gamma_{1,\text{FC}}$ of 0.3855, and a kurtosis $\gamma_{2,\text{FC}}$ of 3.0180 [240]. The values are normalized to the installed wind generation capacity.

Table 9.3: Parameters of the wind forecast error [240].

Parameter		Value
Distribution type		Hyperbolic
Mean value	μ_{FC}	0.0162
Std. deviation	σ_{FC}	0.0514
Skewness	$\gamma_{1,\text{FC}}$	0.3855
Kurtosis	$\gamma_{2,\text{FC}}$	3.0180

9.2.1.10 Optimization Parameters and Fuzzy Logic Configuration

The cuckoo-search algorithm is executed with 45 nests and a total of 80 iterations. The cuckoo-search's parameter standard deviation σ_{CS} is 0.4 and its mean value μ_{CS} is 0.5. The simulation is run eight times to account for the stochastic mechanisms of cuckoo-search and to ensure that the result is not a single outlier.

The fuzzy logic controller uses the power system's current net load, the BESS's SOC, the diesel generator state (must run or must remain off), and the diesel generator's time since the last state change as input. The fuzzy logic controller uses two membership functions for the net load and three membership functions for each of the remaining inputs. Each possible combination of input membership functions is assigned to an output membership function, resulting in 54 output singletons. The chosen number of membership functions performed best among all 16 tested combinations. The algorithm considers a look ahead time period of 24 hours and the parameters are optimized four times each day at 3 AM, 10 AM, 1 PM, and 4 PM. Table 9.4 gives an overview of the input parameters and the membership functions.

Table 9.4: Configuration of fuzzy logic controller for island grid case.

Parameter	membership functions
net load	2
SOC	3
diesel generator state	3
time since diesel generator state change	3
output	54

9.2.2 Results

9.2.2.1 Results of PV-Home Storage

Figure 9.6 shows the achieved self-sufficiency rates by the BESS with different operation strategies. The white bars on the left represent the self-sufficiency rate achieved with the ideal forecast. The blue bars on the right of each group illustrate the self-sufficiency rate based on the flawed forecast.

The self-sufficiency rate of the analyzed PV-home without BESS is 33.6%. The ideal self-sufficiency rate for the given BESS is 59.1% achieved by the *Dynamic Feed-in Limit* operation strategy. Forecast errors reduce the self-sufficiency rate to 46.2%. Fuzzy logic control with ideal forecast and two inputs net load and SOC achieves a smaller self-sufficiency rate of 56.5%. Prediction errors further reduce the achieved self-sufficiency rate to 53.5%. Similar values are achieved with the fuzzy logic controller that considers the forecast energy generation. In this case, the self-sufficiency rate achieved with perfect prediction is 56.7% and 54.2% with the erroneous forecast.

The self-sufficiency rates achieved by the fuzzy logic controllers are lower for the perfect prediction case but are less sensitive to flawed prediction compared to the forecast based pre-scheduling of the BESS power.

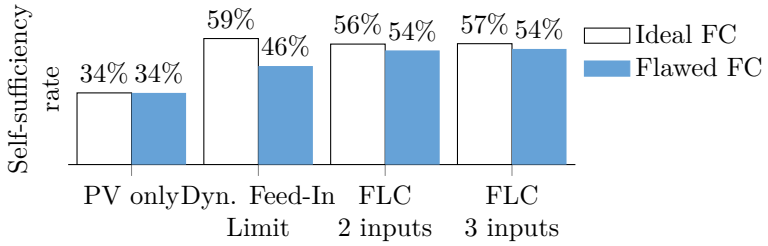

Figure 9.6: Self-sufficiency rates of reference algorithm and optimized fuzzy logic controllers for ideal and erroneous forecast.

The power flows of the household operating the BESS are shown in Figure 9.7 for two exemplary days. The top left figure (a) is the BESS with *Dynamic Feed-in Limit* with perfect prediction. The bottom left plot (b) shows the *Dynamic Feed-in Limit* with forecast error. This is equivalent to an optimization based controller without adaption to prediction uncertainties. The top right figure (c) shows an exemplary fuzzy logic controller with two inputs net load P_{net} and SOC. The bottom right figure (d) depicts an exemplary fuzzy logic controller that in addition considers the generated energy forecast of the look-ahead period $E_{\text{PV}}^{\text{FC}}$. Both fuzzy logic controllers shown are tuned with erroneous predictions of load and generation. The black line represents the net load of the household, the blue area is the battery power, and the green area is the power exchanged between the household and the electricity grid. The grey and yellow area are, respectively, the household load and PV-generation

that determine the net load. The feed-in peaks of each day are denoted with red dashed lines and the respective value.

The *Dynamic Feed-in Limit* with perfect forecast (a) achieves maximum self-sufficiency rate and feed-in peak reduction. However, the performance deteriorates, if the operation strategy is confronted with prediction errors (b). The output of the BESS is pre-determined for each time-step based on the prediction. Any deviation immediately reflects on the performance. Feed-in peaks are not well-predicted and therefore not well-handled. The last peak on the second day, for example, has not been well-predicted and the BESS even discharges at that time, instead of charging, because of the deviating forecast. The inappropriate discharge is marked with a red circle. A similar issue occurs at the evening of day one, where the operation strategy expects a larger load and discharges the BESS, resulting in grid feed-in. Both events do not conform to regulations of the applications and illustrate that forecast-based optimization of the power output is not suitable for real-time energy management of BESS.

Both fuzzy logic controllers generally exhibit better results than the prediction based pre-scheduling, when forecast errors are present. The shown profile of the fuzzy logic controller with two inputs reveals, that the controller charges too quickly on the first day and cannot reduce the feed-in in the second half of the peak generation period and is even worse than the pre-scheduled *Dynamic Feed-in Limit* with forecast errors (b). Introducing the forecast energy generation as an input variable for the fuzzy logic controller leads to slightly better feed-in peak reduction on the first day (d). However, the last feed-in peak of the second day is not well handled by the fuzzy logic controller with three inputs (d). In this specific case, the simpler fuzzy logic controller with two inputs leads to a better feed-in peak reduction.

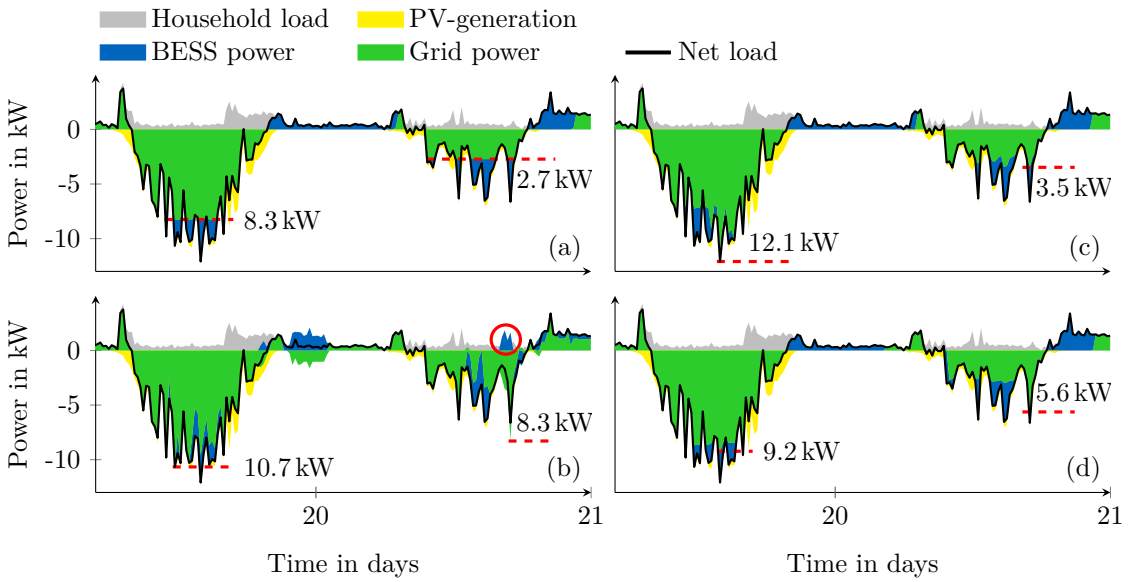

Figure 9.7: Profiles of PV-home BESS. The left figures show the BESS output with *Dynamic Feed-in Limit*. The upper plot (a) is shown with perfect forecast. The bottom figure (b) is the case with prediction error. The two right plots (c) and (d) show the fuzzy logic controllers, both with prediction error. The top plot (c) is the profile of the fuzzy logic controller with two inputs. The bottom plot (d) depicts the fuzzy logic controller with three inputs.

The daily feed-in peak reduction achieved by the BESS with different operation strategies is shown in Figure 9.8. The days are not in a chronological order but the values are sorted in a descending

order of the peak reduction achieved by the respective operation strategy. The dashed lines show the peak feed-in reduction by the operation strategies run with the perfect forecast. The solid lines represent their performance if only non-perfect forecast is available for their optimization. The feed-in peak reduction achieved by the *Dynamic Feed-in Limit* is illustrated by grey lines. The fuzzy logic controller with two inputs (net load and SOC) is represented by blue lines. The fuzzy logic controller's performance with the generated energy forecast as additional input is shown by orange lines.

While the *Dynamic Feed-in Limit* performs perfectly with the ideal forecast, it suffers severely from prediction errors. The feed-in peaks may even increase because of the prediction errors and no correction method is in effect that may prevent unfavorable BESS behavior. Figure 9.8 reveals that this happens in 5 of the 28 analyzed days. This issue is also apparent in Figure 9.7 at the last peak of the second day, where the BESS is scheduled to discharge and consequently raise the grid feed-in power.

The fuzzy logic controllers, in contrast, both achieve a comparably good performance, despite erroneous prediction. In case of perfect prediction, however, they are not capable of utilizing the whole BESS potential for the peak reduction. The fuzzy logic controller with two inputs achieves slightly better results than its three-input equivalent over all days in the flawed forecast case.

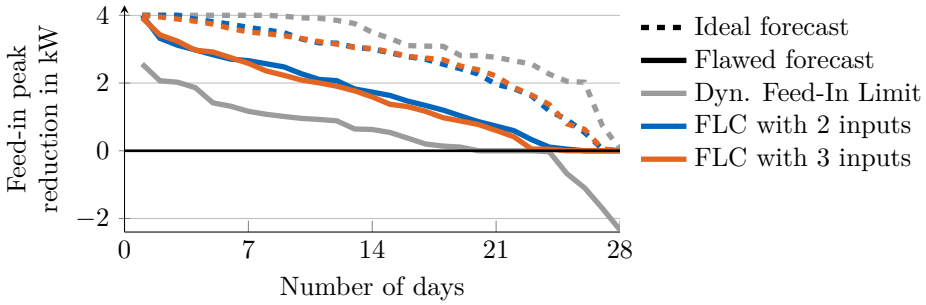

Figure 9.8: Feed-in peak reduction of optimized fuzzy logic controller compared with reference operation strategies for each of the 28 simulated days in descending order.

Figure 9.9 compares the peak reduction of the fuzzy logic controllers and the *Dynamic Feed-in Limit* with erroneous prediction. The increase of feed-in peak-reduction by the fuzzy logic controllers compared to the pre-scheduling by the *Dynamic Feed-in Limit* with forecast errors is shown. The difference in peak reduction of the same days is shown in a descending order. The fuzzy logic controllers consistently achieve better results in the presence of prediction errors. The fuzzy logic controller with two inputs (blue line) only achieves a slightly lower feed-in peak-reduction than the rule-based reference in three days. Adding the generated energy forecast as input for the fuzzy logic controller (orange line) leads to slightly poorer results for the majority of the days.

The proposed control algorithm achieves slightly inferior results compared to the reference operation strategy under perfect conditions but is considerably more robust to prediction errors that are common in real-world applications.

9.2.2.2 Results of Island Grid

The proposed algorithm's performance is evaluated by the fuel reduction compared to the island without BESS. Figure 9.10 shows the profiles of the island for an exemplary day. The top figure shows the *load follow* operation strategy. The optimized fuzzy logic controller is shown in the middle figure. The bottom figure depicts the profiles of the *On-Off* operation strategy. The figures show the load

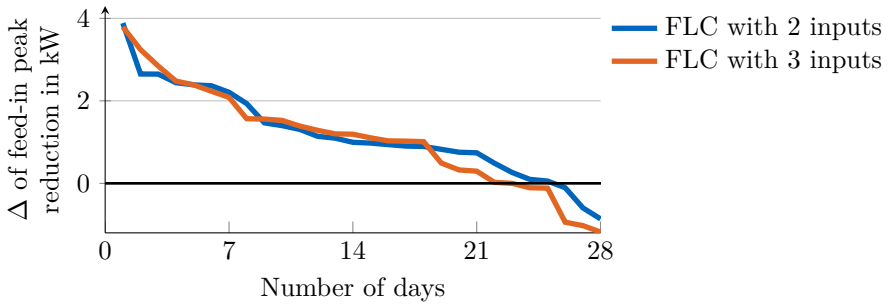

Figure 9.9: Difference of feed-in peak reduction of optimized fuzzy logic controller against the reference operation strategy with forecast error for each of the 28 simulated days in descending order.

(grey area), the wind generation (orange area), the PV-generation (yellow area, stacked on the wind generation), the consequent net load (black line), the DG generation (green area), the BESS power (blue area), and the resulting curtailment (red area).

The *load follow* operation strategy provides the load with the BESS first but does not plan ahead. Instead of charging the BESS with the running DG to prevent later ramp-up, only the minimum power output of the DG is used. The *On-Off* operation strategy leads to larger DG output and higher fuel consumption. However, the BESS is charging the excess power and has sufficient energy to provide the load at the end of the day and prevent an additional ramp-up of the DG. The optimized fuzzy logic controller behaves similarly to the *load follow* operation strategy but does not follow the load as well. It evokes larger DG power output and the curtailment of the RES indicates that the RES are not optimally utilized.

A bar chart with the fuel reduction achieved by operating the BESS is shown in Figure 9.11 (a). The ratio of the load shed to the overall load is depicted in Figure 9.11 (b). The results represent the performance over all of the 28 simulated days compared to an island grid without BESS. The BESS with *On-Off* reduces the fuel consumption by 9.4% and the *load following* algorithm leads to 63.8% reduction of the fuel consumption. The fuzzy logic controller reduces the fuel consumption by 47.4% under perfect conditions. Prediction errors deteriorate the reduction to 34.4% less fuel consumption. The shed load is below 1% of the energy consumption.

The results summarize the BESS behavior shown in Figure 9.10. While the *load following* algorithm is superior in reducing the diesel generation, the fuzzy logic controllers are not sufficiently accurate to achieve comparable results. The *On-Off* algorithm leads to unnecessary power output, as seen in the figure, and is therefore not capable of reducing the diesel generation substantially.

Varying residual energy in the BESS for the different cases has not been taken into account for the results. The island grid without BESS, however, requires the diesel generator to generate 311 MWh of electricity, largely exceeding the BESS's nominal energy capacity of 5.3 MWh.

9.2.2.3 Discussion of both Scenarios

The proposed controller has been demonstrated for different scenarios. The results are in general acceptable, though can probably be improved. Compared to the reference operation strategies, that rely on prediction data, the optimized fuzzy logic controller is more robust against prediction errors.

The optimization recurrence has been varied from several times a day to once every day. The look-

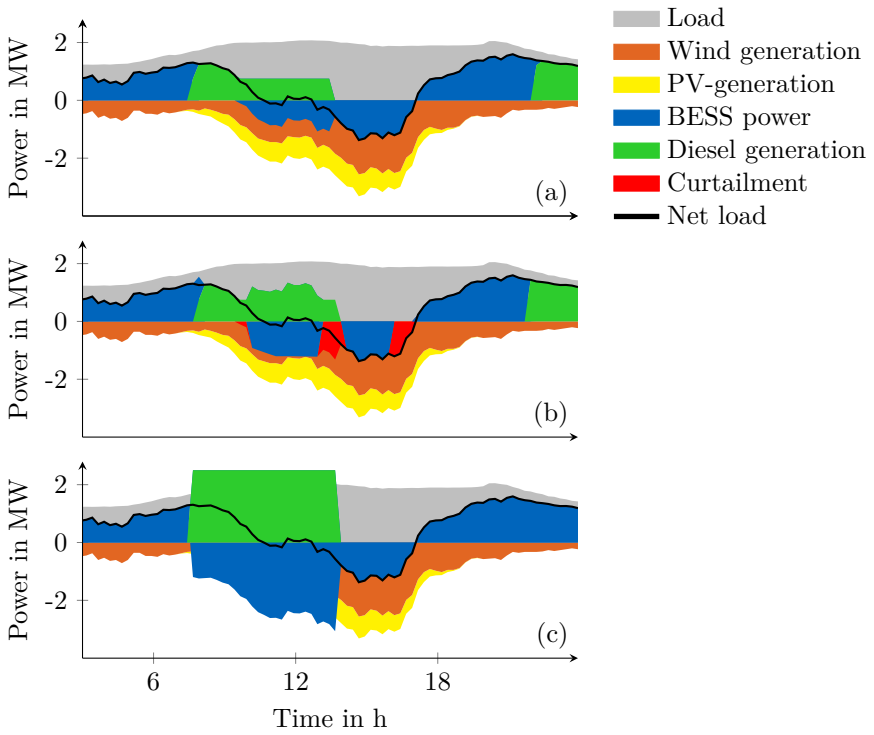

Figure 9.10: Profiles of the island grid of day 238 of 2016 with different operation strategies for the BESS. The figure on top (a) shows the profiles with the *load following* operation strategy. The middle figure (b) illustrates the performance of an optimized fuzzy logic controller with forecast error. The bottom figure (c) depicts the power flows with an *On-Off* operation strategy.

ahead horizon has been varied from one day up to seven days. Longer look-ahead horizons, as well as less frequent optimization, lead to inferior results.

Increasing the use of RES in an island grid is a more straightforward application and the reference operation strategies do not require profile prediction. In this case, the optimized fuzzy logic controller is inferior to the *load follow* reference operation strategy, yet outperforms the non-optimal reference *On-Off* strategy.

More inputs, such as the generated energy forecast provide the controller with additional adaptiveness and, if feasible, lead to better performance. This can be seen in the PV-home case, where the fuzzy logic controller with three inputs is consistently better than the one with two inputs. The increased

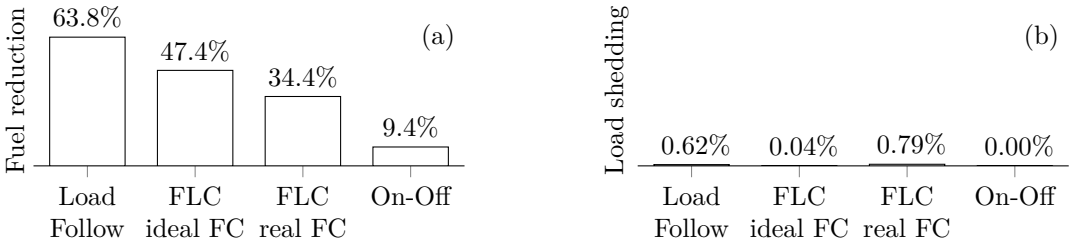

Figure 9.11: Reduction of fuel consumption (a) by reference algorithms and optimized fuzzy logic controller compared to island grid without BESS. The rate of load shedding is depicted in the right Figure (b).

adaptiveness, however, seems to also increase the sensitivity against certain prediction errors, like on day 2, where the fuzzy logic controller with two inputs is superior to its three-input counterpart that underestimates the last feed-in peak. Other input values, such as the time of the day, did not improve the controller's performance and partially increased its sensitivity to forecast uncertainties.

The proposed fuzzy logic control-structure is exploited as a general controller, that can be adapted for a wide range of objectives and system configurations. The property of *fuzziness* reduces the impact of prediction errors, as demonstrated in the PV-home case. At the same time, it does not handle discrete events well, such as preventing the ramp-up of the DG, even though the BESS would be capable of doing so. The controller does not excel at tasks that require the BESS to provide exact values output power.

The proposed algorithm can be deployed for different applications without changing its general structure. The algorithm is more suited for complex applications with high degrees of freedom, where reference operation strategies are not as obvious. The method can be utilized as a systematic approach to gradually develop control algorithms, by varying input membership functions and possible input values. The resulting fuzzy logic controller and its linguistic representation could be used as the basis for the development of a parametric, rule-based controller.

9.3 Summary of Multi-Objective Optimized Control

The proposed algorithm is based on a fuzzy logic controller that is optimized in a recurring manner, by a cuckoo-search algorithm. It shows superior robustness against prediction errors, compared to the reference parametric controllers in the PV-home case. As demonstrated in two example cases, the algorithm may be deployed for different systems and applications. The combination of the fuzzy logic controller with meta-heuristic optimization overcomes the drawback of widespread manual tuning of the fuzzy logic controller. The use of fuzzy logic control allows a wide range of desired behavior based on the momentary input. The cuckoo-search ensures optimality within the ability of the controller for a variety of scenarios instead of the need to optimize parameters for a specific scenario. Results show, however, that the configurations of the fuzzy logic controller with the best performance under realistic forecast uncertainties, do not capture the full potential in the ideal case.

A limitation is the complexity of the controller that requires meta-heuristic optimization, fuzzy logic control, and a system model. It furthermore relies on prediction data, which may not always be available. The use of the controller is limited to applications, that allow a certain freedom to operate. BESS applications that impose fixed rules on the BESS output power, such as primary control reserve are not suitable for the proposed control algorithm.

The proposed method represents a systematic approach to handle prediction uncertainties, associated with renewable energy generation. The controller's real-time capability is ensured by the underlying rule-based fuzzy logic controller. The algorithm uses forecasts with a longer sample time for the parameter optimization than the profiles of the simulation, indicating that it can process shorter sample periods. Optimization to achieve improved results is included with the meta-heuristic search algorithm, to optimize the controller's parameters based on prediction data. The algorithm is adaptive to changing environment because of its receding horizon principle, instead of a one-time offline parameter optimization. This allows exploiting more accurate near-term forecast and adjusted control parameters.

10 Application Stacking

This chapter proposes a concept to operate BESS with the *application stacking* approach. The structure is described in Section 10.1 and illustrated with examples in Section 10.2. A summary (Section 10.3) concludes this chapter. A large proportion of this chapter has been published in [241].

10.1 Structure of Concept

A two-layer concept for the *stacking of applications* is proposed. The first layer consists of a time-ahead planning of the BESS partitions for a defined time period (e.g. a day ahead). The partitions comprise the BESS resources and right of use. The second layer allows shifting of the pre-determined storage partitions between the planning phases.

The first layer determines the expected use of storage partitions of each application for planning purposes and to resolve financial obligations. The second layer allows an exchange of BESS-resources within the operation period of the time-ahead planning between the applications. This allows consideration of forecast uncertainties and to react on them.

10.1.1 Time-Ahead Planning for Battery Resources

The first layer is the pre-planning where BESS resources and right of use (energy capacity, stored energy, priority power value, and rank) for each application are determined, depending on their forecast needs.

The virtual energy capacity segments E_k^C of the BESS are assigned to each stakeholder k. The sum of all n capacity segments is equal to the total physical nominal energy $E_{\mathrm{BESS}}^{\mathrm{nom}}$ of the BESS (10.1). A segment that is not allocated to any application may exist. The physically stored residual energy E^r in the BESS is distributed among the applications and is associated to the state-of-charge (SOC) (10.2). Consequently, the residual energy segments E_k^r may not be negative and must not exceed the corresponding energy capacity segment E_k^C (10.3). This translates to constraints (10.4) and (10.5) for the power P_k assigned to the segments. The variables with a bottom index (k, A or B) denote the segments in general or the specific value for the respective stakeholder.

$$E_{\mathrm{BESS}}^{\mathrm{nom}} = \sum_{k}^{n} E_k^C \tag{10.1}$$

$$E_{\mathrm{BESS}}^{\mathrm{nom}} \cdot \mathrm{SOC} = E^r = \sum_{n}^{k} E_k^r \tag{10.2}$$

$$0 \leq E_k^r \leq E_k^C \quad \forall k \tag{10.3}$$

$$P_k \geq 0 \qquad \text{if } E_k^r = 0 \tag{10.4}$$

$$P_k \leq 0 \qquad \text{if } E_k^r = E_k^C \tag{10.5}$$

An illustration of the energy asset segmentation is shown in Figure 10.1. The physical reality of the BESS is shown on the left, while the virtual segmentation is depicted on the right of the Figure. The residual energy segment E_k^r is the energy stored in the respective energy capacity segment E_k^C. The balanced energy segment $E_k^b = E_k^C - E_k^r$ represents the storable energy until the segment is fully charged.

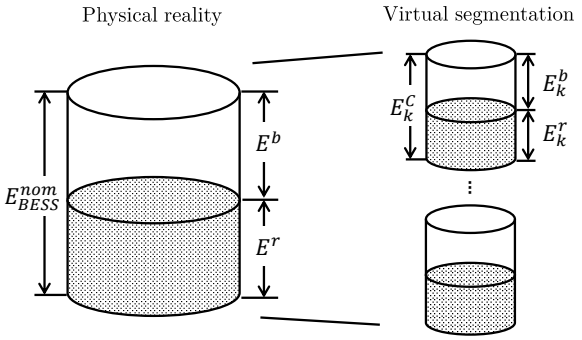

Figure 10.1: Illustration of BESS segmentation and distribution according to the planning stage.

Unlike energy, power is only limited by momentary values, instead of persisting system states. The constraints for the power distribution are therefore not as strict as the energy constraints. The sum of assigned power values determines the physical output of the BESS. Each application is given a rank R_k and yields a priority power value P_k^P.

Equations (10.6) to (10.9) describe the power allocation to each application if the total requested reference power $\sum_k P_k^{\text{ref}}$ exceeds the nominal power $P_{\text{BESS}}^{\text{nom}}$ of the system. During the first distribution, a maximum of prioritized power value P_k^P is assigned.

Equations (10.6) to (10.8) are computed for each application sequentially in the order of their rank R_k. If physical power is available after assigning the powers $\tilde{P}_k$ for all applications in the first step, the unmet reference powers $\tilde{P}_k^{\text{ref}}$ (10.8) are met with the remaining BESS power capability P^{rem} (10.6). The ratios of the unmet reference powers $\tilde{P}_k^{\text{ref}}$, after execution of (10.6) to (10.8) for all applications, determine the allocation of the power for each application P_k (10.9). If the BESS reaches its power limit $P_{\text{BESS}}^{\text{nom}}$ at any step of the power assignment, the current value is set to maximize the output power. All following reference powers are then set to 0.

$$P^{\text{rem}} = P_{\text{BESS}}^{\text{nom}} - \left| \sum_k^n \tilde{P}_k \right| \tag{10.6}$$

$$\tilde{P}_k = \begin{cases} \min\left\{P_k^{\text{ref}}, P^{\text{rem}}, P_k^P\right\} & \text{for } P_k^{\text{ref}} \geq 0 \\ -\min\left\{-P_k^{\text{ref}}, P^{\text{rem}}, P_k^P\right\} & \text{for } P_k^{\text{ref}} < 0 \end{cases} \tag{10.7}$$

$$\tilde{P}_k^{\text{ref}} = P_k^{\text{ref}} - \tilde{P}_k \tag{10.8}$$

$$P_k = \tilde{P}_k + \frac{\tilde{P}_k^{\text{ref}}}{\left|\sum_l^n \tilde{P}_l^{\text{ref}}\right|} \cdot P^{\text{rem}} \quad \forall k \tag{10.9}$$

10.1.2 Intra-Day Battery Resource Shifting for Real-Time Control

The second layer allows re-allocation of resources in cases of prediction errors. Stakeholders may require obtaining additional resources to fulfill their objectives because of prediction errors. The control algorithm may detect the shortage of resources for each stakeholder individually during operation and trigger the request for more resources from another resource holder.

These new resources allow the receiving stakeholder to meet his objectives, while the resource provider may suffer performance losses and consequently financial losses. The terms of the transactions and the respective compensation that the parties agreed on in the first operation layer apply.

A general description and the associated constraints of the transactions and the implications on the BESS state are given in (10.10) to (10.12). Energies (both energy capacity E_k^C or residual values E_k^r) may be changed at any time (10.10), given that any increase ΔE_k is taken from other segments (10.11). This ensures the overall energy balance (10.1) and (10.2). The superscript star denotes the new value E_k^*, the superscript 0 denotes the previous value E_k^0. The redistribution is not limited to pairs of applications but may include more parties (10.12). ΔE_{kl} denotes an energy transfer from application k to application l. The notation with shifting residual energy implies that the shifting of energy capacity refers to *empty* capacity. If both energy capacity and residual energy should be shifted, this is done in two separate operations.

$$E_k^* = E_k^0 + \Delta E_k \quad \forall k \tag{10.10}$$

$$\sum_k^n \Delta E_k = 0 \tag{10.11}$$

$$\Delta E_k = \sum_l^n \Delta E_{lk} \quad \forall k \tag{10.12}$$

10.2 Illustrating Examples

The first examples in this Section show the proposed behavior of the BESS with two stakeholders. Charging power is defined by positive power values. Negative power values represent a discharging. Suppose a BESS with following states and allocation of the properties to each stakeholder A and B.

The physical properties and states are the nominal energy capacity $E_{\text{BESS}}^{\text{nom}} = 100\,\text{kWh}$, nominal power $P_{\text{BESS}}^{\text{nom}} = 50\,\text{kW}$ and the stored (residual) energy $E^r = E_A^r = 5\,\text{kWh}$. The properties of application A, application B, and the total values, are given in Table 10.1.

Table 10.1: Example values of the right of BESS-use and virtual states of applications.

Application k	Energy Capacity E_k^C	Residual Energy E_k^r	Priority Power P_k^P	Rank R_k
A	75 kWh	5 kWh	10 kW	2
B	25 kWh	0 kWh	20 kW	1
Total	100 kWh	5 kWh	30 kW	-

Negating Output Powers

Opposing power requests P_k^{ref} of the stakeholders' operation strategy negate each other and the residual power is executed by the BESS if all relevant constraints are fulfilled. Suppose application A requires a power P_A^{ref} of 30 kW and application B requests a power P_B^{ref} of -25 kW, the resulting reference power is the sum of both reference powers (10.13).

$$\sum_{k}^{n} P_k^{\text{ref}} = 5\,\text{kW} \tag{10.13}$$

Energy Capacity Allocation

The next example illustrates how the allocated energy capacity segments E_k^C of stakeholder k limits the requested power P_k^{ref}. Suppose that both applications request a discharging power of both 10 kW (10.14). As application B has no energy left for discharge (Table 10.1), its residual energy is at the limit and the application must keep the energy constraint (10.3). Consequently, application B does not discharge (10.15). The overall output power of the BESS is equivalent to the output of application A (10.16).

$$P_A^{\text{ref}} = P_B^{\text{ref}} = -10\,\text{kW} \tag{10.14}$$

$$P_B \geq 0\,\text{kW} \rightarrow P_B = 0\,\text{kW} \tag{10.15}$$

$$P = P_A + P_B = -10\,\text{kW} \tag{10.16}$$

Hierarchical Distribution of Power

If the sum of the requested power exceeds the nominal power (10.17), a priority based distribution of the BESS's nominal power to the requested output of each application is executed. Suppose the reference power of application A is $P_A^{\text{ref}} = 50\,\text{kW}$ and application B requires $P_B^{\text{ref}} = 30\,\text{kW}$. Application A is assigned power first because it has a higher rank $R_A = 2$ than application B with a rank of $R_B = 1$.

In the first step, A receives its reference power up to a maximum of its prioritized power P_A^P or the remaining power P^{rem} (10.18). Since no power allocation has taken place in this iteration yet, the remaining power P^{rem} equates to the nominal power $P_{\text{BESS}}^{\text{nom}}$ (10.6). $\tilde{P}_A$ is the preliminary power that is allocated in the first step according to (10.7). The remaining power P^{rem} (10.19) is then assigned to application B (10.20), with the same rules that the priority power P_B^P and remaining capacity P^{rem} limit the allocated power $\tilde{P}_B$ (10.7).

After assigning all preliminary powers $\tilde{P}_k$, the remaining power P^{rem} (10.21) is distributed among the residual $\tilde{P}_k^{\text{ref}}$ powers (10.8) according to their proportions (10.9) and the definite powers P_k are

assigned to the applications (10.22) and (10.23). Figure 10.2 graphically represents (10.18) to (10.21).

$$\sum_{k}^{n} P_k^{\text{ref}} = 80\,\text{kW} > P_{\text{BESS}}^{\text{nom}} \tag{10.17}$$

$$\tilde{P}_A = \min\left\{P_A^{\text{ref}}, P^{\text{rem}}, P_A^P\right\} = \min\left\{50\,\text{kW}, 50\,\text{kW}, 10\,\text{kW}\right\} = 10\,\text{kW} \tag{10.18}$$

$$P^{\text{rem}} = P_{\text{BESS}}^{\text{nom}} - \tilde{P}_A = 50\,\text{kW} - 10\,\text{kW} = 40\,\text{kW} \tag{10.19}$$

$$\tilde{P}_B = \min\left\{P_B^{\text{ref}}, P^{\text{rem}}, P_B^P\right\} = \min\left\{30\,\text{kW}, 40\,\text{kW}, 20\,\text{kW}\right\} = 20\,\text{kW} \tag{10.20}$$

$$P^{\text{rem}*} = P^{\text{rem}0} - \tilde{P}_B = 40\,\text{kW} - 20\,\text{kW} = 20\,\text{kW} \tag{10.21}$$

$$P_A = \tilde{P}_A + \frac{\tilde{P}_A^{\text{ref}}}{\left|\sum_k^n \tilde{P}_k^{\text{ref}}\right|} \cdot P^{\text{rem}} = 10\,\text{kW} + \frac{40\,\text{kW}}{50\,\text{kW}} \cdot 20\,\text{kW} = 26\,\text{kW} \tag{10.22}$$

$$P_B = \tilde{P}_B + \frac{\tilde{P}_B^{\text{ref}}}{\left|\sum_k^n \tilde{P}_k^{\text{ref}}\right|} \cdot P^{\text{rem}} = 20\,\text{kW} + \frac{10\,\text{kW}}{50\,\text{kW}} \cdot 20\,\text{kW} = 24\,\text{kW} \tag{10.23}$$

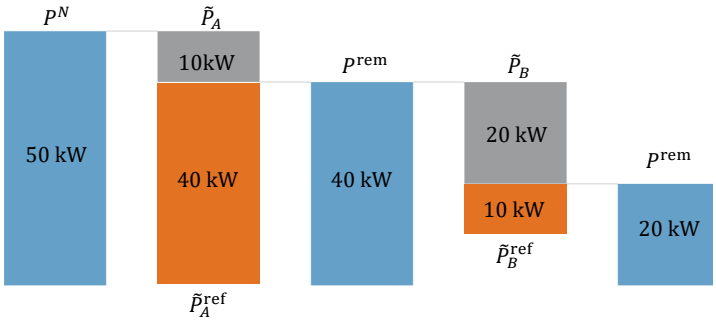

Figure 10.2: Sequential assignment of available power to the power demands.

Shifting of Stored Energy

Equations (10.24) to (10.27) illustrate how residual energy is exchanged between two parties (10.26) and (10.27), while the allocated energy capacities remain (10.24) and (10.25). The superscript star denotes the new value E_k^*, the superscript 0 denotes the previous value E_k^0. This is a mere re-declaration of ownership. The equations ensure that the physical energy within the BESS remains identical to the assigned energy to their owners. This example procedure is intended to compensate for single-events where stakeholder A needs to shed energy ΔE_{AB}^r that stakeholder B is willing to receive. The constraint of the redistributed energy (10.11) is fulfilled because $\Delta E_{AB} = -\Delta E_{BA}$.

$$E_A^{C*} = E_A^{C0} \tag{10.24}$$

$$E_B^{C*} = E_B^{C0} \tag{10.25}$$

$$E_A^{r*} = E_A^{r0} + \Delta E_{BA}^r \tag{10.26}$$

$$E_B^{r*} = E_B^{r0} + \Delta E_{AB}^r \tag{10.27}$$

The example is graphically illustrated in Figure 10.3. A redistribution of the residual energies E_k^r also changes the SOC of the application and generates a discontinuity in the graph. The amount of ΔE_{AB}^r is shifted from E_A^r to E_B^r. This way stakeholder A is able to store more energy in the future.

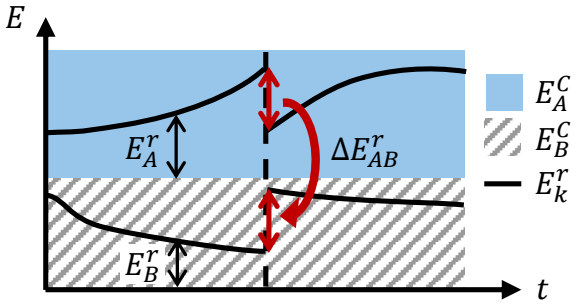

Figure 10.3: Illustration of shifting residual energy E^r between applications triggered by short-term control outside of bidding.

Shifting of Energy Capacity

The next example illustrates a re-assignment of each application's assigned energy capacity (10.28) and (10.29), but the stored energy remains unchanged (10.30) and (10.31). This transaction is intended for a more persistent increase of energy capacity for application A.

$$E_A^{C*} = E_A^{C0} + \Delta E_{BA}^C \tag{10.28}$$
$$E_B^{C*} = E_B^{C0} + \Delta E_{AB}^C \tag{10.29}$$
$$E_A^{r*} = E_A^{r0} \tag{10.30}$$
$$E_B^{r*} = E_B^{r0} \tag{10.31}$$

The shifting of the energy capacity is illustrated in Figure 10.4. A re-assignment is triggered, where E_A^C is increased by ΔE_{BA}^C. The graphical discontinuity of E_A^r is caused by the shifting of its bottom reference.

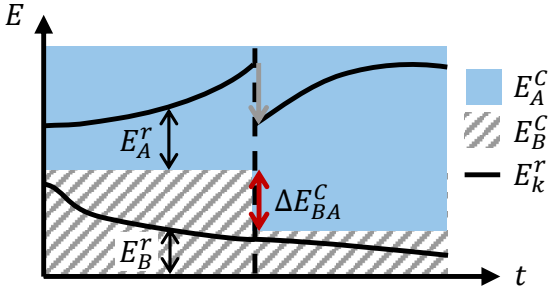

Figure 10.4: Shifting of energy capacity E^C from stakeholder B to stakeholder A.

10.3 Summary of Application Stacking

The proposed *application stacking* concept partitions the BESS into segments of energy capacity and stored energy. The approach consists of two layers. The first layer is the time-ahead-layer, where the auction market determines the technical parameters: control algorithm, energy capacity, priority power, and rank. Optimal allocation of the segments requires model prediction of the achieved benefits in the respective applications. The second layer is the real-time-layer, where the control algorithm

triggers the re-allocation of energy and priority power.

The first auction layer enables a transparent allocation of BESS resources and some certainty for planning. The second auction layer introduces short-term flexibility and additional BESS buffer. Prediction uncertainties and emergency situations are covered, as well as general situations with a low probability could be covered by the second layer instead of completely occupying resources. The flexibility introduced by the redistribution mechanism is expected to avoid the hedging and blocking of BESS resources. Accurate estimation of the SOC is, however, assumed.

As these short-term triggered events are expected to be more elaborate, accurate capacity allocation is probably beneficial for all stakeholders. This short-term event and priority-based re-assignment allow the stakeholders to omit comprehensive hedging by liberally blocking large segments of the BESS. Yet, the added flexibility does not exhibit ambiguity because the explicit occurrence and value of obligations are pre-declared and the flexible BESS deployment is made accountable for all parties. This increases the utilization and thus improves the benefit per BESS energy capacity.

11 Implementation Concepts for Improved Operation

This chapter proposes concepts that allow implementing the presented operating algorithms to adequately map the operation to business logic, that is determining financial obligations. This is especially important in scenarios with multiple stakeholders. The problem in the first place and existing literature regarding auction markets for BESS is outlined in Section 11.1. The blockchain technology is described in Section 11.2. It enables the implementation of low-cost aggregators that are responsible for the market clearing. The concept is proposed in Section 11.3 and Section 11.4 summarizes the chapter.

11.1 Auction Markets to Include Multiple Stakeholders

An auction market to allow operating BESS for multiple stakeholders is proposed. Other approaches require a pre-determined priority setting that all stakeholders need to agree on. It also does not consider changing environment and requirements of the stakeholders. Auction markets, on the other hand, allow the stakeholders determine their priorities themselves by their bidding behavior.

Auction markets for BESS have been proposed to allow a sharing of the BESS among multiple stakeholders [242; 243]. In order to propose a sound mathematical framework, their constraints and assumptions for the markets are rather strict.

He *et al.* [242] are the first to propose a business model that allows the systematic aggregation of several revenue streams of energy storage systems. They propose a series of auctions for the right to utilize the energy storage to ensure non-conflicting usage of the energy storage by different actors. The optimal composition of the stacking is determined with perfectly forecast power profiles. They set the constraint that the charged and discharged energy of each application is equal, to avoid conflicts of interest between the auctions. No consideration of prediction errors has been given.

Brijs *et al.* [243] propose the usage of auction markets, where storage owners can offer rights of physical storage usage. They introduce an aggregator for clearing the auction market. This limits the deployment of the proposed market to large-scale BESS with powers of several MW, as the aggregator adds further operating cost that can only be compensated by large-scale BESS with higher absolute revenue. The deployment of their concept excludes smaller BESS such as community BESS in distribution grids that would address the most severe challenges of RES [64].

Besides setting very strong constraints, both proposed auction market concepts require a clearing of the market by an additional party, the aggregator. This introduces another cost factor that impairs the added economic value of multi-use and thus limits the application to larger BESS for financial reasons. Another systematic issue is the role of the aggregator. Holding the monopoly to market decisions automatically creates strong incentives to exploit market power, requiring complex regulations to remedy these incentives [244].

Even though multi-use has been suggested, no concept has been proposed, that allows for both, optimal,

technical operation and transfer to business logic with multiple stakeholders. Multi-use, as proposed, results in a dynamic dispatch of BESS and is not compatible with rather static electricity markets and regulations. Multiple applications within one system require a conciliating mechanism that maps the BESS efforts and resulting benefits to market-based obligations. This is especially relevant in deregulated energy markets, common in the European Union, where the ownership and operation of BESS need to be decoupled. This allows value generation of shared BESS across multiple market players.

11.2 Blockchain to Enable Automated Low-Cost Aggregators

The blockchain is currently a much-noticed topic that is discussed in a variety of industries. It is mostly known in its application for cryptocurrencies, such as Bitcoin or Ethereum. The blockchain is a distributed database that allows every participant to verify the authenticity of any transaction, registered in the blockchain. Some blockchain projects exist in the energy sector, with the majority dealing with using the blockchain for simple trading transactions [245–249]. Only a few concepts extend the use of blockchain to address technical issues [244; 250–254].

The blockchain technology exhibits properties for trusting agreements, that may enable a more flexible and dynamic use of BESS in the future. Immutable proof of agreements and the utilization of so-called smart contracts hold the potential to enable local auction markets that are compatible with both business logic and flexible multi-use of BESS for optimized performance.

Blockchain Technology

The blockchain is a distributed database where each agent has an identical copy. The database comprises a chain of blocks. Any agent can generate blocks that store the block header, transactions, and smart contracts. The distributed nature, the cryptographic mechanisms, and the proof-of-work mechanism enable transparency and validity of the transactions. The blockchain technology is assumed to be independent of central authorities, yet ensures the agreement between all parties by peer to peer validation. [246]

Generating new blocks start with a new block header that includes a timestamp, a hash of the previous block in the chain, and the result of the proof-of-work that is generated by the mining mechanism. These elements protect the block and prevent a subsequent change of the database entries. Each generated block is broadcast in the blockchain network for validation by each individual agent, before they add that block to their own chain, leading to a synchronization of the distributed blockchains. [250]

Mining is the solving of a pre-defined problem to validate the generated block. Higher complexity of the problem raises the security of the mechanism, but also requires more time and energy to be solved.

A smart contract is a user-defined program in a block that specifies the rules of transactions. They can be reviewed by all blockchain-participants and serve as a substitute for written, legal contracts. [255]

11.3 Structure of Concept

This Section proposes a basic concept that combines two promising topics: multi-use of BESS and blockchain technology. It allows a market-based multi-use of a BESS with several stakeholders while providing flexibility for real-time energy management. The concept consists of a two-layer architecture, combined with a blockchain to implement a business logic that determines the financial obligations. The first layer provides the cyclical (pre-)allocation of the BESS resources and determines the control parameters. The second layer serves the purpose of real-time re-allocation of the resources, triggered by the technical control algorithm. The concept is shown graphically in Figure 11.1.

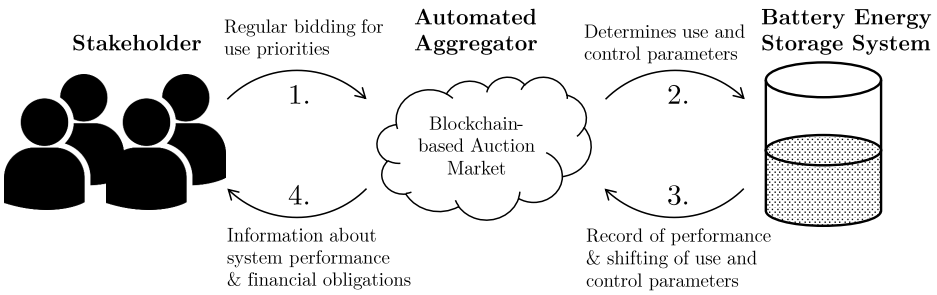

Figure 11.1: Graphical illustration of the proposed multi-use concept. Multiple stakeholders bid on use priorities. An automated aggregator clears the market and sets the operating parameters of the BESS. The behavior of the BESS is recorded and the financial obligations according to the terms agreed on at the bidding process are distinctly determined.

The implementation for the multi-use approach *merging of multiple objectives* can be applied as follows: The stakeholders bid on the weight of their objective that then form the objective function J for the optimization, consisting of the weighted sum of the individual objectives. The operation of the BESS is then optimized by its EMS. This operating mode is more complex than the *application stacking* but allows to reach global optima. It is, however, not suitable for strict applications, like energy wholesale or frequency control, where the output is completely determined.

This implementation concept can be applied to the *stacking of applications* as follows: The first layer, the time-ahead planning of the BESS segments and rights of use are determined by auction. This auction also determines the terms for the second layer, i.e. triggers and (financial) consequences. The blockchain registers all submitted bids. The disclosure of all bids and the rules for the clearing process allow all blockchain participants to acknowledge and verify the results. This is transferred to the market via smart contracts to register the technical transaction and financial obligations in the blockchain. The priorities of the stakeholders depend on their willingness to pay for the BESS service.

A hybrid of stacking and merging is possible. This results in several segments for the *stacking of applications* and any segment can be used for a *merging of multiple objectives*. It is possible to have several segments with a certain set of objectives that are merged into a single objective function J.

Suggested Properties of Blockchain

A permissioned blockchain is advisable because it ensures that only stakeholders with a reasonable interest in operating the BESS may participate in the auction market. With limited agents in the blockchain, the proof-of-work mechanism can be designed as a simple problem to consume only little energy with short computation. Even though this compromises the security against manipulation of

the transactions, the limited access to the blockchain reduces that risk.

The less elaborate proof-of-work enables reasonable mining without high-performance computers and is therefore possible for all or at least a large share of the market participants, to further minimize the risk of manipulation and reinforce the validity of transactions.

11.4 Summary of Auction Markets for Multiple Stakeholders

The issue of multiple stakeholders is a challenge for multi-use concepts. The introduced market for BESS is suitable to handle dynamics in future electricity grids. The multi-use of BESS is combined with blockchain technology to remedy the drawbacks of a conventional aggregator that coordinates the multiple stakeholders. This may be a catalyzing link between technical control and business logic. This extension avoids the need for an expensive aggregator, as automated algorithms are utilized instead. The author suggests a local auction market, where stakeholders bid for use priorities. The suggested blockchain-based aggregator is responsible for automated, computer-based market clearing, BESS execution, proof of delivery, and determination of financial obligations among the stakeholders.

Smart contracts are incorporated in the proposed concept to allow mechanisms that compensate for the intermittency of load and generation with the associated prediction uncertainties. The dynamics of the power grid are expected to increase with growing shares of RES and battery electric vehicles. Instead of adding energy buffer for each stakeholder during the auction, smart contracts allow more flexible sharing of the BESS within the auctioned periods. This consequently prevents oversizing of BESS, but increases their utilization ratio instead and eventually improves their economic value.

The properties of the blockchain technology presumably enable a generic, low-cost solution that can be applied to any BESS-size, down to small systems, such as community BESS with a few tens of kWh energy capacity. Consequently, the majority of applications for stationary BESS is covered [64]. The key-property of blockchain in the proposed multi-use concept for BESS is that all transactions (i.e. auctioned or triggered allocations of BESS use priorities) are registered in the blockchain and allow accountable actions and obligations between all stakeholders, without an added central authority [246]. A few conditions are necessary for the proposed concept to be feasible. First, all relevant stakeholders need to understand and adopt smart contracts and the consequences of the programming code included. Second, these smart contracts need to be legally effective and binding.

An essential issue that remains to be investigated in the according field is to guarantee the congruence of blockchain transactions and physical processes. The transfer between digital and physical world, the tokenization is a general issue of cyber-physical systems. Regulations today require approved measurement devices [81]. The concept is not strictly bound to the blockchain but could be operated with an independent aggregator instead. The benefits of blockchain seem to outweigh its complexity, as the cost for an additional aggregator renders the concept unattractive and creates incentives to exploit the market power [244].

12 Concluding Operation Improvement

Improvement methods for the operation of BESS are proposed in Part III. A classification of multi-use operation is presented: *Multi-objective optimized control* is the energy management of a BESS to serve several technical objectives at the same time. *Application stacking* is the simultaneous execution of several applications, by partitioning the physical BESS into virtual segments and specifically assigning them to applications.

Multi-objective control algorithms exist in literature but exhibit significant drawbacks. An optimization-based algorithm is proposed, that can be deployed for most applications, considers prediction errors, and features real-time capabilities.

The literature on *application stacking* reveals that the approach is suggested to increase the economic benefit of BESS. A concept for operating BESS with *application stacking* is proposed in this thesis. The BESS is partitioned into segments of energy capacity and stored energy. The distinct segmentation of battery resources and priorities strictly separates the operation of different applications. The results may, however, not be optimal, if several objectives lead to resource conflicts.

The issue of multiple stakeholders that would like the BESS to achieve objectives is especially present in unbundled power systems, such as most electricity markets in the European Union. With regard to the proposed the *multi-objective optimized control* method and the *application stacking* approach, multiple stakeholders cause ambiguity of how to segment the BESS partitions or how to weight the different objectives. An auction market is proposed for both approaches to introduce clarity and transparency. Instead of introducing another stakeholder that coordinates and clears the auction market, an automated, computer-based aggregator is proposed.

The remuneration of operating BESS in a *multi-objective optimized control* manner is determined by the physical power output. The contribution of each application to the BESS operation cannot be definitely distinguished. Instead, the stakeholders pay for the weight of their objective(s) in the global objective function J. In this case, the BESS operator bears the responsibility for the achieved value. The optimization stage of BESS control follows the bidding of the auction market, in this approach. This leads to a central optimization by the BESS's energy management system and a cooperative operation with the according weights for each objective.

The accountable revenue of the *application stacking* method is based on virtual profiles. Stakeholders pay for their assigned BESS segment and gain direct control. The stakeholders bear the responsibility to operate their BESS segment to fulfill the task. This causes distributed optimization by each stakeholder, preceding the auction. The BESS resource allocation problem is solved independently and the BESS output is made of the subsequent superposition of BESS segments' operation.

The fulfillment of applications is more comprehensible with *application stacking*. The increased complexity of *multi-objective optimized control* allows less obvious manipulation and requires all stakeholders to trust the BESS operator or the aggregator even more. Hybrid multi-use appeals both stakeholder preferences to either have direct control or just delegate the responsibility.

Part IV

Conclusion and Outlook

13 Conclusion

A comprehensive simulation framework for stationary BESS *SimSES* has been developed and is presented in Part I. The tool enables the simulation of BESS with technical accuracy and embed the system in an application context. Thus, analyses with regard to stress on the system, operating points, and system behavior, as well as its significance for the respective application can be conducted conjointly. It serves as fundamental tool for the study of the remaining topics of this thesis.

Evaluation metrics for BESS are derived in Part II. Both economic and GWP metrics are formulated and reasoned for three applications: increasing the self-consumption, peak-shaving, and integrating RES in an island grid. They describe BESS performance in a global manner and capture the true value of BESS for the operator. The efficiency of BESS is identified as a key parameter that determines the performance of BESS. The overall BESS value in all applications improves with higher efficiencies.

The assessment of BESS with regard to the carbon emissions in literature varies greatly. Narrow scopes of the analyses that neglect important aspects are common. A generic method for approximating the carbon emissions of producing BESS is derived Part II. It can be generally applied to BESS with varying sizes and technologies. The overall impact on the carbon emissions by operating BESS is derived for the three applications. A holistic approach is ensured to capture the key-effects of BESS operation. The prevents neglecting relevant processes and yields more credible results.

Case studies show the potential of BESS in the applications and illustrate that several metrics should be used for a reasonable assessment. Isolated metrics may not be informative. Thorough study of such results and cases is necessary.

GWP analyses reveal that economic incentives for deploying ESS in different applications do not necessarily align with carbon reduction objectives. This is described in detail for the case study of increasing the self-consumption in the residential context. While the carbon footprint of the individual household is reduced on a narrow scope, increasing the self-consumption raises the overall carbon emissions. The importance of operation strategies is shown in this case: BESS that only avoid curtailment losses achieved the most favorable carbon reduction.

The next step is to accomplish an improvement of BESS with regard to the presented metrics. This task is covered in Part III of the thesis. Large body of literature deals with optimal sizing and design of components. The literature review on control of BESS unveils weaknesses of existing approaches. Rule-based operation strategies for specific applications are state of the art. They are not necessarily optimal and need to be developed for each scenario. Optimization-based approaches display optimal results, but are deteriorated by prediction errors.

A novel control algorithm is proposed that is versatile, uses prediction for optimal performance, and withstands forecast errors. The method uses the fuzzy logic control approach for the controller and recurrently optimizes the control parameters with a cuckoo-search algorithm. A case study with the two applications PV-home storage and hybrid renewable-diesel island grid display the versatility of the algorithm. While the method achieves inferior results compared to the optimal reference opera-

tion strategies it features better robustness against forecast uncertainties. The fuzzy logic controller possesses real-time capabilities and compensates for prediction errors. The cuckoo-search algorithm provides optimality for the control parameters and enables the use of freely chosen objective functions. The method is, however, rather complex and relies on a system model, prediction data, fuzzy logic controller, and cuckoo-search.

Unbundled electricity markets constitute the majority of electricity markets in Europe and introduce a new issue: Multiple stakeholders that want the BESS to achieve their objectives. The introduced multi-use, more specifically the *application stacking* addresses this issue. The *application stacking* method partitions the BESS into virtual energy capacity segments with associated residual energy segments. The energy segments are assigned to serve individual applications. A power distribution scheme is included in the segment assignment. The method's structure is based on existing power planning approaches. The planning of the BESS segmentation recurs after for a defined time (e.g. daily). In addition an adjustment mechanism is featured that allows re-allocation of the segments in between the planning phases. This introduces the flexibility to act on prediction errors. The flexibility is expected to avoid hedging/blocking of BESS resources for buffering against prediction errors and a higher utilization of BESS instead.

Multiple stakeholders are incorporated in this concept by an auction market for the segments. The bidding determines the energy segments for the stakeholders. This way the distribution of the energy segments and associated power distribution scheme are clear and transparent to all stakeholders. The auction market is proposed to use the *Blockchain* technology for the automated, computer-based aggregator that is responsible for the market clearing of the bidding. This allows a low-cost solution, applicable to smaller BESS, such as community storage systems, and reaches the grid issues in the low voltage-distribution grid. Existing auction markets are limited to utility-scale BESS of several megawatt hours.

The proposed auction market is also applicable to *multi-objective optimized control*, but the attribution of the achieved values to distinct stakeholders and the associated financial obligations is not straightforward, in contrast to the *application stacking* approach. The *application stacking* method is therefore more appropriate than the *multi-objective optimized control* in a multi-stakeholder scenario with distinct applications. The *multi-objective optimized control* is more adequate in a single-operator scenario because it can exploit the technical BESS capability more exhaustively. A hybrid approach is possible, where individual segments use the *multi-objective optimized control* for their purpose.

14 Outlook

14.1 Evaluating Stationary Battery Storage Systems

The efficiency of BESS is an important factor that needs to be considered in future improvements of the systems. The measures for increasing the system efficiency are technical improvements of the inverter, battery, and the standby consumption of the system components.

Besides using improved components, operational enhancements can reduce energy losses as well. The conversion efficiency may be increased by improving the internal power distribution, in case several inverters exist in the system. The power distribution algorithm would avoid partial load for the inverter and consequently prevent operating points with low-efficiency. Improved thermal management and the ability to completely shut down idle components would reduce the standby consumption of the system. The influence on battery aging and the reaction of the system with increased ramp-up time need to be analyzed before implementing such measures.

The assessment of BESS with regard to the GWP is disunited. Even with the ISO standards for life-cycle assessment, the chosen scopes are often too narrow and important aspects are neglected. A derivation of global effects for additional applications than covered in this thesis is necessary. A comparison with alternative options, such as hydrogen storage also supports the endeavor of reducing the carbon emissions caused by the power systems.

The presented methods can be improved. The PV-home case, for example, can be further extended: Self-consumption and capping of the feed-in power are the only tasks investigated under German regulations. Time-of-use schemes instead of fixed rate assumptions need to be investigated for evaluating the use of self-consumption under different circumstances. It may especially be more beneficial if the prices are correlated to the carbon emission factor of the instantaneous production.

The assumptions for replacing conventionally produced energy presumably underestimates the benefit of exporting the PV produced energy into the grid. A more precise analysis that reflects the dispatch behavior of generators further elaborates the evaluation of the GWP impact of PV-home storage systems. An appropriate approach has been presented by Zheng, who considered the dispatch curve of generators in a power system [136]. Appen *et al.* [190] discuss the effect of PV-home storage systems. They conclude that regulatory framework needs to change, to incentivize grid-supporting operation of residential BESS.

Misalignment of incentives and general public benefits are presented in Part II. The author of this thesis suggests care inspection of effective regulations and adjustments to align the incentives with global benefits. The *multi-objective optimized control* framework combined with the proposed GWP metrics and economic incentives enable the investigation of possible incentive frameworks and the congruency with global usefulness. The approach reproduces the shortened BESS capabilities in the presence of prediction errors, in contrast to pure optimization based operation strategies. This way more effective incentives can be designed and proposed for policymakers.

14.2 Improving Battery Storage Operation

The *multi-objective optimized controller* has been proposed in this work. It represents the first working version and can be further developed and investigated.

The deployment of the controller for more input variables, BESS applications, and objective goals needs to be conducted to further analyze the algorithm's performance. Further investigation of the influence of varying forecast quality and simulation over a full year add value to the assessment of the proposed algorithm. In addition, the real-time capability has not been explicitely demonstrated. However, fuzzy logic controller are used for applications that require fast responses. Its capability, especially for the island grid case, should be demonstrated in the future.

Battery aging, for example, could be regarded as an objective for the control of the BESS and included in the simulation to be minimized. This allows finding a trade-off between the marginal cost of efficiency loss and battery aging, against the achievable revenue of operation.

The specific choice of cuckoo-search and fuzzy logic control is expected to be non-essential. The proposed algorithm structure could be tested with other optimization methods and other algorithms for the rule-based controller. Smarter initial values for the optimization algorithm based on previously found optimal solutions could improve the convergence of the cuckoo-search and should be investigated in the future. Another enhancement of the algorithm could be, to expand the control of a single BESS to controlling more units in a microgrid.

For the actual implementation of the presented controller, a cloud architecture is proposed, where the CPU-intensive cuckoo-search for optimization of the fuzzy logic controller's parameters is run on a central computer. The fuzzy logic controller's optimal parameters are then transmitted to the local controller of the BESS, that is responsible for the real-time control with an implemented fuzzy logic controller. The parameters comprise of about 3 times the number of membership functions and the execution of a fuzzy logic controller can be handled with low computational effort.

As for the *application stacking* method, the proposed algorithm needs to be simulated in the future to quantify its capabilities. This allows a sound comparison of the expected benefits with the single-use operation. Especially the rules for power distribution need further elaboration for handling more than two applications. The impact of inaccurate state-estimation with regard to SOC and aging needs to be analyzed and finally, an extension to other units than BESS should be developed to obtain a general framework for the control of microgrids with multiple stakeholders.

Other distributed ledgers, such as *tangle*, may be more suitable for the proposed method, than *blockchain* [256]. A potential analysis of different technologies and a comparison to the concept of a dedicated aggregator, are necessary for the future to prove the cost benefits claimed in this thesis. Further research on new methods that address security issues associated with tokenization is necessary, the transfer between physical reality and virtual data. This is not only beneficial for the proposed concept but concerns all fields, where tokenization is necessary.

The present thesis combines two relevant topics in the field of BESS: Evaluation of operating BESS and control algorithms that set the operation to optimize these evaluation objectives. Future research needs to further deepen the understanding of how BESS influences the power system in terms of technical, financial, and GWP-related benefits. Aligning economic incentives for BESS with carbon reduction operation is crucial for a reasonable transformation of the power system. Further improvement of BESS control ensures beneficial operation.

List of References

[1] *State of Climate: Global Climate Report for Annual 2017*. Online, 2018. URL: https://www.ncdc.noaa.gov/sotc/global/201713 (visited on 09/13/2018).

[2] T. Stocker, D. Qin, G.-K. Plattner, M. Tignor, S. K. Allen, J. Boschung, A. Nauels, V. Xia, and V. Bex. *Climate change 2013: The physical science basis: Working Group I contribution to the Fifth assessment report of the Intergovernmental Panel on Climate Change*. Cambridge, United Kingdom and Newyork, NY, USA: Cambridge University Press, 2014.

[3] J. M. Melillo, T. Richmond, and G. W. Yohe, eds. *Climate Change Impacts in the United States: The Third National Climate Assessment*. 2014. DOI: 10.7930/J0Z31WJ2.

[4] G. A. Meehl et al. "Global Climate Projections". In: *Contribution of working group I to the fourth assessment report of the intergovernmental panel on climate change, 2007*. Ed. by Cambridge University Press. Cambridge, United Kingdom and New York, NY, USA, 2007, pp. 747–846. URL: http://www.ipcc.ch/publications_and_data/publications_ipcc_fourth_assessment_report_wg1_report_the_physical_science_basis.htm (visited on 09/13/2018).

[5] N. Stern. "The economics of climate change". In: *American Economic Review* 98.2 (2008), pp. 1–37. URL: www.jstor.org/stable/29729990.

[6] C. Mora et al. "The projected timing of climate departure from recent variability". In: *Nature* 502.7470 (2013), pp. 183–187. DOI: 10.1038/nature12540.

[7] United Nations. *Kyoto Protocol to the United Nations Framework Convention on Climate Change*. 1998. URL: https://unfccc.int/process-and-meetings/the-kyoto-protocol/what-is-the-kyoto-protocol/what-is-the-kyoto-protocol.

[8] United Nations. *Paris Agreement*. 2016. URL: https://unfccc.int/process-and-meetings/the-paris-agreement/the-paris-agreement.

[9] O. Edenhofer et al., eds. *Climate Change 2014: Mitigation of Climate Change: Contribution of Working Group III to the Fifth Assessment Report of the Intergovernmental Panel on Climate Change*. Cambridge, United Kingdom and New York, NY, USA: Cambridge University Press, 2014. URL: https://www.ipcc.ch/report/ar5/wg3/.

[10] F. Birol. *World Energy Outlook 2010*. Berlin, 2010. URL: http://www.oecd.org/berlin/46389140.pdf.

[11] T. Klaus, C. Vollmer, K. Werner, H. Lehmann, and K. Müschen. *Energieziel 2050: 100% Strom aus erneuerbaren Quellen*. Ed. by Umweltbundesamt. Dessau-RoSSlau, 2010.

[12] BDEW. *Stromerzeugung in Deutschland nach Energieträgern*. 2017. (Visited on 05/25/2017).

[13] Angela Merkel. *Regierungserklärung von Bundeskanzlerin Angela Merkel zur Energiepolitik: Der Weg zur Energie der Zukunft*. Berlin, 2011. URL: https://www.bundesregierung.de/ContentArchiv/DE/Archiv17/Regierungserklaerung/2011/2011-06-09-merkel-energie-zukunft.html (visited on 09/15/2018).

[14] D. Jahn and S. Korolczuk. "German exceptionalism: The end of nuclear energy in Germany!" In: *Environmental Politics* 21.1 (2012), pp. 159–164. ISSN: 0964-4016. DOI: 10.1080/09644016.2011.643374.

[15] W. Zander et al. *Netzflexstudie: Optimierter Einsatz von Speichern für Netz- und Marktanwendungen in der Stromversorgung*. Ed. by Deutsche Energie-Agentur GmbH. Berlin, 2017. URL: https://www.dena.de/themen-projekte/projekte/energiesysteme/netzflexstudie/ (visited on 09/13/2018).

[16] T. Engel. *EnergyMap - Auf dem Weg zu 100% EE - Der Datenbestand*. 2016. URL: http://www.energymap.info/download.html (visited on 05/25/2017).

[17] H. Wirth and K. Schneider. "Recent facts about photovoltaics in Germany". In: *Fraunhofer ISE* 92 (2015).

[18] D. Zarrilli, A. Giannitrapani, S. Paoletti, and A. Vicino. "Energy Storage Operation for Voltage Control in Distribution Networks: A Receding Horizon Approach". In: *IEEE Transactions on Control Systems Technology* (2017), pp. 1–11. ISSN: 1063-6536. DOI: 10.1109/TCST.2017.2692719.

[19] H. Chandler. *Harnessing variable renewables: A guide to the balancing challenge*. Paris: OECD/IEA, 2011. ISBN: 9789264111387.

[20] G. Fuchs, B. Lunz, M. Leuthold, and D. U. Sauer. *Technology Overview on Electricity Storage - Overview on the potential and on the deployment perpectives of electric storage technologies*. 2012. URL: http://www.sefep.eu/activities/projects-studies/120628_Technology_Overview_Electricity_Storage_SEFEP_ISEA.pdf.

[21] B. Dunn, H. Kamath, and J.-M. Tarascon. "Electrical energy storage for the grid: a battery of choices". In: *Science (New York, N.Y.)* 334.6058 (2011), pp. 928–935. ISSN: 1095-9203. DOI: 10.1126/science.1212741.

[22] H. Hesse, M. Schimpe, D. Kucevic, and A. Jossen. "Lithium-Ion Battery Storage for the Grid—A Review of Stationary Battery Storage System Design Tailored for Applications in Modern Power Grids". In: *Energies* 10.12 (2017), p. 2107. ISSN: 10.3390/en6083951. DOI: 10.3390/en10122107.

[23] X. Luo, J. Wang, M. Dooner, and J. Clarke. "Overview of current development in electrical energy storage technologies and the application potential in power system operation". In: *Applied Energy* 137 (2015), pp. 511–536. DOI: 10.1016/j.apenergy.2014.09.081.

[24] P. T. Moseley and J. Garche. *Eletrochemical Energy Storage for Renewable Sources and Grid Balancing*. Elsevier Science, 2014. ISBN: 978-0-444-62616-5.

[25] U.S. Department of Energy. *DOE Global Energy Storage Database*. 2016. URL: https://www.energystorageexchange.org/.

[26] M. C. Bozchalui and R. Sharma. "Operation strategies for energy storage systems in distribution networks". In: *2014 IEEE PES general meeting*. Piscataway, NJ: IEEE, 2014, pp. 1–5. ISBN: 978-1-4799-6415-4. DOI: 10.1109/PESGM.2014.6939483.

[27] A. Garces, C. A. Correa, and R. Bolanos. "Optimal operation of distributed energy storage units for minimizing energy losses". In: *2014 IEEE PES Transmission & Distribution Conference and Exposition - Latin America (PES T&D-LA)*. Ed. by P. Beltran. Piscataway, NJ: IEEE, 2014, pp. 1–6. ISBN: 978-1-4799-6251-8. DOI: 10.1109/TDC-LA.2014.6955220.

[28] M. Naumann, R. C. Karl, C. N. Truong, A. Jossen, and H. C. Hesse. "Lithium-ion Battery Cost Analysis in PV-household Application". In: *Energy Procedia* 73 (2015), pp. 37–47. ISSN: 4989289269. DOI: 10.1016/j.egypro.2015.07.555.

[29] C. N. Truong, M. Naumann, R. Karl, M. Müller, A. Jossen, and H. Hesse. "Economics of Residential Photovoltaic Battery Systems in Germany: The Case of Tesla's Powerwall". In: *Batteries* 2.2 (2016), p. 14. ISSN: 2313-0105. DOI: 10.3390/batteries2020014.

[30] SolarPower Europe. *Unleashing the Potential of Solar & Storage*. 2018. URL: http://www.solarpowereurope.org/unleashing-the-potential-of-solar-storage/ (visited on 09/12/2018).

[31] C. N. Truong, L. Viernstein, M. Schimpe, R. Witzmann, A. Jossen, and H. C. Hesse. "Maximizing Solar Home Battery Systems' Contribution to the Energy Transition of the Power System". In: *NEIS 2017*. Ed. by D. Schulz. Berlin: VDE Verlag GMBH, 2018, pp. 133–140. ISBN: 9783800744459.

[32] C. Jägemann, S. Hagspiel, and D. Lindenberger. *The economic inefficiency of grid parity: The case of German photovoltaics*. 2013. URL: https://www.econstor.eu/bitstream/10419/92970/1/775175242.pdf.

[33] M. Resch, B. Ramadhani, J. Bühler, and A. Sumper. "Comparison of control strategies of residential PV storage systems". In: *International Renewable Energy Storage Conference*. 2015, pp. 1–18. DOI: 10.13140/RG.2.1.3668.2084.

[34] M. Resch, J. Bühler, M. Klausen, and A. Sumper. "Impact of operation strategies of large scale battery systems on distribution grid planning in Germany". In: *Renewable and Sustainable Energy Reviews* 74 (2017), pp. 1042–1063. DOI: 10.1016/j.rser.2017.02.075.

[35] B. Nykvist and M. Nilsson. "Rapidly falling costs of battery packs for electric vehicles". In: *Nature Climate Change* 5.4 (2015), pp. 329–332. DOI: 10.1038/nclimate2564.

[36] G. Fitzgerald, J. Mandel, J. Morris, and T. Hervé. "The Economics of Battery Energy Storage: How multi-use, customer-sited batteries deliver the most services and value to customers and the grid". In: *Rocky Mountain Institute* (2015). URL: http://www.rmi.org/electricity_battery_value.

[37] A. Stephan, B. Battke, M. D. Beuse, J. H. Clausdeinken, and T. S. Schmidt. "Limiting the public cost of stationary battery deployment by combining applications". In: *Nature Energy* 1.7 (2016), p. 16079. ISSN: 2058-7546. DOI: 10.1038/nenergy.2016.79.

[38] T. Weitzel and C. H. Glock. "Energy Management for Stationary Electric Energy Storage Systems: A Systematic Literature Review". In: *European Journal of Operational Research* (2017). ISSN: 03772217. DOI: 10.1016/j.ejor.2017.06.052.

[39] A. Malhotra, B. Battke, M. Beuse, A. Stephan, and T. Schmidt. "Use cases for stationary battery technologies: A review of the literature and existing projects". In: *Renewable and Sustainable Energy Reviews* 56 (2016), pp. 705–721. DOI: 10.1016/j.rser.2015.11.085.

[40] K.-P. Kairies, D. Haberschusz, D. Magnor, M. Leuthold, J. Badeda, and D. U. Sauer. *Wissenschaftliches Mess- und Evaluierungsprogramm Solarstromspeicher Jahresbericht 2015*. Aachen, 2015.

[41] J. Hoppmann, J. Volland, T. S. Schmidt, and V. H. Hoffmann. "The economic viability of battery storage for residential solar photovoltaic systems – A review and a simulation model". In: *Renewable and Sustainable Energy Reviews* 39 (2014), pp. 1101–1118. DOI: 10.1016/j.rser.2014.07.068.

[42] J. Moshövel, K.-P. Kairies, D. Magnor, M. Leuthold, M. Bost, S. Gährs, E. Szczechowicz, M. Cramer, and D. U. Sauer. "Analysis of the maximal possible grid relief from PV-peak-power impacts by using storage systems for increased self-consumption". In: *Applied Energy* 137 (2015), pp. 567–575. DOI: 10.1016/j.apenergy.2014.07.021.

[43] Bundestag. *Gesetz für den Vorrang Erneuerbarer Energien*. Berlin, 2000. DOI: 10.1007/978-3-540-33950-2_2.

[44] Bundestag. *Gesetz für den Ausbau erneuerbarer Energien*. Berlin, 2014.

[45] S. You and C. N. Rasmussen. "Generic modelling framework for economic analysis of battery systems". In: *IET Conference on Renewable Power Generation* (2011), p. 122. ISSN: 978-1-84919-536-2. DOI: 10.1049/cp.2011.0147.

[46] B. Battke, T. S. Schmidt, D. Grosspietsch, and V. H. Hoffmann. "A review and probabilistic model of lifecycle costs of stationary batteries in multiple applications". In: *Renewable and Sustainable Energy Reviews* 25 (2013), pp. 240–250. DOI: 10.1016/j.rser.2013.04.023.

[47] J. Weniger, T. Tjaden, and V. Quaschning. "Sizing of Residential PV Battery Systems". In: *Energy Procedia* 46 (2014), pp. 78–87. ISSN: 4989289269. DOI: 10.1016/j.egypro.2014.01.160.

[48] C. Rathgeber, E. Lävemann, and A. Hauer. "Economic top–down evaluation of the costs of energy storages—A simple economic truth in two equations". In: *Journal of Energy Storage* 2 (2015), pp. 43–46. DOI: 10.1016/j.est.2015.06.001.

[49] F. Marra, G. Yang, C. Traeholt, J. Ostergaard, and E. Larsen. "A Decentralized Storage Strategy for Residential Feeders With Photovoltaics". In: *IEEE Transactions on Smart Grid* 5.2 (2014), pp. 974–981. ISSN: 1949-3053. DOI: 10.1109/TSG.2013.2281175.

[50] J. Weniger, J. Bergner, and V. Quaschning. "Integration of PV power and load forecasts into the operation of residential PV battery systems". In: *4th Solar Integration Workshop*. 2014. URL: http://pvspeicher.htw-berlin.de.

[51] A. Zeh and R. Witzmann. "Operational Strategies for Battery Storage Systems in Low-voltage Distribution Grids to Limit the Feed-in Power of Roof-mounted Solar Power Systems". In: *Energy Procedia* 46 (2014), pp. 114–123. ISSN: 4989289269. DOI: 10.1016/j.egypro.2014.01.164.

[52] R. Bao and W. Zhang. "Optimal scheduling of active distribution networks with energy storage systems considering environmental cost". In: *Proceedings of the 5th IEEE International Conference on Electric Utility Deregulation, Restructuring and Power Technologies (DRPT2015)*. Piscataway, NJ: IEEE, 2015, pp. 642–647. ISBN: 978-1-4673-7106-3. DOI: 10.1109/DRPT.2015.7432321.

[53] E. L. Ratnam, S. R. Weller, and C. M. Kellett. "An optimization-based approach to scheduling residential battery storage with solar PV: Assessing customer benefit". In: *Renewable Energy* 75 (2015), pp. 123–134. DOI: 10.1016/j.renene.2014.09.008.

[54] A. Zeh, M. Rau, and R. Witzmann. "Comparison of decentralised and centralised grid-compatible battery storage systems in distribution grids with high PV penetration". In: *Progress in Photovoltaics: Research and Applications* 24.4 (2016), pp. 496–506. ISSN: 10627995. DOI: 10.1002/pip.2566.

[55] C. A. Hill, M. C. Such, D. Chen, J. Gonzalez, and W. M. Grady. "Battery Energy Storage for Enabling Integration of Distributed Solar Power Generation". In: *IEEE Transactions on Smart Grid* 3.2 (2012), pp. 850–857. ISSN: 1949-3053. DOI: 10.1109/TSG.2012.2190113.

[56] O. C. Rascon, B. Schachler, J. Buhler, M. Resch, and A. Sumper. "Increasing the hosting capacity of distribution grids by implementing residential PV storage systems and reactive power control". In: *2016 13th International Conference on the European Energy Market (EEM)*. Piscataway, NJ: IEEE, 2016, pp. 1–5. ISBN: 978-1-5090-1298-5. DOI: 10.1109/EEM.2016.7521338.

[57] F. Marra, Y. T. Fawzy, T. Bülo, and B. Blai. "Energy Storage Options for Voltage Support in Low-Voltage Grids with High Penetration of Photovoltaic". In: *IEEE PES ISGT Europe 2012*. IEEE, 2012. URL: http://orbit.dtu.dk/files/9860589/Paper_%20ID238.pdf.

[58] T. Kneiske, J. von Appen, and M. Braun. "Voltage control using PV storage systems in distribution systems". In: *CIRED 2013: Electricity distribution systems for a sustainable future*. IET/CIRED: Institution of Engineering and Technology, 2013, p. 1396. ISBN: 978-1-84919-732-8. DOI: 10.1049/cp.2013.1217.

[59] J. Tant, F. Geth, D. Six, P. Tant, and J. Driesen. "Multiobjective Battery Storage to Improve PV Integration in Residential Distribution Grids". In: *IEEE Transactions on Sustainable Energy* 4.1 (2013), pp. 182–191. DOI: 10.1109/TSTE.2012.2211387.

[60] H. Nazaripouya, Y. Wang, P. Chu, H. R. Pota, and R. Gadh. "Optimal sizing and placement of battery energy storage in distribution system based on solar size for voltage regulation". In: *2015 IEEE Power & Energy Society General Meeting*. IEEE, 2015, pp. 1–5. ISBN: 978-1-4673-8040-9. DOI: 10.1109/PESGM.2015.7286059.

[61] L. Wang, D. H. Liang, A. F. Crossland, P. C. Taylor, D. Jones, and N. S. Wade. "Coordination of Multiple Energy Storage Units in a Low-Voltage Distribution Network". In: *IEEE Transactions on Smart Grid* 6.6 (2015), pp. 2906–2918. ISSN: 1949-3053. DOI: 10.1109/TSG.2015.2452579.

[62] B. Idlbi, J. von Appen, T. Kneiske, and M. Braun. "Cost-Benefit Analysis of Battery Storage System for Voltage Compliance in Distribution Grids with High Distributed Generation". In: *Energy Procedia* 99 (2016), pp. 215–228. ISSN: 4989289269. DOI: 10.1016/j.egypro.2016.10.112.

[63] F. R. Segundo Sevilla, D. Parra, N. Wyrsch, M. K. Patel, F. Kienzle, and P. Korba. "Techno-economic analysis of battery storage and curtailment in a distribution grid with high PV penetration". In: *Journal of Energy Storage* 17 (2018), pp. 73–83. DOI: 10.1016/j.est.2018.02.001.

[64] M. Müller, L. Viernstein, C. N. Truong, A. Eiting, H. C. Hesse, R. Witzmann, and A. Jossen. "Evaluation of grid-level adaptability for stationary battery energy storage system applications in Europe". In: *Journal of Energy Storage* (2017). DOI: 10.1016/j.est.2016.11.005.

[65] M. A. Acquah, S. Han, H. Kim, S. Park, and H. Han. "Real-Time Peak Control algorithm using Stochastic Optimization". In: *IEEE CCWC - 2017*. Ed. by S. Chakrabarti. Piscataway, NJ: IEEE, 2017, pp. 1–6. ISBN: 978-1-5090-4228-9. DOI: 10.1109/CCWC.2017.7868470.

[66] F. Halfmann, F. Alhaider, J. Wendiggensen, and S. Gerhard. “A Predictive Control Strategy for Battery Energy Storage Systems to combine Peak Shaving with Primary Frequency Control”. In: *NEIS Conference 2016*. Ed. by D. Schulz. Wiesbaden: Springer Vieweg, 2017, pp. 113–118. ISBN: 978-3-658-15028-0. DOI: 10.1007/978-3-658-15029-7_18.

[67] X. Han, T. Ji, Z. Zhao, and H. Zhang. “Economic evaluation of batteries planning in energy storage power stations for load shifting”. In: *Renewable Energy* 78 (2015), pp. 643–647. DOI: 10.1016/j.renene.2015.01.056.

[68] E. Reihani, M. Motalleb, R. Ghorbani, and L. Saad Saoud. “Load peak shaving and power smoothing of a distribution grid with high renewable energy penetration”. In: *Renewable Energy* 86 (2016), pp. 1372–1379. DOI: 10.1016/j.renene.2015.09.050.

[69] E. Telaretti and L. Dusonchet. “Battery storage systems for peak load shaving applications: Part 1: Operating strategy and modification of the power diagram”. In: *2016 IEEE 16th International Conference on Environment and Electrical Engineering (EEEIC)*. Piscataway, NJ: IEEE, 2016, pp. 1–6. ISBN: 978-1-5090-2320-2. DOI: 10.1109/EEEIC.2016.7555793.

[70] A.-H. Mohsenian-Rad, V. W. S. Wong, J. Jatskevich, R. Schober, and A. Leon-Garcia. “Autonomous Demand-Side Management Based on Game-Theoretic Energy Consumption Scheduling for the Future Smart Grid”. In: *IEEE Transactions on Smart Grid* 1.3 (2010), pp. 320–331. ISSN: 1949-3053. DOI: 10.1109/TSG.2010.2089069.

[71] P. Palensky and D. Dietrich. “Demand Side Management: Demand Response, Intelligent Energy Systems, and Smart Loads”. In: *IEEE Transactions on Industrial Informatics* 7.3 (2011), pp. 381–388. ISSN: 1551-3203. DOI: 10.1109/TII.2011.2158841.

[72] W. Gu, W. Liu, Z. Wu, B. Zhao, and W. Chen. “Cooperative Control to Enhance the Frequency Stability of Islanded Microgrids with DFIG-SMES”. In: *Energies* 6.8 (2013), pp. 3951–3971. ISSN: 10.3390/en6083951. DOI: 10.3390/en6083951.

[73] D. S. Miranda, Y. Sun, J. Cobben, and M. Gibescu. “Impact of energy storage on island grid dynamics: A case study of Bonaire”. In: *2016 IEEE International Energy Conference (ENERGYCON)*. Piscataway, NJ: IEEE, 2016, pp. 1–7. ISBN: 978-1-4673-8463-6. DOI: 10.1109/ENERGYCON.2016.7513940.

[74] K. Y. Lau, M. Yousof, S. Arshad, M. Anwari, and A. Yatim. “Performance analysis of hybrid photovoltaic/diesel energy system under Malaysian conditions”. In: *Energy* 35.8 (2010), pp. 3245–3255. DOI: 10.1016/j.energy.2010.04.008.

[75] M. Ross, R. Hidalgo, C. Abbey, and G. Joós. “Energy storage system scheduling for an isolated microgrid”. In: *IET Renewable Power Generation* 5.2 (2011), p. 117. DOI: 10.1049/iet-rpg.2009.0204.

[76] G. Merei, C. Berger, and D. U. Sauer. “Optimization of an off-grid hybrid PV–Wind–Diesel system with different battery technologies using genetic algorithm”. In: *Solar Energy* 97 (2013), pp. 460–473. DOI: 10.1016/j.solener.2013.08.016.

[77] C. N. Truong, M. Schimpe, M. Naumann, A. Jossen, and H. C. Hesse. “Impact of Sub-Components on the Overall Performance of Stationary Battery Systems: Insights on the Prototype Energy Neighbor”. In: *International ETG Congress*. ETG-Fachbericht. Berlin and Offenbach: VDE Verlag, 2017. ISBN: 9783800745050.

[78] T. Thien, H. Axelsen, M. Merten, S. Zurmühlen, J. Münderlein, M. Leuthold, and D. U. Sauer. "Planning of Grid-Scale Battery Energy Storage Systems: Lessons Learned from a 5 MW Hybrid Battery Storage Project in Germany". In: (2015). URL: http://www.battcon.com/PapersFinal2015/18%20Thien%20Paper%202015.pdf.

[79] M. Koller, T. Borsche, A. Ulbig, and G. Andersson. "Review of grid applications with the Zurich 1MW battery energy storage system". In: *Electric Power Systems Research* 120 (2015), pp. 128–135. DOI: 10.1016/j.epsr.2014.06.023.

[80] M. Lodl, R. Witzmann, and M. Metzger. "Operation strategies of energy storages with forecast methods in low-voltage grids with a high degree of decentralized generation". In: *IEEE Electrical Power and Energy Conference (EPEC), 2011*. Piscataway, NJ: IEEE, 2011, pp. 52–56. ISBN: 978-1-4577-0405-5. DOI: 10.1109/EPEC.2011.6070252.

[81] A. Zeh, M. Müller, H. C. Hesse, A. Jossen, and R. Witzmann. "Operating a Multitasking Stationary Battery Storage System for Providing Secondary Control Reserve on Low-Voltage Level". In: *ETG Congress 2015*. Bonn, 2015, pp. 1–8. DOI: 10.13140/RG.2.1.1807.7202.

[82] Deutsche Gesetzliche Unfallversicherung. *Qualifizierung für Arbeiten an Fahrzeugen mit Hochvoltsystemen: DGUV 200-005*. 2012.

[83] S. C. Nagpure, B. Bhushan, and S. S. Babu. "Multi-Scale Characterization Studies of Aged Li-Ion Large Format Cells for Improved Performance: An Overview". In: *Journal of The Electrochemical Society* 160.11 (2013), A2111–A2154. ISSN: 0013-4651. DOI: 10.1149/2.001311jes.

[84] M. Schimpe, M. Naumann, N. Truong, H. C. Hesse, S. Santhanagopalan, A. Saxon, and A. Jossen. "Energy efficiency evaluation of a stationary lithium-ion battery container storage system via electro-thermal modeling and detailed component analysis". In: *Applied Energy* 210 (2018), pp. 211–229. DOI: 10.1016/j.apenergy.2017.10.129.

[85] M. Naumann and C. N. Truong. *SimSES - Software for techno-economic simulation of stationary energy storage systems*. 2017. DOI: 10.14459/2017mp1401541.

[86] M. Naumann, C. N. Truong, M. Schimpe, D. Kucevic, A. Jossen, and H. C. Hesse. "SimSES: Software for techno-economic Simulation of Stationary Energy Storage Systems". In: *International ETG Congress*. ETG-Fachbericht. Berlin and Offenbach: VDE Verlag, 2017, pp. 442–447. ISBN: 9783800745050.

[87] G. Notton, V. Lazarov, and L. Stoyanov. "Optimal sizing of a grid-connected PV system for various PV module technologies and inclinations, inverter efficiency characteristics and locations". In: *Renewable Energy* 35.2 (2010), pp. 541–554. DOI: 10.1016/j.renene.2009.07.013.

[88] K. Rumpf, M. Naumann, and A. Jossen. "Experimental investigation of parametric cell-to-cell variation and correlation based on 1100 commercial lithium-ion cells". In: *Journal of Energy Storage* 14 (2017), pp. 224–243. DOI: 10.1016/j.est.2017.09.010.

[89] M. Naumann, M. Schimpe, P. Keil, H. C. Hesse, and A. Jossen. "Analysis and modeling of calendar aging of a commercial LiFePO 4 /graphite cell". In: *Journal of Energy Storage* 17 (2018), pp. 153–169. DOI: 10.1016/j.est.2018.01.019.

[90] M. Schimpe, M. Edler von Kuepach, M. Naumann, H. C. Hesse, K. Smith, and A. Jossen. "Comprehensive Modeling of Temperature-Dependent Degradation Mechanisms in Lithium Iron Phosphate Batteries". In: *ECS Transactions* 80.10 (2017), pp. 147–170. ISSN: 1938-6737. DOI: 10.1149/08010.0147ecst.

[91] A. Millner. “Modeling Lithium Ion battery degradation in electric vehicles”. In: *2010 IEEE Conference on Innovative Technologies for an Efficient and Reliable Electricity Supply*. IEEE, 2010, pp. 349–356. ISBN: 978-1-4244-6076-2. DOI: 10.1109/CITRES.2010.5619782.

[92] S. B. Peterson, J. Apt, and J. F. Whitacre. “Lithium-ion battery cell degradation resulting from realistic vehicle and vehicle-to-grid utilization”. In: *Journal of Power Sources* 195.8 (2010), pp. 2385–2392. DOI: 10.1016/j.jpowsour.2009.10.010.

[93] Y. Miyaki, K. Hayashi, T. Makino, K. Yoshida, M. Terauchi, T. Endo, and Y. Fukushima. “A Common Capacity Loss Trend: LiFePO4 Cell’s Cycle and Calendar Aging”. In: *Meeting Abstracts* MA2012-02.10 (2012), p. 1091.

[94] M. Ecker, N. Nieto, S. Käbitz, J. Schmalstieg, H. Blanke, A. Warnecke, and D. U. Sauer. “Calendar and cycle life study of Li(NiMnCo)O2-based 18650 lithium-ion batteries”. In: *Journal of Power Sources* 248 (2014), pp. 839–851. DOI: 10.1016/j.jpowsour.2013.09.143.

[95] M. Dubarry, C. Truchot, and B. Y. Liaw. “Cell degradation in commercial LiFePO4 cells with high-power and high-energy designs”. In: *Journal of Power Sources* 258 (2014), pp. 408–419. DOI: 10.1016/j.jpowsour.2014.02.052.

[96] B. Guinot, B. Champel, F. Montignac, E. Lemaire, D. Vannucci, S. Sailler, and Y. Bultel. “Techno-economic study of a PV-hydrogen-battery hybrid system for off-grid power supply: Impact of performances’ ageing on optimal system sizing and competitiveness”. In: *International Journal of Hydrogen Energy* 40.1 (2015), pp. 623–632. ISSN: 03603199. DOI: 10.1016/j.ijhydene.2014.11.007.

[97] M. Ashari and C. V. Nayar. “An optimum dispatch strategy using set points for a photovoltaic (PV)–diesel–battery hybrid power system”. In: *Solar Energy* 66.1 (1999), pp. 1–9. DOI: 10.1016/S0038-092X(99)00016-X.

[98] M. Bortolini, M. Gamberi, A. Graziani, and F. Pilati. “Economic and environmental bi-objective design of an off-grid photovoltaic–battery–diesel generator hybrid energy system”. In: *Energy Conversion and Management* 106 (2015), pp. 1024–1038. DOI: 10.1016/j.enconman.2015.10.051.

[99] R. Edwards, V. Mahieu, J.-C. Griesemann, J.-F. Larivé, and D. J. Rickeard. “Well-to-Wheels Analysis of Future Automotive Fuels and Powertrains in the European Context”. In: *2004 SAE Fuels & Lubricants Meeting & Exhibition*. SAE Technical Paper Series. SAE International400 Commonwealth Drive, Warrendale, PA, United States, 2004. DOI: 10.4271/2004-01-1924.

[100] KfW-Bank. *KfW-Programm Erneuerbare Energien Speicher - Merkblatt*. Frankfurt, 2016.

[101] J. Weniger, T. Tjaden, and V. Quaschning. “Sizing and grid integration of residential PV battery systems”. In: *8th International Renewable Energy Storage Conference and Exhibition*. Vol. 18. 2013, p. 20.

[102] B.-B. Energiespeicher eV and B.-B. Solarwirtschaft eV. “„Effizienzleitfaden für PV-Speichersysteme “”. In: *Berlin, März* (2017).

[103] M. Naumann. “Techno-economic evaluation of stationary battery energy storage systems with special consideration of aging”. Dissertation. München: Technische Universität München, 2018.

[104] P. Arun, R. Banerjee, and S. Bandyopadhyay. “Optimum sizing of photovoltaic battery systems incorporating uncertainty through design space approach”. In: *Solar Energy* 83.7 (2009), pp. 1013–1025. DOI: 10.1016/j.solener.2009.01.003.

[105] I. B. Askari and M. Ameri. “Optimal sizing of photovoltaic—battery power systems in a remote region in Kerman, Iran”. In: *Proceedings of the Institution of Mechanical Engineers, Part A: Journal of Power and Energy* 223.5 (2009), pp. 563–570. ISSN: 0957-6509. DOI: 10.1243/09576509JPE717.

[106] S. Avril, G. Arnaud, A. Florentin, and M. Vinard. “Multi-objective optimization of batteries and hydrogen storage technologies for remote photovoltaic systems”. In: *Energy* 35.12 (2010), pp. 5300–5308. DOI: 10.1016/j.energy.2010.07.033.

[107] J. K. Kaldellis, D. Zafirakis, E. L. Kaldelli, and K. Kavadias. “Cost benefit analysis of a photovoltaic-energy storage electrification solution for remote islands”. In: *Renewable Energy* 34.5 (2009), pp. 1299–1311. DOI: 10.1016/j.renene.2008.09.014.

[108] P. Denholm and R. M. Margolis. “Evaluating the limits of solar photovoltaics (PV) in electric power systems utilizing energy storage and other enabling technologies”. In: *Energy Policy* 35.9 (2007), pp. 4424–4433. ISSN: 0301-4215. DOI: 10.1016/j.enpol.2007.03.004.

[109] Z. Wissem, K. Gueorgui, and K. Hédi. “Modeling and technical–economic optimization of an autonomous photovoltaic system”. In: *Energy* 37.1 (2012), pp. 263–272. DOI: 10.1016/j.energy.2011.11.036.

[110] J. Weniger, T. Tjaden, J. Bergner, and V. Quaschning. “Emerging Performance Issues of Photovoltaic Battery Systems”. In: *32nd European Photovoltaic Solar Energy Conference and Exhibition* (2016), pp. 2377–2385. DOI: 10.4229/EUPVSEC20162016-6DP.2.1.

[111] G. Merei, J. Moshövel, D. Magnor, and D. U. Sauer. “Optimization of self-consumption and techno-economic analysis of PV-battery systems in commercial applications”. In: *Applied Energy* 168 (2016), pp. 171–178. DOI: 10.1016/j.apenergy.2016.01.083.

[112] I. Pawel. “The Cost of Storage – How to Calculate the Levelized Cost of Stored Energy (LCOE) and Applications to Renewable Energy Generation”. In: *Energy Procedia* 46 (2014), pp. 68–77. ISSN: 4989289269. DOI: 10.1016/j.egypro.2014.01.159.

[113] S. Quoilin, K. Kavvadias, A. Mercier, I. Pappone, and A. Zucker. “Quantifying self-consumption linked to solar home battery systems: Statistical analysis and economic assessment”. In: *Applied Energy* 182 (2016), pp. 58–67. DOI: 10.1016/j.apenergy.2016.08.077.

[114] E. Hittinger, J. F. Whitacre, and J. Apt. “What properties of grid energy storage are most valuable?” In: *Journal of Power Sources Volume 100* 206 (2012), pp. 436–449. ISSN: 0378-7753. DOI: 10.1016/j.jpowsour.2011.12.003.

[115] R. Jallouli and L. Krichen. “Sizing, techno-economic and generation management analysis of a stand alone photovoltaic power unit including storage devices”. In: *Energy* 40.1 (2012), pp. 196–209. DOI: 10.1016/j.energy.2012.02.004.

[116] A. N. Celik, T. Muneer, and P. Clarke. “Optimal sizing and life cycle assessment of residential photovoltaic energy systems with battery storage”. In: *Progress in Photovoltaics: Research and Applications* 16.1 (2008), pp. 69–85. ISSN: 10627995. DOI: 10.1002/pip.774.

[117] C. Heymans, S. B. Walker, S. B. Young, and M. Fowler. “Economic analysis of second use electric vehicle batteries for residential energy storage and load-levelling”. In: *Energy Policy* 71 (2014), pp. 22–30. ISSN: 0301-4215. DOI: 10.1016/j.enpol.2014.04.016.

[118] C. Goebel, V. Cheng, and H.-A. Jacobsen. “Profitability of Residential Battery Energy Storage Combined with Solar Photovoltaics”. In: *Energies* 10.7 (2017), p. 976. ISSN: 10.3390/en6083951. DOI: 10.3390/en10070976.

[119] H. Hesse, R. Martins, P. Musilek, M. Naumann, C. N. Truong, and A. Jossen. "Economic Optimization of Component Sizing for Residential Battery Storage Systems". In: *Energies* 10.7 (2017), p. 835. ISSN: 10.3390/en6083951. DOI: 10.3390/en10070835.

[120] M. Braun, K. Büdenbender, D. Magnor, and A. Jossen. "Photovoltaic self-consumption in Germany: Using lithium-ion storage to increase self-consumed photovoltaic energy". In: *24th European Photovoltaic Solar Energy Conference (PVSEC)*. 2009.

[121] N. DiOrio, A. Dobos, S. Janzou, et al. *Economic analysis case studies of battery energy storage with SAM*. National Renewable Energy Laboratory Denver, CO, USA, 2015.

[122] A. Colmenar-Santos, S. Campíñez-Romero, C. Pérez-Molina, and M. Castro-Gil. "Profitability analysis of grid-connected photovoltaic facilities for household electricity self-sufficiency". In: *Energy Policy* 51 (2012), pp. 749–764. ISSN: 0301-4215. DOI: 10.1016/j.enpol.2012.09.023.

[123] B. Battke and T. S. Schmidt. "Cost-efficient demand-pull policies for multi-purpose technologies – The case of stationary electricity storage". In: *Applied Energy* 155 (2015), pp. 334–348. DOI: 10.1016/j.apenergy.2015.06.010.

[124] K.-H. Pettinger and W. Dong. "When Does the Operation of a Battery Become Environmentally Positive?" In: *Journal of The Electrochemical Society* 164.1 (2016), A6274–A6277. ISSN: 0013-4651. DOI: 10.1149/2.0401701jes.

[125] P. Denholm and G. L. Kulcinski. "Life cycle energy requirements and greenhouse gas emissions from large scale energy storage systems". In: *Energy Conversion and Management* 45.13-14 (2004), pp. 2153–2172. DOI: 10.1016/j.enconman.2003.10.014.

[126] A. Immendoerfer, I. Tietze, H. Hottenroth, and T. Viere. "Life-cycle impacts of pumped hydropower storage and battery storage". In: *International Journal of Energy and Environmental Engineering* 8.3 (2017), pp. 231–245. ISSN: 2008-9163. DOI: 10.1007/s40095-017-0237-5.

[127] M. Hiremath, K. Derendorf, and T. Vogt. "Comparative life cycle assessment of battery storage systems for stationary applications". In: *Environmental science & technology* 49.8 (2015), pp. 4825–4833. ISSN: 0013-936X. DOI: 10.1021/es504572q.

[128] L. Vandepaer, J. Cloutier, and B. Amor. "Environmental impacts of Lithium Metal Polymer and Lithium-ion stationary batteries". In: *Renewable and Sustainable Energy Reviews* 78 (2017), pp. 46–60. DOI: 10.1016/j.rser.2017.04.057.

[129] P. Stenzel, J. C. Koj, A. Schreiber, W. Hennings, and P. Zapp. "Primary control provided by large-scale battery energy storage systems or fossil power plants in Germany and related environmental impacts". In: *Journal of Energy Storage* (2016). DOI: 10.1016/j.est.2015.12.006.

[130] M. Arbabzadeh, J. X. Johnson, R. de Kleine, and G. A. Keoleian. "Vanadium redox flow batteries to reach greenhouse gas emissions targets in an off-grid configuration". In: *Applied Energy* 146 (2015), pp. 397–408. DOI: 10.1016/j.apenergy.2015.02.005.

[131] P. Stenzel, A. Schreiber, J. Marx, C. Wulf, M. Schreieder, and L. Stephan. "Environmental impacts of electricity generation for Graciosa Island, Azores". In: *Journal of Energy Storage* 15 (2018), pp. 292–303. DOI: 10.1016/j.est.2017.12.002.

[132] E. McKenna, M. McManus, S. Cooper, and M. Thomson. "Economic and environmental impact of lead-acid batteries in grid-connected domestic PV systems". In: *Applied Energy* 104 (2013), pp. 239–249. DOI: 10.1016/j.apenergy.2012.11.016.

[133] C. Jones, V. Peshev, P. Gilbert, and S. Mander. “Battery storage for post-incentive PV uptake? A financial and life cycle carbon assessment of a non-domestic building”. In: *Journal of Cleaner Production* 167 (2017), pp. 447–458. ISSN: 09596526. DOI: 10.1016/j.jclepro.2017.08.191.

[134] F. J. de Sisternes, J. D. Jenkins, and A. Botterud. “The value of energy storage in decarbonizing the electricity sector”. In: *Applied Energy* 175 (2016), pp. 368–379. DOI: 10.1016/j.apenergy.2016.05.014.

[135] Y. Lin, J. X. Johnson, and J. L. Mathieu. “Emissions impacts of using energy storage for power system reserves”. In: *Applied Energy* 168 (2016), pp. 444–456. DOI: 10.1016/j.apenergy.2016.01.061.

[136] M. Zheng. *Smart households: Economics and emission impacts of distributed energy storage for residential sector demand response*. 2015. DOI: 10.7916/D89P315H.

[137] A. Abdon, X. Zhang, D. Parra, M. K. Patel, C. Bauer, and J. Worlitschek. “Techno-economic and environmental assessment of stationary electricity storage technologies for different time scales”. In: *Energy* 139 (2017), pp. 1173–1187. DOI: 10.1016/j.energy.2017.07.097.

[138] M. Arbabzadeh, J. X. Johnson, and G. A. Keoleian. “Parameters driving environmental performance of energy storage systems across grid applications”. In: *Journal of Energy Storage* 12 (2017), pp. 11–28. DOI: 10.1016/j.est.2017.03.011.

[139] M. Finkbeiner, A. Inaba, R. Tan, K. Christiansen, and H.-J. Klüppel. “The New International Standards for Life Cycle Assessment: ISO 14040 and ISO 14044”. In: *The International Journal of Life Cycle Assessment* 11.2 (2006), pp. 80–85. ISSN: 1614-7502. DOI: 10.1065/lca2006.02.002.

[140] J. Dewulf, G. van der Vorst, K. Denturck, H. van Langenhove, W. Ghyoot, J. Tytgat, and K. Vandeputte. “Recycling rechargeable lithium ion batteries: Critical analysis of natural resource savings”. In: *Resources, Conservation and Recycling* 54.4 (2010), pp. 229–234. ISSN: 09213449. DOI: 10.1016/j.resconrec.2009.08.004.

[141] D. A. Notter, M. Gauch, R. Widmer, P. Wäger, A. Stamp, R. Zah, and H.-J. Althaus. “Contribution of Li-ion batteries to the environmental impact of electric vehicles”. In: *Environmental science & technology* 44.17 (2010), pp. 6550–6556. ISSN: 0013-936X. DOI: 10.1021/es903729a.

[142] M. Buchert, W. Jenseit, C. Merz, and D. Schüler. *Ökobilanz zum "Recycling von Lithium-Ionen-Batterien" (LithoRec)*. Ed. by Öko-Institut e.V. 2011. URL: https://www.oeko.de//oekodoc/1500/2011-068-de.pdf.

[143] G. Majeau-Bettez, T. R. Hawkins, and A. H. Strømman. “Life cycle environmental assessment of lithium-ion and nickel metal hydride batteries for plug-in hybrid and battery electric vehicles”. In: *Environmental science & technology* 45.10 (2011), pp. 4548–4554. ISSN: 0013-936X. DOI: 10.1021/es103607c.

[144] S. Amarakoon, J. Smith, and B. Segal. *Application of life-cycle assessment to nanoscale technology: Lithium-ion batteries for electric vehicles*. 2013.

[145] L. Ahmadi, S. B. Young, M. Fowler, R. A. Fraser, and M. A. Achachlouei. “A cascaded life cycle: Reuse of electric vehicle lithium-ion battery packs in energy storage systems”. In: *The International Journal of Life Cycle Assessment* 22.1 (2017), pp. 111–124. ISSN: 1614-7502. DOI: 10.1007/s11367-015-0959-7.

[146] G. Wernet, C. Bauer, B. Steubing, J. Reinhard, E. Moreno-Ruiz, and B. Weidema. "The ecoinvent database version 3 (part I): Overview and methodology". In: *The International Journal of Life Cycle Assessment* 21.9 (2016), pp. 1218–1230. ISSN: 1614-7502. DOI: 10.1007/s11367-016-1087-8.

[147] S. Solomon, D. Qin, M. Manning, Z. Chen, M. Marquis, K. B. Averyt, M. Tignor, H. L. Miller, et al. *Contribution of working group I to the fourth assessment report of the intergovernmental panel on climate change, 2007*. Ed. by Cambridge University Press. Cambridge, United Kingdom and New York, NY, USA, 2007.

[148] I. P. o. C. Change. *Climate Change 2013 - The Physical Science Basis*. Cambridge: Cambridge University Press, 2014. ISBN: 9781107415324. DOI: 10.1017/CBO9781107415324.

[149] A. Hu, L. Huang, S. Lou, C.-H. Kuo, C.-Y. Huang, K.-J. Chian, H.-T. Chien, and H.-F. Hong. "Assessment of the Carbon Footprint, Social Benefit of Carbon Reduction, and Energy Payback Time of a High-Concentration Photovoltaic System". In: *Sustainability* 9.1 (2017), p. 27. ISSN: 2071-1050. DOI: 10.3390/su9010027.

[150] R. C. Hierle. "Lebenszyklusanalyse eines stationären Batteriespeichersystems: Der Energy Neighbor". Masterarbeit. München: Technische Universität München, 2017.

[151] J. F. Peters, M. Baumann, B. Zimmermann, J. Braun, and M. Weil. "The environmental impact of Li-Ion batteries and the role of key parameters – A review". In: *Renewable and Sustainable Energy Reviews* 67 (2017), pp. 491–506. DOI: 10.1016/j.rser.2016.08.039.

[152] M. de Simón-Martín, M. Díez-Mediavilla, and C. Alonso-Tristán. "Real Energy Payback Time and Carbon Footprint of a GCPVS". In: *AIMS Energy* 5.1 (2017), pp. 77–95. ISSN: 2333-8334. DOI: 10.3934/energy.2017.1.77.

[153] H. Birch. *A Study Into The Feasibility of Local Renewable Energy Systems With Storage, Using Security and Sustainability Metrics for Optimisation and Evaluation*. 2016. URL: http://etheses.whiterose.ac.uk/id/eprint/16725.

[154] J. C. Koj, A. Schreiber, P. Stenzel, P. Zapp, J. Fleer, and I. Hahndorf. "Life Cycle Assessment of a large-scale battery system for primary control provision". In: 2014. URL: http://hdl.handle.net/2128/9179.

[155] J. Peng, L. Lu, and H. Yang. "Review on life cycle assessment of energy payback and greenhouse gas emission of solar photovoltaic systems". In: *Renewable and Sustainable Energy Reviews* (2013).

[156] B. Burger. *Energy Charts*. 2017. URL: https://www.energy-charts.de/.

[157] International Energy Agency OECD/IEA. *Electricity Information 2017*. Ed. by IEA Publishing. 2017. URL: https://www.iea.org/publications/freepublications/publication/ElectricityInformation2017Overview.pdf (visited on 07/31/2018).

[158] International Energy Agency OECD/IEA. *Electric power transmission and distribution losses*. Ed. by IEA Statistics. 2018. URL: https://data.worldbank.org/indicator/EG.ELC.LOSS.ZS?end=2014&locations=DE&start=1960&view=chart (visited on 07/31/2018).

[159] Tesla Motors Inc. *Powerwall Product Homepage*. 2015. URL: http://www.teslamotors.com/de_DE/powerwall (visited on 11/16/2015).

[160] Bundesverband der Energie- und Wasserwirtschaft e.V. *Energie-Info: Stromverbrauch im Haushalt*. Berlin, 2014. URL: https://www.bdew.de/internet.nsf/id/6966C7CB65D8D8FAC1257D5E0043D565/file/705_Charts_BDEW_Stromverbrauch%20im%20Haushalt_September%202014.pdf.

[161] Deutsche Übertragungsnetzbetreiber. *EEG-Anlagenstammdaten*. 2015. URL: http://www.netztransparenz.de/de/Anlagenstammdaten.htm (visited on 11/17/2015).

[162] C. A. Rosenkranz, U. Köhler, and J. L. Liska. "Modern battery systems for plug-in hybrid electric vehicles". In: *23rd International Battery, Hybrid and Fuel Cell Electric Vehicle Symposium and Exhibition (EVS-23)*. Anaheim, 2007. URL: http://www.lifepo4.info/Battery_study/Batteries/Modern_Battery_Systems_for_Plug_In_Hybrid_Vehicles.pdf.

[163] Z. Shahan. *38,000 Tesla Powerwall Reservations In Under A Week (Tesla / Elon Musk Transcript)*. 2015. URL: http://cleantechnica.com/2015/05/07/38000-tesla-powerwall-reservations-in-under-a-week-tesla-elon-musk-transcript/ (visited on 11/23/2015).

[164] Bundesministerium der Finanzen. *AfA-Tabelle für die allgemein verwendbaren Anlagegüter ("AV")*. 2000. URL: https://www.bundesfinanzministerium.de/Content/DE/Standardartikel/Themen/Steuern/Weitere_Steuerthemen/Betriebspruefung/AfA-Tabellen/2000-12-15-afa-103.html.

[165] S. Diaf, M. Belhamel, M. Haddadi, and A. Louche. "Technical and economic assessment of hybrid photovoltaic/wind system with battery storage in Corsica island". In: *Energy Policy* 36.2 (2008), pp. 743–754. ISSN: 0301-4215. DOI: 10.1016/j.enpol.2007.10.028.

[166] R. Dufo-López. "Optimisation of size and control of grid-connected storage under real time electricity pricing conditions". In: *Applied Energy* 140 (2015), pp. 395–408. DOI: 10.1016/j.apenergy.2014.12.012.

[167] H. Yang, Z. Wei, and L. Chengzhi. "Optimal design and techno-economic analysis of a hybrid solar–wind power generation system". In: *Applied Energy* 86.2 (2009), pp. 163–169. DOI: 10.1016/j.apenergy.2008.03.008.

[168] A. Zucker and T. Hinchliffe. "Optimum sizing of PV-attached electricity storage according to power market signals – A case study for Germany and Italy". In: *Applied Energy* 127 (2014), pp. 141–155. DOI: 10.1016/j.apenergy.2014.04.038.

[169] Bundesverband der Energie- und Wasserwirtschaft e.V. *BDEW-Strompreisanalyse August 2015*. Berlin, 2015.

[170] S. Philipps and W. Warmuth. *Photovoltaics Report 2015*. 2015. URL: https://www.ise.fraunhofer.de/en/news/news-archive/news-2012/fraunhofer-ise-publishes-photovoltaics-report.

[171] W. G. van Sark, P. Muizebelt, J. Cace, A. de Vries, and P. de Rijk. "Price development of photovoltaic modules, inverters, and systems in the Netherlands in 2012". In: *Renewable Energy* 71 (2014), pp. 18–22. DOI: 10.1016/j.renene.2014.05.008.

[172] G. Di Francia. "On the cost of photovoltaic electricity for small residential plants in the European Union". In: *International Journal of Renewable Energy Research (IJRER)* 4.3 (2014), pp. 610–617. URL: http://www.ijrer.org/ijrer/index.php/ijrer/article/view/1373.

[173] KfW-Bank. *KfW-Programm Erneuerbare Energien "Speicher" - Merkblatt*. Frankfurt, 2015.

[174] EPEX SPOT. *Börsenstrompreis am EPEX-Spotmarkt für Deutschland/Österreich von September 2014 bis September 2015*. 2015. URL: http://de.statista.com/statistik/daten/studie/289437/umfrage/strompreis-am-epex-spotmarkt/.

[175] T. Autrup et al. *Batteriespeicher in der Nieder- und Mittelspannungsebene: Anwendungen und Wirtschaftlichkeit sowie Auswirkungen auf die elektrischen Netze: VDE-Studie*. Ed. by VDE ETG. Frankfurt am Main, 2015.

[176] G. Kerber. "Aufnahmefähigkeit von Niederspannungsverteilnetzen für die Einspeisung aus Photovoltaikkleinanlagen". Dissertation. München: Technische Universität München, 2010.

[177] M. Wagler and R. Witzmann. "Erstellung und Evaluierung eines synthetischen Haushaltslastprofilgenerators für Wirk- und Blindleistung". In: *14. Symposium Energieinnovation*. Graz/Austria, 2016, pp. 1–11.

[178] P. Icha and G. Kuhs. "Entwicklung der spezifischen Kohlendioxid-Emissionen des deutschen Strommix in den Jahren 1990 - 2016". In: (2017). URL: https://www.umweltbundesamt.de/sites/default/files/medien/1410/publikationen/2017-05-22_climate-change_15-2017_strommix.pdf (visited on 05/27/2017).

[179] N. V. Ramana. *Power system analysis*. Noida India: Pearson, 2011.

[180] VDE. *VDE-AR-N 4105 Anwendungsregel: Generators connected to the low-voltage distribution network*. 8.2011.

[181] M. Steen. *Greenhouse gas emissions from fossil fuel fired power generation systems*. Institute for Advanced Materials, Joint Research Centre, European Commission, 2000.

[182] M. L. Mittal, C. Sharma, and R. Singh. "Estimates of Emissions from Coal Fired Thermal Power Plants in India". In: (2012). URL: https://www3.epa.gov/ttnchie1/conference/ei20/session5/mmittal.pdf.

[183] D. Neves and C. A. Silva. "Optimal electricity dispatch on isolated mini-grids using a demand response strategy for thermal storage backup with genetic algorithms". In: *Energy* 82 (2015), pp. 436–445. DOI: 10.1016/j.energy.2015.01.054.

[184] Red Eléctrica de Espana. *Canary electricity demand in real-time*. 2018. URL: http://www.ree.es/en/activities/canary-islands-electricity-system/canary-electricity-demand-in-real-time (visited on 06/08/2018).

[185] A. Colmenar-Santos, A.-R. Linares-Mena, D. Borge-Diez, and C.-D. Quinto-Alemany. "Impact assessment of electric vehicles on islands grids: A case study for Tenerife (Spain)". In: *Energy* 120 (2017), pp. 385–396. DOI: 10.1016/j.energy.2016.11.097.

[186] M. Carrion and J. M. Arroyo. "A Computationally Efficient Mixed-Integer Linear Formulation for the Thermal Unit Commitment Problem". In: *IEEE Transactions on Power Systems* 21.3 (2006), pp. 1371–1378. DOI: 10.1109/TPWRS.2006.876672.

[187] Q. Tang, N. Liu, and J. Zhang. "Optimal Operation Method for Microgrid with Wind/PV/Diesel Generator/Battery and Desalination". In: *Journal of Applied Mathematics* 2014 (2014), pp. 1–12. DOI: 10.1155/2014/857541.

[188] S. Lüers, A.-K. Wallasch, and K. Rehfeldt. "Kostensituation der Windenergie an Land in Deutschland–Update". In: *Deutsche WindGuard GmbH im Auftrag von BWE und VDMA. Varel. Abgerufen am* 14 (2015).

[189] R. McKenna. "The double-edged sword of decentralized energy autonomy". In: *Energy Policy* 113 (2018), pp. 747–750. ISSN: 0301-4215. DOI: 10.1016/j.enpol.2017.11.033.

[190] J. von Appen and M. Braun. "Strategic decision making of distribution network operators and investors in residential photovoltaic battery storage systems". In: *Applied Energy* 230 (2018), pp. 540–550. DOI: 10.1016/j.apenergy.2018.08.043.

[191] T. Bocklisch. "Hybrid energy storage approach for renewable energy applications". In: *Journal of Energy Storage* 8 (2016), pp. 311–319. DOI: 10.1016/j.est.2016.01.004.

[192] A. J. Pimm, T. T. Cockerill, and P. G. Taylor. “The potential for peak shaving on low voltage distribution networks using electricity storage”. In: *Journal of Energy Storage* 16 (2018), pp. 231–242. DOI: 10.1016/j.est.2018.02.002.

[193] J. Pascual, J. Barricarte, P. Sanchis, and L. Marroyo. “Energy management strategy for a renewable-based residential microgrid with generation and demand forecasting”. In: *Applied Energy* 158 (2015), pp. 12–25. DOI: 10.1016/j.apenergy.2015.08.040.

[194] J. Kennedy, P. Ciufo, and A. Agalgaonkar. “Voltage-based storage control for distributed photovoltaic generation with battery systems”. In: *Journal of Energy Storage* 8 (2016), pp. 274–285. DOI: 10.1016/j.est.2016.10.007.

[195] J. Fleer and P. Stenzel. “Impact analysis of different operation strategies for battery energy storage systems providing primary control reserve”. In: *Journal of Energy Storage* 8 (2016), pp. 320–338. DOI: 10.1016/j.est.2016.02.003.

[196] T. Lühn and J. Geldermann. “Operating Strategies for Battery Storage Systems in Low-Voltage Grids to Limit the Feed-In Power of Solar Power Systems Using Fuzzy Control”. In: *Zeitschrift für Energiewirtschaft* 79.2 (2017), p. 652. DOI: 10.1007/s12398-017-0198-7.

[197] D. Arcos-Aviles, F. Guinjoan, M. P. Marietta, J. Pascual, L. Marroyo, and P. Sanchis. “Energy management strategy for a grid-tied residential microgrid based on Fuzzy Logic and power forecasting”. In: *Proceedings of the IECON2016 - 42nd Annual Conference of the IEEE Industrial Electronics Society*. Piscataway, NJ: IEEE, 2016, pp. 4103–4108. ISBN: 978-1-5090-3474-1. DOI: 10.1109/IECON.2016.7793088.

[198] R. Arghandeh, J. Woyak, A. Onen, J. Jung, and R. P. Broadwater. “Economic optimal operation of Community Energy Storage systems in competitive energy markets”. In: *Applied Energy* 135 (2014), pp. 71–80. DOI: 10.1016/j.apenergy.2014.08.066.

[199] N. Jayasekara, M. A. S. Masoum, and P. J. Wolfs. “Optimal Operation of Distributed Energy Storage Systems to Improve Distribution Network Load and Generation Hosting Capability”. In: *IEEE Transactions on Sustainable Energy* 7.1 (2016), pp. 250–261. DOI: 10.1109/TSTE.2015.2487360.

[200] V. Marano, G. Rizzo, and F. A. Tiano. “Application of dynamic programming to the optimal management of a hybrid power plant with wind turbines, photovoltaic panels and compressed air energy storage”. In: *Applied Energy* 97 (2012), pp. 849–859. DOI: 10.1016/j.apenergy.2011.12.086.

[201] Y. Lu, J. Zhou, H. Qin, Y. Wang, and Y. Zhang. “Environmental/economic dispatch problem of power system by using an enhanced multi-objective differential evolution algorithm”. In: *Energy Conversion and Management* 52.2 (2011), pp. 1175–1183. DOI: 10.1016/j.enconman.2010.09.012.

[202] R. R. nejad, S. M. Hakimi, and S. M. Tafreshi. “Smart virtual energy storage control strategy to cope with uncertainties and increase renewable energy penetration”. In: *Journal of Energy Storage* 6 (2016), pp. 80–94. DOI: 10.1016/j.est.2016.03.001.

[203] J. Choi, Y. Shin, M. Choi, W.-K. Park, and I.-W. Lee. “Robust Control of a Microgrid Energy Storage System using Various Approaches”. In: *IEEE Transactions on Smart Grid* (2018), p. 1. ISSN: 1949-3053. DOI: 10.1109/TSG.2018.2808914.

[204] Y. Zhang, B. Liu, T. Zhang, and B. Guo. "An intelligent control strategy of battery energy storage system for microgrid energy management under forecast uncertainties". In: *Int. J. Electrochem. Sci* 9 (2014), pp. 4190–4204.

[205] I. Ranaweera, O.-M. Midtgård, and M. Korpås. "Distributed control scheme for residential battery energy storage units coupled with PV systems". In: *Renewable Energy* 113 (2017), pp. 1099–1110. DOI: 10.1016/j.renene.2017.06.084.

[206] W. Qi, J. Liu, and P. D. Christofides. "A distributed control framework for smart grid development: Energy/water system optimal operation and electric grid integration". In: *Journal of Process Control* 21.10 (2011), pp. 1504–1516. ISSN: 09591524. DOI: 10.1016/j.jprocont.2011.05.010.

[207] Y. Zheng, J. Zhao, Y. Song, F. Luo, K. Meng, J. Qiu, and D. J. Hill. "Optimal Operation of Battery Energy Storage System Considering Distribution System Uncertainty". In: *IEEE Transactions on Sustainable Energy* (2017), p. 1. DOI: 10.1109/TSTE.2017.2762364.

[208] A. B. Forough and R. Roshandel. "Lifetime optimization framework for a hybrid renewable energy system based on receding horizon optimization". In: *Energy* 150 (2018), pp. 617–630. DOI: 10.1016/j.energy.2018.02.158.

[209] M. Arnold and G. Andersson. "Model predictive control of energy storage including uncertain forecasts". In: *Power Systems Computation Conference (PSCC), Stockholm, Sweden*. Vol. 23. 2011, pp. 24–29.

[210] V. de Oliveira, J. Jäschke, and S. Skogestad. "Optimal operation of energy storage in buildings: Use of the hot water system". In: *Journal of Energy Storage* 5 (2016), pp. 102–112. DOI: 10.1016/j.est.2015.11.009.

[211] R. Kumar, M. J. Wenzel, M. J. Ellis, M. N. ElBsat, K. H. Drees, and V. M. Zavala. "A Stochastic Model Predictive Control Framework for Stationary Battery Systems". In: *IEEE Transactions on Power Systems* (2018), p. 1. DOI: 10.1109/TPWRS.2017.2789118.

[212] Z. Li, C. Zang, P. Zeng, and H. Yu. "Combined Two-Stage Stochastic Programming and Receding Horizon Control Strategy for Microgrid Energy Management Considering Uncertainty". In: *Energies* 9.7 (2016), p. 499. ISSN: 10.3390/en6083951. DOI: 10.3390/en9070499.

[213] T. Niknam, F. Golestaneh, and A. Malekpour. "Probabilistic energy and operation management of a microgrid containing wind/photovoltaic/fuel cell generation and energy storage devices based on point estimate method and self-adaptive gravitational search algorithm". In: *Energy* 43.1 (2012), pp. 427–437. DOI: 10.1016/j.energy.2012.03.064.

[214] J. D. Lara, D. E. Olivares, and C. A. Canizares. "Robust Energy Management of Isolated Microgrids". In: *IEEE Systems Journal* (2018), pp. 1–12. ISSN: 1932-8184. DOI: 10.1109/JSYST.2018.2828838.

[215] Y. Wang, X. Lin, and M. Pedram. "Adaptive Control for Energy Storage Systems in Households With Photovoltaic Modules". In: *IEEE Transactions on Smart Grid* 5.2 (2014), pp. 992–1001. ISSN: 1949-3053. DOI: 10.1109/TSG.2013.2292518.

[216] J. Qin, Y. Chow, J. Yang, and R. Rajagopal. "Online Modified Greedy Algorithm for Storage Control Under Uncertainty". In: *IEEE Transactions on Power Systems* 31.3 (2016), pp. 1729–1743. DOI: 10.1109/TPWRS.2015.2440355.

[217] J. Sachs and O. Sawodny. “A Two-Stage Model Predictive Control Strategy for Economic Diesel-PV-Battery Island Microgrid Operation in Rural Areas”. In: *IEEE Transactions on Sustainable Energy* 7.3 (2016), pp. 903–913. DOI: 10.1109/TSTE.2015.2509031.

[218] L. Barelli, G. Bidini, F. Bonucci, and A. Ottaviano. “Residential micro-grid load management through artificial neural networks”. In: *Journal of Energy Storage* 17 (2018), pp. 287–298. DOI: 10.1016/j.est.2018.03.011.

[219] J. Müller, M. Ahrens, I. Mauser, and H. Schmeck. “Achieving Optimized Decisions on Battery Operating Strategies in Smart Buildings”. In: *Applications of Evolutionary Computation*. Ed. by K. Sim and P. Kaufmann. Cham: Springer International Publishing, 2018, pp. 205–221. ISBN: 978-3-319-77538-8.

[220] M. Abdoos and M. Ghazvini. “Multi-objective particle swarm optimization of component size and long-term operation of hybrid energy systems under multiple uncertainties”. In: *Journal of Renewable and Sustainable Energy* 10.1 (2018), p. 015902. ISSN: 1941-7012. DOI: 10.1063/1.4998344.

[221] G. Henri, N. Lu, and C. Carrejo. “Design of a novel mode-based energy storage controller for residential PV systems”. In: *2017 IEEE PES Innovative Smart Grid Technologies Conference Europe (ISGT-Europe)*. Piscataway, NJ: IEEE, 2017, pp. 1–6. ISBN: 978-1-5386-1953-7. DOI: 10.1109/ISGTEurope.2017.8260258.

[222] A. Mamun, I. Narayanan, D. Wang, A. Sivasubramaniam, and H. K. Fathy. “Multi-objective optimization of demand response in a datacenter with lithium-ion battery storage”. In: *Journal of Energy Storage* 7 (2016), pp. 258–269. DOI: 10.1016/j.est.2016.08.002.

[223] P. Musilek, P. Krömer, R. Martins, and H. C. Hesse. “Optimal Energy Management of Residential PV/HESS Using Evolutionary Fuzzy Control”. In: *Congress on Evolutionary Computation*. 2017, pp. 1–8.

[224] J. P. Fossati, A. Galarza, A. Martín-Villate, J. M. Echeverría, and L. Fontán. “Optimal scheduling of a microgrid with a fuzzy logic controlled storage system”. In: *International Journal of Electrical Power & Energy Systems* 68 (2015), pp. 61–70. ISSN: 01420615. DOI: 10.1016/j.ijepes.2014.12.032.

[225] A. S. Tsagkou, E. D. K. D. I. Doukas, D. P. Labridis, A. G. Marinopoulos, and T. Tengner. “Stacking grid services with energy storage techno-economic analysis”. In: *2017 IEEE Manchester PowerTech*. Piscataway, NJ: IEEE, 2017, pp. 1–6. ISBN: 978-1-5090-4237-1. DOI: 10.1109/PTC.2017.7981004.

[226] Z. Wu and X. Xia. “Optimal switching renewable energy system for demand side management”. In: *Solar Energy* 114 (2015), pp. 278–288. DOI: 10.1016/j.solener.2015.02.001.

[227] O. Megel. *Storage in Power Systems: Frequency Control, Scheduling of Multiple Applications, and Computational Complexity*. 2017. DOI: 10.3929/ethz-b-000171342.

[228] D. Metz and J. T. Saraiva. “Simultaneous co-integration of multiple electrical storage applications in a consumer setting”. In: *Energy* 143 (2018), pp. 202–211. DOI: 10.1016/j.energy.2017.10.098.

[229] F. Soyck, F. Schilling, M. Schmidt, and B. Engel. “Real time calculation of virtual meter points for simultaneous multiple use of PV storage systems”. In: *International ETG Congress 2015; Die Energiewende - Blueprints for the new energy age*. 2015, pp. 1–7.

[230] R. Hollinger, L. M. Diazgranados, F. Braam, T. Erge, G. Bopp, and B. Engel. “Distributed solar battery systems providing primary control reserve”. In: *IET Renewable Power Generation* 10.1 (2016), pp. 63–70. DOI: 10.1049/iet-rpg.2015.0147.

[231] C. N. Truong, D. C. May, R. Martins, P. Musilek, A. Jossen, and H. C. Hesse. “Cuckoo-search optimized fuzzy-logic control of stationary battery storage systems”. In: *2017 IEEE Electrical Power and Energy Conference (EPEC)*. Ed. by Institute of Electrical and Electronics Engineers. Piscataway, NJ: IEEE, 2017, pp. 1–6. ISBN: 978-1-5386-0817-3. DOI: 10.1109/EPEC.2017.8286239.

[232] M. N. Ab Wahab, S. Nefti-Meziani, and A. Atyabi. “A comprehensive review of swarm optimization algorithms”. In: *PloS one* 10.5 (2015), e0122827. DOI: 10.1371/journal.pone.0122827.

[233] X.-S. Yang and S. Deb. “Cuckoo Search via Levy Flights”. In: *X.-S. Yang, S. Deb, Cuckoo search via Levy flights, in: Proc. of World Congress on Nature & Biologically Inspired Computing (NaBIC)* (2009).

[234] X. Li and M. Yin. “Modified cuckoo search algorithm with self adaptive parameter method”. In: *Information Sciences* 298 (2015), pp. 80–97. ISSN: 00200255. DOI: 10.1016/j.ins.2014.11.042.

[235] X.-S. Yang and S. Deb. “Multiobjective cuckoo search for design optimization”. In: *Computers & Operations Research* 40.6 (2013), pp. 1616–1624. ISSN: 03050548. DOI: 10.1016/j.cor.2011.09.026.

[236] J. Zhao and B. K. Bose. “Evaluation of membership functions for fuzzy logic controlled induction motor drive”. In: *Proceedings of the 28th annual conference of the IEEE Industrial Electronics Society*. Piscataway, NJ: IEEE Operations Center, 2002, pp. 229–234. ISBN: 0-7803-7474-6. DOI: 10.1109/IECON.2002.1187512.

[237] T. Takagi and M. Sugeno. “Fuzzy identification of systems and its applications to modeling and control”. In: *IEEE Transactions on Systems, Man, and Cybernetics* SMC-15.1 (1985), pp. 116–132. ISSN: 0018-9472. DOI: 10.1109/TSMC.1985.6313399.

[238] J. Zhang et al. “Baseline and target values for regional and point PV power forecasts: Toward improved solar forecasting”. In: *Solar Energy* 122 (2015), pp. 804–819. DOI: 10.1016/j.solener.2015.09.047.

[239] Q. Jiang, M. Xue, and G. Geng. “Energy management of microgrid in grid-connected and stand-alone modes”. In: *IEEE Trans. Power Syst* 28.3 (2013), pp. 3380–3389.

[240] B.-M. Hodge et al. “Wind Power Forecasting Error Distributions: An International Comparison”. In: *11th Annual International Workshop on Large-Scale Integration of Wind Power into Power Systems as well as on Transmission Networks for Offshore Wind Power Plants Conference*. 2012, pp. 1–6. (Visited on 01/16/2013).

[241] C. N. Truong, M. Schimpe, U. Bürger, H. C. Hesse, and A. Jossen. “Multi-Use of Stationary Battery Storage Systems with Blockchain Based Markets”. In: *Energy Procedia* 155 (2018). 12th International Renewable Energy Storage Conference, IRES 2018, 13-15 March 2018, Düsseldorf, Germany, pp. 3–16. ISSN: 1876-6102. DOI: https://doi.org/10.1016/j.egypro.2018.11.070.

[242] X. He, E. Delarue, W. D’haeseleer, and J.-M. Glachant. “A novel business model for aggregating the values of electricity storage”. In: *Energy Policy* 39.3 (2011), pp. 1575–1585. ISSN: 0301-4215. DOI: 10.1016/j.enpol.2010.12.033.

[243] T. Brijs, D. Huppmann, S. Siddiqui, and R. Belmans. "Auction-based allocation of shared electricity storage resources through physical storage rights". In: *Journal of Energy Storage* 7 (2016), pp. 82–92. DOI: 10.1016/j.est.2016.05.009.

[244] E. Munsing, J. Mather, and S. Moura. *Blockchains for Decentralized Optimization of Energy Resources in Microgrid Networks*. 2017. URL: http://escholarship.org/uc/item/80g5s6df.pdf.

[245] F. Imbault, M. Swiatek, R. de Beaufort, and R. Plana. "The green blockchain: Managing decentralized energy production and consumption". In: *2017 IEEE International Conference on Environment and Electrical Engineering and 2017 IEEE Industrial and Commercial Power Systems Europe (EEEIC / I&CPS Europe)*. IEEE, 2017, pp. 1–5. ISBN: 978-1-5386-3917-7. DOI: 10.1109/EEEIC.2017.7977613.

[246] N. Zhumabekuly Aitzhan and D. Svetinovic. "Security and Privacy in Decentralized Energy Trading through Multi-signatures, Blockchain and Anonymous Messaging Streams". In: *IEEE Transactions on Dependable and Secure Computing* (2016), p. 1. ISSN: 1545-5971. DOI: 10.1109/TDSC.2016.2616861.

[247] I. Kounelis, G. Steri, R. Giuliani, D. Geneiatakis, R. Neisse, and I. Nai-Fovino. "Fostering consumers' energy market through smart contracts". In: *2017 International Conference in Energy and Sustainability in Small Developing Economies (ES2DE)*. 2017, pp. 1–6. DOI: 10.1109/ES2DE.2017.8015343.

[248] M. E. Peck and D. Wagman. "Energy trading for fun and profit buy your neighbor's rooftop solar power or sell your own-it'll all be on a blockchain". In: *IEEE Spectrum* 54.10 (2017), pp. 56–61. ISSN: 0018-9235. DOI: 10.1109/MSPEC.2017.8048842.

[249] Oxygen Initiative. *Oxygen Initiative brings Blockchain technology for charging stations to the U.S.* 2018. URL: https://oxygeninitiative.com/blockchain-4-charging-stations/.

[250] P. Danzi, M. Angjelichinoski, . Stefanovi, and P. Popovski. *Distributed Proportional-Fairness Control in MicroGrids via Blockchain Smart Contracts*. 2017.

[251] K. Kvaternik, A. Laszka, M. Walker, D. Schmidt, M. Sturm, M. Lehofer, and A. Dubey. "Privacy-Preserving Platform for Transactive Energy Systems". In: *ACM/IFIP/USENIX Middleware*. 2017, pp. 1–6.

[252] C. Pop, T. Cioara, M. Antal, I. Anghel, I. Salomie, and M. Bertoncini. "Blockchain Based Decentralized Management of Demand Response Programs in Smart Energy Grids". In: *Sensors (Basel, Switzerland)* 18.1 (2018). ISSN: 1424-8220. DOI: 10.3390/s18010162.

[253] TenneT. *TenneT unlocks distributed flexibility via blockchain*. 2017. URL: https://www.tennet.eu/news/detail/tennet-unlocks-distributed-flexibility-via-blockchain/.

[254] Ponton. *Ponton Develops a Smart Market for Germany Flexibility Providers*. 2017. URL: https://enerchain.ponton.de/index.php/13-ponton-develops-a-smart-market-for-german-flexibility-providers.

[255] K. Delmolino, M. Arnett, A. Kosba, A. Miller, and E. Shi. "Step by Step Towards Creating a Safe Smart Contract: Lessons and Insights from a Cryptocurrency Lab". In: *Financial Cryptography and Data Security*. Ed. by J. Clark, S. Meiklejohn, P. Y. Ryan, D. Wallach, M. Brenner, and K. Rohloff. Vol. 9604. Lecture Notes in Computer Science. Berlin, Heidelberg and s.l.: Springer Berlin Heidelberg, 2016, pp. 79–94. ISBN: 978-3-662-53356-7. DOI: 10.1007/978-3-662-53357-4_6.

[256] S. Popov. “The Tangle”. In: *Whitepaper* (2017). URL: https://iota.org/IOTA_Whitepaper.pdf.

[257] T. Vorbuchner. “Optimierung der Betriebsstrategie stationärer Energiespeicher für Peak-Shaving Anwendungen unter Berücksichtigung der Batteriealterung”. Masterarbeit. München: Technische Universität München, 2017.

List of Figures

List of Tables

Appendix

A Additional Data

Nam Truong

Von: [redacted]
Gesendet: Montag, 2. Juli 2018 13:48
An: Nam Truong
Cc: [redacted]
Betreff:

Hallo zusammen,
[redacted] hat mich gerade entsprechend gebrieft und ich will gerne einen Richtpreis für die angefragte Modulmenge angeben. Zu unserem üblichen Listenpreis ist das ein Sonderprojekt – Preis den wir normalerweise bei Größenordnungen von 2 MWh und darüber anbieten.

1 x Batteriemodul mit 4,8 kWh (100% DOD; 1C) inkl. ABO (Active Battery Optimizer) 2.347,10 €

Das ist nur der Preis für das blanke Batteriemodul mit dem Balancing (ABO), es ist keinerlei Batterie Management System, Modulverbinder, Schrank etc. enthalten.

Ich hoffe das reicht so aus, wenn nicht bitte einfach bei mir melden…

Mit freundlichen Grüßen | With best regards

Figure A.1: Quotation for battery price.

Table A.1: Grid charges in Germany. Overview of ten national and ten municipal distribution grid operators. Prices are from 2017 for a usage period larger than 2700 h per year. [257]

Grid operator	Power charge / EUR/kW/a	
	LV	MV
Netze BW GmbH	113.18	79.63
Bayernwerk	115.65	**139.12**
Westnetz	49.87	83.77
NEW Netz	65.72	60.77
EnergieNetzMitte	114.72	113.76
TEN	147.83	141.31
Avacon	128.52	140.04
E.DIS	98.64	72.60
WEMAG	155.38	137.89
Schleswig-Holstein Netz	146.76	122.26
Stromnetz Berlin	92.55	**41.88**
Stromnetz Hamburg	48.62	51.20
Stadtwerke München	143.00	109.80
Rheinische NetzGesellschaft	88.68	57.14
NetzDienste RheinMain	97.10	67.65
Stuttgart Netze	55.94	67.65
Düsseldorf Netz Düsseldorf	59.36	77.00
Dortmund Dortmund Netze	63.46	83.16
Leipzig Netz Leipzig	127.59	**180.71**
Bremen Wesernetz	55.28	93.65

Table A.2: Bill of materials of the *Energy Neighbor*. Components of 230 V supply.

Bezeichnung im Schaltplan	Menge	Hersteller	Artikel Nummer	Beschreibung
F02				NA-Sicherung, von KWH spezifiziert
F02				NA-Sicherung, von KWH spezifiziert
FI1	1	SIEMENS	5SV3312-6	FI Schutzschalter 25A/0,03A 2pol. für 230 V Steckdosen
F1	1	SIEMENS	5SY6116-6	Sicherungsautomat 1pol.B16A für 230 V Steckdosen
F51	1	SIEMENS	5SY6116-7	Einpoliger Leitungsschutzschalter; C-16A für Alarmanlage
F52	1	SIEMENS	5SY6325-7	Dreipoliger Leitungsschutzschalter; C-25A für Klimasystem
F100	1	SIEMENS	3RV2411-1HA10	Leistungsschalter A-AUSL. 5,5...8A, N-AUSL. 163A, für 24 V Netzteile
F_NA1	1	SIEMENS	5SY6306-6	Dreipoliger Leitungsschutzschalter; B-6A für NA-Schutz

WA – D 250 Ausführung „G“
mit manueller Schaltanlage & Ölauffangwanne

STROMERZEUGER AUF GRUNDRAHMEN Ausführung „G“

Modell	kVA	KW	Gewicht	Motortyp	Leistung	Verbrauch	Ampere
Modell	*100%*	*100%*	*KG*			*bei 100 % Last*	*Genschalter*
WA- D 20 „G“	20	16	550	F3M 2011	20,0 KW	6,7 L/h	28
WA- D 30 „G“	30	24	640	F4M 2011	27,6 KW	8,9 L/h	43
WA- D 40 „G“	40	32	720	BF4M 2011	36,4 KW	11,6 L/h	57
WA- D 60 „G“	60	48	820	BF4M 2011 C	52,0 KW	14,4 L/h	86
WA- D 85 „G“	85	68	1.240	BF4M 1013 E	78,5 KW	21,0 L/h	122
WA- D 100 „G“	100	80	1.300	BF4M 1013 ECG2	91,1 KW	25,8 L/h	144
WA- D 130 „G“	130	104	1.480	BF4M 1013 FC	117,8 KW	32,3 L/h	187
WA- D 150 „G“	150	120	1.580	BF6M 1013 EC	138,1 KW	38,5 L/h	216
WA-D 180 „G“	180	144	1.610	BF6M 1013 FCP	159,8 KW	45,90 L/h	260
WA- D 200 „G“	200	160	1.820	BF6M 1013 FCG2	178,6 KW	50,8 L/h	288
WA- D 250 „G“	250	200	2.200	TCD 2013 L06 4V	216 KW	49,9 L/h	360
WA- D 300 „G“	300	240	2.660	BF6M 1015 C	271 KW	76,6 L/h	432
WA- D 380 „G“	380	304	2.740	BF6M 1015 CP	327 KW	94,3 L/h	547
WA- D 430 „G“	430	344	3.300	BF8M 1015 C	369 KW	103,5 L/h	619
WA- D 450 „G“	450	360	3.350	BF8M1015 C2	-/- KW	117,5 L/h	648
WA- D 500 „G“	500	400	3.600	BF8M 1015 CP	440 KW	131,3 L/h	720

PREISE ab Werk Verl zzgl. MwSt.

Modell	Verkabelt auf Klemmleiste	manueller Start mit 3 pol. Genschalter	inkl. integrierte Notstromautomatik / AMF mit Generatorschalter 4-polig (ohne Netzschalter)	externe Umschaltung mit Netzschalter / ATS 4-polig
	Nettopreis in € ab Werk	*Nettopreis in € ab Werk*	*Nettopreis in € ab Werk*	*Nettopreis in € ab Werk*
WA- D 20 „G“	7.752	8.337	8.711	474
WA- D 30 „G“	8.103	8.730	9.119	520
WA- D 40 „G“	9.167	9.869	10.146	586
WA- D 60 „G“	11.295	12.003	12.219	678
WA- D 85 „G“	13.803	14.561	14.925	755
WA- D 100 „G“	14.990	15.633	15.698	927
WA- D 130 „G“	17.513	18.373	18.786	1.224
WA- D 150 „G“	19.353	20.542	20.859	1.224
WA- D 180 „G“	21.750	23.124	23.619	1.224
WA- D 200 „G“	24.699	25.839	26.291	1.760
WA- D 250 „G“	28.430	29.973	30.871	2.819
WA- D 300 „G“	36.117	37.674	38.721	2.819
WA- D 380 „G“	42.315	44.190	45.018	2.819
WA- D 430 „G“	46.112	48.477	49.070	2.819
WA- D 450 „G“	51.971	50.726	51.971	3.008
WA- D 500 „G“	53.910	56.331	56.805	3.008

Figure A.2: Price list for diesel generators. The price assumption is based on the diesel generator *WA- D 500 “G”* with a nominal power of 440 kW. The configuration with integrated backup power automation and 4-pin generator switch is chosen (56,805 EUR). An external switching with a 4-pin power switch is included (3008 EUR). A VAT of 19% is added to the given net price resulting in a gross price of 70,613 EUR or 162 EUR/kW.

bayernwerk

Netzentgelte für Entnahmestellen mit Leistungsmessung - Jahresleistungspreis - (Preisblatt LG JLP)

Gültig ab 01. Januar 2017

Das Entgelt für die Vorhaltung sowie die Inanspruchnahme der Netzkapazität während eines Abrechnungsjahres wird anhand der Jahresabrechnungsleistung in Abhängigkeit der erreichten Benutzungsstunden bestimmt.

Jahresbenutzungsdauer	< 2.500 Bh		≥ 2.500 Bh	
Entnahmestelle	Leistungspreis €/ kW*a	Arbeitspreis ct/kWh	Leistungspreis €/ kW*a	Arbeitspreis ct/kWh
Umspannung Höchst-/ Hochspannung	16,97	3,30	94,15	0,22
Hochspannung	15,85	3,95	111,69	0,12
Umspannung Hoch-/ Mittelspannung	16,05	4,05	114,85	0,10
Mittelspannung	12,78	5,55	139,12	0,50
Umspannung Mittel-/ Niederspannung	12,85	5,66	142,50	0,47
Niederspannung	14,17	5,63	115,65	1,57

Bei Entnahme der elektrischen Energie aus der Mittelspannungsebene und deren Erfassung durch eine niederspannungsseitige Messeinrichtung wird ein Zuschlag für Transformatorenverluste in Höhe von 1,5 % auf die Arbeitsmengen und die Leistungswerte erhoben.

Die Jahresbenutzungsdauer (h/a) wird als Quotient aus der im Abrechnungsjahr bezogenen Verrechnungswirkarbeit (kWh) und der Verrechnungsleistung (kW) ermittelt.

Der Preis in €/a für die Nutzung des Netzes ergibt sich als Summe der beiden Produkte:
- ‚Maximale jährliche Leistung P' x ‚Leistungspreis LP' sowie
- ‚Jahresenergie W' x ‚Arbeitspreis AP'

Figure A.3: Price list for power price of electricity provider *Bayernwerk* of 2017.

Table A.3: Bill of materials of the *Energy Neighbor*. Components of 24 V supply.

Bezeichnung im Schaltplan	Menge	Hersteller	Artikel Nummer	Beschreibung
SITOP1, SITOP2, SITOP3	3	SIEMENS	6EP1437-2BA20	SITOP PSU300S 40A; geregelte 24 V Stromversorgung, mit jeweils 40 A;
USV	1	SIEMENS	6EP4137-3AB00-2AY0	SITOP UPS1600 40A; 24 V USV-Einheit mit 40 A und Ethernet Schnittstelle
Bat	1	SIEMENS	6EP4135-0GB00-0AY0	SITOP UPS1100; Batterie für USV mit 12Ah
F101	1	SIEMENS	5SY6116-7	Einpoliger Leitungsschutzschalter; C-16A für USV-Einheit
F_Licht	1	SIEMENS	5SY6110-6	Einpoliger Leitungsschutzschalter; B-10A für Beleuchtung
F_Lüfter	1	SIEMENS	5SY6125-7	Einpoliger Leitungsschutzschalter; C-25A für LE-Schrank- und Containerlüfter
F-Sicherheit	1	SIEMENS	5SY6106-6	Einpoliger Leitungsschutzschalter; C-25A für Hauptschalter und NA-Schutz Signale
F_RCMU	1	SIEMENS	5SY6106-7	Einpoliger Leitungsschutzschalter; C-6A für RCMU
F_IT	1	SIEMENS	5SY6106-7	Einpoliger Leitungsschutzschalter; C-6A für sämtliche IT Komponenten im LE-Schrank
F_NotAus	1	SIEMENS	5SY6306-6	Einpoliger Leitungsschutzschalter; B-6A für Not Aus Schaltgerät
F-HS_1 ... F-HS_2	2	SIEMENS	5SY6113-7	Einpoliger Leitungsschutzschalter; C-13A für Hauptschalter
F-Janitza	1	SIEMENS	5SY6306-6	Einpoliger Leitungsschutzschalter; B-6A für Janitza Messgerät
F_LS_S1 ... F_LS_S8	8	SIEMENS	5SY6113-7	Einpoliger Leitungsschutzschalter; C-13A für Stringschalter
F_LE1 ... F_LE8	8	SIEMENS	5SY4106-8	Einpoliger Leitungsschutzschalter; D-6A für Wechselrichtereinheiten
F_R1 ... F_R8	8	SIEMENS	5SY6110-7	Einpoliger Leitungsschutzschalter; C-10A für Rackversorgung
F_R1_USV ... F_R8_USV	8	SIEMENS	5SY6110-7	Einpoliger Leitungsschutzschalter; C-10A für USV-Rack-Versorgung

Table A.4: Bill of materials of the *Energy Neighbor*. Safety and control components.

Bezeichnung im Schaltplan	Menge	Hersteller	Artikel Nummer	Beschreibung
NA 1	1	SIEMENS	5TT3427	Spannungs- und Frequenzrelais 5TT3 427 zur Überwachung von Netzeinspeisungen gröSSer 30 kVA
OR_1, OR_2	2	Weidmüller	8218440000	Oder-Funktionsbaustein für Inselnetzerkennung
Insel	1	SIEMENS	LZS:RT3A4L24	Steckrelais, 1 Wechsler, 24 V
RCMU	1	Bender	RCMS 490 D	Differenzstrom-Überwachungssystem
AN1, AN2	2	Bender	AN110	Netzgerät für allstromsensitive Messwandler
W1 ... W8	8	Bender	W20AB	Allstromsensitive Messwandler in den Stringabgängen
KEMS_S	1	SIEMENS	LZS:RT3A4L24	Steckrelais, 1 Wechsler, 24 V
K100	1	SIEMENS	3SK1111-2AB30	Sicherheitsschaltgerät (Not Aus)
S100	2	Ähnlich zu:	Ähnlich zu:	Not Aus Schalter neben Eingangstüre und in LE-Schrank
S100.1		SIEMENS	3SB3000-1HA20	
S101	1	Ähnlich zu: SIEMENS	Ähnlich zu: 3SB3001-0AA61	Not Aus Reset Taster
PilotR1_rück ... PilotR8_rück	8	POENIX CONTACT	RIF-1-RPT-LDP-24DC/2X21AU	Steckrelais, 2 Wechsler, 24 V
PilotLE1 ... PilotLE8	8	SIEMENS	LZS:RT3A4L24	Steckrelais, 1 Wechsler, 24 V

Table A.5: Bill of materials of the *Energy Neighbor*. AC switching gear components.

Bezeichnung im Schaltplan	Menge	Hersteller	Artikel Nummer	Beschreibung
LS1, LS2	2	SIEMENS	3VA2340-5HL32-0AA0	Leistungsschalter (Hauptschalter)
	4	SIEMENS	3VA9988-0AA12	Hilfsschalter, je zwei in LS1 und LS2 integriert.
Mo1, Mo2	2	SIEMENS	3VA9467-0HA10	Motor für Leistungsschalter LS1 und LS2
USA_Mo1, USA_Mo2	2	SIEMENS	3VA9908-0BB11	Unterspannungsauslöser
LS_S1 ... LS_S8	8	SIEMENS	3VA1110-4EE36-0AA0	Leistungsschalter (Stringschalter)
	8	SIEMENS	3VA9988-0AA12	Hilfsschalter, je zwei in LS1 und LS2 integriert.
MO_S1 ... MO_S8	8	SIEMENS	3VA9157-0HA10	Motor für Leistungsschalter LS_S1 bis LS_S8
USA_S1 ... USA_S8	8	SIEMENS	3VA9908-0BB11	Unterspannungsauslöser

Table A.6: Bill of materials of the *Energy Neighbor*. IT-components.

Bezeichnung im Schaltplan	Menge	Hersteller	Artikel Nummer	Beschreibung
Switch_innen, Switch_auSSen	2	POENIX CONTACT	FL SWITCH SF 16TX	Ethernet Switch, 16 TP-RJ45-Ports, 100 Mbit/s
Switch_WAN	1	POENIX CONTACT	FL SWITCH SFNB 5TX	Ethernet Switch, 5 TP-RJ45-Ports, 100 Mbit/s
EMS_Speicher	1	SIEMENS	6AG4140-6BL20-1HA0	IPC mit CORE I7-3517UE Prozessor
PoKey1	1	VARTA	–	Ethernet to I/O-Wandler
PoKey_Lüfter 1, PoKey_Lüfter 2	2	VARTA	–	Ethernet to I/O-Wandler (Lüftersteuerung)

Table A.7: Bill of materials of the *Energy Neighbor*. Inverter components.

Bezeichnung im Schaltplan	Menge	Hersteller	Artikel Nummer	Beschreibung
CU1 ... CU8	8	SIEMENS	6SL3040-1MA01-0AA0	Control Unit CU320-2
AIM1 ... AIM6	6	SIEMENS	6SL3100-0BE23-6AB0	Active Interface Module für 36 kW Wechselrichter
AIM7, AIM8	2	SIEMENS	6SL3100-0BE21-6AB0	Active Interface Module für 16 kW Wechselrichter
ALM1 ... ALM6	6	SIEMENS	6SL3130-7TE23-6AA3	Active Line Module: bidirektionaler 36 kW Wechselrichter
ALM7, ALM8	2	SIEMENS	6SL3130-7TE21-6AA4	Active Line Module: bidirektionaler 16 kW Wechselrichter
VSMR1 ... VSMR8	8	SIEMENS	6SL3053-0AA00-3AA1	Voltage Sensing Module; Spannungsmesskomponente für Wechselrichtereinheit
	8x3	MAGNETEC	M-614	Filterringe für Zwischenkreisfilterung (voraussichtlich drei Stück pro String)

Table A.8: Bill of materials of the *Energy Neighbor*. Auxiliary components.

Bezeichnung im Schaltplan	Menge	Hersteller	Artikel Nummer	Beschreibung
UMG1	1	Janitza	UMG 96RM-E	Leistungsmessgerät
I1, I3	3	Janitza	6A315.3	Messwandler für Leistungsmessgerät
LE_Lüfter_1 ... LE_Lüfter_4	4	EBM Papst	RG 220-43/14/2TDMO	Radiallüfter mit Gehäuse für LE-Schrank Lüftung
Container_Lüfter	1	EBM Papst	RG 220-43/14/2TDMO	Radiallüfter mit Gehäuse für Lüfter an Luftlanze
A1	1	SIEMENS	5SD7443-1	Überspannungsschutzeinrichtung

Table A.9: Bill of materials of the *Energy Neighbor*. Components of a battery rack (1/2).

Bezeichnung im Schaltplan	Menge	Hersteller	Artikel Nummer	Beschreibung
	1	Rittal	8606009 / TS8	TS8 Schrank mit IT-Türe, Anschlag wahlweise rechts oder links, incl. Rückwand und Deckel
	1	Rittal	8106235	Seitenwände, paarweise verpackt.
	-1	Rittal	8609060	Alternativ: Trennwand
	-1	Rittal	8800470	Anreihbefestigung zur Verbindung der Trennwände (8 Stück pro Verpackungseinheit)
	-1	Rittal	8800490	Anreihbefestigung zur Verbindung nebeneinander stehender Schränke (6 Stück pro Verpackungseinheit)
	1	Rittal	8100000	Sockel für die Racks (4 Stück pro Verpackungseinheut)
	1	Rittal	8100600	Blenden für Sockel (2 Stück pro Verpackungseinheit)
	1	VARTA-Storage		Luftlanze und Regalböden
Modul1 ... Modul13	13	VARTA-Storage / TUM		Batteriemodule
BMS-Master	1	TUM		Master BMS
EMS-Rack	1	VARTA-Storage		Rack EMS
	2	POENIX CONTACT	VS-08-A-RJ45/MOD-1-IP20	RJ45 Anbaurahman,
	2	POENIX CONTACT	VS-08-BU-RJ45/BU	RJ45 Buchseneinsatz (Buchse auf Buchse)
	1	POENIX CONTACT	HDFK 50	Durchführungsklemme bis 150 A
	1	POENIX CONTACT	HDFK 50/Z	Durchführungsklemme bis 150 A mit Rastzapfen
	1	POENIX CONTACT	DP-HDFK 50/7,2	Distanzplatte für Durchführungsklemme bis 150 A
	1	POENIX CONTACT	UW 4	Durchführungsklemme bis 41 A
	5	POENIX CONTACT	UW 4/S	Durchführungsklemme bis 41 A mit Rastzapfen
	2	POENIX CONTACT	DP-UW 4	Distanzplatte für Durchführungsklemme bis 41 A
	13	POENIX CONTACT	VC-TFS 5/1M-PEA	Stecker: Kontakteinsatz für Leistungspins
	13	POENIX CONTACT	VC-TFS 8	Stecker: Kontakteinsatz für Signalpins

Table A.10: Bill of materials of the *Energy Neighbor*. Components of a battery rack (2/2).

Bezeichnung im Schaltplan	Menge	Hersteller	Artikel Nummer	Beschreibung
24V_Versorgung	1	POENIX CONTACT	RIF-0-RPT-24DC/ 1AU	Steckrelais, 1 SchlieSSer, 24 V
R_HV_P, R_HV_N	2	POENIX CONTACT	RIF-1-RPT-LDP-24DC/2X21AU	Steckrelais, 2 Wechsler, 24 V
Switch_Rx	1	POENIX CONTACT	FL SWITCH SFNB 5TX	Ethernet Switch, 5 TP-RJ45-Ports, 100 Mbit/s
	diverse	POENIX CONTACT	PT 2,5-QUATTRO	Durchgangsklemmen
X1_FR1, X1_FR2	2	POENIX CONTACT	ZFK 6-DREHSI (6,3X32)	Zugfeder-Sicherungsklemme für G-Sicherungseinsätze
X1_FR1, X1_FR2	2	SIBA	7017240	G-Sicherungseinsatz 6,3 x 32 mm
IsoW	1	Bender	ISOMETERő iso685	Isolationsüberwachungsgerät
I_DC	1	Isabellen-hütte	IVT-100-U3-TOI-CAN2-24	Stromsensor
GV200_P, GV200_N	2	GIGAVAC	GIG/GV200CAB-1	DC-Leistungsrelais
LS_DC	1	ABB	1SDA054183R0001	Leistungsschalter
LS_DC	1	ABB	1SDA054910R0001	Hilfskontakt für Leistungsschalter
LS_DC	1	ABB	1SDA054929R0001	Drehantrieb für Leistungsschalter
LS_DC	1	ABB	1SDA055006R0001	Anbausatz für Leistungsschalter (Anschlussbolzen)
Lüfter	1	ebmpapst	RER220-44/14/2TDMO	Racklüfter
	3			Mini Kunststoff Schaltdosen

Emissions of Producing Auxiliary Electronics

The components are grouped into several categories: Cables, 24 V supply, AC-switchgear, IT-components, 230 V supply, safety and control components, and miscellaneous components. The cables are included in the bill of materials and are estimated based on an existing BESS [154]. The 24 V supply converts the 230 V grid power to 24 VDC. It consists of power circuit breaker, converter, and an interruptible power supply. The AC-switchgear is responsible for connecting and disconnecting the BESS from the local electricity grid. Components such as power circuit breaker, servomotors for switches, and undervoltage releases belong to this group. IT-components are the sum of (micro-) processors, switches, and ethernet I/O converters. 230 V supply allows lighting and other standard devices to work with standard power supply. Components that fall into this category are power circuit breakers and fuses. The devices that belong to the safety and control group ensure the monitoring of the BESS and enable safety functions, as well as control of the BESS. Voltage and frequency supervision relays, differential current monitors, and emergency switches belong to this group. Miscellaneous devices comprise sensors and the ventilation system.

A breakdown of the electronic component groups regarding their carbon emissions is given in Table A.11.

Table A.11: Production emissions of auxiliary electronics of the *Energy Neighbor*.

		Spec. emissions (kg CO_2eq/kg)		Total emissions (kg CO_2eq)	
Component	Mass (kg)	Min.	Max.	Min.	Max.
Cables	322.00	0.79	1.43	254.22	461.55
24 V supply	24.23	60.82	83.80	1473.54	2030.03
AC-switchgear	8.11	15.56	17.39	126.19	140.96
IT-components	4.71	96.92	190.28	456.61	896.50
230 V supply	1.79	4.28	8.60	7.68	8.60
Safety and control	1.77	49.55	82.98	87.47	148.24
Misc.	5.00	17.77	20.76	88.90	103.86
Total	367.61			2494.61	3789.74

B Profiles for Simulation

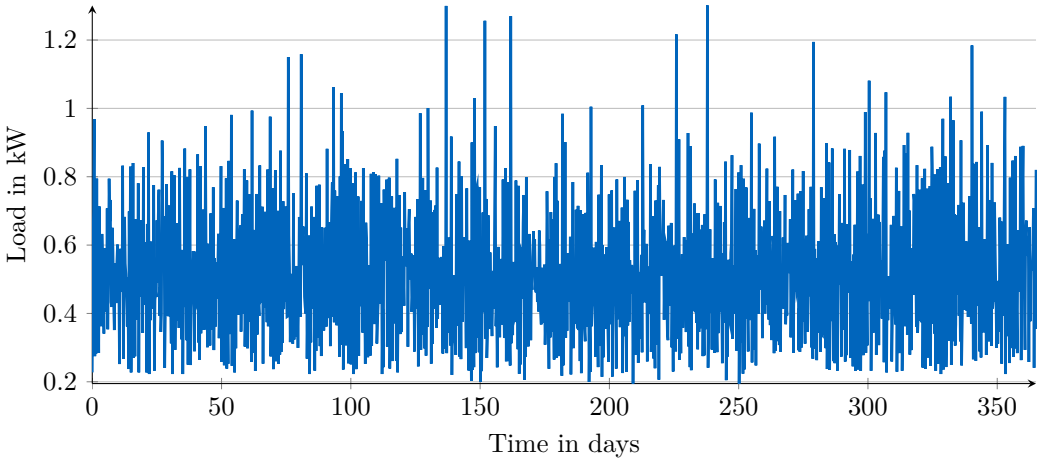

Figure B.1: Load profile for PV-home simulation

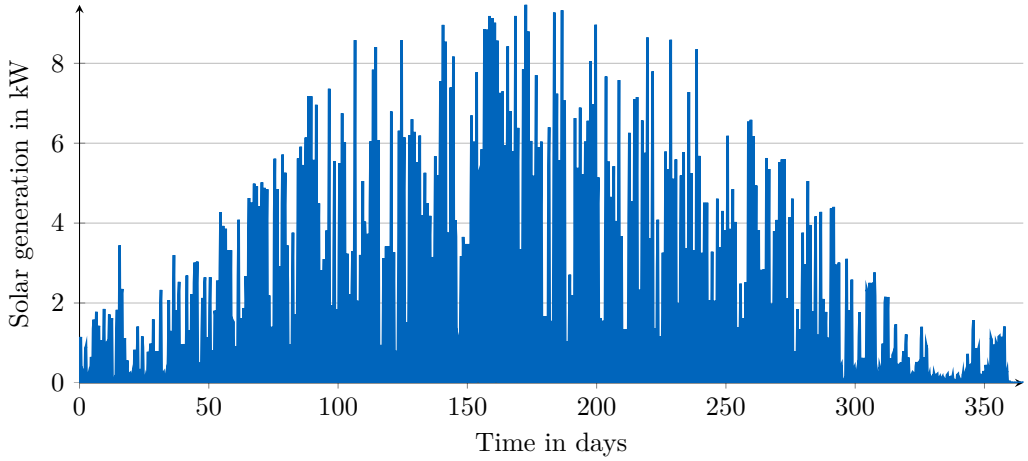

Figure B.2: Solar generation profile for PV-home simulation

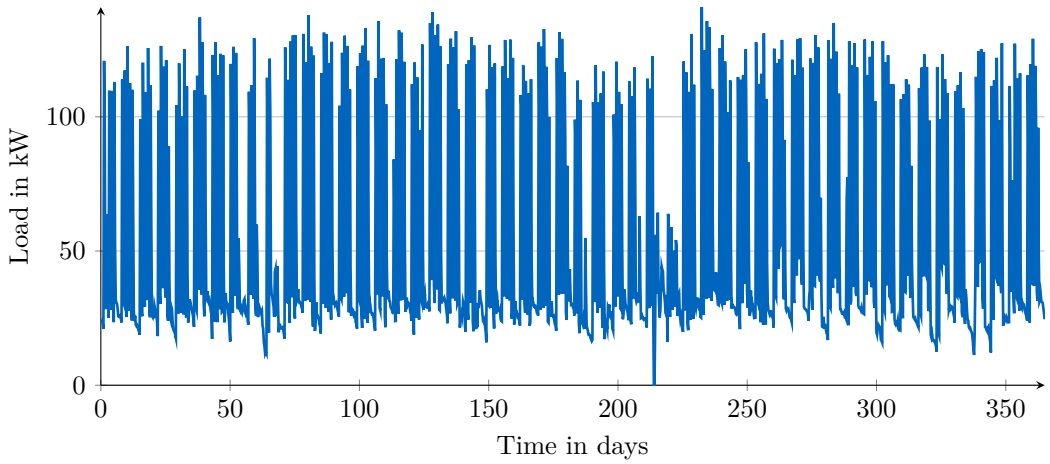

Figure B.3: Load profile of sawmill for peak-shaving simulation

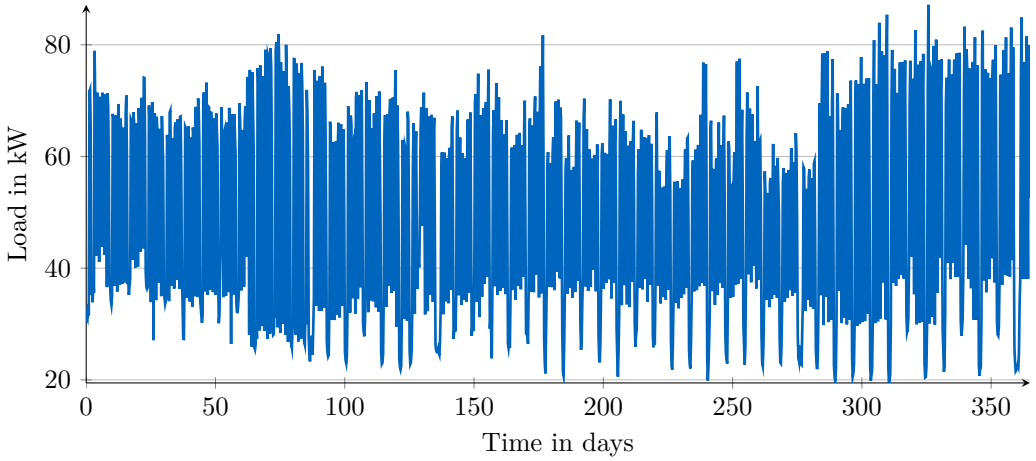

Figure B.4: Load profile of grocery store for peak-shaving simulation

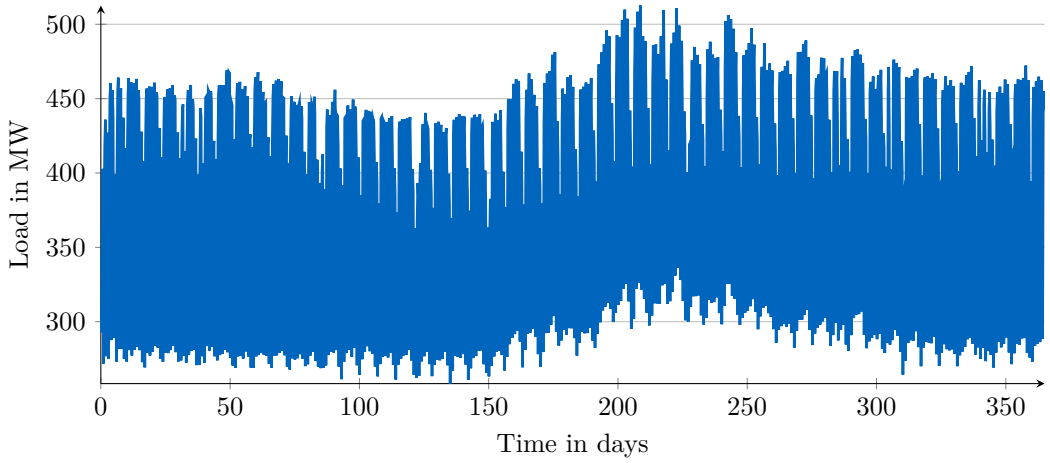

Figure B.5: Load profile of island for island grid simulation

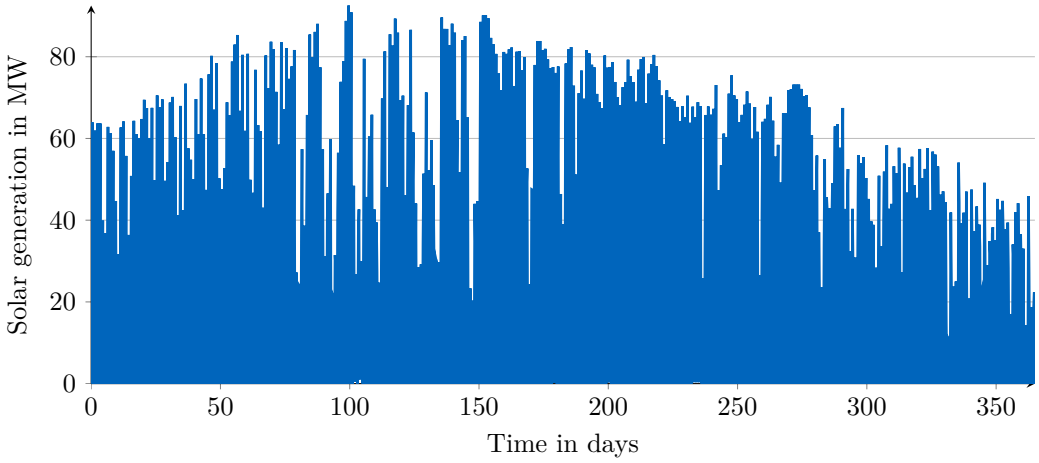

Figure B.6: Solar generation profile for island grid simulation

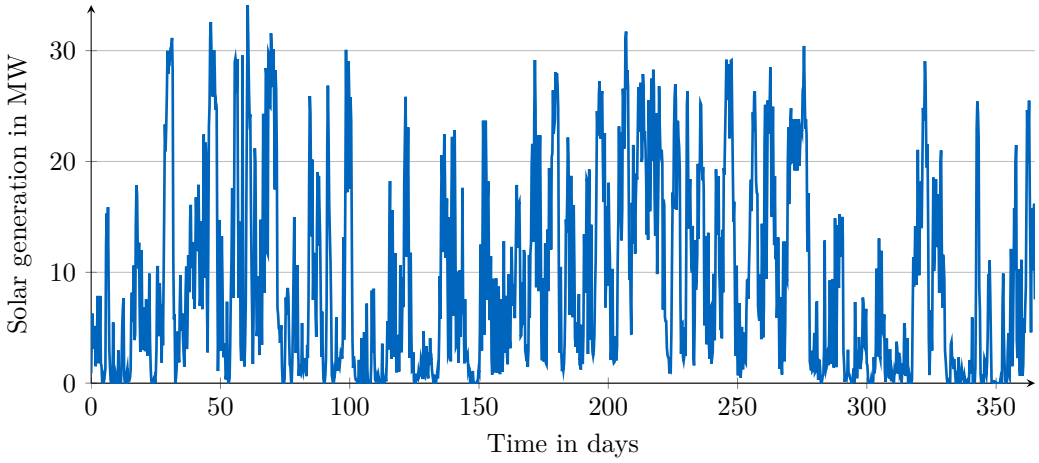

Figure B.7: Wind generation profile for island grid simulation